Advanced vision tests for optimising aircrew performance

James Richard Ellis Sadler

Doctor of Philosophy

City, University of London

Centre for Applied Vision Research

School of Health Sciences

March 2021

Contents

List of tables

List of figures

Acknowledgements

I would like to thank my academic supervisor, Prof. John Barbur for always asking what seems like the unanswerable question and for introducing me to pupillometry. I would also like to thank Dr Desmond Connolly, without whom this adventure would have never started. Your gentle guidance and support were invaluable in getting me across the line.

To Ben and Emsal, thank you for being there to bounce ideas off and Tracy for all your help.

I am grateful to all those who participated in my studies, without your vision, and patience, this project would never have happened.

I also must thank QinetiQ for sponsoring the PhD and the Human Performance management team for making the time available to complete the project. The trial of SP802 was made easier with your support. Vivienne, thank you, for your help. To Antony and Sarah for giving me the time and gentle prods as to what is important. To Sally for taking me up, and down, to 10,000 ft so smoothly. To Dom and Henry for those endless linearity checks, and Alec and Tim for getting me going and being there to help when needed.

I would like to thank my family and I am grateful for the support provided by both my parents and in-laws. Boys, it has been a roller-coaster and I am sorry that I have not been around to share in your lockdown adventures as much as I would have loved to. I hope that one day, you will pick this up, from its place propping open the study door, and understand at least part of what I have been working on.

Lastly to my wife, for holding the fort and giving me the space to get my head into gear. I could not have done this without you and all your loving support.

For P, A and L

Declaration

I grant powers of discretion to the University Librarian to allow this thesis to be copied in whole or in part without further reference to me. This permission covers only single copies made for study purposes, subject to normal conditions of acknowledgement.

Abstract

This research project has considered how advanced vision tests can be used to optimise aircrew performance both as a means for characterising visual function of aircrew and as a method of better understanding mesopic visual function.

The first study defined a test protocol for the Rod Cone Sensitivity (RCS) test with the aim of characterising the sensitivity of rod and cone mediated vision to mean modulated flickering stimuli presented at the fovea and peripherally at 5° eccentricity. The luminance, chromaticity, and temporal modulation of the two stimulus conditions were configured to promote either a rod or cone mediated response after a short adaptation time of two minutes. Subsequently, the test was utilised to characterise binocular summation both at the fovea and at 5° eccentricity with results confirming cone mediated vision based up probability summation at the fovea. The study also identified that binocular summation of stimuli presented peripherally resulted from a combination of probability and neural summation processes for both test stimulus conditions of the RCS test.

The second study confirmed that the chromaticity of the rod condition instigated a rod mediated response based upon the scotopic dependency of the pre-stimulus diameter of the pupil light reflex. Using the two stimulus conditions to characterise the transient pupil light reflex to a 100% contrast stimulus for luminance values from -3 to 2 log cdm^{-2} enabled models for the constriction amplitude and latency as a function of retinal illuminance to be developed. The results have assisted in determining the transition point between rod and cone mediated visual function as a function of scotopic retinal illuminance and how this point might be affected by changes caused by aging to the optics of the eye and retina.

The last study applied the RCS test enabling the comparison of visual function under conditions of: normobaric normoxia; hypobaric hypoxia equivalent to 3048m altitude; and normobaric hyperoxia (100%). The participants demonstrated a statistically significant loss of sensitivity at 5° eccentricity at $0.5cd.m^{-2}$ and $24cd.m^{-2}$ due to hypobaric hypoxia, when compared to the normobaric hyperoxia condition. In addition, the study demonstrated that an inspired fraction of 43% oxygen was able to mitigate against the effects of hypobaric hypoxia at 3048m altitude.

Together the studies have highlighted the differences in sensitivity and function of the retina at the fovea and at 5° eccentricity at mesopic light levels, and how the peripheral retina is more sensitive to changes in choroidal oxygen tension.

Abbreviations and symbols

SI units are represented conventionally. All other units, symbols and abbreviations that have been used are listed below.

μ	Mean
σ	Standard Deviation
α	Alpha
ρ	Apodisation factor
λ	Wavelength
ϕ	Pupil diameter
AD	Anderson-Darling
ADP	Adenosine Di-Phosphate
AFC	Alternative Forced Choice
amu	Atomic mass units
ANOVA	Analysis Of Variance
Ar	Argon
arcmin	arc minute
ASI	Alternative Summation Index
ATP	Adenosine Tri-Phosphate
AVOT	Advanced Vision and Optometric Tests
BL	Bottom Left
bpm	Beats per minute
BR	Bottom Right
BSI	Binocular Summation Index
BSR	Binocular Summation Ratio
C	Cone mediated stimulus
Ca^{2+}	Calcium cation
CAA	Civil Aviation Authority
CAAT	Contrast Acuity Assessment Test
CAD	Colour Assessment and Diagnosis
Cap	Capacitance
C_B	Binocular contrast sensitivity
$cd.m^{-2}$	Candela per square meter
cGMP	cyclic Guanosine Mono-Phosphate
CIE	Commission Internationale de l'Eclairage
C_L	Left eye contrast sensitivity
C_M	Monocular contrast sensitivity
c_n	Coefficient where n defines the index.
CO_2	Carbon Dioxide

cpd	Cycles/degree
C_R	Right eye contrast sensitivity
CSF	Contrast Sensitivity Function
D	Stimulus that is a metameric match to D65 illuminant
D65	CIE illuminant which is a metameric match to daylight.
e^-	electron
$E(\lambda)$	Radiance spectrum
ECG	Electrocardiogram
EMAIL	Eye Movement And Integrated Latency
E_{Ph}	Photopic retinal illuminance
E_{Sc}	Scotopic retinal illuminance
EW	Edinger Westphal
F_IO_2	Fractional Inspired Oxygen concentration
fMRI	Functional Magnetic Resonance Imaging
FMT	Flicker Modulation Threshold
ft	Feet
GMP	Guanosine Mono-Phosphate
HMD	Helmet Mounted Display
Hz	Hertz
ICAO	International Civil Aviation Organisation
IHADSS	Integrated Helmet And Display Sighting System
IIT	Image Intensifier Tube
INL	Inner Nuclear Layer
IPI	Interocular Percentage Increase
IPL	Inner Plexiform Layer
ipRGC	intrinsically photoreceptive Retinal Ganglion Cell
IQR	Inter-Quartile Range
IS	Inner segment
ISL	Integrated Saccade Latency
K^+	Potassium cation
L	Long wavelength sensitive cone
L	Luminance
LEDs	Light Emitting Diodes
LGN	Lateral Geniculate Nucleus
lm	Lumen
logMAR	Logarithm of Minimum Angle of Resolution
lux	Unit of photopic illumination
M	Medium wavelength sensitive cone
M	Molecule

m/q	Mass to Charge ratio
$M^{+\bullet}$	Radical ion
MBTR	Monocular/Binocular Threshold Ratio
Mg^{2+}	Magnesium cation
Mk	Mark
mlux	milli-lux
mmHg	millimetres of Mercury
MOD	Ministry Of Defence
MR	Modulation Ratio
n	A number
N_2	Nitrogen
Na^+	Sodium cation
nm	nanometres
NVG	Night Vision Goggle
O_2	Oxygen
ONL	Outer Nuclear Layer
OPL	Outer Plexiform Layer
OPN	Olivary Pretectal Nucleus
OS	Outer segment
P_ACO_2	Partial Pressure of Carbon Dioxide
P_AO_2	Alveolar Partial Pressure of Oxygen
P_B	Barometric Pressure
PCO	Pressure Chamber Operator
PCO_2	Partial Pressure of Carbon Dioxide
PDE	phosphodiesterase
PET	Positron Emission Tomography
$P_{ET}CO_2$	End tidal partial pressure of Carbon Dioxide
$P_{ET}O_2$	End tidal partial pressure of Oxygen
pH	Potential of Hydrogen
Ph	Photopic
PI	Principal Investigator
P_IO_2	Inspired Partial Pressure of Oxygen
PIPR	Post Illumination Pupil Response
PJND	Perceived Just Noticeable Difference
PLR	Pupil Light Reflex
P*n*	Pupillometry participant number where *n* defines the index, e.g. P3.
PNS	Para-sympathetic Nervous System
PO_2	Partial Pressure of Oxygen
psig	Pounds per Square Inch Gauge

P_x	Probability of detecting a stimulus
QEC	QinetiQ Ethics Committee
QSI	Quadratic Summation Index
R	Respiratory Exchange Ratio
R	Rod mediated stimulus
R*	Photoactive Rhodopsin
R^2	Coefficient of determination
RAF	Royal Air Force
RCS	Rod Cone Sensitivity
RCS-C	Rod Cone Sensitivity test cone enriched condition
RCS-R	Rod Cone Sensitivity test rod enriched condition
RGC	Retinal Ganglion Cell
RPE	Retinal Pigment Epithelium
S	Short wavelength cone
S/P	Scotopic/Photopic ratio
SC	Superior Colliculus
Sc	Scotopic
SCN	Supra-Chiasmatic Nucleus
SHS	School of Health Sciences
SMO	Supervising Medical Officer
SNO	Standard Normal Observer
SNS	Sympathetic Nervous System
SpO_2	Blood oxygen saturation
T	Transducin
T*	Photoactive Transducin
T_B	Binocular Threshold
Td	Troland
T_L	Left eye Threshold
TL	Top Left
T_{Pupil}	Transmission of pupil
T_R	Right eye Threshold
TR	Top Right
US	United States
USAF	United States Air Force
V(λ),	Photopic luminosity function
V'(λ)	Scotopic luminosity function
VPT	Visual Processing Time
VS	Visual System

1 Introduction

1.1 Overview

1.1.1 Background

The motivation behind this research project originates from a previous investigation of the visual information, i.e. the types of features and their location in the visual scene, used by military helicopter aircrew to complete tasks within the rotary wing stability and control manoeuvre set (Sadler *et al* 2016). This set of tasks includes hovering, landing, and taking off, all of which are often performed in challenging visual conditions within the theatre of operations as well as during training. Within the scope of the previous investigation, a survey of incident reports made by aircrew highlighted that there are times when aircrew miss or misinterpret visual cues. This is further supported by the result of the European Union Aviation Safety Review where 33% of the incidents involving commercial air transport and air-taxi aeroplanes were attributed to situational awareness and sensory events (EASA 2020). For specialised operations aeroplanes, e.g. parachuting and air shows, this proportion is 44% (EASA 2020). These were attributed to either the visual cues not being prominent enough to be assimilated effectively, or that stressors, e.g. fatigue, hypoxia, or operational tempo, were acting in isolation or jointly to reduce the pilot's ability to operate effectively. It should be noted that not all aircrew are pilots, with the rear crewman in a helicopter providing a third pair of eyes during some manoeuvres.

To assist aircrew when operating in challenging visual conditions, technological aids are used to enhance visual performance. Night Vision Goggles[1] (NVGs) and other advanced technologies and systems have extended the operational environments within which both civilian and military aircrew operate. Whilst this has benefits to maintaining operational tempo, it can lead to an increase in cognitive workload (Sekiguchi *et al* 1978) and physical fatigue (Caldwell 2005) as well as the human operator working in visually challenging environments with the potential for spatial disorientation (Stot 2013). With increased levels of fatigue comes an associated degradation in performance and an increased probability of human error, which could ultimately lead to an accident. Fatigue itself is often cited as a contributing factor in aviation accidents (Caldwell 2005). Additionally, operating at altitudes of 2,438m (8,000ft) and above, without supplementary oxygen, has been shown to result in a degradation in the ability to see fine detail and discriminate colours with the onset of hypoxia under mesopic conditions (Connolly 2011). This reduction in visual performance is due to the reduced oxygen levels in the blood supply to the choroid

[1] NVGs are an electro-optic device that aids vision in low light conditions, typically below 200mlux. Light from the outside scene is focused by an objective lens onto the photocathode of the Image Intensifier Tubes (IITs) inside the NVG. The resulting photo-electrons are accelerated to the micro-channel plate resulting in the generation of a cascade of electrons. This increased flux of electrons is subsequently accelerated towards a phosphor screen generating an intensified version of the image formed on the photocathode. Typically, the gain of these devices is ~10,000 resulting in an image with a luminance of 5 - 8cd.m^{-2}. The NVG eyepiece provides an image scaled to match the external scene.

located behind the retina coupled with increased oxygen demand from rod photoreceptors depriving cones in the periphery (Connolly *et al* 2008, Connolly 2011, Wangsa-Wirawan and Linsenmeier 2003).

Vision tests enable a greater understanding of the properties of the visual system (VS), whether this is measuring the response to a stimulus or as a method of diagnosing vision related diseases, e.g. glaucoma. Vision tests have become a regulatory requirement in the selection of personnel for specific roles: aircrew and air traffic controllers. Similarly, the use of psychophysical vision tests has become more widespread as toolboxes are developed for common scientific computing applications, e.g. MATLAB. This has enabled researchers to understand more about how the VS functions and thus provide a method of investigating visual function within the wider topic of human performance.

1.1.2 Scope

In the context of this research project, vision tests have been considered both for characterising an individual's visual function and as a method to gain greater understanding of mesopic visual function to facilitate the development of new technologies or systems designed to optimise aircrew performance. The scope of the studies reported in this thesis thus reflect these two roles that vision tests can play in optimising aircrew performance. The definition and characterisation of a new test protocol in the first study provides a method to characterise a participant's visual function at high mesopic and low photopic light levels. In the second study, pupillometry has been used to complement the new test protocol by examining how high mesopic and low photopic light levels affect involuntary pupil responses. In the last study, experiments were undertaken to investigate the effects of altitude and oxygen concentration on peripheral visual function extending the work previously undertaken by Connolly (2008).

The outcomes of the project are of direct relevance to aircrew who routinely operate during the periods of dawn and dusk, whether they be military aircrew working in unpressurised aircraft or commercial pilots who are generally older.

1.1.3 Aims

The aim of this research project was to learn more about human visual function under mesopic lighting conditions, enabling the development of vision tests that can characterise mesopic visual function and inform the development of new technologies or systems to optimise aircrew performance.

In support of this aim, three studies were undertaken. The aim of the first study was to characterise a new test protocol to assess flicker modulation thresholds at high mesopic and low photopic light levels to better understand visual function at this crossover point. The aims of the second study were to support the findings of the first study, and to characterise the effects of age on mesopic visual function using pupillometry. Lastly, the new test protocol was applied with the aims of gaining: a greater understanding of the effects of mild hypoxia on peripheral visual function at high mesopic and low photopic light levels; and a better understanding how increasing the inspired concentration of oxygen can be used as a countermeasure.

These aims are revisited in the discussion of the research project's findings presented in chapter 6.

1.1.4 New findings

The findings listed below are believed to be new. These are in addition to the investigations undertaken that have verified results of previous studies to validate the techniques used.

Within the context of the first study, to define the protocol and establish a basis for the utility of the Rod Cone Sensitivity test, the following are believed to be new findings.

- The development of a new test protocol to characterise the flicker modulation thresholds at low photopic ($24cd.m^{-2}$) and high mesopic ($0.5cd.m^{-2}$) with a requirement for 2 minutes pre-test adaptation to the test conditions.
- The demonstration that the binocular summation ratio at 5° eccentricity is ~$1.25\sqrt{2}$ and is independent of photoreceptor type at this eccentricity.
- The demonstration that sighting eye dominance can be predicted using the Rod Cone Sensitivity (RCS) test protocol from monocular response for both eyes.

The second study used the chromaticities of the two Rod Cone Sensitivity test stimulus conditions to investigate the contributions of rods and cones to the transient pupil light reflex with the following novel results.

- The demonstration that the model proposed by Stanley and Davies (1995) for predicting pupil diameter as a function of corneal flux can be used to describe the transient peak constriction pupil diameter and constriction latency as a function of scotopic retinal illuminance.
- The demonstration that the transient constriction amplitude of the pupil can be fitted by a Gaussian function combined with a fixed pedestal.
- As a function of age, the following aspects of the transient pupil light reflex response have been demonstrated:
    - The scotopic retinal illuminance at which peak constriction amplitude occurs decreases.
    - The pupil onset constriction latency decreases.
    - The scotopic retinal illuminance of the intersection of the constriction latencies measured for the rod enriched and cone enriched test stimuli decreases.

In the final study, the effects of altitude and oxygen concentration were evaluated using the Rod Cone Sensitivity test, defined in the first study, along with another test to assess the time taken to identify stimuli presented in the periphery of the visual field. The new findings arising from this study are given below.

- There is not a significant difference in the time required to binocularly detect and identify a 30% contrast Landolt C, with a gap of 4 arcmin, at 8° eccentricity when participants were mildly hypoxic, equivalent to 3048 m (10,000 ft), compared to the respiratory conditions of normoxia or hyperoxia (100% oxygen) at ground level.

- The effects of mild hypoxia at 3,048m can be overcome by breathing supplementary oxygen with a concentration of 43% and that the resulting visual performance is broadly comparable to an inspired fraction of 29% at ground level.

1.2 The visual system (VS)

1.2.1 Overview

Within the scope of the project, Advanced Vision and Optometric Tests (AVOT) have been used to characterise mesopic visual function and provide greater understanding of the effects of operating at 3,048m (10,000ft) where mild hypoxia is known to affect visual function. The AVOT tests have reduced variability, small within subject variability and allow configuration of stimulus parameters. Drawing on the themes of visual performance and the effect of stressors, the following sections consider the VS in terms of both imaging and non-imaging functions and the effect of altitude on visual function.

Vision encompasses the method by which light entering the eye is converted to inputs to wider cortical functions in the brain enabling visual perception of the world. These inputs allow decisions to be made through the application of context to a situation leading to a greater sense of spatial awareness. The processing of light entering the eye is not limited to the forming and processing of images via photo-transduction but extends to the non-visual function regulating the sleep-wake cycle by the process of photoentrainment.

Psychophysical vision tests assist in developing understanding of the functional properties and in particular, the sensitivity of the system. Where relevant, experiments on mammals with a shared physiology enable a better understanding of some visual processes through direct monitoring of signals or blood flow and chemical concentrations that assist in gaining a more detailed understanding of the VS.

1.2.2 Anatomy of the eye

The eye develops within the embryo as an extension of the central nervous system, sharing both anatomical and physiological properties with the brain. The asymmetric sphere, some 25 mm long, with its optics at one end, is designed to focus light onto the retina located within the posterior of the eye, as illustrated in Figure 1-1. The retina consists of cells, organised in functional layers, whose combined function is to convert photons of light into electrical impulses that undergo initial spatial, temporal, and chromatic processing prior to transmission to the visual cortex via the optic nerve. The visual cortex applies further processing to abstract meaning from the continuous stream of signals received via the optic nerve. Afferent signals are also processed by areas of the mid brain resulting in instigation of efferent responses that are often regulated by signals from the cortex, e.g. pupil constriction in response to an increase in retinal illuminance.

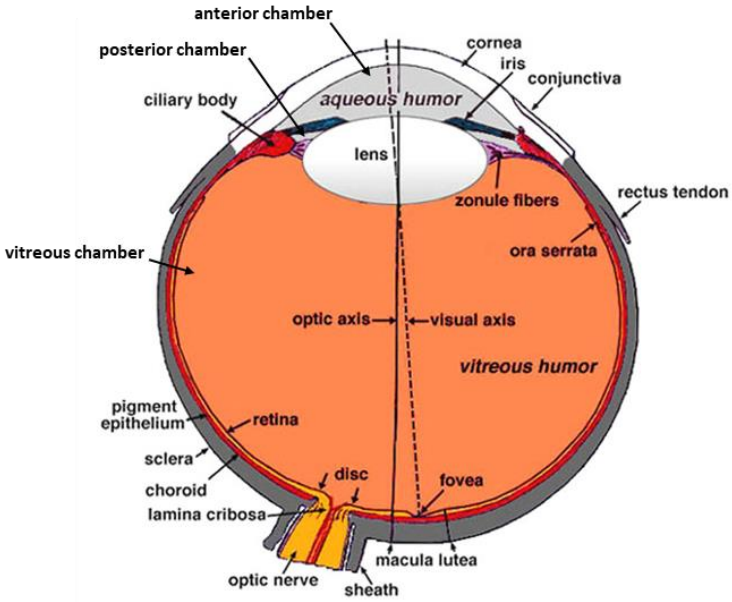

Figure 1-1: Anatomy of the human eye. Modified from Kolb (2018).

Physical protection of the eye is provided by the bony walls of the orbit located in the skull. The optic nerve leaves the eye through an aperture at the rear of the orbit. The orbit provides fixation points for the six muscles that enable the eye to move in azimuth and elevation. The eyelids, anterior to the eye, provide additional physical protection and light shielding from the external environment. They also provide a method of lubricating and clearing the anterior surface of the eye with secretions from the tear ducts.

The eye is supplied with blood from the ophthalmic artery, a branch of the carotid artery, through one of three branches: central retinal artery; anterior ciliary arteries; posterior ciliary arteries. Entering the orbit via the aperture at the rear, the central retinal artery runs along and enters the optic nerve to emerge within the globe at the optic disc (Figure 1-1), providing a blood supply to the inner aspect of the retina via layers of capillaries. The blood supply to the outer retina is provided via diffusion from the choroid, which is supplied directly by the posterior ciliary arteries which enter the back of the globe. The anterior and posterior ciliary arteries also supply the ciliary body and musculature controlling the shape of the lens and pupil size. The blood supply to the retina provides oxygen to maintain visual function. The blood supply also sustains the intraocular pressure of the eye, maintaining its asymmetric shape.

Three structural layers provide the basis for three compartments that are filled with intraocular fluids. The outer fibrous layer of a young, healthy eye comprises of the transparent cornea, white sclera and lamina cribrosa. As the eye ages, the cornea starts to become opaque as a result of fluid accumulation (Gipson 2013). In addition, the lens starts to take on a yellow appearance as the lens density increases which has the effect of attenuating blue light (Kessel *et al* 2010).

The middle layer consists of three structures, i.e. the iris, the ciliary body, and the choroid. The anterior of the ciliary body is attached to the iris, whilst its posterior is continuous with the choroid and retina.

The iris is a muscular ring-shaped membrane and its image in the cornea forms the pupil of the eye. Constriction, or miosis, of the iris sphincter muscle reduces the pupil's diameter as part of a

parasympathetic nervous response. The pupil dilates when the dilator pupillae muscle contracts and is a sympathetic nervous response. The diameter of the pupil primarily varies as a function of retinal illuminance to modulate the light incident on the retina; this autonomic response is referred to as the Pupil Light Reflex (PLR), which is considered in section 1.3.

The choroid is an important layer within the eye. Research by Linsenmier (1986) indicates that the choroid is responsible for the provision of oxygen to the outer layer of the retina containing the photoreceptors responsible for image formation. Hypoxia (oxygen deficiency) affects photoreceptor function, observed as reduction in luminance and chromatic sensitivity, considered in section 1.5.

The inner, nervous layer of the eye, i.e. the retina, has three functional elements that enable vision: the Retinal Pigment Epithelium (RPE), retinal photoreceptors and retinal neurons. The interconnections between the cells in the retina define the initial processing applied to the signals generated from photo-transduction in the photoreceptors. A more detailed consideration of photoreceptors and processing of their signals within the retina is provided in sections 1.2.4 and 1.2.5 respectively.

The compartments of the eye are located either side of the iris and the lens (Figure 1-1). The anterior chamber is the compartment between the cornea and the iris, whilst the posterior chamber is between the iris and the lens and the ring of zonule fibres that control the shape of the lens. The vitreous chamber is the space behind the lens and zonule fibres. From a clinical perspective, the eye can be separated into two segments, i.e. the lens and all structures anterior to it, and those structures posterior to the lens.

The aqueous humour is a watery, optically transparent solution of electrolytes which normally has a low protein content. This fills the anterior and posterior chambers providing nourishment to both cornea and lens. The vitreous humour is a transparent gel within the vitreous chamber filling the space between the posterior surface of the lens, ciliary body and retina. A three-dimensional structure of collagen fibres provides its gelatinous properties. Debris within the vitreous humour causes what is commonly referred to as floaters, which can detract from the visual scene being processed by the VS.

Blood is the last of the three intraocular fluids and has several key functions. The flow rate of blood within the choroid is one of the largest per unit tissue mass in the body (Wong-Riley 2010). In addition to maintaining the intraocular pressure, it has been suggested that blood has a role in the thermal management of the eye, enabling thermal energy to be absorbed as light strikes the retinal pigment epithelium (Galloway *et al* 2006). This is analogous to the use of a heat sink to remove the thermal energy generated within a photodetector as part of an electronic light detection/imaging system.

1.2.3 Optical function of the eye

The key optical elements within the eye are the cornea, pupil, lens, and the retinal photoreceptors. Although light is transmitted through the aqueous and vitreous humour, these media do not have an active role in controlling the path of light entering the eye or the process of phototransduction. The refractive properties of the cornea's fixed curvature coupled with the ability of the lens to change shape enables light to be focused onto the photoreceptors within the retina. The pupil acts as an aperture stop, controlling the amount of light entering the eye, like a camera.

The optimum pupil diameter for acuity is reported as 2.4mm, with smaller pupil diameters resulting in worsening retinal image quality because of increased diffraction (Campbell and Gubisch 1966). As pupil diameter increases, the effect of light scatter and higher order aberrations become more apparent. Light scatter is attributed mostly to the lens with smaller contributions from the cornea and the aqueous and vitreous humour. As pupil diameter increases, spherical aberration increases rapidly. Chromatic aberration is also significant in the human eye resulting in a degradation in retinal image quality when white light is involved. Chromatic aberrations arise due to the wavelength dependency of the refractive index of the cornea and lens. This results in shorter wavelengths of light being focused closer to the lens when compared with longer wavelengths. Campbell and Gubisch (1966) report that the optical quality reduces as the pupil dilates with more attenuation at spatial frequencies below 20 cycles/degree (cpd). This has the effect of reducing the contrast sensitivity for medium scale features in the retinal image by around 50% for a 6.6 mm pupil compared to a 2.4mm pupil. High spatial frequencies are affected by the reduction in the eye's modulation transfer function as it approaches the limiting resolution of the visual system. This is primarily defined by photoreceptor separation within the fovea.

Humans have evolved to function in an environment where the primary light source is the sun; a black body emitter with a temperature of 5,778K. Through evolution this has dictated the spectral response of the photoreceptors within the eye which reflects the peak available electromagnetic radiation at the Earth's surface. The result is a system that responds to wavelengths from 380nm to 780nm, the visible spectrum. The comfortable range of viewing conditions for the eye, as illustrated in Figure 1-2 in terms of luminance, can also be considered in terms of illumination conditions that vary from 10^5 lux for a bright sunny day to 10^{-4} lux for an overcast sky at night with no artificial lighting. The diameter of the pupil across this dynamic range varies between 1mm to 8mm (Williams and Warwick 1980) although Watson and Yellott (2012) quote a range in the order of 2 mm to 8 mm. Based upon the latter range of pupil diameters, which is more widely accepted, the area of the pupil changes by a factor of 16 as light levels transition from scotopic to photopic.

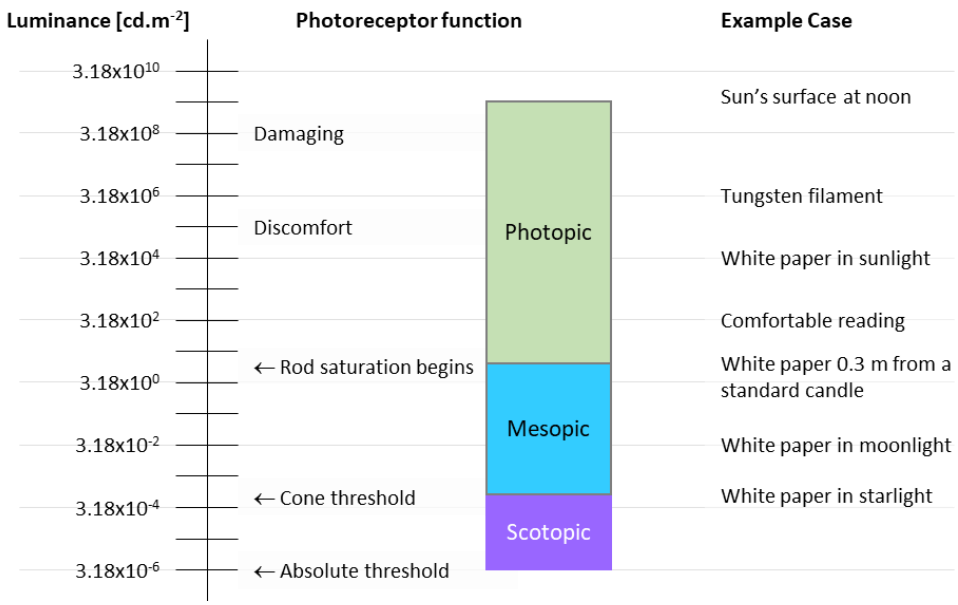

Figure 1-2: Functional limits of the visual system in terms of luminance.

1.2.4 Photoreceptors

1.2.4.1 The duplex retina

To enable visual function during both day and night, a duplex retina has evolved with two types of photoreceptors: cones and rods. Their names come from the appearance of their outer segments, as illustrated in Figure 1-3. Rods have a long cylindrical outer segment. The cones in the periphery of the retina have an outer segment that tapers to a point whilst those within the fovea are more elongated and rod like (Hood and Finkelstein 1986). Rods are more sensitive, enabling vision under low light levels, i.e. scotopic vision. Cones provide vision during daytime conditions, i.e. photopic vision, when the photon flux is much higher. The interim, mesopic, region aligns to the set of conditions when both rods and cones are sensitive. These three ranges are illustrated in Figure 1-2.

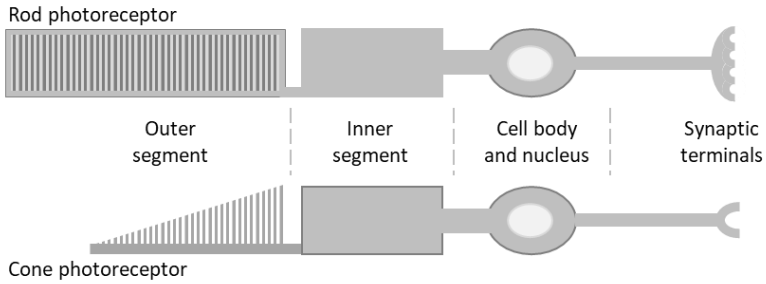

Figure 1-3: Diagram of a rod and cone showing the main segments of the photoreceptors.

The outer segment of the rod photoreceptor contains around 800 disc-like membranes containing ~100 million light sensitive pigment rhodopsin molecules (Lamb and Pugh 2004). Discs are produced at the base of the outer segment and over the space of 10 days transit up the outer segment before being phagocytosed within the RPE against which the tip of the outer segment abuts. The rod inner segment contains ellipsoids packed with mitochondria. At the base of the rod photoreceptor is the spherule that connects with bipolar and horizontal cells. The cone photoreceptor has a similar structure but with some key differences. The outer segment of the cone consists of discs formed by the folded layers of the cell membrane. The disc renewal process takes a longer time in cones compared to rods.

Cones have developed into three types which are classified based upon their spectral responsivity to light of different wavelengths: short (S), medium (M) and long (L). The relative spectral response curves for rods and the three classes of cones are provided in Figure 1-4. A third photosensitive cell type exists within the retina. Melanopsin containing intrinsically photoreceptive Retinal Ganglion Cells (ipRGCs) are a sub-population of Retinal Ganglion Cells (RGCs) and are discussed in more detail in section 1.3.

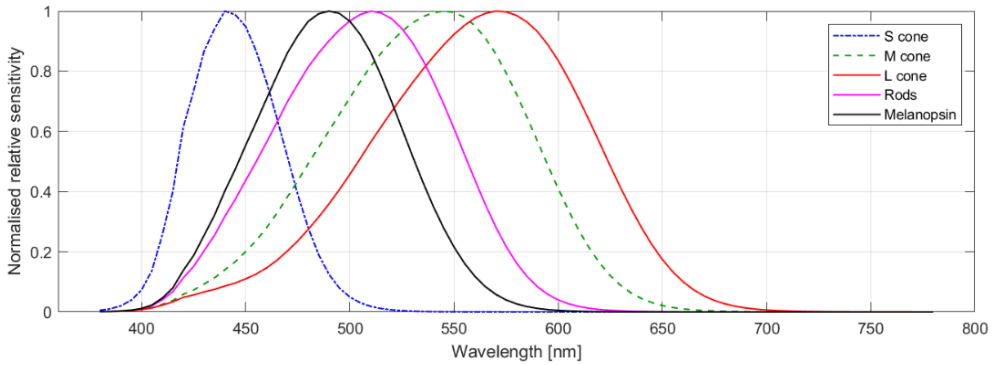

Figure 1-4: Relative spectral responses of the short (S), medium (M) and long (L) wavelength sensitive cone types as well as those of rods and melanopsin.

The abstraction of chromatic response is summarised in Figure 1-5 showing how the perception of colour arises from the summation and differencing of the cone signals. The summation of signals from L and M cones gives rise to the perception of luminance.

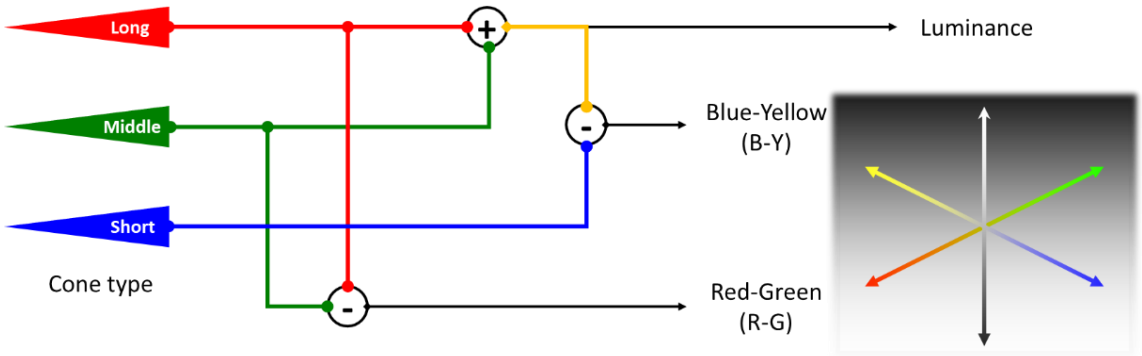

Figure 1-5: Perception of colour from opponent colour processing, where (+) is summation, (-) is differencing operation.

Unlike the rods, cones are sensitive to the angle of incident light, referred to as the Stiles Crawford effect (Stiles and Crawford 1933). To account for this angular dependence, a weighting function can be applied to the retinal illuminance for cone signals. The resulting transmission, T_{Pupil}, as a function of pupil diameter is given in Equation 1, where ρ is the apodisation factor[2].

$$T_{Pupil}(\emptyset) = 10^{-\rho\frac{\emptyset^2}{4}}$$

Equation 1: Apodisation of the pupil's transmission as a function of its diameter.

The resulting reduction in transmission as pupil diameter increases arises from the increased range of angles that light can enter the eye as the pupil diameter increases. As the angular direction of the incident light with respect to the axis of a cone photoreceptor increases, the probability of the light being absorbed by the cone decreases. Since all cones point towards the centre of the pupil, the Stiles-Crawford effect applies to cones over the whole of the retina.

[2] The value of ρ has been taken to be 0.0226 based upon data supplied by academic supervisor.

1.2.4.2 Distribution of photoreceptors

The distribution of photoreceptors varies across the retina as a function of location and photoreceptor type. Of the two photoreceptor types, rods are more numerous with the average human retina containing 92 million rods (Curcio *et al* 1990). The foveola, an area at the centre of the retina along the visual axis corresponding to a horizonal diameter of 1.25°, or 0.350mm, is almost free of rods (Curcio *et al* 1990). As illustrated in Figure 1-6, the density of rods increases as a function of eccentricity peaking at ~155,000 to 165,000rods/mm^2 around 15° to 20°. The noticeable dip in photoreceptor density on the nasal side of the retina corresponds to the eccentricity of the optic disc, where the optic nerve exits the eye. Beyond this eccentricity, the density of rods decreases. The density of rods is biased towards the nasal and superior sections of the retina. In contrast the average number of cones is 4.6 million with an average peak density of 199,000cones/mm^2, although the variation between individuals results in a range of 100,000 to 324,000cones/mm^2 (Curcio *et al* 1990). Unlike rods, cone density is at its highest at the fovea and decreases rapidly with increasing eccentricity. The horizontal meridian aligns to a streak of higher cone density. The cone density is 40-45% higher on the nasal compared to the temporal retina. There is also a bias towards the midperipheral inferior region compared to the superior retina. The figures quoted above differ from those quoted by Osterberg (1935) which are slightly higher: between 110 to 125 million rods and 6.3 to 6.8 million cones. Osterberg's data was based upon a single specimen that was sampled at greater eccentricities that the samples used by Curcio *et al* leading to the higher estimate of rods and cones (Curcio *et al* 1990). The distribution of the three cone sub-types is not uniform. The fovea is populate by L and M cones in the approximate ratio of 2:1 (Carroll *et al* 2002). The S cones are distributed outside the fovea.

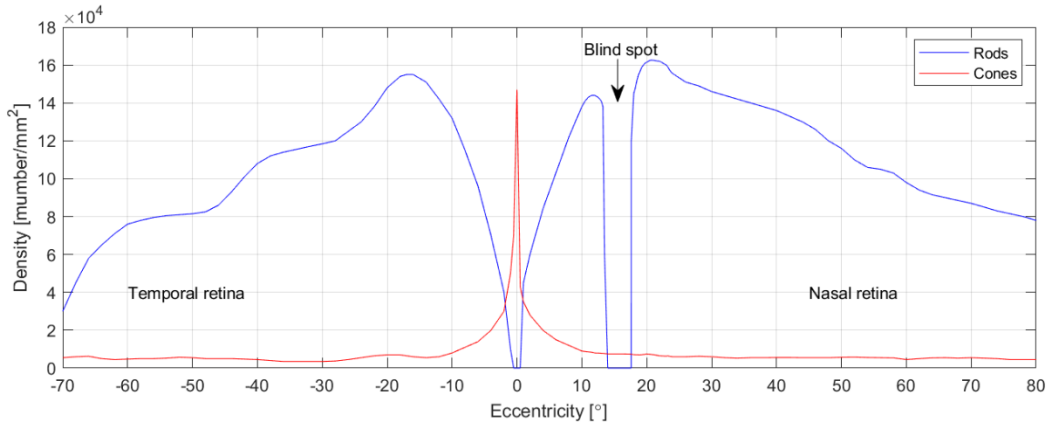

Figure 1-6: Density of photoreceptors as a function of eccentricity for the left eye, based upon Osterberg (1935).

The density and distribution of photoreceptors changes with age. Curcio *et al* (1993) found that the population of cones did not consistently change, whereas the density of rods decreased with age. The reduction in rod density, which starts in midlife, results in an annulus of loss as age increases between 0.5mm and 3mm eccentricity. For reference, the region of peak rod density corresponds to an eccentricity between 3mm and 5mm (Curcio *et al* 1993). Where rod density is reduced, rod coverage is maintained by larger rod inner segments and it is concluded that the loss of sensitivity at scotopic (and mesopic) light levels is due to post-receptoral factors (Curcio *et al* 1993).

1.2.4.3 Phototransduction

Phototransduction is the process by which photons of light incident upon a photoreceptor are converted into an electrophysiological response. It is a complex process which has been the subject of detailed reviews (Baylor 1987, Lamb and Pugh 2004, Lamb 2013) as understanding of the biochemistry has developed. The following is a simplified explanation of the key processes.

Phototransduction can be explained by comparing the movement of positively charged ions (cations) within a rod photoreceptor under two different lighting conditions: when it is in the dark; and when exposed to photons of light.

When the photoreceptor is in the dark, a current (known as the dark current) is generated by ions moving in a circuit from the extracellular fluid, through the outer and inner segments of the cell and back into the extracellular fluid, as illustrated in Figure 1-7. The dark current flowing in the outer segment arises from the movement of three ions: 80% - 90% Sodium (Na^+), 10% – 15% Ca^{2+}, and to a lesser degree Magnesium (Mg^{2+}). The current from the inner segment is primarily due to Potassium ions (K^+). An ion pump at the boundary of the inner segment with the extracellular fluid exchanges extracellular K^+ for intracellular Na^+. This pump is reliant upon metabolic energy in the form of Adenosine Tri-Phosphate (ATP), which is produced by the mitochondria within the inner segment of the photoreceptor using oxygen present in blood flowing through the choroid (Wong-Riley 2010). In addition, four Na+ are transferred into the outer segment of the cell in exchange for a Ca^{2+} and a K^+.

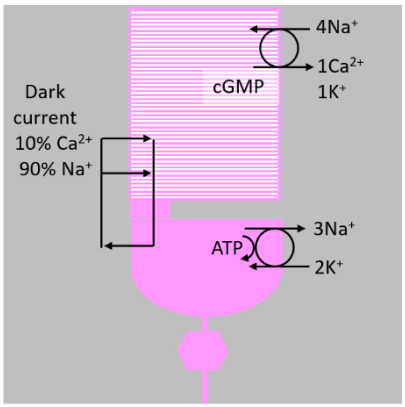

Figure 1-7: Illustration of the movement of cations in a rod in the dark and the dark current flowing from the extracellular fluid, through the outer segment to the inner segment.

The dark current is sustained by the maintenance of the Na^+ concentration gradients within the segments resulting in the Na^+ defining the resting membrane potential and the cell membrane is described as depolarised. The depolarisation of the cell membrane results in the release of the neurotransmitter glutamate. The darker the photoreceptor is the more the cell membrane depolarises, the more neurotransmitter is released, and the more work the inner segment ion pumps must undertake to expel the intracellular Na^+ and recover the K^+ from the extracellular fluid.

Exposure of the photoreceptor to light causes the cation channels in the outer segment to close. This resets the equilibrium point to match that of K^+ resulting in hyperpolarisation of the membrane potential and the release of glutamate is reduced. The closure of the cation channels in the outer segment is directly

linked to the exposure of, and resulting transformation of, the photopigment molecule, which in rods is rhodopsin.

The photosensitive pigments are based upon a form of vitamin A, the chromophore, and a protein called opsin. The link with vitamin A explains the notion of British World War II pilots improving their night vision by eating carrots, a vegetable high in vitamin A.

The absorption of a photon of light causes the isomer of retinaldehyde (11-*cis* retinal) to change shape to its all-*trans* form. In human rods the photopigment rhodopsin is composed of 11-*cis* retinal. The photopigment in cones also contains the 11-*cis* retinaldehyde but with different opsins, which explains the different spectral sensitivity of cones compared to rods. The absorption of light and the resulting change in shape causes the bleached appearance of the photopigment.

The light-induced isomerisation of rhodopsin triggers a sequence of reactions in the photoreceptor's outer segment that reduces the levels of cyclic Guanosine Mono-Phosphate (cGMP), as illustrated in Figure 1-8. The cascade of reactions occurs quickly with the effects amplified as they progress. First photoactive rhodopsin (R*) within the discs of the outer segment converts the protein transducin (T) to its active form (T*). This then stimulates the activation of phosphodisterase (PDE) to its active form PDE* which has the effect of reducing the concentration of cGMP through its conversion to GMP. The reduced concentration of cGMP closes the cation channels in the outer segments. Closing these cation channels reduces the influx of Na+ leading to the hyperpolarisation of the cell that in turn reduces the release of glutamate. The isomerisation of one rhodopsin molecule in the outer segment decreases the dark current by ~3% (Baylor *et al* 1979) demonstrating the scale of the amplification that occurs. Subsequent connections to bipolar cells and RGCs in the retina result in modification of the nerve impulses being transmitted down the optic nerve.

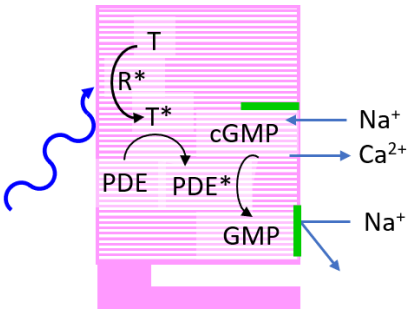

Figure 1-8: Enzymic reactions within the outer segment resulting from the light-induced isomerisation of rhodopsin to the photoactive rhodopsin (R) that eventually causes the closing of the cation channels (shown in green) reducing the influx of Na^+.*

The regeneration of rhodopsin from its all-*trans* form back to 11-*cis* retinal in part determines how quickly photoreceptors can recover from the interaction with a photon and regain sensitivity. The process of recovery involves the inactivation of the R* by multiple phosphorylations and binding with arrestin. T* inactivates itself slowly resulting in a similar reduction in the activation of PDE to PDE* and a slowing of the conversion of cGMP to GMP. At the same time, the activity of the enzyme that forms cGMP from GMP is enhanced by the reduction in Ca^{2+} concentration. The result is that cGMP concentration increases, opening the cation channels in the outer segments and restoring the photoreceptor membrane to its

depolarised state. Once Ca^{2+} concentration is restored to its original levels, the enzymic generation of cGMP ceases.

1.2.5 Retinal processing

The retina has a layered structure consisting of different cell types, illustrated in Figure 1-9. It is the connections between the different layers of cells that enables processing of signals from photoreceptors giving rise to spatial acuity, and the perception of luminance, colour, and temporal effects such as the perception of flicker and motion. The following consideration of the retinal processing starts at the outer retina and moves towards the inner surface, where photons first enter the retina.

The RPE consists of a single layer of cells that absorb photons of light not absorbed by the photoreceptors. The rod and cone photoreceptors span three layers within the retina's structure. The Outer Segments (OS) of the photoreceptors form a layer with the Inner Segments (IS) forming a second layer beneath it. The Outer Nuclear Layer (ONL) is formed by the photoreceptor nuclei. The Outer Plexiform Layer (OPL) contains the dendrites of the bipolar and horizontal cells that form synapses with the rod spherules and cone pedicles. The Inner Nuclear Layer (INL) consists of the horizontal, bipolar and amacrine cell nuclei. The horizontal cells are located at the outer region of the INL whilst the amacrine cells are located close to the boundary with the Inner Plexiform Layer (IPL), which consists of the synaptic connections between the Retinal Ganglion Cells (RGCs), amacrine and bipolar cells.

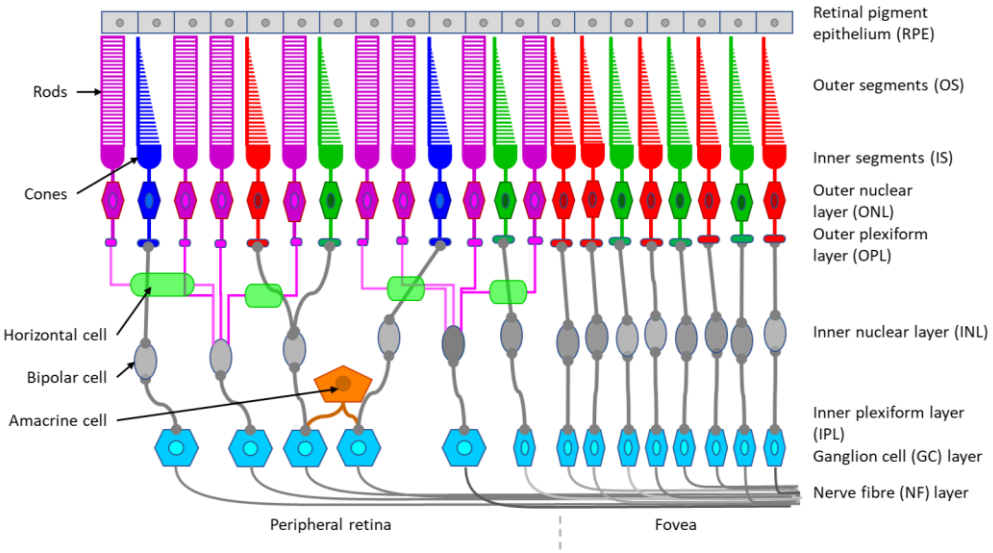

Figure 1-9: Structure of the retina illustrating some of the interconnections between cell types.

As eccentricity from the fovea increases, the density of connections between cell types changes. Within the fovea, where the density of cone photoreceptors is at its greatest, there is close to a 1:1 mapping of cones to RGCs leading to higher cortical magnification compared to the periphery of the retina (increased visual acuity). This underpins the ability to resolve higher spatial frequencies. As eccentricity increases, multiple photoreceptors connect to a smaller number of bipolar cells which then connect a similar number of RGCs. This leads to greater spatial summation and a reduction in acuity (Duncan and Boynton 2003). The grouping of multiple photoreceptors connected to a single RGC via a bipolar cell, forms a receptive field. Depending upon bipolar cell type, the output from the RGC signals either positive or negative contrast. From a practical perspective, the result of combining the outputs from multiple photoreceptors

reduces the number of bipolar cells and RGCs required, and subsequently minimises the number of connections necessary to transmit signals to the visual cortex via the optic nerve. Peak rod density of ~150,000 cells/mm^2 occurs at an eccentricity between 3 mm and 5mm (Curcio *et al* 1990, 1993). For the same region, the peak rod bipolar density is ~10,000 cells/mm^2 and the ratio of rods to rod bipolar cells is 75:4 (Lee *et al* 2019). Within the same region the density of cones is 8,500 cells/mm^2. At 1mm eccentricity the ratio of rods to rod bipolar cells reduced to 20:2.3 (Lee *et al* 2019).

The two types of bipolar cell are characterised by the connection they make to the photoreceptor. The invaginating (on) bipolar cell responds by depolarising its membrane potential in response to photoreceptor hyperpolarisation. The synapse between the photoreceptor and the on bipolar cell is defined as sign-inverting. Conversely the flat (off) bipolar cell conserves the polarity of the photoreceptor hyperpolarisation. Only cones connect with the flat bipolar cell type. Rods connect only to the on bipolar cell type.

Connections between multiple photoreceptors and a single bipolar cell are made via the horizontal cells. The horizontal cells assist in mediating the response to hyperpolarisation of the photoreceptors in the region surrounding the central photoreceptor connected to the sign-inverting on bipolar cell. The resulting sensing element, illustrated in Figure 1-10, leads to a centre-surround organisational structure within the retina, which can detect edge features within the image formed on the retina.

The functionality of centre-surround processing can be illustrated by considering the RGC firing rate in response to illumination of either or both the centre and surround region of a receptive field, see Figure 1-11. For the on-centre case, when the stimulus is aligned to the centre region, the firing rate of the RGC is increased. The RGC firing rate is significantly reduced, or inhibited, if the surround of the on-centre field is illuminated and the centre is not stimulated. For the case where both the centre and surround are both uniformly illuminated, the RGC firing rate is not affected as the response from the off-surround inhibits the response from the on-centre. For the off-centre case, the RGC firing rate is increased when stimulus is incident upon the surround region. This opposite interaction is referred to as lateral inhibition.

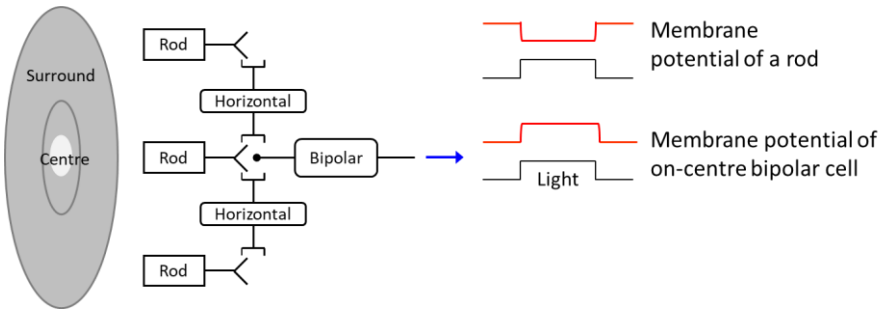

Figure 1-10: Receptive field formed of rod photoreceptors connected to an on-centre bipolar cell and horizontal cells and the onward connection to the retinal ganglion cell. Blue arrows indicate the membrane potentials of the rod and the bipolar cell in response to a spot of light on the retina. Adapted from McIlwain (1998)

As the photoreceptors respond to changes in light intensity, there is also a response when the stimulus is removed from the respective region. For the on-centre case, when the stimulus is removed from the surround region, there is an increase in the RGC firing rate. This is mimicked by the off-centre case when the stimulus is removed from illuminating the centre of the receptive field structure. Although the

example below is illustrated for changes in luminance, the same methodology can be applied to the processing of signals from cones leading to the opponent processing of L and M cones and the combined response from L and M cones (L+M) and S cone.

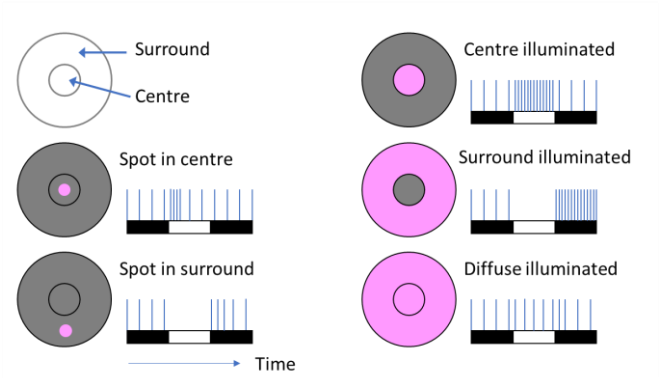

Figure 1-11: Response of RGCs to stimulation of an on-centre receptive field by a source that illuminates the respective areas of receptive field for a short time shown by the white bar.

Amacrine cells are an interneuron located within the inner retina. A subset of amacrine cells, the amacrine II cell, has been linked with transmission of rod signals to RGCs. For single photon absorption events at low light levels, it is thought that there is a pathway between rod on-bipolar cells via amacrine II cells which are connected to both on and off cone bipolar cells (Sharpe and Stockman 1999). Additionally, the distribution of the amacrine II cell type has been attributed as contributing to limiting the spatial resolution of scotopic vision at eccentricities less than 15° (Lee *et al* 2019). Amacrine cells have also been linked to a theory proposing their role in the perception of motion with the cells providing a pathway between bipolar cells and a RGC (McIlwain 1998).

The different types of RGC are intermingled across the retina, with each cell type having specific functional properties and processing pathways. The size of the RGCs' dendritic fields within the central retina are small compared to those at greater eccentricities. This is a function of both the photoreceptor type they connect to, as well as RGC cell type.

The two main RGC types are midget and parasol cells. Midget RGCs have small dendritic fields and are primarily found within the fovea. They have been linked to both spatial and chromatic (red-green) opponency, receiving inputs from L and M cone types (Dacey 2000). This is based upon +L/-M, -L/+M, +M/-L and -M/+L centre inputs combined with opposing mixed inputs from L and M cones, i.e. the surround input is not limited to one cone input but the comparison of signals from two types. Midget RGCs make up about 80% of RGCs and have been associated with lower contrast sensitivity than parasol RGCs (Callaway 2005). It is inferred that they have higher spatial frequency selectivity. They map to the parvocellular layers of the Lateral Geniculate Nucleus (LGN) within the thalamus and the primary visual cortex, being associated with a slow, tonic, response. This slow response is illustrated by the midget RGCs' response to temporal varying signals with a frequency of 5 to 10Hz, which is linear as a function of contrast.

Parasol RGCs, as their name suggests, have large dendritic fields, and are considered as broadband, or achromatic. They make up about 10% of the RGCs projecting to the LGN and are associated with having a

high contrast sensitivity (Callaway 2005). They have low spatial frequency selectivity, with their dendritic fields being about three times the size of the midget RGCs. Parasol RGCs connect to the LGN and visual cortex via the magnocellular pathway and are associated with a transient, phasic, response. This is reflected in the temporal response of parasol RGCs which has an optimal response at ~20Hz.

There are other distinct types of RGC but their function has yet to be fully characterised. Of these, the small bistratified ganglion cell has been linked to the processing of signals from the S cone – on bipolar cell pathway from 'blue-ON' receptive fields (Dacey 1996) that connect to koniocellular neurones located within the LGN (Callaway 2005, Mollon 1999).

1.2.6 Processing beyond the retina

1.2.6.1 Optic Chiasm

The axons from the RGCs form the optic nerve that projects to the LGN via the optic chiasm. Within the optic chiasm, the axons from both eyes meet and the connections corresponding to the nasal half of each retina decussate. In effect, the optic chiasm is the hub at which sensory inputs from both retinas are combined based upon the hemifield the signals originated. This is illustrated in Figure 1-12 in terms of image forming function (and in Figure 1-16 in terms of the PLR). For example, the signals processed by the temporal retina of the left eye are combined with those of the nasal retina of the right eye to pass, eventually, via the left optic radiation to the left visual cortex. In this way, common features can be combined at a signal level, shown by the coloured sections of the imaged scene, except that each fovea has bilateral cortical representation.

After the optic chiasm, the signals proceed along the optic tracts to the LGN within the thalamus. In addition to signals being transmitted to the LGN, additional connections (not illustrated in Figure 1-12) are made to the Supra Chiasmatic Nucleus (SCN), Olivary Pretectal Nucleus (OPN) and Edinger Westphal (EW) Nucleus located within the mid-brain. The role of the OPN and EW nucleus in mediating the PLR are discussed in more detail in section 1.3.

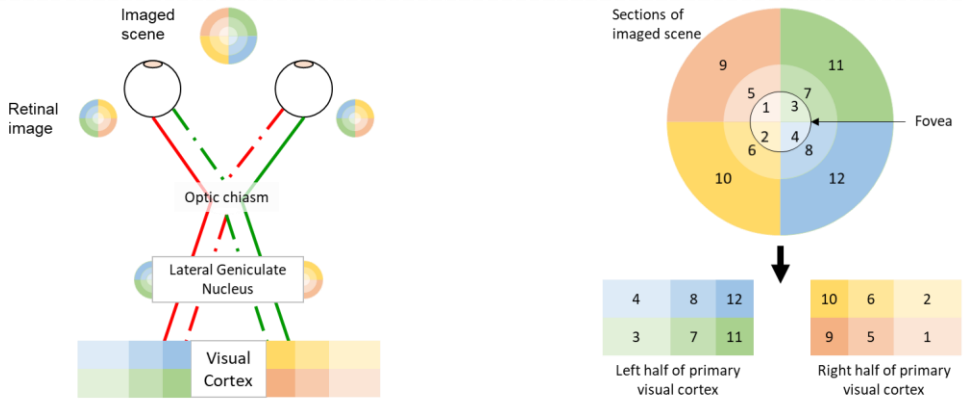

Figure 1-12: Functional diagram showing the decussation of signals from the nasal halves of the two retinas at the optic chiasm (left) and the mapping of regions in the imaged scene to regions in the visual cortex (right).

1.2.6.2 Lateral Geniculate Nucleus (LGN)

The LGN is formed of six layers, or laminae, with each lamina receiving input from only one eye: laminae 2, 3 and 5 from the ipsilateral temporal retina; laminae 1, 4 and 6 from the contralateral nasal retina. This

arrangement enables signals from the same object within the visual scene to be processed topographically by the same part of the brain.

The LGN neurons replicate the response characteristic of the source RGC type with the achromatic and chromatic signals of the magnocellular and parvocellular pathways projecting to the laminae of the LGN based upon their information content. The first two laminae of the LGN are primarily connected to the magnocellular pathway. The remaining laminae are split between the off-centre (laminae 3 and 4) and on-centre (laminae 5 and 6) parvocellular pathways. This alternating arrangement of excitatory and inhibitory signals provides the basis for orientation selectivity within the visual cortex. The LGN neurons mainly project to the first visual area (V1) of the visual cortex.

1.2.6.3 Visual cortex

The central visual field, especially at the fovea, is mapped to a greater proportion of the visual cortex than is the periphery, as illustrated in Figure 1-12. This can be represented using a log-polar projection to map the topography of the retina to regions of the visual cortex, as suggested by Grill-Spector and Malach (2004). The log-polar projection assists in visualisation of the cortical magnification and the areas of the visual cortex that the fovea maps to compared to the rest of the visual field. There is a division between the regions that monocular inputs map to compared to other regions that respond to stimuli presented to either eye, i.e. bilateral cortical representation. Ocular dominance is present within the visual cortex with some layers responding more strongly to one eye compared to the other.

There are three properties of the imaged scene that the visual cortex tries to categorise: colour opponency, disparities and orientation. Colour opponency gives rise to the perception of colour along the axes illustrated in Figure 1-5. Binocular disparities between similar regions of the visual field results in the perception of depth which can be abstracted to understand the location of an object within the visual scene.

Motion is determined based upon disparities in the visual scene as a function of time. Whilst, as scientists, we like to arrive at a single model for how the visual system processes information, not every aspect of vision can be defined by a single theory. The case of motion-in-depth is one such case. Experimental validation has demonstrated that there are two independent mechanisms for the perception of motion-in-depth within a normal population (Nefs *et al* 2010). The two mechanisms rely on either the change in binocular disparity as a function of time or the disparity between monocular motion maps to generate the perception of motion in depth. The ability to determine the direction of motion, is the fourth key attribute of the processing undertaken within the visual cortex. Furthermore, visual disparities also drive involuntary control of eye movements leading to convergence.

From the perspective of understanding its function, the visual cortex is separated into six visual areas, V1 to V6, with increasing abstraction occurring as the signals are processed through the respective visual areas. Additional higher level processing centres, V7 and V8, are introduced in the literature but nomenclature and boundaries of these regions are yet to be agreed (Grill-Spector and Malach 2004).

The function of the visual areas has been determined using a range of techniques with more recent studies making use of modern imaging techniques: Positron Emission Tomography (PET) (Zeki *et al* 1991) and

functional Magnetic Resonance Imaging (fMRI) (Grill-Spector and Malach 2004), and the more traditional approach of staining. Together these and other studies have demonstrated that vision areas V1/V2 and V4 have a functional involvement in colour vision, whilst areas V1/V2 and V5 are linked to motion perception (Ffytche *et al* 1995). Vision area V3 is associated with processing of disparities which enables the processing of depth. The specification of V1/V2 draws through the point raised by Zeki *et al* (1991), that they found it hard to distinguish between these two areas when trying to define the visual areas associated with the processing of colour and motion.

As illustrated by the summary above, the processing undertaken in V1 defines the information from which visual features are abstracted in the subsequent areas. Visual area V1, also known as the striate cortex, is formed of six principal layers, and sub-layers, in bands parallel to the surface of the cortex. The axons from the magnocellular and parvocellular layers in the LGN map respectively to neurons in sublayers 4Cα and 4Cβ. The parvocellular signals are split into two new pathways with one aligned to the processing of colour (P-B), and the second associated with orientation and high acuity perception (P-I). The two pathways are complementary. The -B and -I suffices correspond to blob or inter-blob cell types. Blob cells are colour specific, being aligned to specific sections of the visual spectrum, whilst the inter-blob cells are likewise orientation selective. The layered structure of V1, which is also prevalent in V2, enables the flow of visual information to be tracked through the visual cortex, as illustrated in Shipp and Zeki's study on macaque monkeys (Shipp and Zeki 2002).

1.2.6.4 Additional processing centres

In addition to the visual cortex, there are other processing centres that have specific roles in the provision of visual and non-visual functions. Eye movements, or saccades, are controlled by the Superior Colliculus (SC), a layered structure at the top of the brain stem (Carpenter 2000). The superior layers of the SC are sensory whilst the deeper layers control motor function. This enables the SC to provide the required innervation of the respective muscles to move the eye to its new fixation point. Carpenter (2000) highlights a time period of 100-200ms from stimulus onset before a saccade, in effect a latency, that broadly agrees with measurements made by Llapashtica (2019) using the Eye Movement And Integrated Latency (EMAIL) test (Barbur 2017), described later in section 1.4.2.

Accommodation is the process by which the shape of the lens is adjusted to bring near objects into focus. In addition, for near objects it is necessary for the optical axis of the two eyes to converge onto the object of interest by rotating the eyes inwards. The process of convergence enables the image of the object to be projected onto similar sections of the retina. The amount of convergence and the accommodative state of the eye are used in the perception of the object's depth. In addition to changes in accommodation and convergence, there may also be a constriction of the pupil. The controlling pathways for these functions interface with the SC and pretectal nuclei and where the pupil is involved, the Edinger-Westphal nucleus.

The non-visual function of photoentrainment involves the SCN with projections from melanopsin containing intrinsically photosensitive RGCs (Berson *et al* 2002). Neurons within the SCN exhibit a sustained response to light which continues post stimulus offset (Drouyer *et al* 2007), similar in nature to

the Post Illumination Pupil Response (PIPR) to a blue stimulus at photopic luminance values, as described in section 1.3.6.

1.2.6.5 Binocular summation

The VS pools information from two eyes to provide a single representation of the world. This is observed as improved sensitivity to variations in luminance. The magnitude of the improvement is generalised to a factor of $\sqrt{2}$ (Campbell and Green 1965), however the review by Baker *et al* (2018) suggests that value is higher and has a dependency on the test methodology used. Binocular summation relies on the contribution of two summation mechanisms: probability summation and neural summation.

Probability summation describes how the chance of detecting a stimulus is independent of the eye used. There is an equal chance a photon will result in a detection event in either eye and hence the chance of detecting a photon with either the left or right eye can be expressed respectively as P_L and P_R. According to Pirenne's equation (Pirenne 1943), the probability of detecting the stimulus binocularly, P_B, is given by Equation 2. If P_L and P_R both equal 0.5, then P_B equals 0.75. To return the P_B back to the threshold condition of 0.5, the luminance of the binocularly viewed stimulus must be reduced.

$$P_B = P_L + P_R - (P_L \times P_R)$$

Equation 2: Pirenne's equation

Neural summation describes the convergence of the signals from the monocular pathways into a single response to a stimulus. The impression conveyed by Blake and Fox (1973), is that determining the contribution of neural summation is at times difficult. The basis for evaluating the neural summation component relies on determining the contribution of probability summation. Having accounted for the probabilistic component, the magnitude of the neural component can be derived.

The combined result of the two summation mechanisms has been characterised by considering the effect of probability summation on the detection of: two simultaneous stimuli at widely separated locations in the same eye; and two non-simultaneous stimuli presented at the same location (Thorn and Boynton 1974). The stimuli were presented both monocularly and binocularly to fully dark-adapted participants. The result provided evidence for neural summation with the binocular threshold being lower than those recorded for the monocular conditions.

1.2.7 Dark adaptation

In a darkened environment, the process of dark adaptation results in an increase in sensitivity as a function of time typically measured following exposure to a bright light ('retinal bleach'), as illustrated in Figure 1-13. The resulting curve can be separated into two parts corresponding to the adaptation of cones followed by rods. Being less sensitive, the adaptation of cones takes between 1 and 12 minutes, depending upon the intensity of the bright light that bleaches photopigments in the photoreceptors. In contrast, rods take at least 30 minutes to reach a plateau in sensitivity which does not change significantly for an extended period of 3 hours (Hecht *et al* 1935). Aligned with the initial plateau in the dark adaptation curve, Hecht *et al* (1937) noted that the violet colour of the stimulus changed to colourless with increasing time. This change in appearance corresponds to the transition to purely rod mediated vision based on

threshold light perception. Above this threshold, cones enable the perception of both colour and luminance. The length of time required for full adaptation to occur is dependent upon the intensity of the initial bleaching stimulus. This aligns to the degree of photopigment bleaching and the time required for its replenishment. At lower adapting intensities, the dark adaptation process transitions directly into the rod adaptation curve since cones are not involved. Hecht *et al* (1937) also noted that although the cone portion of the adaptation curve varies as a function of adapting intensity, the rod portion has a defined time period to reach maximum sensitivity. Domey *et al* (1960) demonstrated that age influences the sensitivity of the photoreceptors, illustrated in Figure 1-14. Based upon these results, it is observed that from the fourth decade of life there is a loss of sensitivity as a function of age that is present for both cone and rod mediated vision. The peak in sensitivity between the age of 20 – 29 agrees with the change in chromatic sensitivity as a function of age observed by Barbur and Rodriguez-Carmona (2015). In terms of aircrew performance, it will take older aircrew longer to get to the same dark-adapted state as a younger colleague if operating in a darkened cockpit. However, lighting form the cockpit instruments and displays result in aircrew never becoming fully dark adapted. To mitigate this, military aircrew will use NVGs to intensify the external night-time scene. This has the additional benefit of overcoming the differences in sensitivity because of age. It may still take older aircrew longer to adapt to the external scene if they need to identify navigational lights by looking under their NVGs. The Image Intensifier Tubes (IITs) inside an NVG only amplify light; they do not reproduce colour.

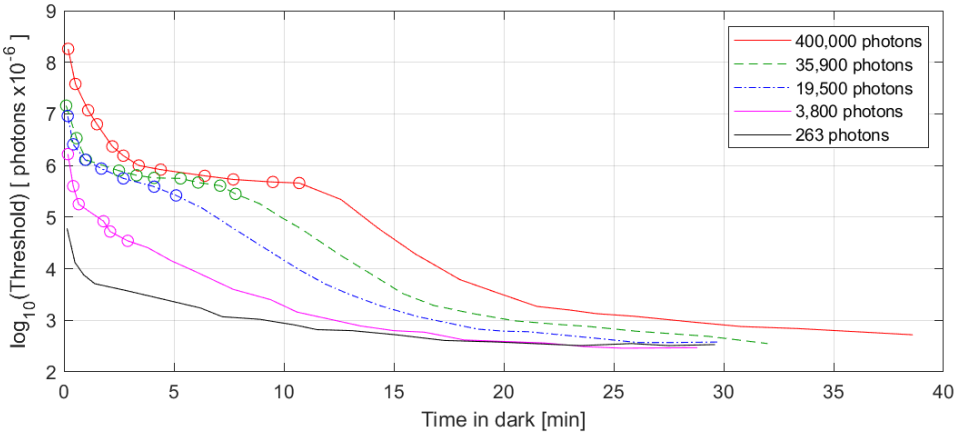

Figure 1-13: Dark adaptation curves for a violet light following a bleaching event of differing intensities. Symbols correspond to the cone function indicated by the identification of the stimulus' violet colour. Replotted from results of Hecht et al (1937).

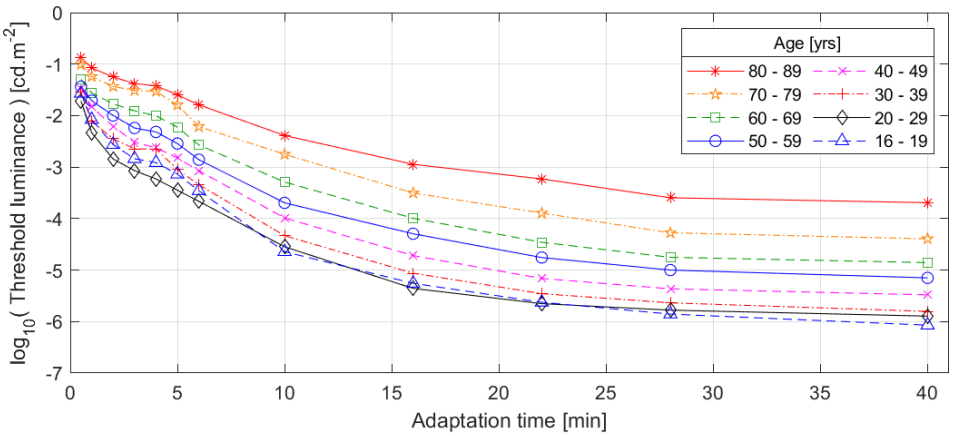

Figure 1-14: Dark adaptation curves as a function of age. Replotted from Domey et al (1960).

1.2.8 Spatial and temporal contrast sensitivity

As discussed in section 1.2.5 and 1.2.6, the distribution of cells within the retina, their interconnections, along with the processing undertaken within the retina and visual cortex, all contribute to defining the spatial and temporal contrast sensitivity of the VS. Where the spatial distribution of photoreceptors connected to bipolar cells is large, the resulting receptive field responds to low spatial frequency, or coarse features. Conversely, the ~1:1 mapping of cones in the fovea results in higher spatial acuity defined primarily by the period of the inter-cone spacing.

The spatial and temporal Contrast Sensitivity Functions (CSFs) characterise the response of the visual system, with experiments mapping sensitivity in terms of retinal illuminance or stimulus luminance. Examples of the resulting CSFs are illustrated in Figure 1-15. For the foveal region, both CSFs are at their maximum extent. The limiting spatial frequency is at 60cpd with a peak sensitivity ~6cpd for a participant with normal trichromatic vision[3] (Curcio *et al* 1990, Campbell and Gubisch 1966, Hess and Nordby 1986a). For a rod monochromat, i.e. a subject who lacks any functioning cone photoreceptors, the maximum acuity is limited to 6cpd at a lower retinal illuminance of 180ScTd compared to 6 cpd at 2000ScTd for the normal trichromat (Hess and Nordby 1986a, 1986b). The peak in spatial CSF aligns with luminance values in the order of 100cd.m^{-2}. Beyond this peak between 200cd.m^{-2} to 300 cd.m^{-2} achromatic contrast sensitivity has been shown to reduce sharply for background luminance values in the order of 1,000cd.m^{-2} (Wuerger *et al* 2020). This last point is highly relevant for military aircrew and the use of Helmet Mounted Displays (HMDs) when flying at altitude with background scene content comprising sun-illuminated cloud or snow. Both conditions will result in background scene luminance levels in the order of 1,000 to 10,000cd.m^{-2}. To counteract these conditions, a dark visor with a typical transmission of 10% is used to attenuate the background scene luminance. This has the effect of overcoming any degradation in sensitivity, returning aircrew to a perceived background luminance better aligned to the optimum sensitivity of the VS. Additional attenuation is provided by the cockpit transparency, but this is small compared to that of the dark visor. As the luminance of the stimulus is reduced, the shape of the spatial

[3] A normal trichromat is a person who has all three cone types and can thus see the three primary colours.

CSF changes from band pass to a low pass filter with a reduction in the limiting frequency of the VS. This change in functionality aligns with the transition from cone to rod mediated vision.

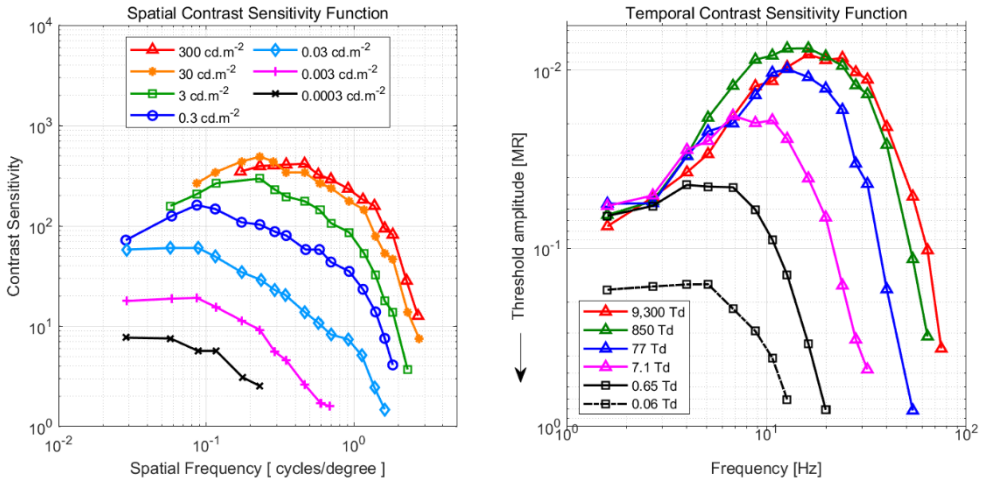

Figure 1-15: Spatial (left) and temporal (right) contrast sensitivity functions based respectively upon van Nes and Bouman (1967) and Kelly (1961).

Barten (2003) raises an interesting point about the background luminance to which the participant is adapted. This can have an effect on contrast sensitivity, something which Blackwell and Blackwell (1980) parameterised in their Relative Contrast Sensitivity measure that was subsequently utilised in the calculation of the Perceived Just Noticeable Difference metric used to define requirements for military cockpit displays (Vassie 1998, MOD 2011).

The combination of spatial distribution of photoreceptors and the underlying network of bipolar and RGCs along with the time required to replenish bleached photopigments in the photoreceptor outer segments provides the underlying spatial and temporal properties of the initial processing of the retinal image. The temporal properties of the VS are linked to Bloch's law, given in Equation 3, that relates the threshold for a stimulus of fixed size to its duration (t) and luminance (L). Bloch's law demonstrates that if the stimulus luminance is low, it needs to be presented for a longer duration. This can be thought of in terms of needing a threshold number of photons received before a stimulus can be declared as detected or identified. The relationship has an upper limit of ~100 ms for the stimulus duration.

$$L.t = Const.$$

Equation 3: Bloch's law

For stimuli of longer duration and larger extent, the relationship between stimulus threshold and luminance is best described by Weber's law (Barlow 1958). Similar temporal relationships link visual acuity and stimulus duration (Baron and Westheimer 1973) resulting in visual acuity increasing with exposure durations above the upper bound of Bloch's law.

In a similar manner to spatial contrast sensitivity, the VS has a temporal contrast sensitivity, with the relative amplitude, or modulation ratio (MR), being analogous to the modulation contrast represented in the spatial CSF (Kelly 1961). This is illustrated in Figure 1-15 where the spatial and temporal CSFs are presented together. The form of the temporal CSF is like that of the spatial CSF with a band pass behaviour

for high illuminance values. At the lowest illuminance values, the temporal CSF behaves like a low pass filter.

What is noticeable is the asymptotic behaviour for all but the 0.06 Td function. The relative amplitude sensitivity has a value of 15 – 17 for an adaptation level of 0.65 – 850Td. At 9,300Td, this value drops to ~13. The 9,300Td peak of the temporal CSF is also lower than the results for 850 Td. This reduction in sensitivity to the 9,300 Td stimulus may be linked to the degradation in spatial CSF at high luminance values (Wuerger *et al* 2020). The luminance of the two stimuli are similar: ~4930cd.m^{-2} for Kelly (1961) compared to 2,000 and 7,000cd.m^{-2} for Wuerger *et al* (2020). This inference is supported by Kelly's comments that he "noticed some discomfort at this level" and this test point was excluded in his later study (Kelly 1962). The peak sensitivity is between 10 – 20Hz, whilst for the 0.06Td case it lies at ~5Hz. These differences are indicative of the response of the two photoreceptor types: rods being slower compared to the response of cone mediated vision. For the 0.06Td stimulus the sensitivity is minimal for a 15Hz modulation frequency, providing an insight into how a stimulus to measure flicker modulation thresholds can be designed to promote a rod or cone mediated response by controlling the frequency of modulation in combination with the background luminance to which the participant is adapted.

Kelly (1961) used an edgeless 68° field resulting in a response that is driven by the temporal properties of the stimulus without any confounding spatial cues, or spatial transients, resulting from seeing the edge of a smaller stimulus presented against a larger, adapting background field. By using an artificial pupil, it was possible to control the retinal illumination whilst minimising the influence of the Stiles Crawford effect, i.e. the dependency of cones to the incidence angle of the illumination source (Stiles and Crawford 1933).

1.3 Pupil Light Reflex (PLR) Response

1.3.1 Overview

The PLR has been a topic of study due to its role in controlling the illumination level at the retina, but also the insight it can give on neurological conditions. This review is a short summary of the PLR and its role in visual function. More extensive reviews have been undertaken (McDougal and Gamlin 2015, Douglas 2018) and books have been written on the topic (Loewenfeld 1999).

1.3.2 Function

The PLR is an autonomic response to changes in ambient illumination (Gamlin *et al* 2007). An increase in light intensity results in constriction (miosis) of the pupil. A reduction in retinal illumination results in the dilation (mydriasis) of the pupil. The latency of constriction ranges from 500ms to 180ms as illumination increases (Douglas 2018). The diameter of the pupil is reduced by constriction of the circular sphincter pupillae, that runs around the pupil's circumference. The pupil increases in size by the constriction of the radial dilator muscle, which runs from the iris root radially to the periphery of the pupil.

The diameter of the pupil, and thus area, has been shown to be dependent upon luminance, size of the adapting field, age of subject and whether one or both eyes are adapted (Watson and Yellott 2012). Other factors that can influence pupil size are; the accommodation state of the eye (Spector 1990); use of stimulants/depressants (Hou *et al* 2006, Wilhelm *et al* 2014); emotional state (Partala and Surakka 2003,

Bradley *et al* 2008, Oliva and Anikin 2018); tiredness (Lowenstein *et al* 1963); and cognitive load (Hess and Polt 1964, Piquado *et al* 2010, Daniels *et al* 2012, Kang *et al* 2014).

1.3.3 Experimental studies

As highlighted by Douglas (2018), experimental studies characterising the PLR generally use brief flashes of light less than a second in duration, often of high intensity, to trigger a constriction of the pupil. The resulting PLR, whilst experimentally interesting, does not necessarily replicate the rate and magnitude of changes of illumination that naturally occur. Whilst short flashes are partially representative of the case of aircrew emerging into bright sun-illuminated sky or cloud, however, changes in illumination at dawn/dusk are more gradual. As a result, there is an argument for the use of smaller increments in stimulus luminance when characterising the dynamics of the pupil as a function of retinal illumination levels that more closely relate to the operating conditions of aircrew, especially those associated with mesopic visual function.

Additionally, it is often hard to compare different studies due to the way that results are presented. Pupil size can be reported either in terms pupil area or diameter as an absolute or relative value. There are also slight variations in how constriction latency is defined with the point of peak acceleration (Bergamin and Kardon 2003, Ellis 1981) or the onset of pupil constriction in terms of pupil diameter (Yu *et al* 2007) being used. The latter method is dependent on defining the variation in pupil diameter resulting from experimental measurement errors and what correlates to the actual onset of the constriction. The former method aligns better with the physical properties of a dynamic system. To address the variations in techniques and definition of metrics, there has been a movement to standardise practices and define best practice (Kelbsch *et al* 2019).

1.3.4 Consensual pupil response

In humans, the effect of an increment in retinal illuminance in one eye will result in a consensual response in the un-stimulated eye, in addition to the direct response in the stimulated eye. The magnitude of the constriction when one eye is stimulated is less than when both eyes are simultaneously stimulated. From this it might be suggested that the summation of signals from both eyes may influence the magnitude of the overall response. Visual thresholds are lower, i.e. there is a greater sensitivity, when a stimulus is viewed binocularly than when viewed monocularly and similarly the magnitude of the constriction is larger when viewed binocularly. This provides an indication of the pathways and processing centres by which the response is mediated.

1.3.5 Neural pathways of the Pupil Light Reflex (PLR)

As illustrated in Figure 1-16, the signals from the retina that mediate the PLR follow a similar path to those from the RGCs bound ultimately for the visual cortex. The signals flow along the optic nerve and decussate within the optic chiasm and onto the OPN. Each OPN receives inputs from the temporal retina of the ipsilateral eye and the nasal retina of the contralateral eye. The output from each OPN goes to both EW nuclei. The interconnections between the OPN and the EW nuclei provides the basis of the consensual PLR as an increment in retinal illumination detected by one retina is transformed into stimulation of both EW nuclei. The signal from each EW nucleus is transmitted along the oculomotor nerve to the ciliary

ganglion. From here it innervates the sphincter pupillae via short ciliary nerves resulting in constriction of the pupil as part of the Parasympathetic Nervous System (PNS). This control mechanism also links to the constriction of the pupil when focussing on a near object, i.e. the accommodative response. Barbur (1995) argues that there are supranuclear inhibitory inputs to the EW nuclei, enhancing signals to the constrictor muscles, that arise from transient disturbances in the cortical inhibitory pathway. The transient reduction in the inhibitory input results in increased parasympathetic innervation observed as a constriction of the pupil.

The dilation of the pupil is linked to the Sympathetic Nervous System (SNS), hence the pupil's dilation in response to stimuli that instigate an emotional response. The SNS nerve impulse is derived from the Cilospinal centre and the superior cervical ganglion with long ciliary nerves innervating the pupil dilator.

The constriction of the pupil is thus driven directly by the PNS, whereas dilation is a combination of the reduction of the PNS input to the sphincter and activation by the SNS of the dilator muscle. It is this balance between the PNS and SNS signals to the two muscles that controls the size of the pupil that explains the effect of age on pupil diameter. As age increases, there is a reduction in pupil size, (senile miosis) along with reductions in the amplitude and velocity of the darkness reflex, which have been attributed to a loss of sympathetic tone (Bitsios *et al* 1996, Korczyn *et al* 1976). This results in there being an imbalance in the constrictor and dilator muscles in the favour of the constrictor resulting in the smaller pupil size.

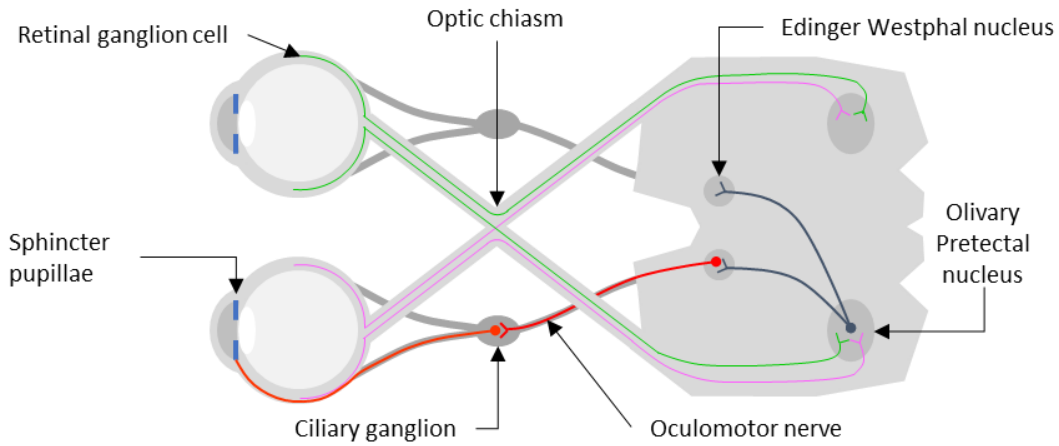

Figure 1-16: Schematic representation of the parasympathetic innervation of the sphincter pupillae.

The starting point for the PLR is within the retina, where rods, cones and a third photosensitive cell type, the ipRGC, have all been shown to contribute (McDougal and Gamlin 2010, Gamlin *et al* 2007, Barrionuevo *et al* 2014). Whilst rods and cones are in the outer retina, melanopsin containing ipRGCs (Lucas *et al* 2003, Dacey *et al* 2005) located within the inner retina have been shown to provide an input to the PLR. In addition, ipRGCs have been linked to regulation of endogenous circadian clocks as a result of photoentrainment and connections to the SCN, the brain's circadian pacemaker (Chen *et al* 2011, Drouyer *et al* 2007, Hattar *et al* 2002, 2003, Ecker *et al* 2010).

As well as being found in human retinas, ipRGCs are also present in other mammals enabling their properties and functions to be studied in more detail. Studies of the effect of blocking signals from either

ipRGCs, rods or cone photoreceptors through breeding has enabled the function of ipRGCs to be defined in mice (Lucas *et al* 2001, Kostic *et al* 2016). The results of similar studies, summarised by Gamlin (2007) and presented in Table 1-1, show that the full PLR function is reliant upon the output from melanopsin containing ipRGCs, and rod and cone photoreceptors, but also that fundamentally pupil constriction is controlled by the ipRGCs. The inference is that, in addition to the pathway that visual signals are transmitted, there is a parallel architecture of connections whereby rods and cones connect to ipRGCs. The resulting signals from the ipRGCs are then transmitted to the OPN via the optic chiasm as illustrated in Figure 1-16. Support for this parallel architecture is provided by the larger and more sparsely populated dendritic fields of the ipRGCs compared to those of parasol and midget RGCs (Dacey *et al* 2005). Within the human retina, ipRGCs form ~0.2% of the total RGC population (Dacey *et al* 2005) which aligns with the values quoted by Hatori and Panda (2010) of a population of up to 3,000 ipRGCs compared to the total population of ~1.5 million RGCs.

The correlation between sustained constriction of the pupil at high retinal illumination, representative of photopic light levels, corresponds to the sustained 'on' response from the ipRGCs (Dacey *et al* 2005) that occurs after stimulus offset. This response is triggered by stimuli with a blue component that aligns to the spectral sensitivity of melanopsin (Lucas *et al* 2001). The spectral sensitivity of melanopsin aligns with the spectral composition of daylight and provides a link to the process of photoentrainment.

		Melanopsin	
		Lacking	Present
Rods and cones	Lacking	No PLR	Pupil constriction in response to high retinal illuminance.
	Present	Abnormal PLR. Pupil fails to fully constrict at high retinal illuminance.	Normal PLR

Table 1-1: Summary of pupil light reflex's dependence on melanopsin, rod, and cone function based upon Gamlin et al (2007).

The constriction of the pupil also has an additional benefit from an optical perspective. The pupil's size influences the quality of the image formed on the retina. A small pupil reduces the effects of spherical aberration whilst increasing the depth of field, i.e. the range over which objects in the scene are perceived to be in focus. Spherical aberration arises from light passing through the periphery of a lens being focused closer to the lens than light passing through the centre of the lens. However, a very small aperture can produce significant diffraction effects which also affect spatial resolution.

1.3.6 Additional functions

As a result of the linkages to photoentrainment, a metric for fatigue has been devised by correlating the magnitude of the PIPR with melatonin levels in saliva over the course of a day (Münch *et al* 2012). Using two separate stimuli whose wavelengths are selected to respectively favour melanopsin (~480nm) and act as a control (~635nm), the change in the magnitude of the PIPR as a function of hours awake was

evaluated. The pupil has also been linked to measures of fatigue based upon the small variation in pupil diameter as a function of time (Lowenstein *et al* 1963, Różanowski *et al* 2015).

Additionally, studies of the pupil and its function have highlighted that the constriction and re-dilation of the pupil is affected not only by the retinal illuminance[4] and the angular subtense of the target stimulus but also its spatial structure, colour and motion (Barbur *et al* 1992, 1998a, 1998b). This introduces a cortical component into the PLR when using complex stimuli suggesting the involvement of central visual pathways in regulating the activity of cells in the EW nucleus, in addition to the pathway illustrated in Figure 1-16.

1.3.7 Research question

A question that arises from this area of vision research is whether it is possible to demonstrate how the signals from human rod and cone photoreceptors contribute to the afferent output of the ipRGC, and subsequently their effect on the efferent signal that drives the PLR at mesopic light levels? This is of interest for the insight it might provide into the mediation of image formation at these light levels, given the cortical component to the PLR as indicated by Barbur *et al* (1992, 1995, 1998a, 1998b).

1.4 Vision tests

1.4.1 Photometry and colorimetry

Vision tests rely on being able to stimulate a specific response based upon defined achromatic or chromatic properties of a stimulus in terms of luminance and co-ordinates in colour-space respectively. This section provides an overview of the definition of luminance and colour and how these quantities can be calculated from the spectro-radiometric properties of an object. The examples below consider the emission spectrum (E_λ), in radiometric units, from a display used to undertake psychophysical vision tests.

In 1931 the Commission Internationale de l'Eclairage (CIE) defined a standard (CIE 2004) for specifying colour based upon work by Maxwell, Abney and Guild as reviewed by Wright (1996). The standard also formalised the method for calculating luminance based upon the photopic luminosity function for a standard observer, which describes the summed response of L and M cones. There are two variants of the luminosity function defined for a 2° and 10° angular subtense, with the former commonly used as it corresponds to the fovea. Since the initial definition of the photopic luminosity function, $V(\lambda)$, there have been a series of updates to better define the function (Judd 1951, Vos 1978, Sharpe *et al* 2005), but these are yet to become fully adopted across industry.

The scotopic luminosity function, $V'(\lambda)$, defines the spectral response of rod mediated vision. The Scotopic/Photopic ratio (S/P) is the ratio of the scotopic and photopic luminance, as defined in Equation 4.

[4] Retinal illuminance is the product of luminance and pupil area of the pupil. Units of retinal illuminance are Trolands (Td).

$$S/P = 1700 \int V'(\lambda)E_\lambda d\lambda \Big/ 683 \int V(\lambda)E_\lambda d\lambda$$

Equation 4

To define the colour of a test patch in CIE 1931 colour-space, its radiance is transformed to a two-dimensional co-ordinate (x, y) in CIE 1931 colour-space. The colour matching functions ($\bar{x}$, $\bar{y}$, $\bar{z}$) are a set of non-negative weighting factors that provide a mathematical simplification of the spectral responses of the L, M and S cones. The $\bar{y}$ matching function is V(λ) scaled between 0 and 1 and as a result Y is equivalent to the luminance of the test patch. The full description of the colour matching functions, and their derivation, is defined by the CIE (CIE 2004). What is presented below is a shortened version of the calculations defined in the standard.

The three tristimulus values (X, Y, Z) are calculated by integrating the product of the colour matching functions with the radiance (E_λ) of the test patch across the visible spectrum, see Equation 5. The constant K_m transforms the units of radiance into the units of luminance and has a value of 683 lm/W. The corresponding scotopic value is 1700 lm/W.

$$X = K_m \int E_\lambda \bar{x} d\lambda \qquad Y = K_m \int E_\lambda \bar{y} d\lambda \qquad Z = K_m \int E_\lambda \bar{z} d\lambda$$

Equation 5

The CIE 1931 colour-space co-ordinates (x, y) are calculated using the relationships described in Equation 6. The resulting values when summed equal 1. Additionally, a constant energy white point is defined when x = y = z = $^1/_3$.

$$x = X/(X+Y+Z) \qquad y = Y/(X+Y+Z) \qquad z = Z/(X+Y+Z)$$

Equation 6

The CIE 1931 colour-space is not a uniform colour-space but does allow the visualisation of our ability to perceive a wide range of shades of green. The non-uniformity of the CIE 1931 colour-space was demonstrated by MacAdam (1942) and as a result the CIE 1976 colour-space (CIE 2015) was defined to try to achieve a more uniform mapping of colour differences. This revised colour space is utilised in the definition of symbology, display system colour gamuts and display design (Vassie 1998, Vassie and Christopher 2000, Laycock 1986). The CIE 1976 colour-space co-ordinates are calculated by applying a transformation, defined in Equation 7, to the CIE 1931 co-ordinates.

$$u' = 4x/(-2x+12y+3) \qquad v' = 9x/(-2x+12y+3)$$

Equation 7

Calibration of a display requires the measurement of both the emission spectra of the display's primaries and the variation of luminance as a function of drive voltage or signal. The latter is known as the display's gamma function. From this information, it is possible to define the required drive signals, in terms of red, green, and blue pixel levels, to generate a specific point within the display's colour gamut by applying reverse transforms between the CIE co-ordinates and the tristimulus values. The result is a look-up table

that characterises the display. It is this that is calculated by the LumCal function developed for use in the Advanced Vision and Optometric Tests (AVOT) software.

1.4.2 Application of vision tests

The US Navy and Air Force undertakes a series of tests to assess the health of a subject's eyes as well as visual function. These largely replicate those performed as part of a clinical examination (US Navy 2017). The nature of these tests has remained unchanged since the second World War, despite continued advancements in aircraft and the cockpit environment. Refractive properties and oculomotor balance can be measured using objective methods. Traditionally the assessment of visual acuity has been undertaken using standardised test charts formed of arrays of letters of reducing size. The letters used have a defined format using the Snellen or Sloan notation. Depending upon whether the sequences of letters are randomised between tests, utilising multiple test cards/slides, it is possible for the aircrew to learn the sequence and manipulate the test (Wright *et al* 2016).

The clinical assessment of visual acuity and colour discrimination have largely remained unchanged until recently. Although the logarithm of Minimum Angle of Resolution (log MAR) chart forms the basis for assessing visual acuity, technological developments have seen the paper-based charts being replaced by computer generated versions presented via a desktop monitor. To obtain the necessary viewing distance, mirrors are used whilst minimising the space required to undertake the test. The ability to randomly select the letters that make up each chart has the advantage of making it impossible to learn the ordering of the letters that make up each line of the chart. This ensures that the test is a true assessment of visual acuity. Despite the technology being available, the test is often restricted to high levels of contrast, i.e. black letters presented on a white background. Such tests do not give an indication of the sensitivity of rod and cone photoreceptors, instead they favour assessing the subject's spatial acuity within the discrete steps of the respective chart.

Within the scientific literature, a series of test methods have been used to better understand photoreceptor function and interconnections within the retina. From the measurement of dark adaptation thresholds through the use of a flash which saturates the photoreceptor(s) (Hecht *et al* 1935, 1937) to the mean modulated and luminance pedestal-based stimuli adopted by Anderson and Vingrys (2000b, 2001). For a pure test of photoreceptor temporal sensitivity function, a test stimulus with luminance varying temporally by an equal amount above and below the background luminance results in thresholds that are more representative of the function of the photoreceptor under evaluation than tests using a luminance pedestal. Anderson and Vingrys (2001) concluded that stimuli using luminance pedestals are subject to interactions between the target and its surround. Depending on the background luminance level used, this can lead to rod-cone interactions and localised dark adaptation.

Several tests exist for the characterisation of colour vision and subsequent detection and classification of colour vision deficiency. Some tests take the diagnosis one step further by determining the severity of the deficiency. The underlying premise of the tests is to present a set of stimuli that will isolate responses in one or more cone types enabling determination of whether the subject is lacking a cone type or has a mutated form of the respective photopigment.

There are several tests of colour vision that are in common use, however there are issues with the results that some of the tests generate. Probably the most well-known colour discrimination test is the Ishihara set of plates. These consist of a series of pseudo-isochromatic plates which present a pattern of coloured dots within which there is a number or a line. By manipulating the chromaticity of the dots making up each test plate, whilst maintaining a constant luminance, a set of plates have been designed that align to a confusion line for a certain dichromat. Although the Ishihara test is primarily defined to characterise red-green colour vision, the technique could be applied to yellow-blue colour vision. The normal observer will see the number or pattern due to the chromatic contrast. To the dichromat, who is the target of the test, the pattern appears to have the same chromaticity as the background. The full set of plates includes a set of plates where those with a colour vision deficiency will see a different pattern to those with normal colour vision. These are augmented by additional plates designed to characterise the type of colour vision deficiency or act as a control. These plates are now so well known within the United States Air Force (USAF) pilot community, that pilots reportedly learn how to recognise the individual plates and, thus can pass the test despite potentially having a colour vision deficiency. As a result, research has been directed towards the development of a reliable test to replace the Ishihara plates. One example is the Rabin Cone Contrast Test (Rabin *et al* 2011). This test presents a series of letters that have been designed to stimulate a single cone type. The other two cone types are stimulated at subthreshold levels by matching the level of excitation for the letter and background with respect to sensitivity function of the respective cone types. Rod inputs are negated by setting the display luminance within the photopic regime at 21.5cd.m^{-2}. The Rabin test has been criticised as it tends to fail since pre-receptoral filters in the eye, such as the macular pigment, and the presence of non-standard cone pigments generate responses in the remaining cones.

The Farnsworth Munsell hue discrimination test consists of a series of coloured caps of different hue which must be arranged in order by the subject. The number of caps used defines the type of test, e.g. D-15 or D-100 for the 15 and 100 cap tests respectively. This test is based upon the Farnsworth Munsell colour system with the individual caps having the same value and chroma but different hue values. The test is traditionally presented on a black background but conducted in photopic conditions using a controlled illuminant to ensure consistency of the appearance of the caps.

In the UK, the Colour Assessment and Diagnosis (CAD) test has been developed over several years to measure small changes in chromatic sensitivity (Barbur *et al* 1994, Rodriguez-Carmona *et al* 2005) and to relate the participant's sensitivity to colour to a standard normal for their age (Barbur and Rodriguez-Carmona 2015). In this way, age related degradations in colour sensitivity due to normal ageing have been accounted for when determining if a subject has a colour vision deficiency. The CAD test utilises both spatial and temporal luminance contrast noise and utilises 16 colour directions to ensure that the discrimination of the colour target from the background is purely based upon the use of either RG or YB colour signals.

Whereas the Ishihara and similar tests utilise a fixed set of plates which are predefined increments, the CAD test can probe the thresholds of the subject's colour vision. This is achieved using a staircase optimisation process and a 4 Alternative Forced Choice (4AFC) procedure. This test methodology enables

the colour vision thresholds for red-green and yellow-blue opponents to be derived over a series of iterations with confidence whilst limiting the opportunities for false results to be generated. The sensitivity of the test has resulted in its use for assessing changes in visual function with the onset of hypoxia (Connolly *et al* 2008), where other tests have been unable to provide reliable results (Hovis *et al* 2013).

In addition to the CAD test, several AVOT have been developed by City, University London, with the aim of characterising aspects of vision and visual performance. These include:

- Contrast Acuity Assessment Test (CAAT) (Barbur and Chisholm 2001);
- Acuity Plus (Rauscher *et al* 2013);
- Flicker Plus (Bi *et al* 2016);
- Eye Movement And Integrated Latency (EMAIL) (Barbur *et al* 2017, Llapashtica *et al* 2017);
- Rod Cone Sensitivity (RCS) test (Hathibelagal *et al* 2020).

The Flicker Plus test was used by Bi *et al* (2016) to assess the effects of normal ageing by measuring the luminance threshold for a 15Hz flickering target on-axis and at 4° eccentricity in the four quadrants of the display along the $\pm 45^{\circ}$ diagonals. The size of the disc stimulus was 20arcmin and 30arcmin for the foveal and peripheral stimuli, respectively. The difference in size allows for the change in visual acuity with eccentricity. The luminance of the stimulus was sinusoidally modulated about the luminance of the background allowing the measurement of the Flicker Modulation Threshold (FMT). The presentation time was equivalent to five cycles (334ms). Photoreceptors are more sensitive to mean modulated flickering stimulus than to a flickering stimulus presented on top of a luminance pedestal (Anderson and Vingrys 2000b, 2001).

By controlling the chromaticity of the background, the test can preferentially stimulate photoreceptors receptive to medium to long wavelengths, i.e. M and L cones, equivalent to the cone modulate luminance response. Coupling this with the range of luminance values, from 0.6cd.m^{-2} to 60cd.m^{-2}, enabled the flicker thresholds to be determined from high mesopic into photopic vision. The selection of background chromaticity had the benefit of reducing the rod signal and thus avoided the destructive interference observed by Sharpe and Stockman (1999) and others. The results reported in Bi *et al* (2016) are only based upon monocular presentations.

In terms of a vision test, the outcome of the investigation by Bi *et al* (2016) is a test protocol that enables characterisation of photoreceptor sensitivity which can detect changes due to ageing. This therefore provides a starting point for a test to assess both photoreceptor function of aircrew for the purposes of selection but also to study the effects of stressors like hypoxia. The use of a flickering mean modulated luminance stimulus isolates the threshold measurement from variation in the perception of the chromaticity of the stimulus between participants. By assessing photoreceptor function both at the fovea and peripherally, the test provides the basis for assessing the sensitivity of rods or cones if a suitable isolating stimulus is used. The starting point for the isolation of rod and cone signals is provided in the method adopted by Barbur (1982) where the chromaticity of the stimulus was selected to preferentially stimulate either a rod or cone mediated response.

One of the most recent developments is the Eye Movement And Integrated Latency (EMAIL) test (Barbur *et al* 2017). This measures the time required to detect, saccade to and then correctly identify a target presented in the periphery of the subject's field of view. The test can provide a measure of the Integrated Saccade Latency (ISL), the minimum stimulus duration required for the subject to detect the peripheral stimulus, to generate a goal-directed saccade and to process the visual information of interest to correctly identify the target. This is all done in a simple experiment without the use of eye-tracking equipment. A four-alternative forced choice method is used to derive the ISL threshold for the correct identification of the orientation of the Landolt C placed at a defined eccentricity and across a limited range of elevations, nominally ±10°. A central fixation marker is used provide a visual reference for the start of each presentation. The test can also be used with an eye tracker to generate data for fitting the test subject's psychometric function using a series of fixed stimulus durations.

1.5 Effect of hypoxia on visual function

Flying at altitude in an unpressurised aircraft, like a helicopter, can induce hypobaric (low pressure) hypoxia (oxygen deficiency) resulting from breathing air at ambient pressure during ascent. The reduced atmospheric pressure reduces the partial pressure of oxygen (PO_2) in the air which in turn reduces the saturation of haemoglobin with oxygen. This then results in a lower concentration of oxygen in the blood reducing the delivery of oxygen to tissues within the body, including the inner retina, while the reduced PO_2 in the choroid reduces the oxygen flux to the photoreceptors in the outer retina (Barbur and Connolly 2011). The photopic vision of occupants of the cabins and cockpits of commercial fixed wing aircraft are largely unaffected as they are usually maintained at a pressure equivalent to less than ~2,438m independent of flying altitude, but mesopic vision may be compromised (Connolly 2011).

Given the altitudes involved, hypoxia is a particular issue for both military and civilian helicopter pilots operating in mountainous regions. A counter measure to the onset of hypoxia is to breathe supplementary oxygen to overcome the effects of oxygen deficiency. This increases the PO_2 resulting in an increased diffusion gradient across tissue boundaries.

The impact of hypoxia on retinal function is centred on the flow of oxygen from the choroid into the inner segments of the photoreceptors within the inner retina. The blood flow in the choroid is not metabolically regulated (Wangsa-Wirawan and Linsenmeier 2003) and as such is reliant upon the retinal oxygen tension (PO_2) to maintain the diffusion into these cellular structures.

The demand for oxygen in photoreceptor inner segments arises from the presence of mitochondria which are responsible for the generation of ATP from oxidation metabolism. The ATP is required for repolarisation of the membrane potential in the photoreceptor after depolarisation as part of photo-transduction (Wong-Riley 2010). The release of energy occurs through the conversion of ATP to Adenosine Di-Phosphate (ADP). The resulting energy assists in the maintenance of the dark current (Barlow 1957). The results of the tests on the feline retina have shown that photoreceptors require more oxygen in dark adapted conditions, compared to the light adapted conditions, due to the increased metabolic processes (Linsenmeier 1986). This is shown by graphs of oxygen tension against retinal depth with the greatest range in values observed when the retina is dark adapted. Whilst the choroidal circulation system is

providing oxygen to the outer retina, the retinal artery supplies the ganglion cells located in the inner retina.

Associated with hypoxia is the contrasting effect of hyperventilation which enhances visual sensitivity (Wald *et al* 1942) and speeds up dark adaptation even negating the effects of hypoxia at 4572m (15,000ft) (Connolly and Hosking 2006) as arterial carbon dioxide tension falls.

Several studies have considered the effects of hypoxia on vision at a range of simulated altitudes from 2438m (8,000ft) to 3568m (15,000ft) using either: breathing air within the confines of a hypobaric chamber; or using mixtures of oxygen and nitrogen to give the fraction of oxygen that corresponds to the desired altitude (by reproducing a representative PO_2).

Much of the research into the effect of hypoxia on visual function has centred on its effect on chromatic sensitivity with a focus on low light conditions aligned with mesopic and low photopic ranges. This range of lighting conditions align with those experienced by aircrew when flying at dusk/dawn and at night when NVGs are used to aid pilotage. The impact of hypoxia on NVG assisted visual function, simulated in a hypobaric chamber at an altitude of 3810m (12,500ft), is reported by Vecchi *et al* (2014) and is considered in more detail later.

Connolly (2008) has reported on a series of studies which have systematically assessed the impact of hypoxia, when compared to normoxia (normal levels of oxygen at mean sea level), on visual thresholds and chromatic sensitivity, as well as generating data on dark adaptation rates when the subject is hypoxic and with hyperoxia. These studies have also included a consideration of the effects of hyperventilation[5] and resulting hypocapnia[6] on visual function and constructively sought to minimise its effect on the results reported. It is on this basis that Connolly's studies form a reference point against which other results are compared.

Hypoxia at 4572m (15,000ft) was found to delay dark adaptation giving rise to a shallower cone adaptation curve which corresponds to a decrease in sensitivity of the cones (Connolly and Hosking 2006). A similar effect was noted with rod adaptation with participants taking longer to fully adapt. The effects of hypoxia on rod and cone adaptation curves were shown to increase with altitude, i.e. decreasing PO_2. The effect of hyperoxia, achieved by breathing supplementary oxygen (100%) at ground level, was to increase the rate of dark adaptation with both curves for rods and cones being shifted to the left. The effect was more pronounced for rod than cone dark adaptation. In discussing the results of their study, Connolly and Hosking (2006) put forward the hypothesis that rod photoreceptors may be 'functionally hypoxic when

[5] Hyperventilation increases the rate of ventilation and results in a decrease in PCO_2. Visually it has the benefit of decreasing dark adaptation time and lowering thresholds (Connolly and Hosking 2006).

[6] Hypocapnia is defined as the deficiency of carbon dioxide in the arterial blood. The onset of hypocapnia occurs when the partial pressure of carbon dioxide (PCO_2) is less than 35mmHg. Moderate hypocapnia can be induced by voluntary hyperventilation (Connolly and Hosking 2008).

breathing air under normal conditions'. This suggests that breathing elevated concentrations of oxygen may improve their performance without the need to use concentrations of oxygen as high as 100%.

Connolly *et al* (2006) also introduce the concept of fast and slow adapters depending upon an individual's ability to recover from a hypoxic state by breathing supplementary oxygen. The development of a test of rod and cone sensitivity that does not require long adaptation times may be of benefit in determining those with greater visual function when hypoxic and those individuals that have a faster onset/recovery from the condition.

The effect of hypoxia and hyperoxia on chromatic sensitivity in the mesopic range was also investigated using the CAD test (Connolly *et al* 2008, Connolly 2011, Barbur and Connolly 2011). Instead of using a hypobaric chamber, participants breathed gas mixtures to simulate the effects of mild hypobaric hypoxia at 2438m (15.2% oxygen) and 3048m (14.1% oxygen) compared to normoxia (20.95% oxygen) and hyperoxia (100% oxygen). The participant's achromatic spatial contrast sensitivity was also assessed as part of the test. The results of both studies indicate that mesopic vision is affected by the oxygenation state with a reduction in chromatic and temporal contrast sensitivity when hypoxic. Visual function was not affected at photopic luminance values. The inclusion of the lower altitude, 2438m (8,000ft) indicates the impact that hypoxia has on operational performance of aircrew.

The lack of a significant effect on photopic visual function for static or flicker perimetry between normoxia and hypoxia induced by breathing 12% oxygen, balanced with nitrogen, was also noted by Feigl *et al* (2011). Feigl *et al* suggest that the lower metabolic demand under photopic, compared to mesopic or scotopic, conditions influenced the results. Additional tests, using a small (n=3) set of young subjects of mesopic field sensitivities did indicate a significant reduction in visual sensitivity at all eccentricities during hypoxia.

Connolly *et al* (2008) suggest that 'chromatic sensitivity may be more vulnerable to hypoxia with distance from the fovea'. This suggests that hypoxia may affect a pilot's ability to detect coloured cues in peripheral vision when operating in mesopic conditions at altitude. Any resulting increase in reaction time and degradation of contrast sensitivity at mesopic levels will contribute to a degradation in aircrew performance with the potential for loss of situational awareness leading to spatial disorientation.

Connolly also highlights that the effect of hypoxia can vary both on an inter and intra subject basis. This raises the question whether there are some subjects who are more, or less, susceptible to the effects of hypoxia. If this is the case, then is there a subset of aircrew that have a reduced risk of experiencing hypoxia induced spatial disorientation? Could a test, or sequence of tests, identify these individuals?

Other researchers have further considered the impact of hypoxia on chromatic thresholds both for normal as well as those with colour deficiencies. Hovis *et al* (2013) utilised three colour tests: CAD, Cambridge Colour Test, and Cone Specific Contrast Test. Of the three tests, only the CAD test was sensitive to the changes in chromatic thresholds due to onset of hypoxia. The resulting reductions in chromatic sensitivity were described as a rotation of the discrimination ellipse. In addition, the increases in CAD thresholds were positively associated with age although this could be linked to the effects of natural ageing on the

sensitivity of photoreceptors (Jackson *et al* 1999, Owsley 2011). These changes in chromatic thresholds are hypothesised as being similar to a lowering of retinal illuminance.

The theory behind these results, put forward by Feigl *et al* (2011) and Connolly *et al* (2008), is that under mesopic conditions, the greater metabolic demand of rods for oxygen compromises the oxygenation state of cones and as a result cone function. This results in a degradation in the chromatic sensitivity and luminance contrast sensitivity from cone photoreceptors because of the inhibitory effect of the oxygen starved rods.

Fiegl *et al* (2011) suggest that a perimetric test, undertaken under mesopic light conditions may have increased sensitivity to hypoxic retinal disorders. The Rod Cone Sensitivity test, if it is proved to isolate rod and cone sensitivities at mesopic and photopic light conditions respectively, should provide a suitable starting point for such an assessment of retinal function.

In contrast to the above studies, Tinjust *et al* (2002) report that it is the inner retina which is more affected by hypoxia. Their experiment was undertaken using photopic test conditions where cones mediate vision. Their results can be explained by the lower susceptibility of cones to a reduction in PO_2 at photopic luminance, when rods are saturated (rod oxygen consumption is minimised), which would change the bias so that any changes in the performance of RGCs become more apparent. Janáky *et al* (2007) also conclude that the inner retina is more affected by acute hypoxia characterised by a 15min exposure at 5486m (18,000ft). This altitude is higher that the conditions for studies considered previously. It is highly possible that at this higher altitude, the relative oxygen concentration will be significantly reduced in both choroid and retinal arteries leading to both inner and outer retinas being severely depleted of oxygen.

The effect that hypoxia has on the intensified view of the world provided by NVGs has been investigated by Vecchi *et al* (2014). Their experiments were undertaken in a hypobaric chamber replicating conditions at 3810m (12,500ft) with 16 male subjects, aged 41.2±4.7 years. The test comprised an assessment of their visual acuity and contrast sensitivity looking through the NVG at a test chart provided by the Hoffman 20/20 test set, which stimulates the NVG to provide a simulation of light levels equivalent to full moon luminance and starlight in a clear, moonless sky. The luminance of the intensified image provided by the NVG is between 5–8cd.m^{-2}. The test chart comprises two parts. In the centre are nine grating patterns equivalent to Snellen acuities of 20/20 to 20/70. Around this central area in a ring are eight greyscale steps between bright (1) and opaque (8) to determine the dynamic state of the NVG, as shown in Figure 1-17. The experiment consisted of a 60 min exposure to the simulated altitude prior to a descent to ground level. Acuity and contrast sensitivity were measured at 15min intervals with the first measurement, taken before ascent, used as the baseline. A set of control measurements was undertaken at ground level; normoxia condition. The acuity measurements in sequence show the onset of hypoxia during the 60min period with a reduction in visual acuity for both the test set's high light and low light settings. The results for contrast sensitivity did not show any statistically significant reduction in sensitivity with exposure to hypoxia under both lighting conditions. Vecchi *et al* (2014) attribute this to the amplification provided by the NVG's image intensifier tube, which is a plausible conclusion.

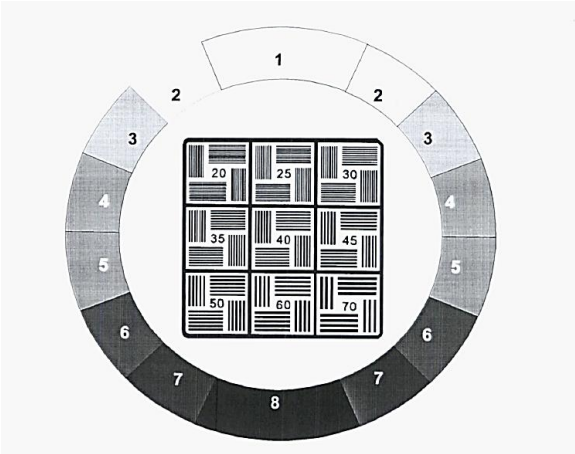

Figure 1-17: Test chart used in the Hoffman ANV-20/20 Test Set.

The set of eight contrast levels displayed in the Hoffman ANV-20/20 test set is not a true measure of contrast sensitivity so has limited utility in quantitatively assessing changes in NVG assisted vision when hypoxic. In normal viewing conditions, the results exceeded the manufacturer's expectation for the NVG/Hoffman 20/20 test set combination reported by Vecchi *et al* (2014). This appears to be more a problem of selecting the correct method of assessing contrast sensitivity using NVGs. On this basis, a different method should be applied to the quantitative assessment of changes in contrast sensitivity due to hypoxia when using NVGs.

Within the literature on the effects of hypoxia on vision, the focus has been on chromatic discrimination and contrast sensitivity as these are the main metrics by which visual function can be related back to flying task performance. If there is a degradation in chromatic and achromatic sensitivity, there is likely to be a reduction in the ability for aircrew to see the features they use to judge velocity and detect hazards, e.g. pylons and wires. With the FAA's Aeronautical Information Manual (FAA 2017), there is a reference to the onset of tunnel vision at altitudes above 4572m (15,000ft) but this has not been highlighted in the literature mainly due to its focus on foveal vision. Apart from a study assessing the effect of reaction times to peripheral stimuli during exercise under hypoxia (Ando *et al* 2010), there does not appear to have been any assessments of how wider visual function and information processing is affected by hypoxia. Ando *et al* (2010) concluded that 'exercise at high altitude may compromise visual perceptual performance'. Within the cockpit environment, aircrew are not necessarily exercising vigorously, however sustained physical interaction with the aircraft is required. If because of hypoxia, reaction times are increased, along with the time taken to perceive an object either within foveal region or peripherally, this could provide an insight into what contributes to a loss of situational awareness and spatial disorientation.

In summary, within the literature for altitudes from 2438 m to 5486 m the effects of hypoxia have been defined as a slowing of dark adaptation as altitude increases. Chromatic discrimination is affected during mesopic vision as rod photoreceptors' demand for oxygen inhibits cone function. In some cases, this has been reported as an anti-clockwise rotation of discrimination ellipses produced by the CAD test. The effect of hypoxia on contrast sensitivity of NVG-assisted vision report by Vecchi *et al* (2014) is thought to be questionable and given the opportunity, it may be of interest to re-evaluate using a different method of assessing contrast sensitivity.

Using a test that can isolate rod and cone sensitivity will provide a different viewpoint on how the function of each photoreceptor type is affected by hypoxia as well as wider confirmation of current understanding. Lastly, utilisation of a test that can quantitatively assess if there is any degradation in the detection and identification of peripheral cues will assist in furthering knowledge into how hypoxia affects wider visual function and the processing of visual information under stressing conditions. It is recommended that the RCS and EMAIL tests be used to assess the effects of hypoxia at 3048 m. Comparisons should be made to test results for normoxia and hyperoxia at 100% oxygen. Subsequent testing should assess the effect of a lower concentration of supplementary oxygen, between 21% and 100%, as a countermeasure to hypoxia at 3048m.

1.6 Aircrew requirements

Controlling a helicopter in a good visual environment requires the control of the aircraft in six degrees of freedom through the combination of sensory cues from a range of sources, as illustrated in Figure 1-18. Whilst vestibular and somatosensory inputs are dependent on the individual, auditory and visual inputs can be affected by external factors and it is the change in visual cues that can have the biggest impact on task completion. From previous work (Sadler *et al* 2016), it is the availability of textural cues and edge based features that form the basis of visual cues utilised by the pilots to maintain fine control of the aircraft when landing or maintaining a stable hover. When these cues are absent, e.g. when flying over a flat sea at night, there is a greater risk of controlled flight into terrain as highlighted in accident reports (Safety Regulation Group Civil Aviation Authority 2007).

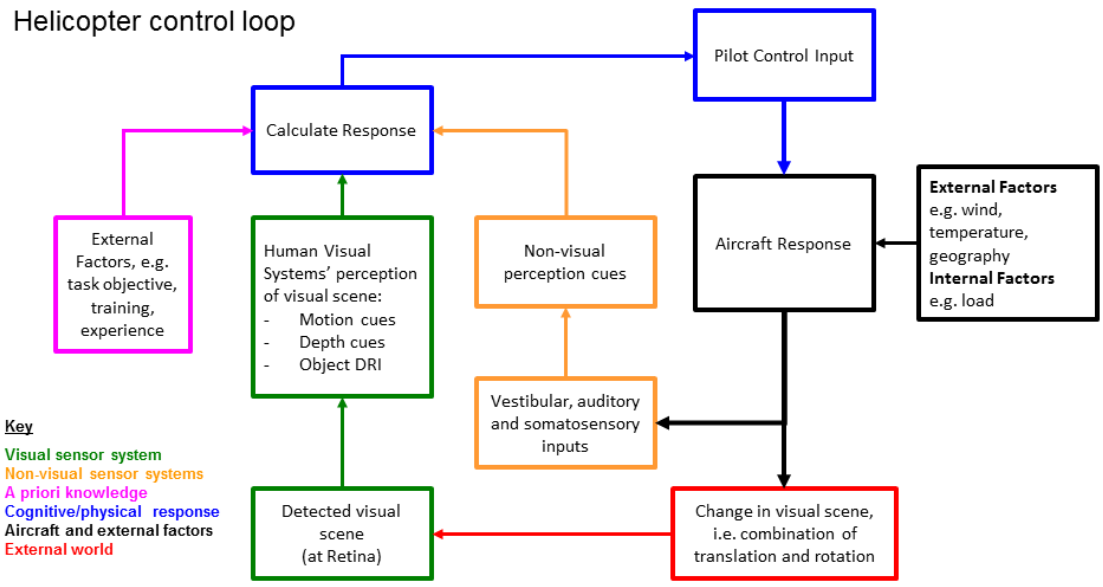

Figure 1-18: Helicopter control loop (Sadler et al 2016)

The onset of hypoxia reduces photoreceptor sensitivity, as identified in section 1.5, whilst fatigue degrades cognitive ability, with both effects likely to be heightened during night-time operations. Changes in environmental conditions, which lead to a degradation in scene contrast and visual cues used to gauge translational and rotation motion, can affect operator effectiveness leading to a loss of situational awareness and increased operator workload.

Being able to quantify the effect of external factors, like hypoxia, on the ability and time required to correctly process and identify peripheral cues assists in the development of training and technological aids. For technological aids, the development is primarily focused on ensuring that the proposed solution does not adversely impact operator performance or restricts the operating envelop for the aircraft. Where there is an impact on operator performance, the focus is to better understand the magnitude of the impact and how it might be mitigated.

1.7 Conclusions

Although the VS is a complex system, its functions can be investigated based upon responses to stimulus luminance, chromaticity, and temporal properties. By controlling these properties, test stimuli can be defined that promote a response from either rod or cone photoreceptors enabling the characterisation of flicker modulation thresholds for each photoreceptor type without the need for a lengthy pre-test adaptation period.

The autonomic nature of the PLR provides a method of assessing contributions from rods and cones across a broad range of light levels without the need to cognitively engage the participant in test outcomes. Assessing the amplitude and latency of the PLR using test stimuli defined to promote a rod or cone mediated response should provide additional insights into mesopic visual function whilst verifying the ability of the stimuli to instigate a rod or cone mediated response. The properties of this non-invasive and involuntary response may also be used to assess the range of light levels normally described as mesopic.

The onset of hypoxia, an effect that is likely to be experienced by rotary wing pilots flying at altitude, affects the rate that aircrew fully dark adapt to the ambient illumination. Additionally, mild hypoxia has been linked to changes in colour perception resulting from cones being deprived of oxygen by rods. Whilst the characterisation of hypoxia has centred on measuring its effects on the central visual field, limited research has been undertaken on effects on peripheral visual function.

As a result, the application of vision tests to characterise rod and cone sensitivity as well as time to process peripheral stimuli would enhance the understanding of mild hypoxia under mesopic illumination conditions.

1.8 Hypotheses to be tested

The main hypotheses considered are listed below for the respective study.

Study 1

a) The RCS test enables the quantitative assessment of the sensitivity of rod and cone-mediated vision.
b) The RCS rod-enriched test condition (RCS-R) produces a rod-mediated response.
c) Increasing the time adapting to the RCS-R test background lowers the measured thresholds (increases sensitivity).

d) Unavoidable changes in the definition of the test protocol did not significantly influence FMT values [7].

e) The RCS FMTs for the four (off-axis) stimuli at 5° eccentricity can be combined into a single metric of parafoveal photoreceptor sensitivity.

f) Monocular RCS FMTs can be used to predict binocular FMTs.

g) Monocular RCS FMTs can be used to predict ocular dominance

Study 2

a) The rod-enriched stimulus from the RCS test (stimulus R[8]) instigates a rod mediated response.

b) For mesopic light levels, rod photoreceptors mediate the steady state pupil diameter.

c) For mesopic light levels, rod photoreceptors mediate the transient response to a positive stimulus of a fixed contrast with respect to the background luminance.

d) If stimulus R and C[9] affect responses primarily mediated by rod and cone photoreceptors respectively, then can the stimuli be used to characterise age dependent changes in the transient pupil response?

Study 3

a) The sensitivity of photoreceptors in the peripheral retina is reduced with oxygen deficiency.

b) The time required to detect, saccade to and correctly identify a target presented in the peripheral visual field will increase as a function of oxygen deficiency within the retina.

c) Peripheral visual function, quantified in terms of photoreceptor sensitivity, computation of saccadic eye movements, and the time to correctly detect and identify a target, can be improved with supplementary oxygen.

[7] A change in the test protocol for both RCS-R and RCS-C test conditions was made due to an undocumented change to the monitor by the manufacturer. See section 3.1.4.

[8] A stimulus condition based upon the RCS rod-enriched (RCS-R) stimulus condition of the RCS test.

[9] A stimulus condition based upon the RCS cone-enriched (RCS-C) stimulus condition of the RCS test.

2 Materials and Methods

This section provides details of the materials and methods that were used in the experiments that are reported in the following chapters. The vision tests employed utilise a similar approach to determining their measure of visual function, the basis of which is reported within this section.

2.1 Vision tests

2.1.1 Alternative Forced Choice (AFC) and adaptive staircases

The technique of measuring the just noticeable difference in defining the thresholds of visual function is a technique which can be traced back to Weber and is still in use today. The Defence Standard 00-970 (MOD 2011) refers to the use of a mathematical method for defining the required luminance and chromatic contrast for a display so that it is visible across the operational envelope of the aircraft. The resulting mathematical method, the Perceived Just Noticeable Difference (PJND) calculation (Vassie 1998, Vassie and Christopher 2000, Laycock 1986), can be linked back to Blackwell and Blackwell's work on contrast thresholds for the Landolt C optotype with a gap width of 4arcmin (Blackwell and Blackwell 1980).

The advanced vision tests used in this research project employ a combination of an Alternative Forced Choice (AFC) methodology coupled to an adaptive staircase to measure a specific aspect of visual function. Increasing the number of alternatives in the AFC methodology reduces the probability of the stimulus being correctly identified by chance whilst reducing the number of trials that need to be completed to obtain a similar result (Vancleef *et al* 2018, Shelton and Scarrow 1984). The number of choices from which the participant can select must be balanced by their ability to distinguish between, and reliably report, the property of the stimulus being altered, e.g. location or orientation. This is a potential issue when using naïve observers who are not experienced with psychophysical testing, as noted by Blackwell (1952). To mitigate this issue, a numeric keypad, Figure 2-1, provided a convenient interface between the participant and the vision test software. The addition of raised elements to the four/five buttons used to record stimulus orientation or location provided a tactile cue to the required response.

The four red buttons on the keypad, corresponding to numbers 1, 3, 7, and 9, have white markers on them that correspond to the orientation of the gap in the Landolt C optotype used for the Eye Movement And Integrated Latency (EMAIL) test. For the Rod Cone Sensitivity (RCS) test, the four red buttons are used in combination with the centre black button, number 5 on the keypad, to record the on-screen location of the test stimulus. Both the RCS and EMAIL tests are described in more detail in section 2.1.4.

The adaptive 2-down, 1-up staircase required the participant to correctly identify the stimulus twice before there was a reduction in the test metric, i.e. stimulus contrast or stimulus duration respectively for the RCS or EMAIL tests. The test metric was increased when the participant incorrectly identified the stimulus. As demonstrated by Rose *et al* (1970), the 2-down, 1-up approach shifts the point of stability[10] on the psychometric function from the 50% point for a simple 1-up, 1-down staircase to 70.7% increasing

[10] The stability point is the point that the probability of a stimulus increase is the same as the probability of a stimulus decrease.

the confidence in the result. The threshold for several stimulus locations can be evaluated by interleaving the staircases for each stimulus, enabling multiple threshold values to be obtain within a single test.

Figure 2-1: An example of the keypad with raised elements on the key buttons the participant used to report stimulus location or orientation.

The magnitude of the change in test metric, between each trial presentation, was reduced as the number of reversals increased according to an exponential function. The exponential reduction in the magnitude of the test metric assists in providing an initial coarse adjustment in the test metric prior to enabling increasing levels of refinement as the number of reversals increases. The number of reversals used to evaluate the final threshold value is a balance between test duration, accuracy of the threshold value, and the attention span of the participant. To reduce the effect of the variation in test value on the test's result, the initial reversal points are not counted towards the final test measurement. The first five reversal are not included for the EMAIL test and the first three reversals of the RCS test are discarded. Both the use of an exponential function to set the increment/decrement in the test metric and discarding initial reversals aligned to coarse adjustments of the test metric address the points raised by Cornsweet (1962) relating to the size and modification of step size during the course of the experiment.

Although there are several methods by which the result or threshold value for the vision test can be calculated (Wetherill *et al* 1966), the method used by the RCS and EMAIL tests calculates the mean of the maxima and minima values of the last *n* reversals, where n is an even number ensuring a balance either side of the (measured) threshold. For the EMAIL test, additional supra-threshold test points are occasionally included, as illustrated in Figure 2-2.

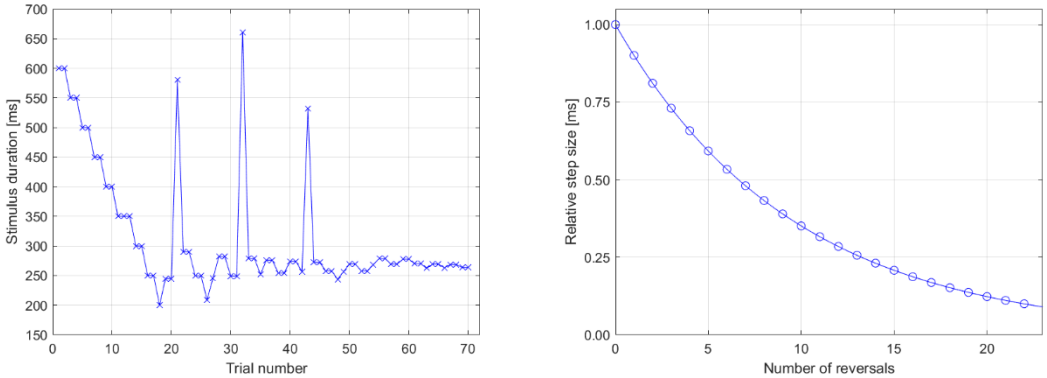

Figure 2-2: An example set of data for the EMAIL test (left) showing three supra-threshold presentations in addition to the main test data. The magnitude of change in stimulus duration with each reversal is plotted (right) showing how the staircase adapts throughout the duration of the vision test.

The starting point for the vision test was defined such that the participant should be easily able to correctly respond to the initial few trials. This builds confidence and assists the naïve participant in completing the test.

Using a 4-AFC methodology has been shown to have benefits with both naïve observers (Jäkel and Wichmann 2006) and for children (Vancleef *et al* 2018), by facilitating attention and vigilance. These points are of direct relevance to the studies undertaken in this research project, especially given the potential for some minor impairment of cognitive function due to the onset of hypoxia.

Whilst other test methodologies, e.g. QUEST, are proposed by other researchers (Watson and Pelli 1983), the combination of a 4-AFC methodology with an adaptive 2-down, 1-up staircase has been proven in other advanced vision tests (Barbur and Chisholm 2001, Barbur *et al* 2006, Bi *et al* 2016).

2.1.2 Equipment

The vision tests were undertaken using a laptop, to run the vision test software, which had been paired with a monitor, used to display the test stimuli to the participant. The laptop, running the 64-bit version of the Windows 7 operating system, connects to the monitor using the DisplayPort interface standard, which is capable of a dynamic range of 10 bits/colour instead of the standard 8 bits/colour commonly used for desktop monitors. This provides the ability to display the small increments in luminance and chromaticity required by the Advanced Vision and Optometric Tests (AVOT) developed at City, University of London. The laptop-monitor pairings used for the studies reported in this thesis are defined in Table 2-1.

Property	System 1	System 2	System 3
Laptop	Hewlett Packard HP ProBook 650 G1	Hewlett Packard HP ProBook 650 G1	Toshiba Part No. PT534E-06301QEN
Monitor	EIZO ColorEdge CS2420	EIZO ColorEdge CS2420	NEC MultiSync PA242W
Sunglasses	S/N C196220	S/N D751767	S/N 91026355
Vision test	RCS	RCS, EMAIL	RCS, EMAIL
Location	City. University of London	City. University of London	MOD Boscombe Down

Table 2-1: Laptop and monitor pairings used for the vision tests undertaken within the research project.

The calibration of the monitor's luminance and chromaticity for each of the primary colours of the visual display was undertaken using a City Occupational software programme, LUMCAL, that generates a look up table that relates the drive signals across the monitor's dynamic range and colour gamut to corresponding luminance and chromaticity values. The resulting look up table is then used by the vision test software to define the drive signals for the monitor to display a stimulus with specific luminance, chromaticity co-ordinates and scotopic/photopic ratio. In addition, the transmission spectra of additional filtering, e.g. neutral density sunglasses, was included in the corrective transformations applied when defining the test condition.

2.1.3 Visual adaptation

The values of the display luminance required for some of the test conditions were below the optimum operating range of the monitor. As a result, it was necessary to use neutral density filters to reduce the luminance at the eye to mesopic light levels. The attenuation of the display luminance was achieved using a pair of Oakley (USA) Holbrook sunglasses fitted with Black Irridium lenses which approximated a neutral density filter of ~10% transmittance. Each set of glasses was supplied calibrated for spectral transmittance and identified within each program. This approach was needed to account for variation in transmittance with wavelength and for differences in spectral transmittance between individual pairs, as illustrated in Figure 2-3. The full spectral transmittance data for each set of sunglasses was used in calculations of photopic and scotopic luminance and chromaticity.

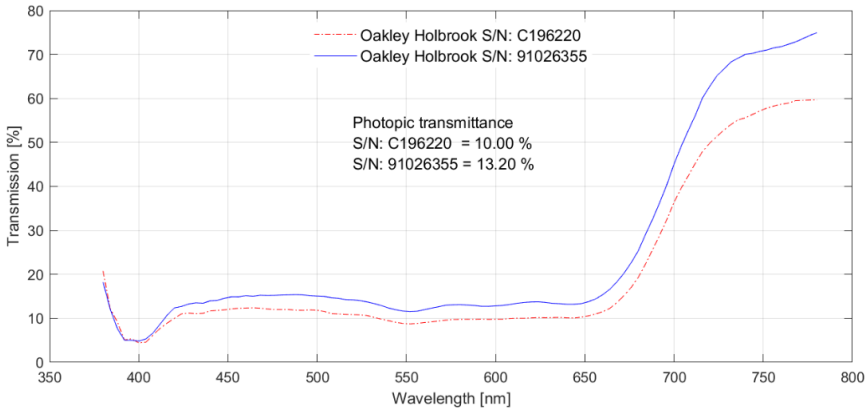

Figure 2-3: Transmission spectra of two pairs of Oakley Holbrook sunglasses fitted with Black Iridium lenses. The Oakley Holbrook sunglasses S/N C196220 were used for testing at City University whilst the sunglasses S/N 91026355 were used for the hypobaric study conducted at MOD Boscombe Down.

Reducing the test stimulus luminance at the eye to the required value for the test is only one part of the process of enabling the measurement of mesopic visual thresholds. The second part was to allow time for the visual system to adapt to the background light level prior to the initiation of the test exposure. A dark adaptation time of 2 minutes was used for all vision tests. This is quite short when compared to the studies by Hecht *et al* (1935), but the steady-state, light adaption levels used in this research project were higher, i.e. high mesopic and low photopic, compared to the fully dark adapted state Hecht *et al* characterised.

Testing at City, University of London was undertaken in the darkened environment of the vision and optics laboratories to maintain full display calibration and to facilitate the process of adaptation.

2.1.4 Psychophysical tests

Three psychophysical vision tests, listed below and introduced in section 1.4.2, have been used in the completion of this research project. These are described in more detail in the following sub-sections.

- Colour Assessment and Diagnosis (CAD) test
- Rod Cone Sensitivity test
    - Rod condition (RCS-R)
    - Cone condition (RCS-C)
- Eye Movement And Integrated Latency (EMAIL) test

2.1.4.1 Colour Assessment and Diagnosis (CAD) test

The CAD test uses a 4-AFC methodology to assess the colour vision of a participant. The participant is presented with a coloured stimulus that moves diagonally across a square foreground centred with respect to a larger uniform background of the same luminance which provided steady-state of light adaptation of the retina. The foreground consisted of a 15 x15 matrix of checks. The luminance of each check varied randomly with equal probability within a range specified as a percentage of background luminance. This produces dynamic luminance contrast noise without changing the mean luminance of the foreground. Both the coloured stimulus and the background are subjected to the same random dynamic luminance contrast noise which masks the detection of any residual luminance contrast signal in the moving-coloured target. This is a result of either of differences in pre-receptoral filters and L/M cone ratios in individual eyes or the presence of variant cone pigments, as expected in subjects with congenital colour deficiency. The use of dynamic luminance contrast noise ensures that it is the chromatic contrast that drives the detection of the stimulus (Barbur *et al* 2002, 2006). The chromaticity of the stimulus is controlled to evaluate chromatic displacement thresholds along a defined set of 16 interleaved directions through the CIE 1931 (x,y) references with respect to the McAdam 'white' background (0.305, 0.323), which is very close in chromaticity to the CIE D65 illuminant. The participant indicates their response using the four red buttons on the keypad, Figure 2-1, to record the direction of the coloured stimulus' movement or simply to guess the direction when unable to see the moving stimulus.

From the resulting threshold values for the 16 interleaved directions, the participant is assessed with respect to the performance of the age adjusted Standard Normal Observer defined with respect to the median of more than 300 young, normal trichromats (Barbur and Rodriguez-Carmona 2015). The output from the test is an assessment of the individual's chromatic sensitivity and allows diagnosis of any colour vision deficiency based upon their red-green and blue-yellow chromatic thresholds.

2.1.4.2 Rod Cone Sensitivity (RCS) test

The RCS test is a development of the Flicker Plus test used by Bi *et al* (2016) to provide a method to isolate and measure the rod and cone mediated Flicker Modulation Thresholds (FMTs) independently using two defined test protocols. This was achieved by defining two background conditions, whose colorimetry and luminance favoured either a rod or cone mediated response. A central, on-axis, stimulus location was surrounded by four, off-axis, possible stimulus locations located diagonally away from central fixation at a fixed eccentricity in each of the four quadrants of the display, as illustrated in Figure 2-4. Prior to a stimulus presentation, a fiducial marker is briefly presented intermittently to direct the participant's attention to the centre of the screen. Diagonal guides are also employed to enhance this effect and provide a guide to the locations of the off-axis stimuli. After a stimulus has been presented, the test software produces an audible beep to trigger the participant to record where they thought the stimulus was presented.

The FMTs for all five stimuli were determined using an interleaved adaptive staircase as part of a 5-AFC procedure using a 2 down, 1 up adaptive staircase. The probability of two sequential correct responses by chance is $^1/_{25}$ for any of the stimulus locations unless the participant always uses one button as their 'don't know' response. To counteract this, participants were briefed to make a best guess of the stimulus'

location. Typically, the test takes between 5 to 10 minutes to complete. More details about the size, eccentricity and luminance of the test stimuli and the background conditions are provided in context of the test procedure in section 3.2.3.

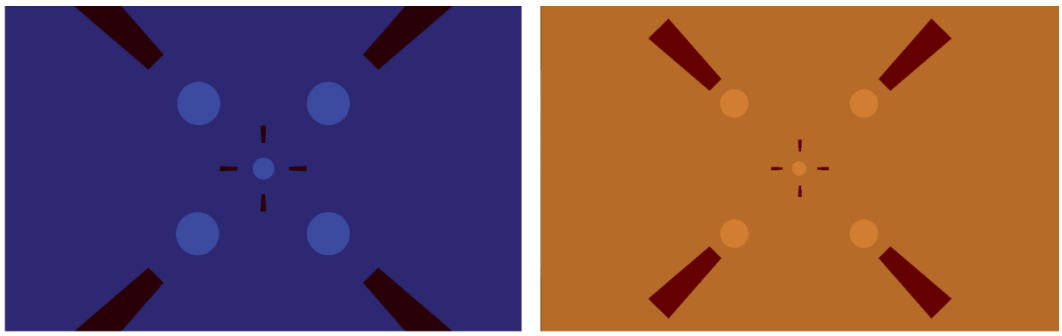

Figure 2-4: The Rod (left) and Cone (right) configuration of the RCS test. The circles in each image show the locations where the 5 stimuli may be presented.

2.1.4.3 Eye Movement And Integrated Latency (EMAIL) test

The origins of the EMAIL test can be traced back to the work of Blackwell (1980) with the use of a Landolt C optotype described in Chisholm and Barbur's work on the CAAT (Barbur and Chisholm 2001) and previous work on saccadic eye movements (Barbur *et al* 1988).

The EMAIL test protocol consists of an initially blank screen with a fixation marker at its centre. The stimulus, a Landolt C, is briefly presented with the gap orientated in the upper left, upper right, lower right or lower left positions. The stimulus itself is surrounded by four, full rings which act as distractors. The latter cause a high degree of visual crowding when presented in visual periphery and this ensures that the subject cannot locate the gap in the Landolt ring and carry out the task in the absence of a saccadic eye-movement. The task for the participant is to detect the location of the stimulus, saccade to it and subsequently identify its orientation, which they record using a numeric keypad, Figure 2-1, by pressing the button corresponding to the orientation of the gap in the C. The duration of the stimulus is varied so as to determine the threshold value for the Integrated Saccade Latency (ISL), i.e. the total time to detect, saccade to and identify the stimulus as set out in Figure 2-6. As outlined in section 2.1.1, the test uses a 4-AFC coupled with an adaptive 2-down, 1-up staircase. In the absence of any signal, the probability of two sequential correct responses occurring by chance is $^{1}/_{16}$. Participants are briefed to make a best guess of the stimulus' orientation.

Although the EMAIL test can be used in conjunction with an eye tracker (Llapashtica 2019), for this research project the test was utilised in a standalone configuration and therefore only the total time for each stimulus presentation was recorded for each trial.

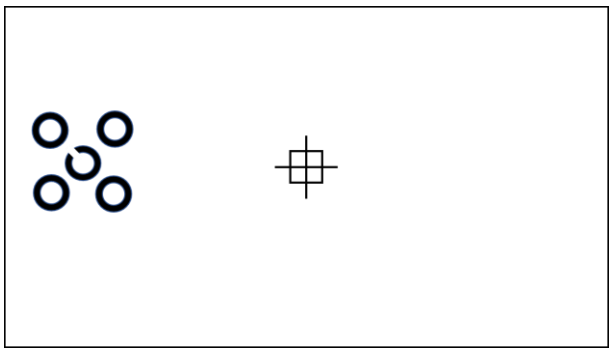

Figure 2-5: Example of the EMAIL test stimulus presented to the participant. (Not to scale.)

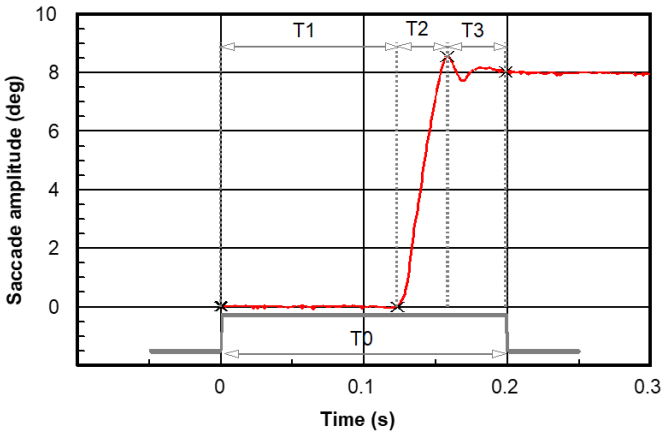

Figure 2-6: Example graph of the displacement of the eye from the centre fixation point as a function of time for a stimulus located at 8 ° eccentricity. T0 is the stimulus presentation time. T1 is the time required to detect the stimulus. T2 is the duration of the saccade to the stimulus. T3 corresponds to the visual processing time.

2.1.5 Training

All participants were familiarised and trained on the vision tests. The training on the RCS vision tests was limited to undertaking the 'learning mode' specific to the test until the participant scored 100%. This was generally achieved within a single run. The training for the EMAIL test consists of a high contrast stimulus being presented for a shortened sequence of presentations. The emphasis of the learning mode is for the participant to achieve reproducible temporal thresholds as well as familiarise themselves with the test protocol.

For the participants of the hypobaric study, investigating the effects of altitude and oxygen concentration on visual function, participants undertook a CAD test in addition to completing the learning modes for the EMAIL and RCS vision tests. It was not a pre-requisite for participants to be experienced altitude participants or experienced with breathing through aircrew masks from pressure demand regulators. All participants received a short familiarisation briefing as required as part of the pre-exposure checks for each test condition.

2.2 Pupillometry

2.2.1 Pupillometer

Although there are commercially available pupillometers and eye tracking systems that are capable of measuring pupil diameter, the nature of the experiments undertaken within the context of this project

required the ability to control the chromatic and spatial properties of the stimulus presented whilst being able to reliably measure pupil diameter.

The P-SCAN pupillometer (Barbur *et al* 1987) is a computer based pupillometry system developed at City University that enables measurements of pupil diameter and eye pointing direction of one or both eyes simultaneously. The system, illustrated in Figure 2-7, provides an overview of the main components and the optical path of the viewer as well as the infra-red (IR) component used to image the participant's pupils. The light field created by the monitor (Sony Triniton Multiscan 500PS, Model No. GDM-500PST), upon which the stimulus is presented, is attenuated by the neutral density filters. These are angled to avoid distracting reflections. Each eye is separately illuminated by IR Light Emitting Diodes (LEDs). The light reflected from the participant's pupil is imaged by the IR sensitive camera which is mounted on a 3-axis translation stage to enable alignment and focusing of the image. The participant's head is maintained in a fixed position using a chin rest and additional head clamps which limit movement of the head in translation and rotation.

The pupil diameter is calculated from the image of the pupil using 64 horizontal line-scans equally spaced vertically across the image. The location of the falling and rising edge of each line scan corresponds to the edge of the pupil. Extraction of these horizontal locations, relative to vertical position of each line scan results in a set of two-dimensional co-ordinates for the circumference of the pupil to which the best circle is fitted and the pupil diameter calculated. This processing is undertaken by the P-SCAN software on the processing computer which synchronises the presentation of the stimulus with the recording of pupil diameter.

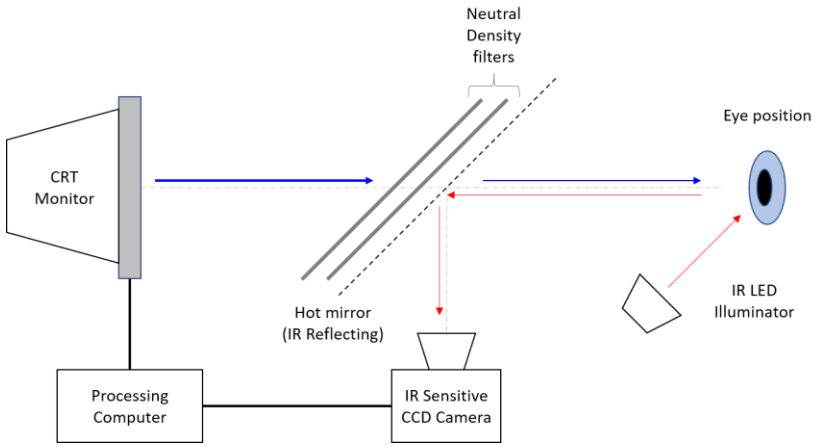

Figure 2-7: Diagram of the P-SCAN system showing the key components and the paths of the optical and infra-red illumination.

The method of processing is resilient to occasions when the pupil drifts to the edges of the camera image as the participant relaxes into the chin rest. Depending upon the severity, this was counteracted by the Principal Investigator adjusting the camera alignment, using the 3-axis translation stage, to bring the pupil back to the centre of the image.

The chromatic properties of the screen were calibrated making it possible to compute the required drive signal to achieve a specific combination of stimulus chromaticity and luminance with the aim of preferentially stimulating a rod or cone mediated response. The transmission characteristics of the neutral

density filters were pre-programmed into the software to ensure that the screen luminance was adjusted to provide the required luminance at the eye. Through adjustment of the spatial extent of the stimulus, it was possible to modulate the corneal flux incident upon the pupil.

2.2.2 Training

The training for the pupillometry was undertaken within the first block of measurements. As a result of the pupil's response to the stimulus onset and offset being involuntary, the training centred on the participant keeping their eyes open during the short measurement period and being ready for the next stimulus presentation.

2.2.3 Metrics

Given the interest in the transient response of the pupil, the metrics used focused on the pupil's response to the onset of the stimulus, as illustrated in Figure 2-8. Whereas previous studies have considered the action spectrum to understand the spectral response, or the magnitude of the stimulus required to instigate a defined pupil constriction amplitude, this study has used a positive stimulus with a fixed value, e.g. 100%, relative to the background luminance condition. Additionally the absolute value of constriction amplitude has been used in this study, however other studies (Fan *et al* 2009) report constriction amplitude relative to the pre-stimulus diameter.

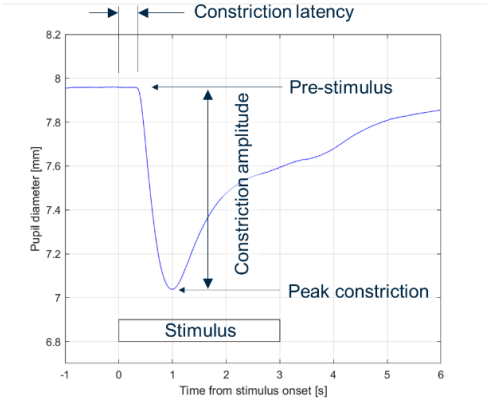

Figure 2-8: Definition of the key metrics used to characterise the transient pupil light response to the onset of the stimulus.

2.3 Simulated altitude exposure

2.3.1 Background

There are several systems that are combined to support undertaking investigations of human performance at altitude. These systems, introduced in the following sub-sections, comprise:

- Hypobaric chamber – provides the ability to simulate the reduction in ambient air pressure with increasing altitude.
- Breathing gas mixtures – enables the evaluation of countermeasures to the reduced ambient partial pressure of oxygen.
- Pressure reducing regulator and pressure demand regulator – these regulate the supply of the breathing gas.

- Aircrew (P/Q) mask – delivery mechanism for the breathing gas.
- Mass spectrometer – technique for breath-by-breath analysis of participant's respired gas composition (oxygenation state).
- Physiological monitoring – provides the ability to ensure that the participant's wellbeing is not being compromised by the experimental exposure.

2.3.2 Hypobaric chamber

Aircrew undertake hypoxia experience training in hypobaric chambers to simulate the effects of hypoxia at altitude. During the training occupants breathe ambient air at the ambient pressure of the chamber. The alveolar gas tensions, produced by the hypobaric exposure, replicate those experienced at the atmospheric pressure corresponding to the altitude.

Alternatively, it is possible to replicate the alveolar gas tension (P_AO_2) in the lungs at altitude by controlling the fractional inspired oxygen concentration (F_IO_2) with a balance of inert gas, i.e. nitrogen (which makes up 78% of atmospheric air). Although this has the benefit of being cheaper than using a hypobaric facility, like the one managed by QinetiQ at MOD Boscombe Down, the effect of a mask leak when simulating an altitude exposure would have a greater effect on the respiratory state of the participant. As a result, the facility was used over the gas mixture approach. There was still a requirement to use gases with different concentrations of oxygen, balanced with nitrogen, but these were used to assess the effect of oxygen concentration as a countermeasure to the onset of hypoxia and explore the degree to which the retina is hypoxic at ground level. The hypobaric facility provided ability to follow these addition lines of enquiry and assess visual function when mildly hypoxic.

The hypobaric chamber facility is split across two levels. The chamber room, on the upper level, is partitioned into the large and small compartment and the capsule. Only the large compartment was used for the trial's activities. On the lower level is the plant room comprising the reservoir and vacuum pumps. The vacuum pumps can evacuate the compartments to an equivalent altitude in excess of 30,480m (100,000ft) at an initial ascent rate of 12,192m.min^{-1} (40,000ft.min^{-1}). In addition to the vacuum pumps for the chamber, oxygen and compressed air supplies, and an uninterruptible power supply are also located in the plant room.

Calibrated pressure transducers in each compartment measure absolute pressure, simulated altitude, and rate of change of altitude. These are augmented by digital displays of absolute pressure, simulated altitude, and analogue gauges of simulated altitude and rate of change of altitude (1,000ft.min^{-1}). The Pressure Chamber Operator (PCO) manually controls the chamber and with experience, a specific altitude or pressure can be held to within 1-2mmHg using a set point indicator.

To support trials activities, the chamber is fitted with a permanent oxygen supply and distribution system and each chamber compartment is fitted with pressure demand regulators. Compressed air, or other mixes of breathing gas, can be supplied to breathing systems inside the chamber from gas cylinders via portals in the side walls of the chamber compartments. The chamber compartments are fitted with safety and emergency alarms which include monitoring of oxygen levels.

Control of the chamber is undertaken in adherence to well established procedures. Checklists are produced and reviewed specifically for each experimental altitude profile. The chamber compartments are fitted with a permanent communications system to enable communication between chamber occupants, investigators who may be inside and/or outside the chamber, and the PCO. Closed circuit television cameras allow remote monitoring of chamber occupants during an exposure with audio and video recordings made for all chamber exposures at altitude.

Illumination inside the chamber compartments is provided by 240V fluorescent strip lights which are controlled externally. The chamber windows were covered with blinds to minimise light ingress and the lights inside the chamber were extinguished during the pre-test adaptation phase prior to and during the vision tests.

2.3.3 Breathing gas mixtures

The process of respiration is driven by the difference in the partial pressures of oxygen and carbon dioxide across the alveolar membrane in the lungs. The F_IO_2 required to produce a partial pressure of oxygen in the alveoli (P_AO_2) is given by the alveolar air equation (Equation 8).

The hypobaric facility at MOD Boscombe Down is located at an elevation of 124m above sea level and a latitude of 51°N (MOD 2019). The barometric pressure at ground level is estimated as 749mmHg based upon the approximation to ground level barometric pressure defined by the International Civil Aviation Authority (ICAO) at 45°N (Harding 2001, ICAO 1993). It is also noted that the barometric pressure will vary due to changes in meteorological conditions on the day.

$$P_AO_2 = P_IO_2 - P_ACO_2 (F_IO_2 + ((1 - F_IO_2) / R))$$

Equation 8: Alveolar air equation

Whilst the inspired gas is dry, there is a need to account for the contribution of water vapour to the overall pressure within the lungs. The dry inspired gas is saturated with water vapour at body temperature by the time it reaches the alveoli. The effect of the water vapour on the inspired partial pressure of oxygen (P_IO_2) is defined by Equation 9.

$$P_IO_2 = F_IO_2 (P_B - P_{H2O})$$

Equation 9: Inspired partial pressure of oxygen as a function of saturated gas

Combining Equation 8 and Equation 9, the amended alveolar gas equation, given by Equation 10, now accounts for the effect of water vapour on the partial pressure of oxygen within the alveoli.

$$P_AO_2 = (F_IO_2 (P_B - P_{H2O})) - P_ACO_2 (F_IO_2 + ((1 - F_IO_2) / R))$$

Equation 10: Alveolar gas equation accounting for the effect of the saturation on the inspired oxygen

Based upon a series of assumptions, listed below, values can be attributed to constants within Equation 10.

- Partial pressure of saturated water vapour (P_{H2O}) at body temperature which can be assumed to be 47mmHg;
- The respiratory exchange ratio, *R*, can be assumed to be 0.845 (Black *et al* 1986);

- Assuming secondary hyperventilation does not occur, it can also be assumed that the partial pressure of carbon dioxide (P_ACO_2) for normocapnia has a value of 40mmHg (Lumb 2017).

After these substitutions, Equation 10 simplifies to Equation 11 below.

$$P_AO_2 = F_IO_2 (P_B – 39.68) – 47.38$$

Equation 11: Simplified expression for alveolar partial pressure of oxygen as a function of inspired oxygen fraction

From the ICAO definition of standard atmosphere, the ambient pressure at 3048m is 523mmHg (ICAO 1993, Harding 2001). Evaluating Equation 11 at ground level and at 3048m for different F_IO_2 values, the effect of hypoxia and hyperoxia on P_AO_2 can be observed, as shown in Table 2-2. Furthermore, by adjusting the F_IO_2 values to account for the reduction in atmospheric pressure due to gain in altitude, similar P_AO_2 values can be achieved for a slightly hyperoxic condition. The required F_IO_2 is balanced by using an inert respiratory gas, i.e. nitrogen, thus the gas mixes identified can be sourced from a commercial supplier in 50L, 200bar cylinders.

Condition		Barometric pressure [mmHg]	F_IO_2 [%]	P_IO_2 [mmHg]	P_AO_2 [mmHg]
Breathing 21% O_2 at ground level	Normobaric normoxia	749	20.95	147	101
Breathing 21% O_2 at 3048 m	Hypobaric hypoxia	523	20.95	100	54
Breathing 100% O_2 at ground level	Normobaric hyperoxia (100% O_2)	749	100.00	702	662
Breathing 29% O_2 at ground level	Normobaric hyperoxia (29% O_2)	749	29.00	204	158
Breathing 43% O_2 at 3048 m	Hypobaric hyperoxia (43% O_2)	523	43.00	205	160

Table 2-2: Alveolar partial pressure of oxygen as a function of altitude and inspired fraction of oxygen.

2.3.4 Regulation of respiratory gases

The flow of gas from the cylinder to the participant is controlled by two regulators in series: the pressure reducing regulator on the cylinder, located externally to the chamber, and the pressure-demand regulator located within the chamber compartment, to which the participant's mask is connected.

All breathing gases used in the trial were delivered using the Honeywell Normalair-Garrett Ltd Mk 7F pressure demand regulator, shown in Figure 2-9. This device is like the pressure demand regulator fitted in fixed wing military aircraft and thus replicates in-service equipment. These devices require a working pressure of 200psig, which is defined by the pressure reducing regulator on the cylinder. There are several key functions of the Mk17F regulator which are of relevance.

Figure 2-9: The Honeywell Normalair-Garrett Mk17F regulator.

Two mixes of the supplied gas are possible:

- Airmix set to 'Normal Oxygen' where the regulator dilutes the supply gas (usually 100% O_2) with air from regulator's ambient environment at a ratio determined by the ambient pressure.
- Airmix set to '100% Oxygen' where the output gas has the same composition as the supply gas and the air inlet shutter is closed.

For the four gas concentrations used in the hypobaric study, each was supplied using a dedicated pressure demand regulator with the airmix selector set to 100% oxygen. In this manner, the specified F_IO_2 was delivered to the participant for the respective trial condition.

The pressure demand regulator, see Figure 2-10, responds when inspiratory demand is placed on the regulator by allowing gas to flow into the breathing hose and onwards to the aircrew mask. By turning the switch at the bottom of the device to 'ON' position, the shut off valve is opened which charges the system and the supply gas flows to a pressure reducer. The gauge on the front of the device provides an indication of the supply pressure. An inspiratory demand reduces the pressure at the output from regulator which results in a deflection of the flexible sensing diaphragm and the demand valve lever allowing gas to enter the sensing chamber. During expiration, the pressure inside the chamber increases as gas flows in until the demand valve closes due to the sensor diaphragm returning to its original position and stopping the flow of gas through the regulator.

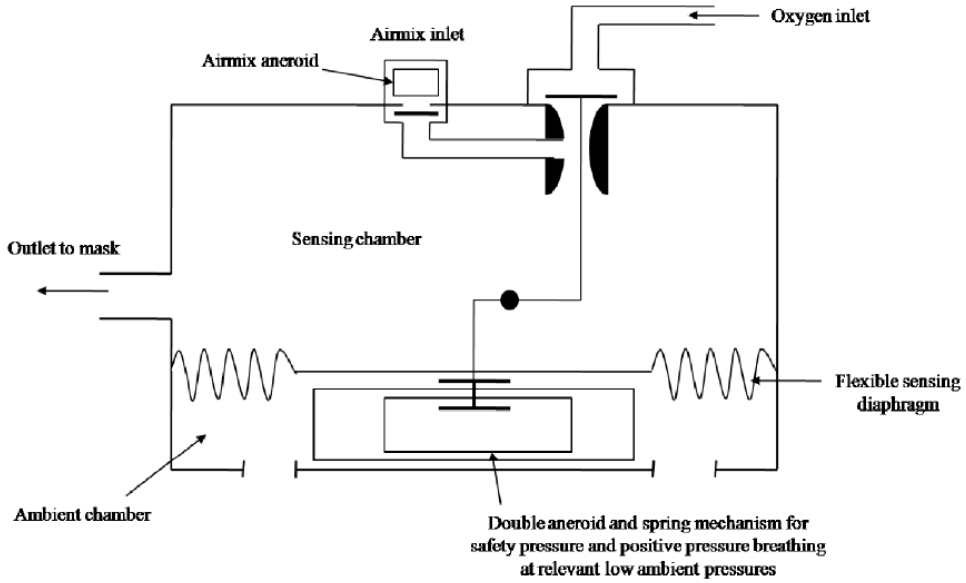

Figure 2-10: Schematic of the Mk17F pressure demand regulator's internal workings.

The pressure demand regulator includes a mechanism, the blinker diaphragm, that detects the flow of gas through the device. The blinker diaphragm is connected to the 'dolls eye' oxygen flow indicator that remains black whilst there is no flow, flipping to a white bar when there is flow.

The device can provide a 'safety pressure', corresponding to ~2-3mmHg, to the breathing diaphragm that in turn opens the demand valve until equilibrium is achieved. In this way, the pressure of gas in the mask, downstream of the regulator, is kept slightly above atmospheric pressure during inspiration. This prevents a reduction in F_IO_2 by ensuring that any face-mask leak is outward from the mask cavity to the external environment.

The pressure demand regulator was used to check that a satisfactory mask seal had been achieved by using the 'Emergency' switch. Having fitted the participant's mask, the regulator's emergency facility was used in conjunction with a breath hold to ensure that there were no leaks. If there was a leak, the dolls eye appeared 'steady white' indicating gas flowing through the system. This method was used to ensure that an adequate mask seal had been achieved prior to the commencement of each test condition.

The pressure demand regulators permanently installed within the hypobaric chamber, used to supply 100% oxygen, were maintained as part of a managed servicing programme whilst the three additional pressure demand regulators, used to supply the breathing gases with 21%, 29% and 43% oxygen, underwent servicing prior to the commencement of the trial. The 21% oxygen gas mix was used to replace breathing air within the chamber so that monitoring the partial pressure of argon could be used to detect a mask leak and the ingress of air from the chamber.

All gases were odourless and tasteless. A colour coded nomenclature was used throughout the trial to refer to the four breathing gases, but no direct reference was made to their composition during the trial, as such the respiratory conditions were masked from the participants.

2.3.5 Breathing gas (oxygen) mask

A Royal Air Force (RAF) Type P/Q Series aircrew oxygen mask was worn by all participants for the study undertaken in the hypobaric chamber. The mask was worn in conjunction with the Type G helmet, as shown in Figure 2-11. The Type P/Q mask is supplied in two sizes: the larger Type P mask and the Type Q mask which provides a better fit for smaller faces. The Type G helmet is available in four sizes. The mask, helmet and RAF coveralls were sized and fitted to the participant prior to their participation in the first phase of the study. (RAF coveralls were used to reduce the risk of oxygen soaking into the participants clothing to minimise the risk of ignition.)

Figure 2-11: The P/Q mask worn in conjunction with the G helmet. Also visible are the Oakley Holbrook glasses used for the rod stimulus condition of the RCS vision test and the blank mass spectrometer probe.

The P/Q mask's moulded soft rubber facepiece, which is supported by a rigid fibreglass exoskeleton, provides a good mask seal. With time, as the rubber facepiece warms, the mask conforms the participant's face. Fit can be further improved by adjustment of a metal strip moulded into the facepiece at the bridge of the nose. The mask is suspended from the G helmet using a chain toggle harness attached to the mask exoskeleton.

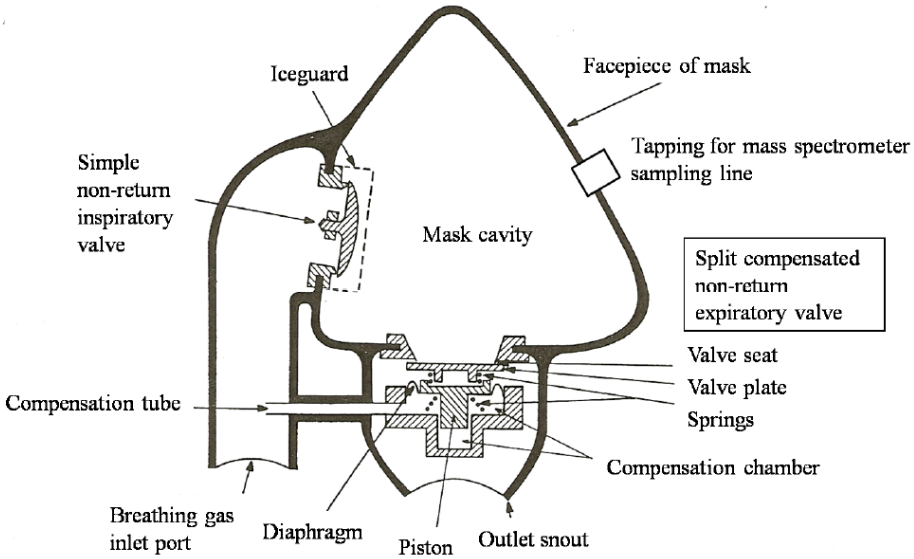

Figure 2-12: Schematic of the P/Q mask showing the inspiratory and expiratory valve assemblies.

The mask contains two valve assemblies: the inspiratory and expiratory valves. The inspiratory valve is a simple non-return valve allowing gas to be drawn into the mask cavity from the mask hose connected to the pressure demand regulator. During expiration, the inspiratory valve closes preventing gas flowing back into the mask hose.

The expiratory valve, located at the base of the mask, is a little more complex. It is a non-return valve formed by a thin metal disc held against the metal valve seat by a light spring which opens with the increase of pressure within the mask cavity during expiration. A compensation tube linking the compensation chamber with the mask hose inlet balances the pressure between the inlet port and the expiratory valve's diaphragm. This prevents the expiratory valve opening in the case of the slight increase in pressure when using safety pressure. A second spring prevents the inadvertent opening of the valve should there be a fall in the inlet port pressure. This arrangement is referred to as a split compensated expiratory valve.

A third valve assembly exists, not shown, which acts as an anti-suffocation valve allowing ambient gas to enter the mask cavity if the mask hose becomes obstructed. This is contingent on sufficient negative pressure being produced in the mask cavity on inspiration.

In addition, as the expired gas is saturated with water vapour, the expiratory valve assembly allows the drainage of moisture from within the mask cavity.

The P/Q masks were modified to provide a portal allowing the mass spectrometer probe to be inserted into the side of the mask opposite the inspiratory valve. When the probe was not connected, a blank probe was inserted to maintain mask cavity integrity, as illustrated in Figure 2-11.

Mounted on the front of the mask is a miniature dynamic microphone and switch assembly which connects to the helmet communications lead (pigtail). This connects via a communications extension lead to the hypobaric chamber's communications system.

2.3.6 Respiratory mass spectrometer

Mass spectrometry enables the identification of a gas from its atomic or molecular mass when ionised whilst the relative abundance of the constituent elements of a mixed gas enables the concentration of each component to be estimated. The underlying technique uses the mass to charge (m/q) ratio of separate ions as the method of identifying the gas species involved.

The gas specimen for analysis is ionised creating positively charged radical ions. These ions are then focused into a beam which is collimated. This is done using a small aperture at the centres of two metal plates that have a potential difference across them. The resulting electric field accelerates the ions between the two plates giving them momentum as they pass through the second aperture.

The mass spectrometer used for this research project utilised a quadrupole to select ions based on their m/q instead of a variable magnetic field used in early systems. The quadrupole consists of four parallel metal rods with direct and alternating current applied to pairs of rods that oppose each other. Ions are selected based upon their interaction with the constant and oscillating electric fields applied to the rods of the quadrupole. This is illustrated in Figure 2-13.

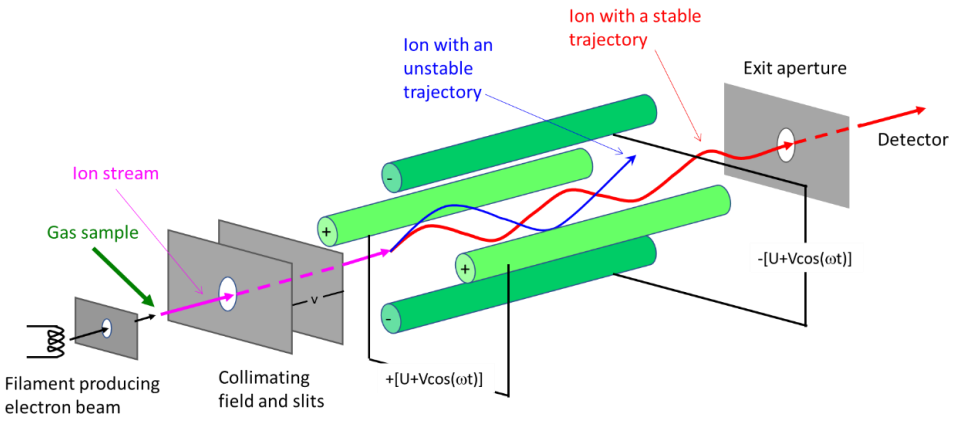

Figure 2-13: Schematic of the mass spectrometer showing the electron beam ionising the gas sample to produce a beam of ions which is collimated. The ions then interact with the oscillating electric fields of the quadrupole enabling the separation of ions with different mass to charge ratio. The resulting beam of ions passes through the exit aperture before being detected.

The process of ionisation is based upon the generation of a positively charged ion of the neutrally charged gas under test by hitting it with a high energy beam of electrons. This process is described by Equation 12. The high energy beam of electrons is produced by thermionic emission, a process where electrons are released from a hot cathode, i.e. a metal filament through which a current is passed. If the gas under test is not ionised, the neutrally charged gas will not interact with the electric and magnetic fields within the mass spectrometer. The vacuum within the ionisation chamber, equivalent to 10^{-6}mmHg, means that the mean free path of the gas molecules is sufficiently long to prevent interactions between molecules. The vacuum is achieved using two vacuum pumps. An initial vacuum is achieved by the low vacuum pump reducing the pressure inside the device to a point where the high vacuum pump can operate efficiently.

$$M + e^- = M^{+\bullet} + 2e^-$$

Equation 12: Process of ionising the molecule M to form a positively charged radical ion that has an unpaired electron, denoted by the •.

The current within the detector, amplified by an electron multiplier, gives rise to a voltage which is digitised within the acquisition hardware and assessed via a computer running data analysis software, PowerLab (ADInstruments, New Zealand).

The mass spectrometer is part of a wider system integrated with the hypobaric chamber, illustrated in Figure 2-14, that includes gases for calibration of the mass spectrometer and data acquisition hardware used in conjunction with data analysis software. A sampling line connects to the inlet to the mass spectrometer's sample reservoir. The sampling line can either be connected to the feed from the calibration gas manifold or to the port in the P/Q mask. Within the mass spectrometer, the sampling pump provides the pressure gradient, approximately 0.5mmHg, required to instigate the flow of gas down the sample line. The sample of gas then enters the ionisation chamber.

Continuous monitoring of inspiratory and expiratory gas composition encompassed those listed below, whilst the other gases in air are present in such small concentrations that they can be ignored for present purposes.

- Diatomic nitrogen (N_2) – 28 atomic mass units (amu)
- Diatomic oxygen (O_2) – 32 amu
- Carbon dioxide (CO_2) – 44 amu
- Argon (Ar) - 40 amu.

The variation in PO_2 and PCO_2 as a function of time corresponds to the inspiratory and expiratory waveforms from which breathing rate can be determined. Further analysis of the waveform enables calculation of the end tidal partial pressures for oxygen and carbon dioxide that reflect alveolar gas composition and the participant's respiratory state.

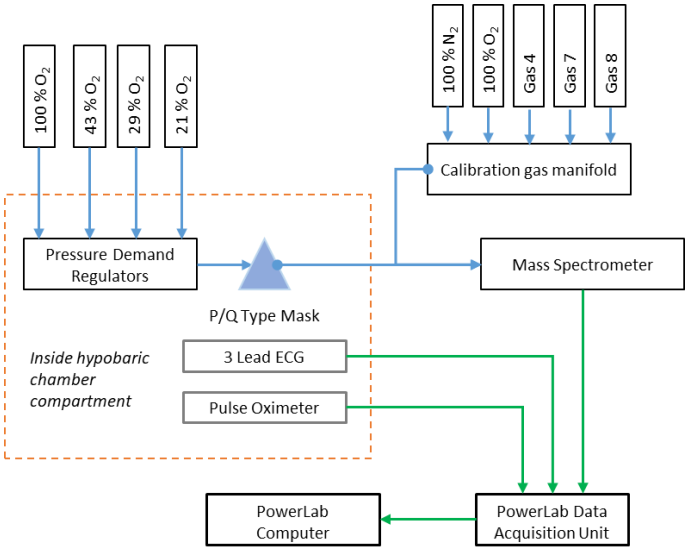

Figure 2-14: Schematic of the system used to monitor and record the physiological condition of the participant. Blue lines show the flow of gas whereas green lines relate to flow of data. Separate pressure demand regulators were used for each breathing gas. Pressure reducing regulators, although not shown, were fitted to each gas cylinder.

To ensure that the mass spectrometer data can be related to the presence of the above gases, data is recorded for a set of reference gases whose composition is defined in Table 2-3. These provide a set of reference points which are used for a two-point calibration of detector voltage as a function of partial pressure for each gas. The calibration, or linearity, checks, were undertaken prior to the commencement of each test condition and at around 25 minutes into each test exposure. The later of these proved more useful when correcting for small variations in atmospheric pressure as all vision tests were completed within 20 minutes of the linearity check. The linearity checks also serve the purpose of reducing the impact of any drift in mass spectrometer sensitivity due to changes in the process of ionising the input gas stream.

Reference Gas	Composition			
	N_2	O_2	CO_2	Ar
Nitrogen	100 %	0 %	0 %	0 %
Oxygen	0 %	100 %	0 %	0 %
4	87 %	65 %	5 %	2 %
7	24 %	60 %	16 %	0 %
8	12 %	80 %	8 %	0 %

Table 2-3: Dry composition of the mass spectrometer calibration gases at ambient temperature and pressure.

Respiratory adaptation

An allowance for respiratory adaptation was built into the experimental protocol for the hypobaric study. This was based around the time to ascend to altitude, i.e. five minutes at 610m.min^{-1}, plus an additional five minutes to adapt to the respiratory conditions. A similar 10 minute adaptation time was utilised with the other test conditions to achieve parity between conditions. This provided enough time to undertake the three vision tests prior to descending from altitude before encroaching on the upper time limit of the altitude exposure of an hour.

Although there is evidence that a longer exposure to altitude will increase the effects of hypoxia (Willmann *et al* 2010), the purpose of the study was to assess the effects on vision during an abrupt exposure reflecting what happens to aircrew. There were other factors, e.g. limiting the effects of fatigue, that also confined the time for respiratory adaptation.

2.3.7 Physiological monitoring

Non-invasive physiological monitoring of the participant's heart rate and arterial oxygen saturation was undertaken for the trial in the hypobaric chamber. These two metrics were monitored throughout by a dedicated observer. Should an issue with the participant's wellbeing be identified, a supervising medical officer was available.

The participant's heart rate was calculated from a three-lead electrocardiogram (ECG) captured using a Charter Kontron Micromon N-xt, (Milton Keynes, UK). The heart rate was produced as an output from the Micromon N-xt device and recorded along with the ECG waveform as separate data inputs to the data acquisition system.

The amount of light absorbed by haemoglobin changes with the degree of oxygen saturation. This can be monitored comparing the absorption of two wavelengths of light, corresponding to red (660 nm) and infra-red (940 nm), through tissue which is perfused with a pulsatile flow of blood (Jubran 2015).

The arterial oxygen saturation was measured using a Kontron Pulse Oximeter 7840 and an ear probe clipped to the participant's left ear. This particular unit has been routinely used for medical monitoring of participants since 2008 for monitoring hypobaric exposures (Connolly 2008). Pressure from the ear cup of the Type G helmet assisted in holding the ear probe in place. Pulse oximeter probes placed on the ear generally have a faster response time to those placed on the finger (Jubran 1999).

The leads for the three-lead ECG and the pulse oximeter probe were passed through an instrumentation port in the side of the large compartment of the hypobaric chamber. These leads were connected to the main electronics unit for each measurement device.

The physiological monitoring data and the output from the mass spectrometer were recorded using PowerLab for subsequent analysis in LabChart (ADInstruments, New Zealand).

2.4 Ethical considerations

2.4.1 Ethical procedures and administration

All studies were conducted in accordance with experimental protocols that were approved in advance by independent local research ethics committees: the School of Health Sciences (SHS) for the trials

undertaken at City, University of London; and the QinetiQ Ethics Committee (QEC) for the trials undertaken in the altitude chamber managed by QinetiQ at MOD Boscombe Down.

All studies adhered to the Declaration of Helsinki. Participants were briefed in detail prior to each individual experiment and provided written informed consent before participating. Participants were free to discontinue an experiment at any time or to withdraw their participation without further explanation.

For the study approved by the QEC, a trials dossier documented all supporting activity for each experiment which included the experimental protocol, Ethics Committee approval, laboratory and experimental risk assessments, participant information sheets, consent forms, medical decision forms, logs of subject exposures and experimental procedures.

2.4.2 Medical supervision

For the study undertaken in the altitude chamber an experienced medical practitioner was available within the laboratory throughout all altitude trials.

2.4.3 Participants

2.4.3.1 Medical screening

Medical screening was only undertaken for the participants of the trial undertaken in the altitude chamber where they were interviewed by independent and experienced aeromedical examiners. The interview was based upon the medical screening questionnaire, Appendix A, and was designed to assess fitness for exposure to pressure change and mild hypoxia. The interview included the topics of being in a confined space and being in the dark, both of which were intrinsic to the trial. The general medical examination included an ear check, i.e. ability for the participant to clear their ears, prior to the hypobaric exposure. Ongoing medical fitness was confirmed before each experiment.

2.4.3.2 Ophthalmic screening

All participants were required to have normal, healthy vision with no history of retinal or systemic disease which could affect retinal function. There were two exceptions to this requirement, where specific attributes of a rod monochromat and a tritanope were utilised to assess specific properties of the rod enhanced stimulus condition.

2.4.3.3 Participant exclusion

Participants for the altitude study were aged between 18 and 40 years. The following exclusion criteria were applied:

- Any conditions that may be aggravated by mild hypoxia;
- Any smoking of cigarettes or a pipe, or the use of e-cigarettes or vaping;
- Any significant cardiovascular or respiratory condition;
- Sickle Cell Disease, however Sickle Cell Trait was not considered a risk for participants of this experimental protocol (Connolly 2014);
- Any regular medication including any eye drops;

- Any significant past or current history of eye disease, eye surgery, eye injury; any significant family history of eye disease; any ocular abnormality; or any obvious visual deficiency including early presbyopia;
- Any fear, phobia or dislike of the dark or confined spaces;
- Any dental procedures performed less than 48 hours prior to altitude exposure;
- Any current neuro-psychiatric disease;
- Any past history of ENT surgery;
- Any use of drugs or medication (prescribed or non-prescribed, with the exception of paracetamol or oral contraceptive pill) in the 24 hours prior to altitude exposure;
- Any exposure to hypobaric or hyperbaric environments in the 24 hours prior to decompression;
- Any intercurrent illness;
- Any other finding or condition considered exclusive by the Supervising Medical Officer.

In addition, female participants for the altitude trial were required to demonstrate a negative urine pregnancy test before each experimental session.

2.4.3.4 Withdrawal criteria

The vision tests and pupillometry undertaken at City, University of London were curtailed if any of the following criteria were met:

- At the participant's request;
- At the request of the Principal Investigator (PI) or any experimenter;
- If the participant demonstrated any signs of distress or impending syncope;
- If the participant of any experimenter expressed any anxiety due to darkness or claustrophobia;
- If the participant complained of or showed signs of discomfort or excessive blinking in the case of the pupillometry study.

The withdrawal criteria for the trial undertaken in the altitude chamber facility, at MOD Boscombe Down which is managed by QinetiQ, are defined in Table 2-4.

Withdrawal criteria	Description
At participant's request	All participants shall be informed that they are free to withdraw from the trial at any time and without giving a reason.
At the request of the PI Senior Medical Officer or other member of the Trial Team	If, at any time, there was any concern that the participant was not entirely well, then the experiment was terminated by the PI. The risk of collapse resulting from hypoxia in this experiment was judged to be negligible. An experiment was curtailed if any of the following criteria were met: • The participant demonstrated any signs of distress or impending syncope. • The participant complained of any new symptoms that developed during the study. • The participant or PI expressed any anxiety due to darkness or claustrophobia. • If the participant, PI or investigators wished to stop the experiment for any reason, which need not be given. • Physiological monitoring showed a SpO2 < 80% or a heart rate rise > 140 bpm.
Failure of any equipment used to monitor withdrawal variables	Any communications failure between chamber occupants and staff outside resulted in immediate cessation of the experiment.

Table 2-4: Withdrawal criteria for the trial undertaken in the altitude chamber.

2.4.3.5 Inconvenience payment

For the vision tests, a single cash inconvenience payment of £10 was made.

For the pupillometry study, a single cash inconvenience payment of £30 was made.

The wearing of G helmets and masks for protracted periods can be uncomfortable and is not part of the participant's normal duties as an employee of QinetiQ. The discomfort was minimised by fitting the mask and G helmet prior to each exposure to ensure both comfort and a good mask seal. A participant inconvenience payment of £35 per day was approved for this trial.

2.4.3.6 Respiratory exposure limits

The duration and severity of the altitude exposure was constrained to a maximum of 1 hour and 3048m (10,000ft) respectively. The time spent at 3048 m was closer to 50 minutes for most participants on the day of the trial. There was a minimum of a week between participants completing the trial's two phases to reduce the confounding effect of the phase 1 on phase 2.

Unlike the previous work undertaken considering visual function at altitude, this study did not set out to instigate hypocapnia or hyperventilation in the participants.

The exposure to oxygen rich breathing gas for brief durations under normobaric or hypobaric conditions, unlike hyperbaric studies, does not induce adverse effects to the respiratory state of the participant.

2.4.3.7 Participant requirements and compliance

For the psychophysical vision tests undertaken at City, University of London, the participants were required to attend either one or two 30 minute sessions in which they would undertake up to 3 vision tests.

The participants for the pupillometry study, were required to have a minimum of 8 hours sleep prior to each test so as to minimise the effect of fatigue on the pupil diameter, e.g. the oscillation in pupil diameter (Lowenstein *et al* 1963, Różanowski *et al* 2015). In addition, the participants were required to abstain from stimulants and depressants, e.g. caffeine and alcohol, in the 8 hour period before testing.

Participants for the altitude study were asked to eat normally and to attend the trial well rested, allowing enough time to be fitted with the appropriate aircrew clothing, consisting of G helmet, mask and coveralls. Given the knowledge that the effect of altitude can be accentuated by alcohol and carbon monoxide from cigarettes will reduce the participant's ability to take on oxygen and thus increase the effects of altitude (McFarland 1971), there was a specific requirement for participants of the altitude study to be non-smokers and to curtail their alcohol intake in the 24 hours prior to participating in the study. Both smoking, more specifically exposure to carbon monoxide, and alcohol have been linked with enhanced effects of hypoxia, i.e. visual and cognitive impairment.

Immediately prior to each session of the altitude trial, participants were requested to complete a lifestyle questionnaire, Appendix B. This enabled assessment of the participant's compliance with the requirements and assist in identification of potential confounding factors.

3 Rod Cone Sensitivity (RCS) test

3.1 Introduction

3.1.1 Purpose

The purpose of this study was to develop and validate a new test protocol for measuring the sensitivity of rod and cone photoreceptors located at the fovea and para-foveal regions of the retina. Unlike other tests of rod photoreceptor sensitivity, the aim was to produce a sensitive test that requires only a short period of dark adaptation. In the future, it is hoped to utilise the test to quantify age related changes in photoreceptor sensitivity.

3.1.2 Background

This work develops from a study by Bi *et al* (2016) into the effects of normal aging on flicker sensitivity, which was undertaken using a monocular stimulus. As the retina ages, the number and distribution of photoreceptors alters (Owsley 2011, Curcio *et al* 1993, Gao and Hollyfield 1992) resulting in the changes in sensitivity observed by Bi *et al* (2016) as age increases beyond 40 to 50 years. Whereas Bi *et al* (2016) used a flicker frequency of 15 Hz, this study has used a lower flicker frequency in order to favour a rod-mediated response to the flickering stimulus in preference to one mediated by cones. This study has also undertaken an assessment of both monocular and binocular Flicker Modulation Thresholds (FMTs).

3.1.2.1 Flicker sensitivity

Characterising an individual's FMT to determine visual function has advantages over spatial contrast sensitivity as it is less affected by scattered light or refractive error. In addition, the attenuation of shorter, blue, wavelengths by the lens as a function of age is a consideration when defining a test for age-related changes in sensitivity and rod photoreceptor function. The sensitivity to contrast is directly related to retinal illuminance, which itself is a function of pupil size. However, whilst a large pupil increases retinal illuminance, the effect of high order aberrations, due mainly to spherical aberrations, also increase rapidly as a function of pupil diameter. Consequently, these have more of an effect under mesopic and scotopic conditions (Barbur and Stockman 2010). The effects of senile miosis will reduce retinal illuminance at these lighting conditions but similarly it reduces the effect of higher order aberrations. Through the adoption of a stimulus that is reliant upon fluctuations in luminance, as opposed to spatial frequency, it should be possible to define a vision test that can characterise changes in photoreceptor sensitivity that is not directly affected by high order aberrations or the reduced ability to resolve higher spatial frequencies under mesopic and scotopic conditions (van Nes and Bouman 1967).

The pathway by which rod signals are transmitted to the retinal ganglion cells influences the way flicker is perceived at mesopic light levels. Under mesopic conditions there is an abrupt transition between the slow, sensitive post-receptoral pathway to a faster, more insensitive path. The phase lags induced between the slower, more sensitive pathway compared to the faster, insensitive pathway give rise to destructive interference for a mesopic stimulus flickering at 15Hz (Sharpe *et al* 1989, Stockman *et al* 1991). To engage the slower, more sensitive rod transmission pathway, Sharpe *et al* found that they needed to limit the luminance of the stimulus to low mesopic values. Although Sharpe *et al* highlight that this

involves cones, it has since been demonstrated that the destructive interference occurs between the two rod pathways (Stockman *et al* 1991). Rod-cone interactions have also been observed for 25Hz flickering stimuli, both in parafoveal and foveal regions of the retina at mesopic background levels (Coletta and Adams 1984).

The 15Hz frequency of flicker modulation used by Bi *et al* (2016) for their investigation into the loss of flicker sensitivity as a function of age corresponds to the peak region reported by Kelly (1961) where maximal visual response was recorded for high photopic levels. As retinal illuminance was reduced, so the peak response shifted to lower frequencies, i.e. at 0.06Td the peak was at 5.1Hz (Kelly 1961). As a result of the temporal sensitivity functions of cones and rods, as reported in this study, two test stimulus conditions were defined that modulate the luminance of the stimulus at 15Hz and 5Hz respectively to promote cone and rod-mediated responses. The resulting RCS test conditions have been defined as RCS-C for the cone-mediating condition, and RCS-R for the rod-mediating condition.

The waveform for the flicker modulation is partially defined by the monitor's refresh rate, which is nominally 60Hz. As illustrated in Figure 3-1, the frame rate of the monitor has an impact on the nature of the temporal modulation of stimulus luminance relative to the background luminance of the screen. Whilst the full waveform of the low frequency sine wave is visible, the higher frequency 15Hz sine waveform is more triangular in nature. Using the interaction between the monitor's refresh rate and the waveform frequency, higher frequency components can be introduced by adopting a square waveform that will preferentially stimulate a cone-mediated response. The eye is however much less sensitive to the 3rd and 5th harmonics of the square wave which may only be detected by cones. Similarly, the 5Hz sine waveform aligns to the low pass frequency response of rods, whilst the 15Hz, square-wave modulation favours cones. These stimulus durations of 333ms and 600ms, respectively for cone and rod stimuli, have also been shown to be sensitive to normal aging (Bi *et al* 2016, Kim and Mayer 1994).

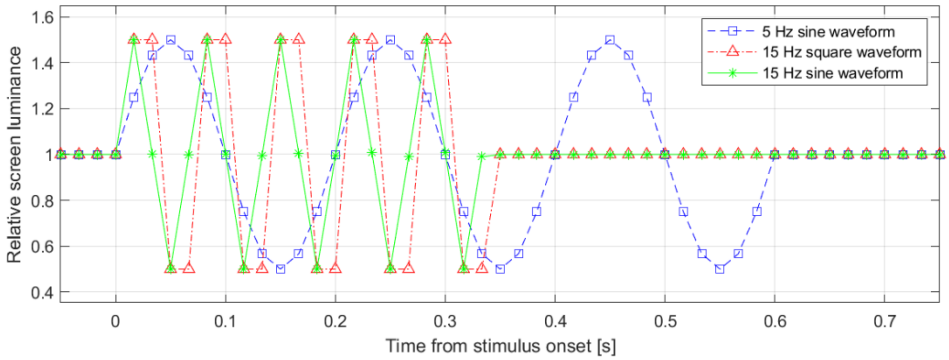

Figure 3-1: The impact of monitor refresh rate on a 50% contrast mean-modulate flickering waveform.

3.1.2.2 Mean modulation versus luminance pedestal

The two methods by which a flickering stimulus can be presented are illustrated in Figure 3-2. Unlike luminance-pedestal thresholds, a mean-modulated flickering stimulus negates any local adaptation that may occur in response to the presentation of the pedestal for the duration of the stimulus (Anderson and Vingrys 2000b). The resulting short-term masking, arising from the pedestal, decays exponentially as

flicker duration is increased. For stimulus durations greater than 500ms, the threshold stabilises but is still elevated, when compared to mean-modulated stimuli, due to the higher time-averaged luminance.

In practice, the luminance pedestal appears as a region of light brighter than its background that reduces the ability to detect the flicker. In contrast, thresholds for mean modulated stimuli remain constant when the stimulus duration is increased (Anderson and Vingrys 2000a). Accordingly mean modulate stimuli have been defined for the new test protocol utilised in this study.

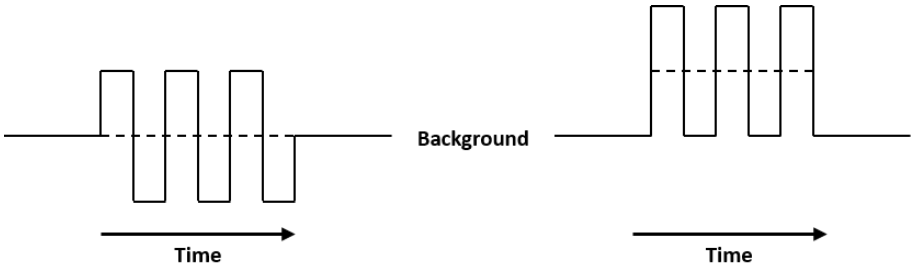

Figure 3-2: Schematic representation of mean-modulated flicker (left) and luminance-pedestal flicker (right). The dashed line equates to the time-averaged luminance experienced by the participant.

3.1.2.3 Spectral properties

Under photopic conditions, the perception of luminance is derived from the additive combination of responses from L and M cones in the ratio of 2L:M (CIE 2004, Carroll *et al* 2002). To maximise its effectiveness, the RCS-C stimulus chromaticity should correspond to a metameric match to the spectral sensitivity of the fovea, where vision is primarily mediated by L and M cones.

The chromaticity of the RCS-R stimulus condition was aligned to the blue end of the visible spectrum, in agreement with the scotopic spectral sensitivity function, to promote a rod- mediated response. With the knowledge of the colour gamut and gamma correction of the display used to present the stimulus, it was possible to generate a stimulus with an increased scotopic content that approximates the narrowband filters used in previous studies to promote rod-mediated responses (Barbur 1982). The was achieved by biasing the contributions of the red, green, and blue components to produce a suitable metameric match with the desired scotopic content. The result is a stimulus, which despite having a low photopic luminance, has a high scotopic luminance and facilitate a rod-mediated response to the fluctuations in the luminance of the circular stimulus. The ratio of the scotopic content to the photopic content is defined as the Scotopic/Photopic ratio (S/P), as described in section 1.4.1. Increasing the scotopic content gives a bluer appearance to the background which aligns to the observations of Adelson (1982).

3.1.2.4 Stimulus luminance

Control of the luminance of the stimulus is also used to preferentially stimulate a rod or cone-mediated response. Historically, rod-mediated responses involved mostly absolute threshold detection measurements in fully dark-adapted eyes. The technique developed for this new protocol utilises a background stimulus condition with a high S/P value in combination with spectrally calibrated neutral density filters, in the form of a pair of Oakley Holbrook sunglasses fitted with Black Iridium lenses. The stimulus conditions selected for this test favour rod-mediated response with only a short adaptation time needed. The test is taken in a darkened room using high mesopic light adaption levels with visual stimuli

that favour the spatial, spectral, and temporal properties of rods. In terms of luminance efficiency, the stimulus employed in the rod test is ~8 times more effective for rods than cones. The stimulus also ensures that only luminance contrast signals are involved, and that the stimulus contrast modulation generated on the retina is independent of any spectrally selective filters that precede photoreceptors in the eye.

Cone-mediated FMT measurements can be adequately characterised at a photopic background luminance of around 24cd.m^{-2} (Kelly 1961, Rovamo *et al* 2000). The spectral properties of the stimulus and the background were also selected to ensure a higher efficiency for cones.

3.1.2.5 Binocular summation and eye dominance

Visual sensitivity, including both contrast and chromatic signal sensitivity, is enhanced (thresholds are lower) when viewing with two eyes rather than one. The integration of the signals from two eyes to achieve this benefit is termed binocular summation. The process of how binocular summation is performed in the brain is still unknown, as noted by Simpson *et al* (2009), and links to other aspects of visual function. For example, motion and depth perception are generally viewed as being dependent upon binocular signals, with two different processing mechanisms being observed experimentally when considering the perception of motion in depth (Harris *et al* 2008).

Within the literature, there are several different metrics that have been applied to model the combination of monocular thresholds to predict binocular thresholds. The following paragraphs discuss some of these metrics and a new metric is introduced.

Previous studies of binocular summation have included assessments of contrast sensitivity and acuity, linking them to the functions of detection and recognition (Home 1978). The aim of Home's tests, undertaken at luminance values from 4.7x10^{-5}cd.m^{-2} to 0.1cd.m^{-2}, was to quantify the sensitivity of the preferred monocular or dominant eye in comparison to the non-dominant eye. His results show that the preferred, dominant eye has a higher sensitivity compared to viewing the stimulus with the non-dominant eye. Home's results for a simple detection task resulted in a ratio of binocular to monocular contrast sensitivity of 1.4 which is equivalent to the value of $\sqrt{2}$ referred to by Legge (1984) and reviews on the subject (Blake and Fox 1973, Blake *et al* 1981). This relationship between binocular thresholds as a function of monocular thresholds, defined in Equation 13, can be explained by in terms of considering the uncorrelated noise between the two eyes. With two observations of the same stimulus, the standard error of the mean observation equates to the standard deviation divided by $\sqrt{2}$. The result of the binocular summation of monocular inputs, it is possible to reduce the effect of the noise on the signal, i.e. increasing the signal to noise ratio, making it possible to detect a smaller signal amplitude resulting in the lower value for the threshold. This relationship links to signal detection theory. Simpson *et al* (2009) describe the noise as either being added centrally after binocular combination, which would result in binocular thresholds being half the monocular value (assuming that left and right monocular thresholds are equal). Alternatively, the noise is added peripherally to each monocular input prior to combination with binocular sensitivity $\sqrt{2}$ times monocular sensitivity. This second model showed better agreement to the results of their investigation. The complication to this simple model are the different sensitivities of the dominant and non-dominant eye quantified by Home (1978).

$$\sqrt{2}T_B = T_M$$

Equation 13: Binocular thresholds (T_B) as a function of monocular thresholds (T_M).

This probabilistic definition of the fusion of two visual information streams (Pirenne 1943, Blake and Fox 1973) has wider applications in the development of biologically inspired methods for combining two or more complementary data sources, e.g. image intensified imagery with long-wave thermal imagery, via the process of image fusion. The resulting fused image facilitates the maintenance of situational awareness at night and in low light conditions as well as providing the ability to see through obscurants, e.g. smoke. One such biologically inspired fusion methodology is that developed by Toet *et al* (1997). In the past there has been interest in image fusion as a method of enhancing aircrew performance.

The combining of information from separate independent monocular responses is picked up by Legge (1984) in his model of quadratic summation which is illustrated in Figure 3-3. In this model, the two monocular contrast sensitivities, C_M and equivalent to $1/T_M$, are summed by quadrature resulting in a binocular contrast sensitivity which is $\sqrt{2}$ greater than the monocular value. This model can also accommodate differences in monocular sensitivities for each eye. This $\sqrt{2}$ model relies on the assumption that monocular inputs are independent samples from the same distribution, however this may not be the case in all participants. Hence whilst some metrics seek to define the summation process, others consider the relative dominance.

Transforming Legge's quadratic summation of contrast sensitivities, Equation 14, into a function based upon the monocular thresholds T_L (left eye) and T_R (right eye), and expressing the result relative to the binocular threshold, leads to the generation of the Quadratic Summation Index (QSI) given in Equation 15. By substituting the relationship in Equation 13 into Equation 15, it can be shown that the theoretical value of the QSI metric equals 1 when both monocular thresholds are equal.

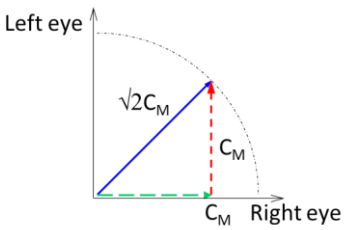

Figure 3-3: Illustration of how the quadratic summation of monocular contrast sensitivity (C_M), where $C_M=1/T_M$, for the left and right eye combine result in a binocular contrast sensitivity equal to $\sqrt{2}C_M$.

$$C_B = \sqrt{C_L^2 + C_R^2}$$

Equation 14: Quadratic summation of contrast sensitivity (Legge 1984). C_L and C_R are the monocular contrast sensitivities of the left and right eyes. C_B is the resulting binocular contrast sensitivity.

$$QSI = T_B \sqrt{T_L^{-2} + T_R^{-2}}$$

Equation 15: Quadratic Summation Index (QSI)

The Binocular Summation Index (BSI) is the ratio of the mean of the two monocular thresholds, T_L and T_R, to the binocular threshold, T_B, as defined in Equation 16. The expected value for this metric is $\sqrt{2}$ (Blake

and Fox 1973) based upon the average monocular threshold equating to the ~1.4 times the binocular threshold.

$$BSI = \frac{T_L + T_R}{2T_B}$$

Equation 16: Binocular Summation Index

The Alternative Summation Index (ASI) is introduced by the author. It is based upon the concept that the eye and more specifically, the connections within the retina, are like the pixels in a camera. The electronics that form the pixels in a camera accumulate charge generated from the photoelectric effect, in a similar manner that the Retinal Ganglion Cells (RGCs) receive the signals resulting from phototransduction in the photoreceptors. In the camera, the charge is stored in a capacitive element within the pixel's electronics prior to reading out to the camera's memory at the end of each frame. Adding the capacitance (Cap_1 and Cap_2) of two pixels in series results in an expression given in Equation 17 for the total capacitance (Cap_{Total}). Equation 18 is derived by substituting for the thresholds of the left and right eye and expressing it relative to the binocular threshold, where the binocular threshold T_B equates to Cap_{Total} and similarly for the left and right eye thresholds to Cap_1 and Cap_2 respectively.

Substituting Equation 13 into this metric results in the theoretical value of $1/\sqrt{2}$, but if the monocular thresholds are double the binocular threshold value, then the ASI metric equates to 1.

$$\frac{1}{Cap_{Total}} = \frac{1}{Cap_1} + \frac{1}{Cap_2}$$

$$Cap_{Total} = \frac{Cap_1 Cap_2}{Cap_1 + Cap_2}$$

Equation 17: Adding capacitances in series

$$ASI = \frac{T_L T_R}{T_L + T_R} . \frac{1}{T_B}$$

Equation 18: Alternative Summation Index (ASI)

When these metrics are applied to the experimental data, if they equate to the theoretical values defined above, then it can be concluded that the model behind the metric provides a good estimate of the binocular summation process.

In addition to considering binocular summation, by applying metrics to the monocular thresholds it should be possible to gain greater understanding of ocular dominance. For aircrew, the issues associated with binocular rivalry and ocular dominance are important especially when symbology is presented monocularly, e.g. the Integrated Helmet And Display Sighting System (IHADSS) Helmet Mounted Display (HMD) used with the AH-64 Apache attack helicopter. Since the introduction of the IHADSS system there have been reports of visual illusions whilst flying using IHADSS HMD (Hiatt *et al* 2004). These illusions can result in false height judgement and undetected and illusory aircraft drift, all of which can lead to controlled flight into terrain resulting in damage to/loss of aircraft and aircrew.

Two metrics, previously used by Gillespie-Gallery *et al* (2013) in their study of the monocular and binocular contrast sensitivity as a function of light level are the Binocular Summation Ratio (BSR) and Interocular

Percentage Increase (IPI). These two metrics, defined in Equation 20 and Equation 21, respectively utilise the best eye threshold, i.e. the minimum of the two monocular thresholds as defined in Equation 19. This is based on the underlying assumption that the best eye equates to the more sensitive eye, and thus will have the lower threshold.

$$Best\ eye\ threshold = \ min([T_L, T_R]).$$

Equation 19: Definition of the best eye threshold

The BSR metric expresses the best eye threshold relative to the binocular threshold. If the monocular thresholds adhere to Equation 13, and the two monocular signals are equal, the BSR metric has the value of √2.

$$BSR = \frac{min([T_L, T_R])}{T_B}$$

Equation 20: Binocular Summation Ratio (BSR)

The IPI metric considers the absolute difference between the two monocular thresholds relative to the threshold of the best eye and so provides an indication of the influence that the best eye has on the summation process. The IPI metric tends to zero as the difference between the two monocular thresholds becomes smaller.

$$IPI = \frac{|T_L - T_R|}{min([T_L, T_R])}$$

Equation 21: Interocular Percentage Increase (IPI)

Together with the binocular summation indices, it is hoped that these metrics will provide a greater understanding of the differences between rod and cone-mediated monocular and binocular thresholds.

Table 3-1 provides a summary of the theoretical values of the three binocular summation and two ocular dominance metrics when evaluated for test cases where monocular thresholds are √2 times (Simpson's peripheral model) and twice (Simpson's central model) the binocular threshold values. These correspond to firstly the model of probability summation, and secondly, the inclusion of an additional neural summation process in addition to the probability summation. It is expected that the lack of equivalency in monocular thresholds will lead to a variation in the actual values from these theoretical predictions.

Quantity	Metric	$T_M = \sqrt{2}T_B$	$T_M = 2T_B$
Binocular summation	BSI	√2	2
	QSI	1	√0.5
	ASI	√0.5	1
Ocular dominance	BSR	√2	2
	IPI	0	0

Table 3-1: Summary of theoretical metric values for quantifying binocular summation and ocular dominance.

3.1.3 Hypotheses

The following hypotheses will be tested within the scope of this study:

a) The RCS test enables the quantitative assessment of the sensitivity of photoreceptors.
b) The RCS-R test condition excites a rod-mediated response.
c) Increasing the time of adaptation to the uniform background field that precedes the RCS-R test, has no significant effect on the measured, rod-mediated thresholds.
d) Unavoidable changes in the test protocol's definition did not significantly influence FMT values [11].
e) The RCS FMTs for the four (off-axis) stimuli at 5° eccentricity can be combined into a single metric of parafoveal photoreceptor sensitivity.
f) Monocular RCS FMTs can be used to predict binocular FMTs.
g) Monocular RCS FMTs can be used to predict ocular dominance

3.1.4 Experimental design

The design of the initial experiments centred on defining the test protocol and factors that could influence the outcome of the test. The parameters for optimisation were those that define the appearance of the stimulus, i.e. size, chromaticity and background luminance, for the two stimulus conditions designed preferentially to enhance either rod or cone-mediated responses. An evaluation was also undertaken to characterise the effect of pre-test adaptation time on the measured FMTs. These initial studies were undertaken by a small cohort ($n \leq 4$). Due to availability not all the participants completed all the characterisation tests, but across the cohort the variation of the FMT as a function of both on and off-axis stimulus size and the stimulus conditions' background luminance were evaluated.

In addition, tests were undertaken by participants with known visual deficiencies to verify that the RCS-R test protocol elicits rod-mediated responses.

Following amendment of the test software and the slight shift in chromaticity of the two stimulus conditions, to address an undocumented change in specification of the EIZO ColorEdge CS2420 monitor by the manufacturer, an analysis was undertaken to determine if the results for the two software versions were comparable. The original version of the test software will be referred to as version 0.102.4, whilst the revised software will be referred to as version 0.102.7.

Having finalised the test protocol, a small study (n=12) was undertaken to measure FMTs for the RCS-R and RSC-C conditions, binocularly and also monocularly using both the left and right eyes. This experiment was completed using version 0.102.7.

The final experiment of the study was to use the RCS test to define a set of normative test data for a population of young normal participants (n=121) to provide a reference point for future studies. Due to the change in test software occurring part way through the experiment, the data has been separated into

[11] A change in the test protocol for both RCS-R and RCS-C test conditions was made due to an undocumented change to the monitor by the manufacturer. See section 3.1.4.

two cohorts: cohort A (n=71) and cohort B (n=38) after exclusions. The test stimuli were viewed binocularly for this experiment.

3.2 Methods

3.2.1 Terminology

When presenting the RCS test results for an individual or the mean result for a cohort, the FMTs have been plotted as a function of meridian position, as illustrated in Figure 3-4. The relationship between on-screen position of the stimuli is also illustrated for reference. When referring to the different stimuli, the centre stimulus will be referred to as the on-axis (line of sight) stimulus. The four outer stimuli are referred to as the off-axis or peripheral stimuli as they are not on the direct line of sight and peripheral, non-foveal, vision is required to identify the location of the stimuli. These outer stimuli correspond to the parafoveal region of the retina. The test protocol requires the participant to maintain fixation on a fiducial at the centre of the screen.

When referring to the test stimuli, the stimulus designed to promote a rod-mediated response will referred to as the RCS-R stimulus or condition, likewise the stimulus designed to promote a cone-mediated response will be referred to as the RCS-C stimulus or condition.

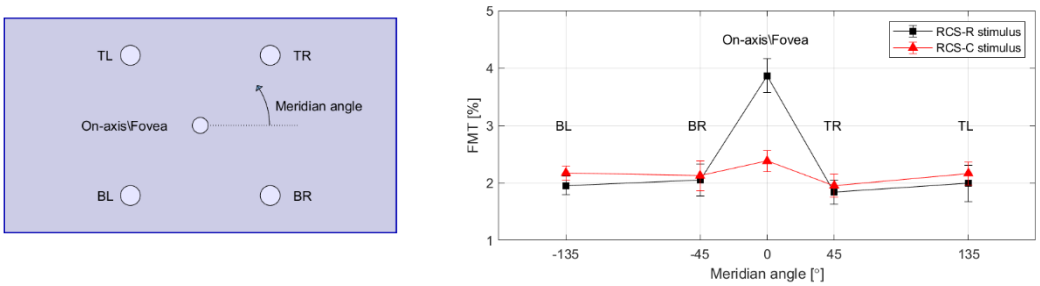

Figure 3-4: Illustration of the on-screen location of the RCS test stimuli (left) and an example set of results for a young participant plotted as a function of meridian position (right) with the corresponding on-screen stimulus locations show in the diagram. (Error bars ±1 standard error.)

3.2.2 Participants

All procedures in the study were conducted in accordance with the tenets of the Declaration of Helsinki. Informed consent was obtained from all participants prior to partaking in the individual studies.

The young, normal participants were recruited from the students and staff of City, University of London. The participants with known visual deficiencies were recruited directly. Participant X had a genetic CNG-B3 achromatopsia, whilst participant Y was a tritanope. The participants for Experiment 5 were between 20 and 27 years old and those for Experiment 6 were between 18 and 30 years old.

3.2.3 Rod Cone Sensitivity test procedure

FMTs were measured at five locations using two stimulus conditions designed to instigate respectively a rod or cone-mediated response. The flickering stimulus was a uniform disc presented either centrally, at the centre of fixation, or at one of four locations of equal eccentricity in the four quadrants of the display, see Figure 2-4.

The size of the stimuli, eccentricity of the peripheral stimuli, and background luminance for both the rod and cone test conditions were determined during an initial period of development testing, undertaken within Experiment 1. The properties of the background and the size, location, duration, and flicker frequency of the stimuli are defined in Table 3-2.

Additional detail, provided in section 2.1.4.2 and 2.1.3, defined the RCS test and the use of the spectrally calibrated sunglasses to attenuate the luminance experienced by the participant for the RCS-R test configuration. The test protocol utilised a 2 down, 1 up adaptive staircase evaluated over 9 reversals for each stimulus location. The staircases for the five stimuli were interleaved and the presentation order was randomised. The FMTs for the five flickering stimuli were calculated as the mean of the last six reversals for each location. The initial amplitude of the luminance flicker was 5% of the background luminance.

Property		**RCS-R test**	**RCS-C test**
Background condition	Luminance at the eye	0.5 cd.m^{-2}	24 cd.m^{-2} (22 cd.m^{-2})
	CIE 1931 co-ordinates (x, y)	(0.18, 0.089) *(0.18, 0.077)*	(0.58, 0.361) *(0.58, 0.322)*
	S/P ratio	8 *(9)*	1 *(0.9)*
Central foveal stimulus	Diameter	45’	30’
Peripheral para-foveal stimuli	Diameter	90’	60’
	Eccentricity	5°	
Temporal properties	Flicker frequency	5 Hz	15 Hz
	Stimulus duration	600 ms	333 ms

Table 3-2: Properties of the centrally and peripherally located stimuli of the RCS-R and RCS-C tests. The luminance of the RCS-R test stimulus is achieved by using a pair of sunglasses. The properties of the background condition are specific to the test software used. The CIE co-ordinates and S/P values in italics relate to software version v0.102.7.

Seated 1 m away from the 611mm (24”) diagonal screen, the participant was instructed to maintain fixation at the centre of the screen for the duration of the test. An initial learning mode was undertaken to familiarise the participant with the keypad interface used to record the location of the flickering stimulus. The buttons on the keypad interface replicated the on-screen location of the five test stimuli.

The tests were undertaken in a darkened room. The illuminance measured on the surface of the display was ~100mlux. Prior to undertaking the rod test, the participant adapted to the background employed in the experiment for 2 minutes whilst wearing the spectrally calibrated sunglasses. The sunglasses were worn over their own spectacles when required. For the cone-enhanced protocol, the adaption period was 1 minute. The tests took up to 10 minutes to complete with a break between the test conditions as required.

3.2.3.1 Monocular thresholds

Monocular thresholds involved the use of an eye patch to occlude the non-tested eye. Monocular thresholds were measured for each eye separately. For the RCS-R test condition, the Oakley sunglasses were worn over the top of the eye patch.

3.2.4 Ocular dominance

The Porta Eye Dominance test (Porta 1593) was used to determine the dominant sighting eye of the participants. The participant pointed at a target located more than 4 metres away whilst viewing it with both eyes. The participant's task was then to close each eye in turn and report whether their finger had moved from the target or not. The sighting dominant eye was determined as the eye for which the perceived target location remained unchanged.

The Porta Eye Dominance test was used because it was simple to administer within the lab environment without additional equipment. Alternative methods of assessing sighting eye dominance exist (Bossi *et al* 2018) that have been shown to produce variable results (Johansson *et al* 2015, Rice *et al* 2008).

3.2.5 Experiments

The study involved six experiments which sought first to define the test, then verify its performance, before characterising the expected values for a cohort of normal participants. The objectives of each experiment were as follows:

Experiment 1: Establish the appropriate selection of stimulus size for the central and peripheral stimuli, peripheral stimulus eccentricity, and background luminance values for both rod and cone conditions.

Experiment 2: Verify that the RCS-R test condition excites a rod-mediated response.

Experiment 3: Assess the effect of increasing pre-test adaptation time for the RCS-R test condition on the measured FMTs.

Experiment 4: Verify that the modification to the chromaticity of the two test protocols, due to the change in display hardware specification, did not significantly influence the FMTs measured using the RCS test.

Experiment 5: Characterise the monocular and binocular FMTs for young normal participants using the RCS tests to assess the advantages of binocular vision in central and peripheral vision.

Experiment 6: Define the Standard Normal Observer (SNO) for the RCS binocular FMTs for a cohort of young normal participants.

3.2.6 Data analysis

Analysis was undertaken using a combination of Microsoft Excel and MATLAB R2018b (Mathworks Inc.) to perform linear regression and additional statistical analyses.

Linear regression analysis and curve fitting were applied to results of Experiments 1, 4, and 6.

Parametric and non-parametric analysis techniques were applied to the data from Experiment2 4 to 6 to determine the results of the test for cohorts of young participants with normal (corrected) vision. Analysis Of Variance (ANOVA) was used to analyse data from Experiment 5 and 6 to establish the relationships between: the two software versions; off-axis FMTs for the two test conditions; left and right monocular, and binocular FMT results for the RCS-R and RCS-C conditions.

3.3 Results

3.3.1 Experiment 1 – Definition of RCS test stimuli

This experiment investigated the effect of the background luminance and stimulus diameter on the FMT measured by the test for the two test conditions. The results, presented below, consider the effect that these parameters have on firstly the RCS-R condition followed by the RCS-C condition.

3.3.1.1 RCS-R stimulus definition

The effect of increasing the background luminance resulted in a decrease in the FMT value recorded for both the central, 45 arcmin on-axis stimulus, at 0° eccentricity, and the four outer, 90 arcmin off-axis stimuli at 5° eccentricity, as presented in Figure 3-5. The background luminance values have been adjusted for the effect of the neutral density glasses and thus represent the luminance of the stimulus at the eye, rather than that at the display. The level of attenuation provided by the neutral density glasses along with the S/P value of the stimulus were accounted for when defining each test condition in the test software. The lowest FMT values were generally achieved by the youngest participants and the highest values by the oldest, suggesting a possible influence of age on FMTs, but this result is limited by the small cohort.

The outcomes of these tests indicate that a background luminance of 0.5cd.m^{-2} gave the greatest scope for variation in FMT for the younger participants, whilst allowing sufficient range for stimuli with sub-threshold FMT to be displayed. This value for the RCS-R background luminance is the lowest value that can be achieved given the dynamic range of the display, the spectral characteristics of the sunglasses and the photometric limits imposed by the primary colours of the display.

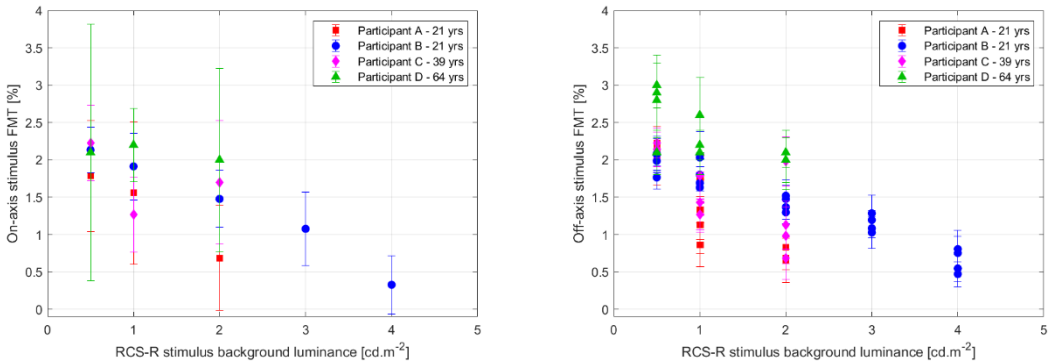

Figure 3-5: The FMT for stimuli located at the screen's centre (left) and at 5 °eccentricity from the screen's centre point (right) for different background luminance values for the RCS-R stimulus condition.

The changes in FMT for the on-axis and off-axis stimuli for the RCS-R condition were explored by varying the angular size of stimulus for background luminance of 0.5cd.m^{-2}, as shown in Figure 3-6 and Figure 3-7 respectively. The eccentricity of the four off-axis stimuli was maintained at 5°. In both cases, the increase in FMT mapped to a power function as stimulus diameter was reduced. For both the on-axis and off-axis stimuli, there is a point where the FMT appears to be independent of any further increase in stimulus diameter. For on-axis and off-axis stimuli respectively this point is around 45 arcmin and 90 arcmin, as marked by the black arrows in the two graphs. These dimensions were used to define the stimulus dimensions for the RCS-R condition.

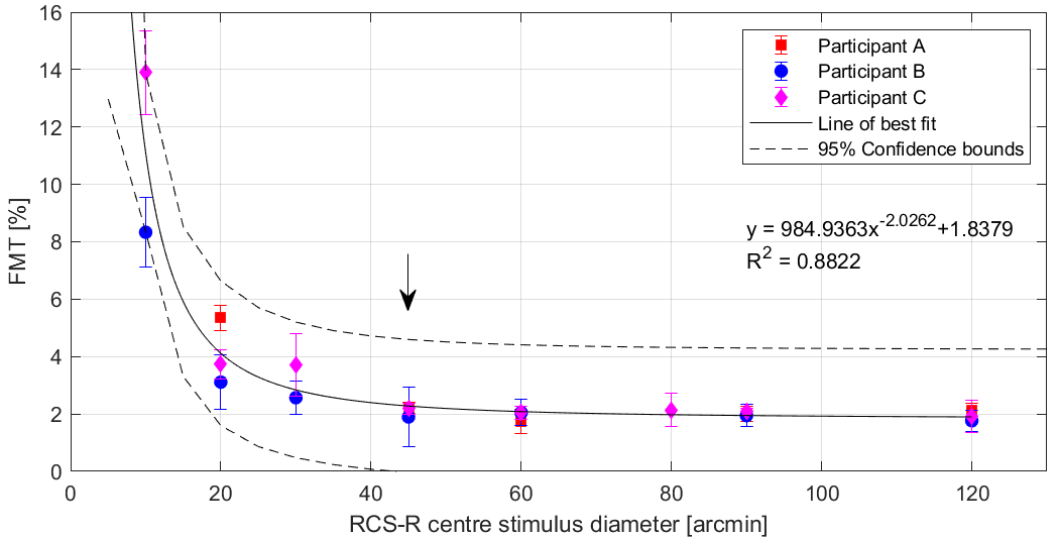

Figure 3-6: The variation of FMT for the on-axis stimulus for the RCS-R background condition at 0.5 cd.m^{-2}. The size of the on-axis stimuli selected for the final test parameters is marked with an arrow.

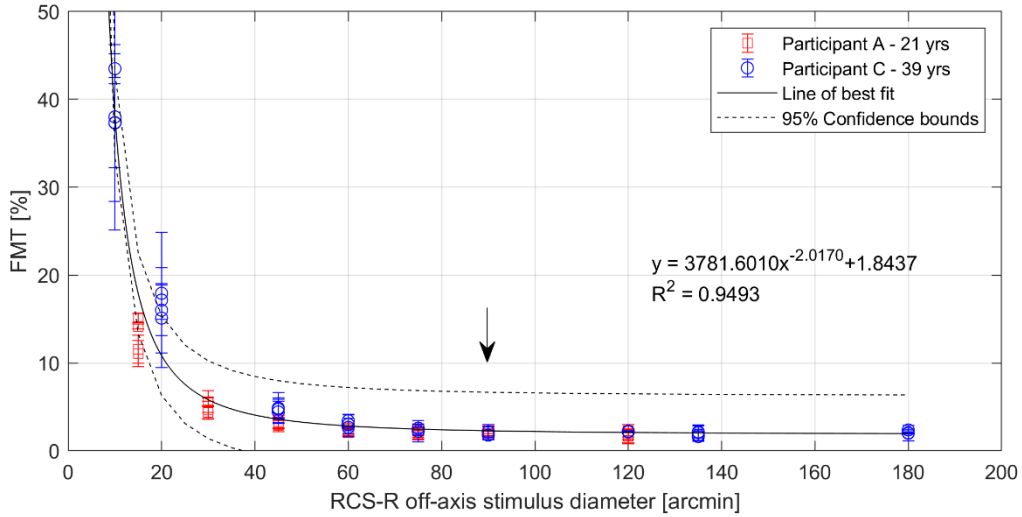

Figure 3-7: Variation of FMT for the stimuli located at 5 ° eccentricity for a RCS-R condition background luminance of 0.5 cd.m^{-2}. The diameter of the off-axis stimulus selected for the final test parameter is marked with an arrow.

Given the age range (21 to 39 years) of the participants in these initial tests, there is good agreement for the FMT values for stimulus diameters beyond the marked points. However, the variation in FMT increases as the diameter of the stimulus is reduced.

3.3.1.2 RCS-C stimulus definition

Decreasing the background luminance of the RCS-C condition had the effect of increasing the FMT values, as illustrated in Figure 3-8. The difference in age between the two participants was thought to be a contributing factor to the variation in FMT values. Participant A recorded the lower set of values presented in Figure 3-5.

To ensure that the test could evaluate the FMTs of both participants with normal vision and those potentially with a vision deficiency, it was necessary to ensure that the presentation of a stimulus with a contrast of 100% relative to the background luminance level could be supported by the dynamic range of the display for the respective stimulus condition. For example, a background luminance of 24cd.m^{-2} will

require the display to be able to present a flickering stimulus with a peak luminance of 48cd.m^{-2} at the required chromaticity. Correspondingly the minimum luminance will be close to 0cd.m^{-2} allowing for a small amount of residual glow from the pixels in their off state. Whilst the display is capable of producing a 64cd.m^{-2} white background, the limitation of the monitor's dynamic range at the required chromaticity of the RCS-C condition resulted in the selection of 24cd.m^{-2} as the background luminance of the RCS-C stimulus condition.

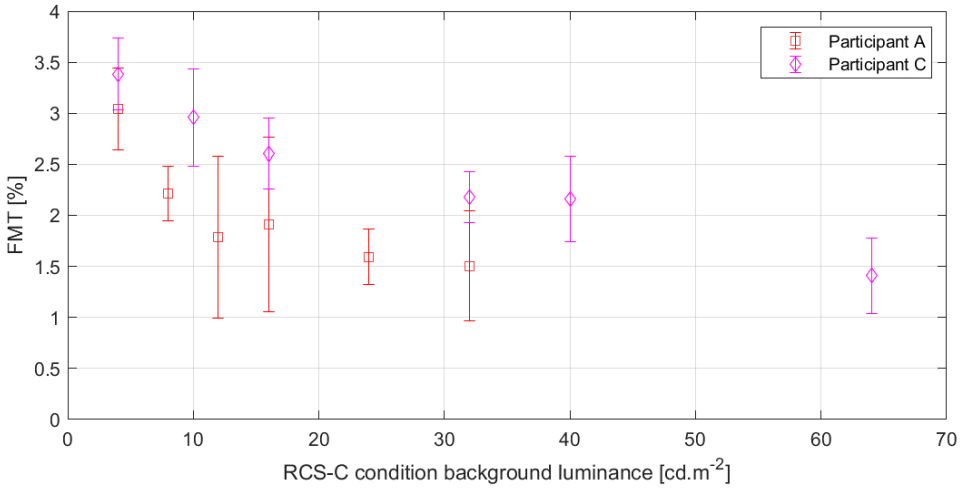

Figure 3-8: Variation of FMT for the centre stimulus location as a function of the cone stimulus background luminance. The stimulus diameter was fixed at 30 arcmin.

The variation in FMT as a function of the on-axis and off-axis RCS-C stimulus diameter is shown in Figure 3-9 and Figure 3-10 respectively. Drawing through the results for the variation of FMT value as a function of RCS-C condition's background luminance, the impact of the characterisation of the on-axis stimulus being undertaken at 32 cd.m^{-2} rather than 24 cd.m^{-2} is minor. The lower luminance increased the FMT for the centre stimulus, but this is still within the variation observed for the three participants. This is further supported by the results presented in Figure 3-10, where there is little difference between the results for the two participants despite the characterisation being undertaken with different background luminance values.

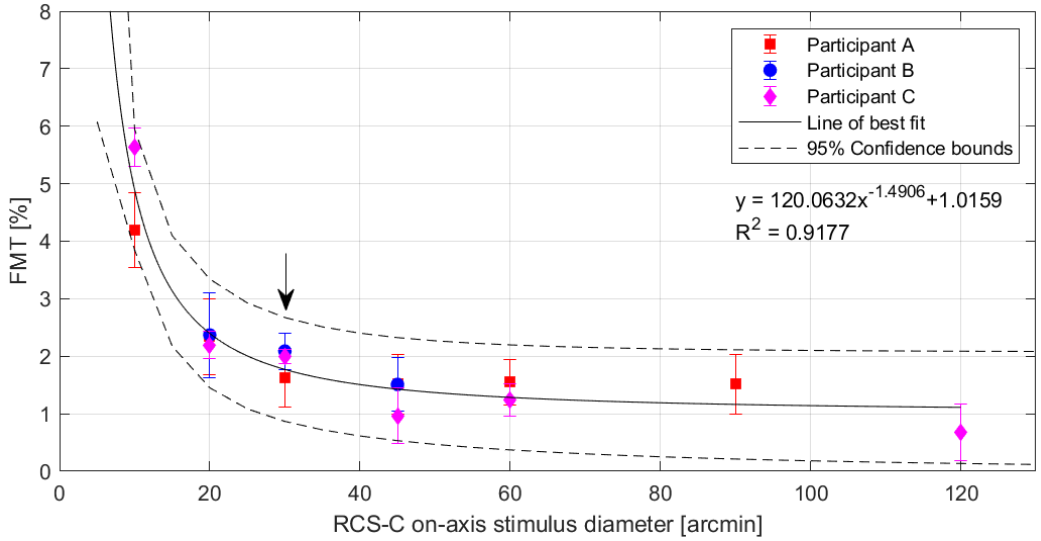

Figure 3-9: Variation in FMT as a function of on-axis stimulus diameter for the RCS-C condition. Measurements undertaken with a background luminance of 32 cd.m^{-2} for all participants.

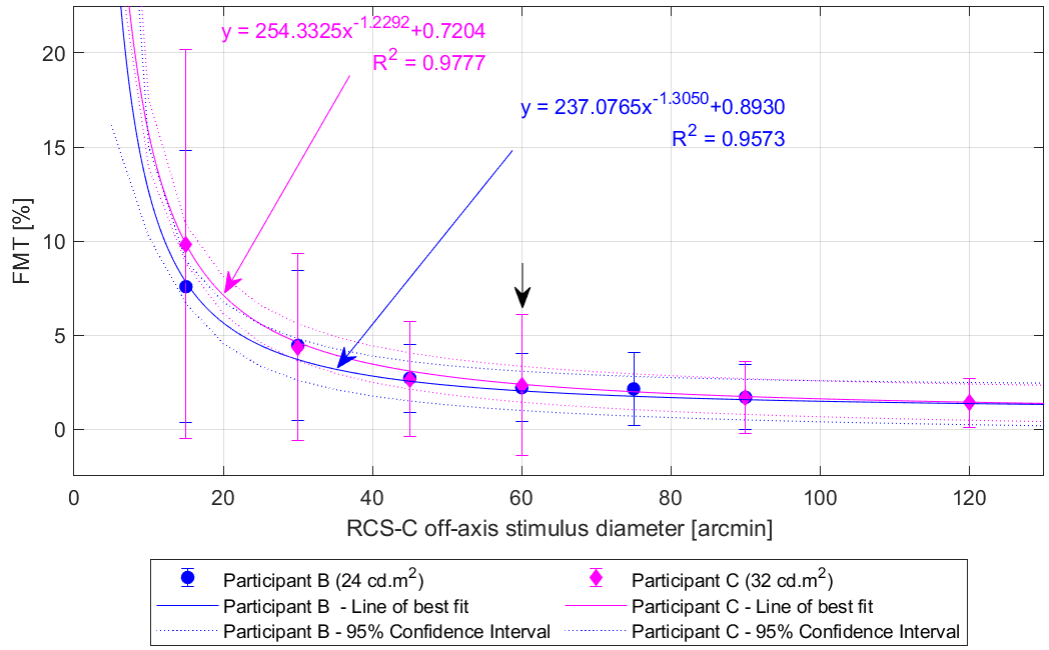

Figure 3-10: Variation in FMT as a function of off-axis stimulus diameter for the RCS-C condition. The background luminance for each participant was different with values quoted in the legend.

The transition point at which the FMT appears to be independent of stimulus size has again been used as the basis for determining the stimulus diameter to be used in the final test. Like the results for the RCS-R condition, this also aligns with FMT values of around 2% for the RCS-C condition. As the stimulus diameter is reduced in size, the FMT values start to increase more rapidly with the potential for greater variance in the data for a SNO.

The resulting set of parameters defining the background luminance for the two test conditions and the size of the on-axis and off-axis stimuli are listed in Table 3-2.

3.3.2 Experiment 2 – Verification of RCS-R condition

The RCS results for a 60 year-old rod monochromat (with the genetic mutation CNG-B3) are provided in Figure 3-11. The results show a reduced sensitivity to the RCS-C stimuli resulting in FMT values greater than 20%, more than 10 times the ~2% FMT value recorded in Experiment 1. The response to the RCS-R condition was broadly equivalent for all off-axis stimulus locations. The higher FMT value for the on-axis stimulus location is attributed to the normal absence of rods at the very centre of the foveal pit. The light from the RCS-R stimuli presented to this individual can only be detected by rods in the region surrounding the fovea through forward scattering. The RCS-R FMT values recorded for the rod monochromat are higher than those expected for a normal participant based upon Experiment 1. This is likely to be a factor of the participant's age or a function of the achromatopsia or a combination of both. As the luminance of the stimulus is in the mesopic range, there is likely to be some cone contribution for a normal participant, even if it is reduced by the test condition's spectral power distribution.

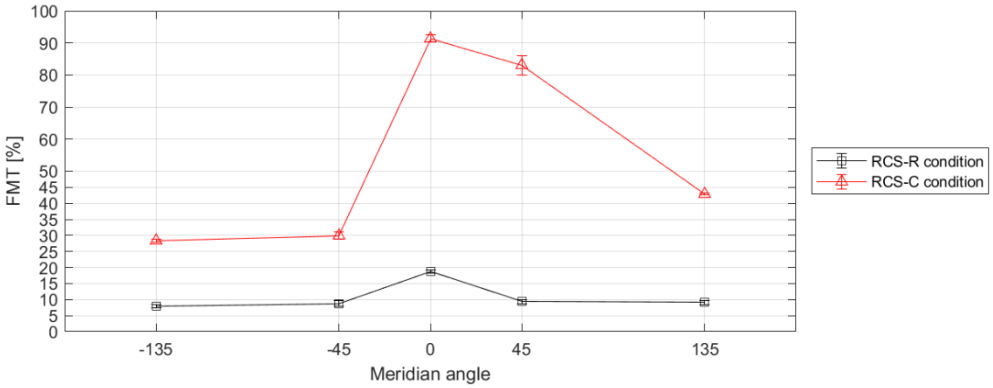

Figure 3-11: FMTs measured for a rod monochromat for the RCS-R and RCS-C conditions. The foveal stimulus is plotted at the centre of each graph. (Age of participant is 60 years.)

The results for the 64 year old tritanope, Figure 3-12, show FMTs for the RCS-R condition that were between 3% and 3.6%, which are normal for the subject's age (Hathibelagal *et al* 2020). If S cones were involved in the detection of the rod condition stimuli, significantly higher FMT values would be expected due to this participant's lack of S cones with thresholds. The reason for the elevated FMT values observed can be attributed to an age related reduction in the density of rod photoreceptors (Owsley 2011) and changes in the optical density of the lens which will attenuate the transmission of blue light (Pokorny *et al* 1987).

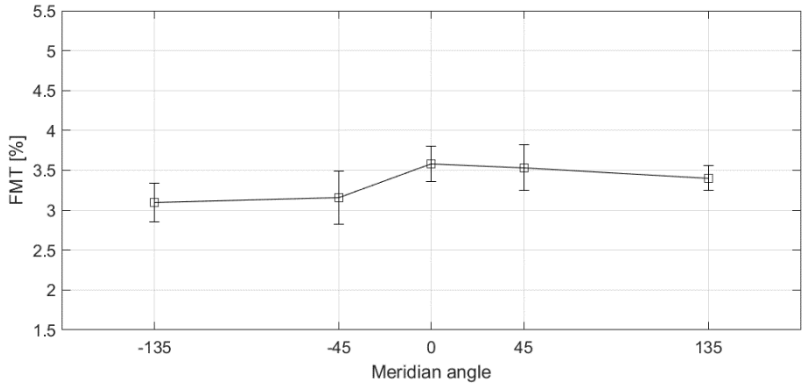

Figure 3-12: FMT for a tritanope measured for the RCS-R condition. (Age of participant is 64 years.)

3.3.3 Experiment 3 – Effect of pre-test adaptation time on RCS-R test thresholds

Having defined the stimulus size and background luminance of the RCS-R test, the impact of the time spent adapting to the background luminance prior to initiation of the test was investigated. The effect of changing the pre-test adaptation time is plotted in Figure 3-13 with lines of best fit calculated for the on-axis stimulus and the mean of the off-axis stimuli. Two effects are evident in the graph. Firstly, the main observation is that there is no effect of changing the adaptation time on the RCS-R test results for off-axis stimuli. The lack of variation in the ±95% confidence intervals for the fitted line provides further evidence that there is no effect on off-axis thresholds as adaption time is increased.

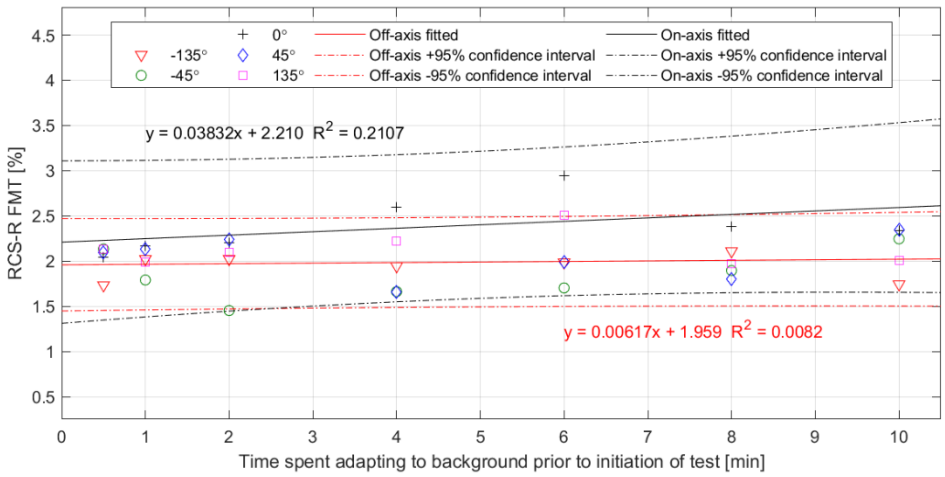

Figure 3-13: Effect on RCS-R test thresholds as a function of time spent adapting to the background test condition.

The second observation is the increase in the on-axis threshold at a rate of 0.04%.min^{-1} indicating a small loss of sensitivity. The localisation of the loss of sensitivity to the central stimulus location suggests a localised change in the sensitivity of rods close to the fovea.

Whilst there may be some desensitisation of cones, the previous experiment demonstrated that cones are less likely to influence the FMT values measured for RCS-R test conditions.

Overall, there is no evidence that limiting the adaptation time compromised the measured FMTs with the outcome of the test suggesting that the practice of allowing 2 minutes pre-test adaptation in a darkened room looking at the RCS-R background stimulus condition was sufficient to enable an assessment of both on and off-axis rod thresholds.

3.3.4 Experiment 4 – Verification that changes in test protocol have not significantly changed test results

To assess if the changes in test protocol had significantly affected the results of mean RCS FMT values measured, the author undertook 16 repetitions of each version of the test using the same display system. The results of this assessment are presented in Figure 3-14.

For both versions of the RCS-R and RCS-C test protocol, the FMT values correlate well, with mean values for one version of the test falling within the error bars, equivalent to ±1 standard deviation, of the other test protocol. This observation is supported by Table 3-3 which shows the results of undertaking two-sample *t*-tests for each test location; these are not statistically significantly different at an α=0.05. For this observer, the results of the two test protocols do not appear meaningfully different.

Stimulus condition	Stimulus location (meridian angle)				
	-135°	-45°	0°	45°	135°
RCS-R	0.69	0.66	0.32	0.10	0.18
RCS-C	0.89	0.45	0.24	0.63	0.58

Table 3-3: P-values for two-sample t-test undertaken for each stimulus location indicating that there are no significant differences between the data for each of the five stimulus locations.

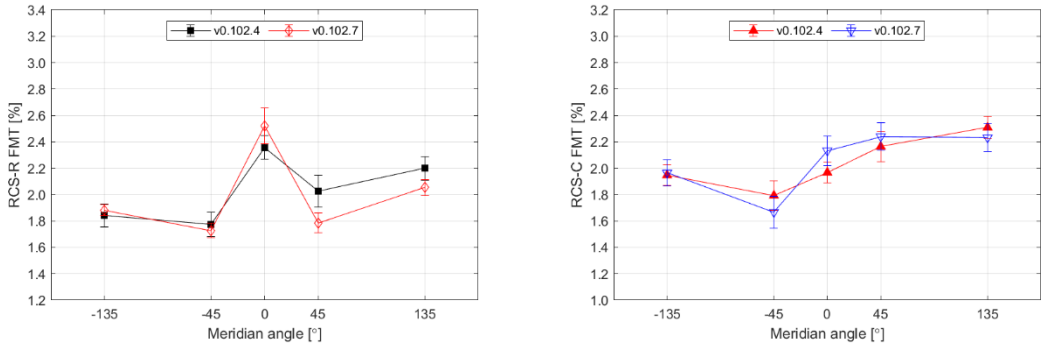

Figure 3-14: Comparison of the results for the RCS-R (left) and RCS-C (right) conditions for the two versions of the test protocol. The error bars equate to ±1 standard error.

Whilst there is no meaningful difference in the means of the sets of data from the two versions of the test, there are differences in the spread of the data indicated by comparing the size of the error bars in Figure 3-14. The standard errors of the off-axis RCS-R thresholds for the v0.102.7 protocol are smaller than those of the v0.102.4 protocol. Conversely, the standard error for the on-axis RCS-R threshold for v0.102.7 of the test are 1.5 times larger than v0.102.4 protocol. The standard errors for the RCS-C condition are closer in magnitude for both the on-axis and off-axis stimuli. The changes in sensitivity observed in the previous experiment, section 3.3.4, are less than the within subject variability demonstrated in these results for both test protocols. Whilst the results of this experiment provide an initial indication, repeating the testing with a larger cohort of participants would provide greater confidence that this is a real effect.

3.3.5 Experiment 5 – Characterisation of monocular and binocular RCS FMTs

This experiment used a small cohort (n=12) of young, normal participants and the new protocol (v0.102.7) to assess monocular and binocular FMTs measured using the RCS test.

In order to better understand the results for the two stimulus conditions, i.e. RCS-R and RCS-C tests, and the three viewing conditions, i.e. monocularly using left and right eyes and binocularly, the data were sorted in ascending order and plotted along with the mean and median values for each stimulus location. An example is illustrated in Figure 3-15 for the RCS-R condition when viewed binocularly and in Figure 3-16 for the RCS-C condition when viewed monocularly with the right eye.

For the peripherally located RCS-R stimuli viewed binocularly, Figure 3-15, the median and mean values of the group are very similar. For these peripherally located targets, the raw data is within ±2.5 standard deviations of the group mean value at each stimulus location. This behaviour is replicated when the RCS-R stimuli are viewed monocularly. The peripherally located targets having a similar median and mean value when the group statistics are calculated for each stimulus location. For the case of the 135° target location, the median and mean are equivalent to two decimal places, i.e. 2.57%.

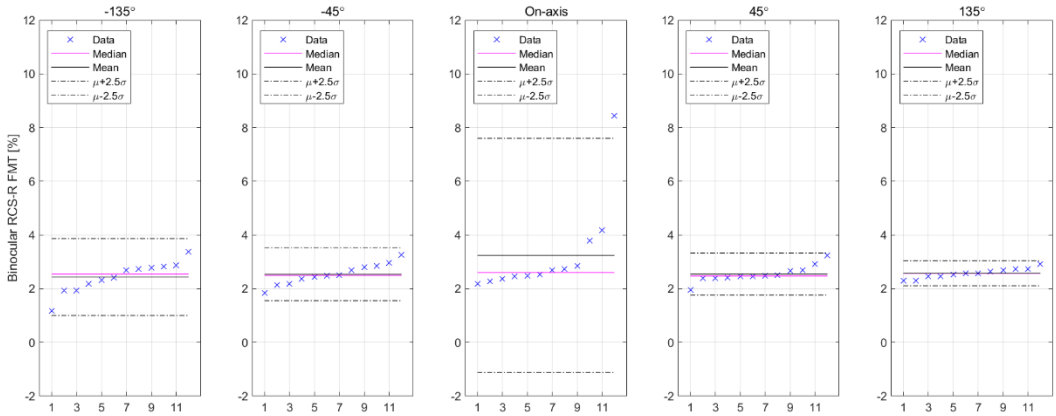

Figure 3-15: Raw binocular RCS-R FMT results for full cohort (blue crosses) plotted along with the group's median and mean value for each stimulus location (solid lines). The dashed lines correspond to the group mean $\pm$ 2.5 standard deviation for each stimulus location in turn.

The results for the RCS-R condition's central stimulus, which aligns to the fovea, have a greater variance, which can be attributed to point 12 in the sorted sequence. The on-axis threshold for this individual is more than 2.5 standard deviations from the group mean and 2.5 times greater than the 75th percentile.

This is either a true reflection of the expected variability in the on-axis threshold or due to other factors, such as fewer rods in central vision requiring a greater amplitude to the luminance modulation. Alternatively, the individual may have very good fixation resulting in the 45 arcmin stimulus being maintained within the rod-free region of the retina. However, the difference in the FMT value compared to the next highest FMT value and the ~2% range of FMT values across the other 11 participants suggest that this might not be a true reflection of the group's on-axis FMTs for the RCS-R condition, i.e. an outlier.

Considering the results for the RCS-C condition in Figure 3-16, a similar relationship is observed for the on-axis stimulus. These on-axis results have a greater variation although the highest ranked point, i.e. point 12, may again be considered as an outlier, based on where it sits relative to the rest of the population. Subsequent analysis identified that this point related to the same participant, identified as point 12, in Figure 3-15. This individual consistently recorded higher on-axis thresholds for all test conditions. For the binocular and monocular viewing conditions, their on-axis FMT values are respectively ~2 and ~1.5 times higher than the next highest FMT values. The inclusion of point 12 in the calculation of the standard deviation for on-axis FMTs results in a negative value for the -2.5 standard deviations, when the data suggest a lower bound closer to ~2%. The minimum on-axis FMT for the binocular RCS-C condition is ~1.2% in comparison. This last point aligns with greater sensitivity at the fovea for the cone-enriched stimulus with more variability in FMT values for peripherally located stimuli.

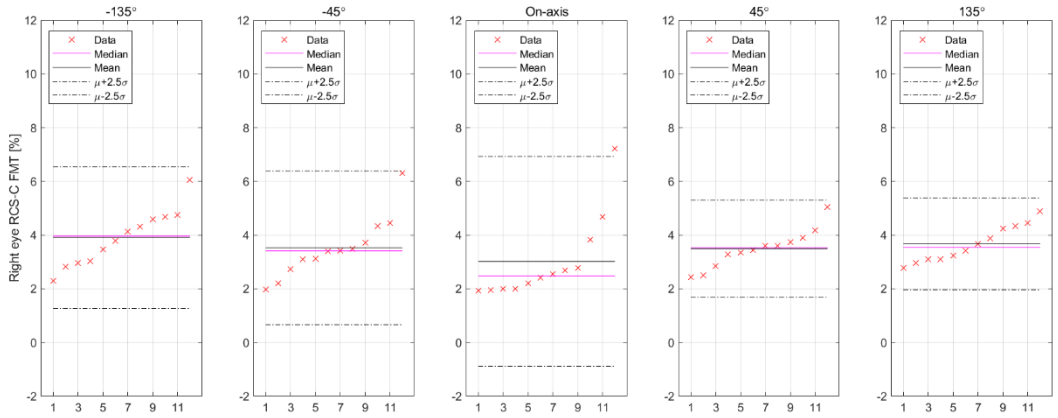

Figure 3-16: Raw FMT results for the full cohort when the RCS-C stimulus was viewed monocularly using right eye (red crosses) plotted alongside the group's median and mean value for each stimulus location (magenta and block solid lines respectively). The dashed lines correspond to the group mean ± 2.5 standard deviations for each stimulus location in turn.

Given that in both examples and the other viewing conditions, the highest ranked point for the on-axis stimulus location appears to be an outlier, and thus could be excluded, is there any statistical evidence for its exclusion? To answer this question, the statistical properties of the remaining data points, once the highest ranked point had been excluded, were considered to determine if the excluded highest ranked point was within ±3.5 standard deviations of the new mean based on the remaining set of data points. The exclusion limits of ±3.5σ was used as this equates to 99.95% of the data for a normal distribution, i.e. it would be very unlikely that the data would be outside of this bound for a sample with n = 12.

The results of applying this methodology to the raw RCS-R and RCS-C data, presented in Figure 3-15 and Figure 3-16, are shown in Figure 3-17 and Figure 3-18. The points identified for exclusion, highlighted by red crosses in the graphs, all relate to the same participant. The ordering of the stimuli in Figure 3-17 and Figure 3-18 has been changed to make it easier to compare the results for the peripherally located stimuli.

Comparing the results for the peripherally located stimuli (±135° and ±45°) in both Figure 3-17 and Figure 3-18, the mean and median values for the two test conditions are similar for the RCS-R and RCS-C stimuli respectively. There is some variation in the upper and lower exclusion limits for the reduced data set, which is more obvious for the RCS-R stimuli when viewed binocularly.

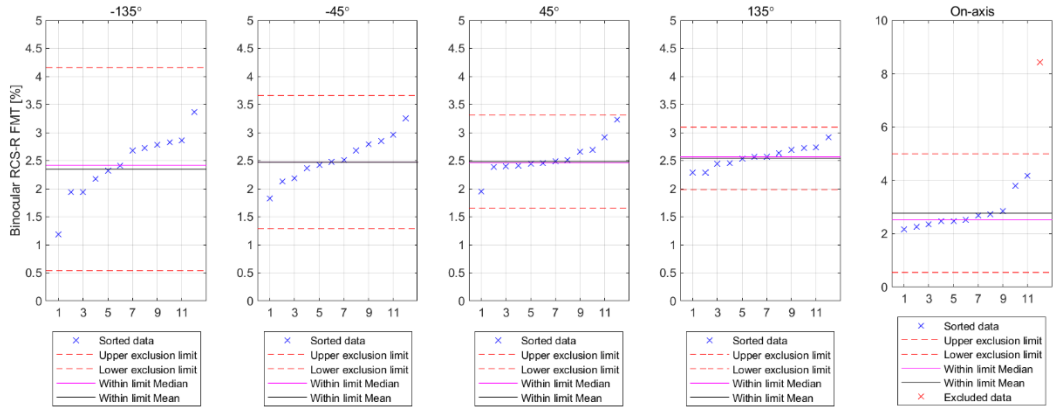

Figure 3-17: The ranked results for the RCS-R condition when viewed binocularly showing point to be excluded (red cross) when the exclusion methodology is applied. (Note the re-ordering of the stimuli.)

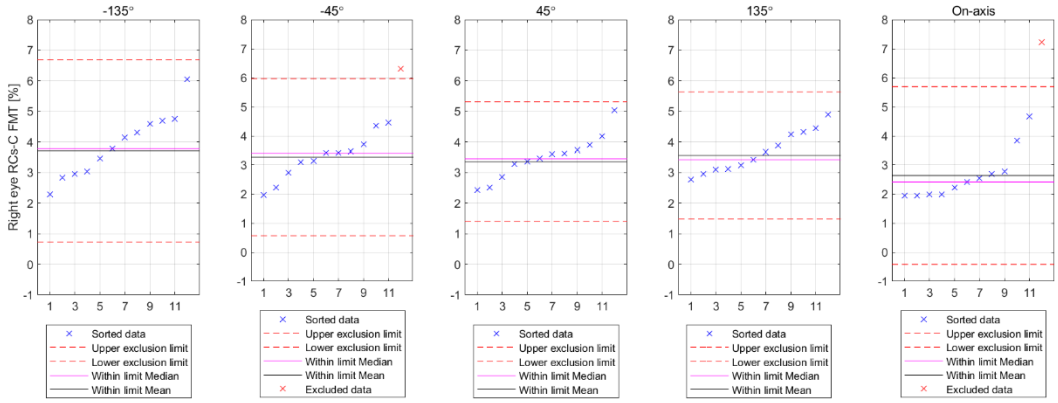

Figure 3-18: The ranked results for the RCS-C condition when viewed monocularly with the right eye. The participant to be excluded (red crosses) when the exclusion methodology is applied correspond to same participant.

The analysis so far has considered only two out of the six conditions under which the tests were completed. Having identified and excluded the outlier, the full set of data is illustrated in Figure 3-19 and Figure 3-20 for the RCS-R and RCS-C conditions respectively for all viewing conditions and target locations.

This pair of graphs show that the monocular FMTs have similar distributions and are between 1.5 to 2 times higher than the binocular FMTs for the corresponding stimulus condition. The range of values for the monocular FMTs is greater than the binocular thresholds, which have lower variance.

Where the distribution of points is skewed, illustrated by the offset between the mean and median values, suggests that the results do not map to a normal distribution. An example is the RCS-R on-axis stimulus, where there is an offset between the monocular mean and median values. For the peripherally located stimuli, the median and mean values are similar suggesting that these data could be combined into a single distribution and the data for the individual stimulus locations conform to a normal distribution. Whether the data conforms to a normal distribution has been assess using the Anderson-Darling (AD) test in section 3.3.5.1. Where the test result has shown that the data does not conform to a normal distribution, alternative distribution types and transformation functions have been assessed. The results of this analysis are presented in Table 3-4 and Table 3-5.

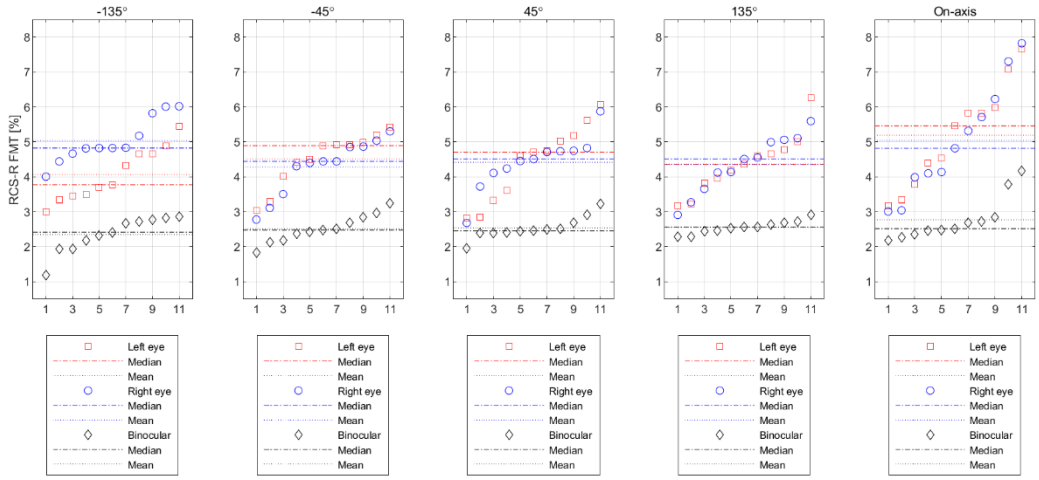

Figure 3-19: Combined results for the RCS-R condition when viewed monocularly with left eye (red), right eye (blue) and binocularly (black) after exclusion of the outlier.

The mean FMTs for the two tests and three viewing conditions have been further summarised in Figure 3-21 where the mean values for each stimulus location are plotted with error bars equivalent to a standard deviation. Except for the stimulus at a meridian angle of -135° viewed with the right eye, the results appear to support the working hypothesis that the off-axis FMTs can be combined into a single off-axis FMT metric. There is still an overlap, within one standard deviation, for the stimulus location at a meridian angle of -135°. The difference for the stimulus at -135° could be attributed to the division of attention when the participants are undertaking the test. This could be assessed by using an eye tracker which would also allow assessment of the participant's ability to main consistent fixation on the centre fiducial.

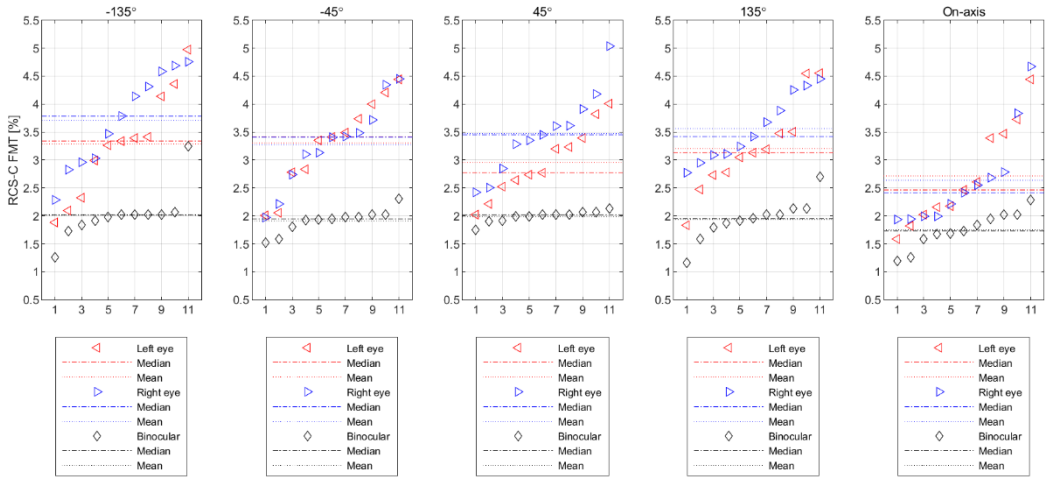

Figure 3-20: Combined results for RCS-C condition when viewed monocularly with left eye (red), right eye (blue) and binocularly (black) after exclusion of the outlier.

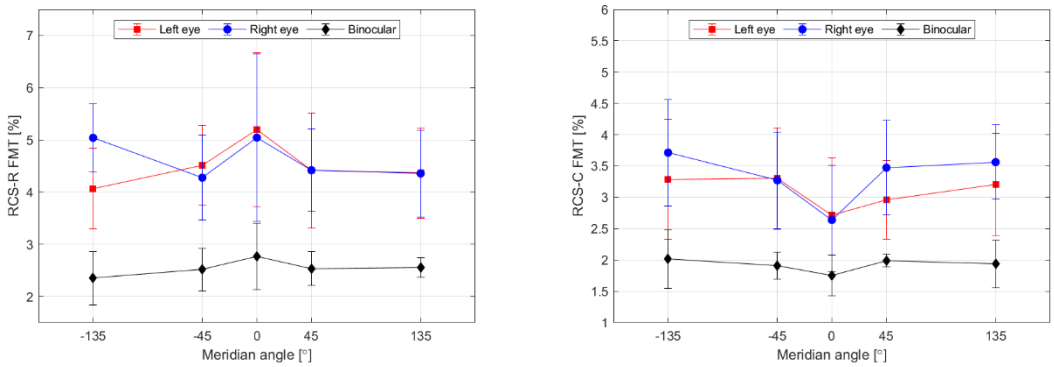

Figure 3-21: The combined FMT results for the RCS-R (left) and RCS-C (right) conditions showing the variation for the five stimulus locations. The mean FMT value has been plotted with error bars of ±1 standard deviation.

Viewing the stimuli monocularly appears to amplify the difference in the FMTs for the on-axis and off-axis stimuli in both the FMT value and its variance. The standard deviation of the binocularly viewed RCS-R on-axis stimuli is larger than the off-axis values reflecting the results of the previous experiment for the single participant. The effect of the lack of rods within the fovea and the corresponding higher cortical magnification of cone-mediated vision at the fovea is demonstrated by the results for the on-axis stimulus location respectively for both test conditions.

This data does not account for ocular dominance, with the result that the monocular data suggests there is no inherent difference between the two eyes. Furthermore, there is scope to combine the monocular data into a single data set. The result of doing this leads to monocular thresholds being ~1.8 and 1.9 times

higher respectively for the off- and on-axis RCS-R condition, and ~1.7 and 1.5 times higher respectively for the off- and on-axis RCS-R condition.

3.3.5.1 Does the data conform to a normal distribution?

The datasets for each stimulus location and for a combined off-axis data set were assessed for a normal distribution using the AD test. The results for the six test cases are provided in Table 3-4. All monocular off-axis datasets, individually and combined as a composite dataset, were consistent with a normal distribution. Some binocular and on-axis data were not normally distributed. However, these assessments of normality are limited by the power of the study, i.e. only having data for 11 participants after exclusion of the outlier, and are sensitive to outlier values and the spread of the data as illustrated in Figure 3-19 and Figure 3-20. Data for two binocular off-axis locations did not conform to a normal distribution:

- RCS-R stimulus at a meridian angle of 45° at the top right of the screen.
- RCS-C stimulus at a meridian angle of -135° at the bottom left of the screen.

For both cases, the asymmetric nature of the distributions caused by values at the extreme of the data sets contributes to the AD test result. The same effect also appears to be contributing to the AD test results for the binocular RCS-R on-axis and RCS-C on-axis stimulus viewed with the right eye. This could either be due to outliers or that the data is naturally skewed with these subsets being representative of the resulting distribution. The value of 0.0005 for the RCS-C binocular off-axis AD test result corresponds to the lowest p-value possible in the MATLAB implementation of the test.

Stimulus	*Viewing condition*	*-135 °*	*-45 °*	*45 °*	*135 °*	*Off-axis*	*On-axis*
RSC-R	Left eye	0.4391	0.1067	0.4127	0.6423	0.1485	0.7395
	Right eye	0.1017	0.1653	0.1410	0.8154	0.0594	0.6819
	Binocular	0.1776	0.9751	*0.0439	0.8758	0.0956	*0.0061
RCS-C	Left eye	0.6800	0.7071	0.8726	0.4237	0.5828	0.3136
	Right eye	0.5017	0.7460	0.7276	0.3925	0.7496	*0.0121
	Binocular	*0.0007	0.0669	0.1408	0.1803	*0.0005	0.7190

*Table 3-4: Anderson-Darling test outcomes (p-values) for the FMT values for the five target locations for the different viewing conditions. (*Cases where the p-value is less than or equal to the significance level of $\alpha = 0.05$ indicating the data are not normally distributed.)*

Additional analysis on the five exceptions, highlighted in bold in Table 3-4, was undertaken to confirm if they conformed to other distribution types by the application of a suitable transformation. This analysis determined that only the RCS-R binocular data for the 45° stimulus location conformed to a normal distribution after being transformed by a natural logarithm or a square root transformation with p-values given in Table 3-5. The only other positive result was that the right eye RCS-C on-axis FMT values conformed to a log normal distribution.

Stimulus	*Viewing condition*	*Location*	*Natural logarithm*	*Square Root*
RCS-R	Binocular	45°	0.0599	0.0535
		On-axis	*0.0346	*0.0149
RCS-C	Right eye	On-axis	0.0838	*0.0345
	Binocular	-135°	*0.0026	*0.0016
		Off-axis	*0.0005	*0.0005

*Table 3-5: Anderson-Darling test outcomes (p-values) for the test conditions previously shown not to conform to a normal distribution. (*Cases where the p-value is less than or equal to the significance level of $\alpha = 0.05$ indicating the data does are not normally distributed.)*

3.3.5.2 Can the off-axis data be considered a single composite dataset?

The means, medians and spread of the off-axis data are similar at each location for the three viewing conditions, as illustrated in Figure 3-19 and Figure 3-20. From this a hypothesis is proposed that the off-axis FMTs can be considered as a single composite dataset. The outcome of the AD test results in Table 3-4 support this hypothesis by indicating that the off-axis data are normally distributed. To test this hypothesis, a series of one-way ANOVAs were undertaken on the data for the six combinations of test and viewing condition to determine if any of the means for a single stimulus location were significantly different from the others between the stimulus locations. The results of these analyses are summarised in Table 3-6. The lack of a statistically significant result for the six ANOVAs confirms the principle that the off-axis stimuli can be considered as a single composite dataset for this experiment.

One-way ANOVA test	*F*	*p-value*
Left eye RCS-R off-axis FMTs	0.51	0.68
Right eye RCS-R off-axis FMTs	2.24	0.10
Binocular RCS-R off-axis FMTs	0.69	0.56
Left eye RCS-C off-axis FMTs	0.42	0.74
Right eye RCS-C off-axis FMTs	0.67	0.58
Binocular RCS-C off-axis FMTs	0.22	0.88

Table 3-6: One-way ANOVA for the off-axis FMTs for the six test conditions.

3.3.5.3 Binocular summation and ocular dominance metrics

The mean values of the three binocular summation metrics and the two ocular dominance metrics are plotted in Figure 3-22. In addition, the reference values of $\sqrt{0.5}$ and $\sqrt{2}$ are plotted, as dashed lines, to assist in the interpretation of the results. Whilst these values are only valid when both eyes can be described by the same means and variances, they do provide a reference against which the results can be compared and alternative models/contributions to the summation process can be assessed.

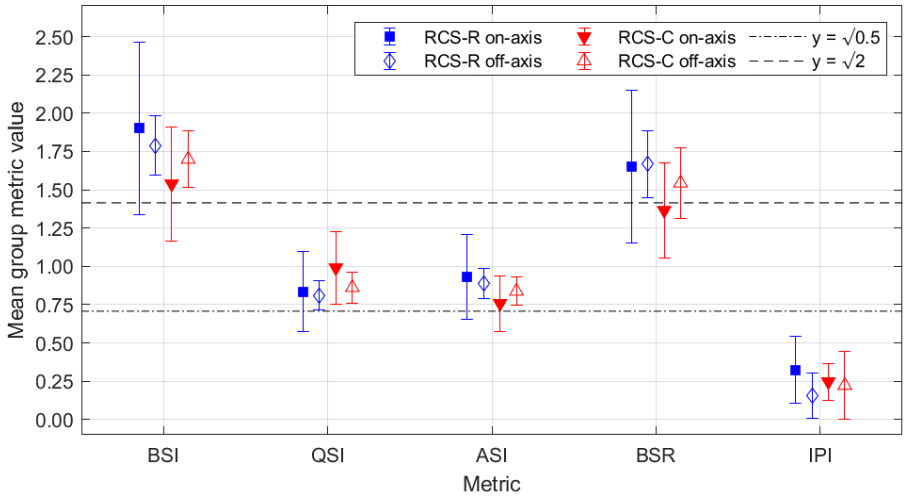

Figure 3-22: Summary of the binocular summation and ocular dominance metric results. Error bars equate to ±1 standard deviation. The three metrics of binocular summation (BSI - Binocular Summation Index; QSI – Quadratic Summation Index; ASI – Alternative Summation Index) and the two ocular dominance metrics (BSR – Binocular Summation Ratio; IPI – Interocular Percentage Increase) were previously defined in section 3.1.2.5.

The results of the summation metrics for the RCS-C on-axis condition show the greatest agreement with the √2 model for binocular summation. This is demonstrated by the closeness of the QSI metric value to its theoretical value of 1. The mean BSI and ASI metric values are also close to their respective theoretical values of √2 and √0.5 for a Monocular/Binocular Threshold Ratio (MTBR) value of √2. These results indicate that cone-mediated photopic vision at the fovea agrees with the probability based peripheral noise model described by Simpson *et al* (2009). However, the ocular dominance metrics for the mean RCS-C on-axis indicate that there is a difference between the two monocular thresholds, as illustrated by the IPI metric value of ~0.25. The BSR metric value of 1.37 is close to √2, the theoretical value for the peripheral noise model assuming equal monocular thresholds. The combination of the IPI and BSR metrics indicate that the monocular thresholds cannot be assumed to be equal and thus ocular dominance exists for photopic foveal vision.

For the off-axis stimuli, there are similarities between metric values for the RCS-R and RCS-C conditions. This makes sense as both conditions are stimulating the same area of the retina with cones contributing either partly or fully to the perception of the luminance modulation. For the BSI metric both values are higher than √2, whilst their QSI values are closer to √0.5. The corresponding ASI metric values are higher than √0.5. For all three metrics, the RCS-R and RCS-C off-axis values are between theoretical MBTR values of √2 and 2 that are based upon the assumption of equal monocular thresholds. The variation in the values of these three metrics, shown by the error bars, indicates greater consistency in the metric values across the cohort compared to the RCS-C on-axis results.

The BSR metric values for the RCS-R and RCS-C off-axis stimuli indicate that there is greater gain in sensitivity through the combination of monocular inputs for peripheral stimuli. This supports the higher MTBR values indicated by the other summation metrics. If it is assumed that the two monocular FMT values are equal, the MBTR value ranges between 1.75 to 1.79 for the three metrics. The IPI values indicate there is a relatively smaller difference between the two monocular RCS-R threshold values. The mean IPI

value for the RCS-R condition is ~10% lower than that for the RCS-C condition at ~25%. This supports the concept of greater enhancement in sensitivity being achieved from viewing the RCS-R peripheral stimuli binocularly compared to that observed in Figure 3-21 for the RCS-C on-axis case. Furthermore, it suggests that the summation process for peripheral stimuli potentially has a neural component in addition to the probabilistic summation contribution.

The results for the RCS-R on-axis condition show greater variability between the monocular values, illustrated by the higher mean IPI metric and the size of the error bars for the BSI and BSR metrics. This greater variability is thought to be the cause of the higher summation metric values that do not align with the theoretical MTBR value of $\sqrt{2}$. If the mean IPI metric was closer to zero, a case could be made for the MTBR value approaching a value of 2, but this is not the case. The results for the RCS-R on-axis condition highlight the variability of the response to this combination of stimulus background/location observed in the left-hand graph in Figure 3-21.

These variations in on-axis and off-axis summation processes are attributed to the different methods by which the two stimulus locations are viewed. Whilst foveal vision is predominantly cone-mediated at upper mesopic luminance values, like those used for the RCS-R condition, the rods surrounding the fovea are thought to contribute to the response to the on-axis stimulus. As a result of fixation eye movements, up to 20 arcmin, the resulting motion of the image of the 45 arcmin stimulus across the retina will ensure some rods are stimulated. The contribution of S cones is minimal based upon the results of the tritanope, Figure 3-12, whilst the chromaticity of the stimulus seeks to minimise the stimulation of L and M cones. For the off-axis stimulus, the increased density of rods results in a greater weight to the rod-mediated response to the RCS-R condition.

The differences in the summation metric values for the RCS-C on-axis and off-axis test cases suggests that there is a difference in the binocular summation for foveal and parafoveal stimuli. This is further supported by the similarity in the summation metric values for the off-axis RCS-R and RCS-C stimuli. The results indicate greater gain being applied to the monocular responses to off-axis, parafoveal stimuli when they are combined to provide binocular vision. The ocular dominance results also indicate greater weight is given to the eye with the lower threshold, i.e. the more sensitive eye in the process of binocular summation.

3.3.5.4 Prediction of ocular dominance

In addition to recording the FMT values for the RCS test, the participant's dominant (sighting) eye was recorded. Using this information, it was possible to determine how well monocular FMT values can predict ocular dominance.

The hypothesis that there is no difference in monocular FMT values between the two eyes was tested by undertaking a paired sample *t*-test on the data. The results, presented in Table 3-7, indicate that null hypothesis can be rejected for the RCS-R off-axis and RCS-C on-axis stimuli at a significance of $p < 0.05$. These two cases, where a statistically significant difference between the FMT values for the reported dominant and non-dominant eye, have been plotted in Figure 3-23.

Condition \ Location	On-axis	Off-axis
RCS-R	0.3225	*0.0354
RCS-C	*0.0401	0.1299

*Table 3-7: Results of paired t-test applied to assess the difference between monocular FMTs for dominant versus non-dominant eye. (*Results highlighted where p-value < 0.05.)*

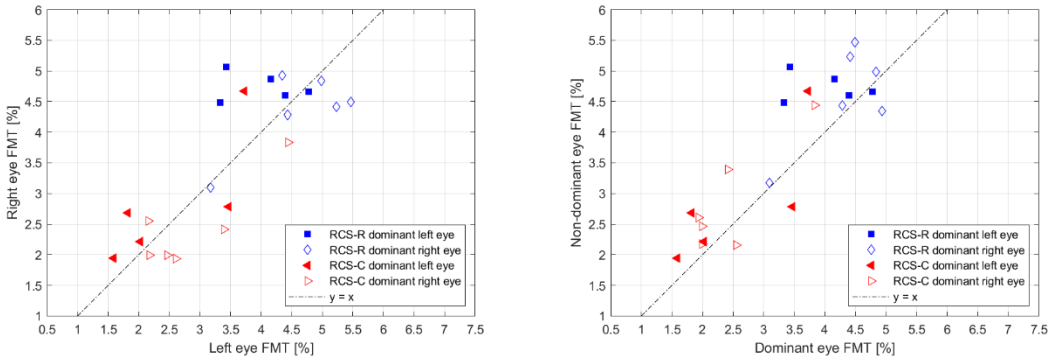

Figure 3-23: The monocular FMT values plotted against each other with the dominant eye highlighted (left). Replotting the same data with the non-dominant eye as a function of dominant eye (right).

The monocular FMT values were initially plotted against each other, as shown in the left-hand graph of Figure 3-23. Where the left eye has been recorded as the dominant eye, the mark is solid for both test conditions. Given the result of the paired *t*-tests there should only be solid markers in the region where y>x and open markers where y<x. When the data are replotted with the FMTs for the non-dominant eye plotted as a function of those for the dominant eye, right-hand graph of Figure 3-23, all but four of the 22 points are in the region where y>x.

The four exceptions to the model, for which y<x in the right-hand graph of Figure 3-23, are not the same pair of individuals but four different participants. Assuming that the same eye was dominant for both the RCS-R and RCS-C test conditions, and the dominant eye has the lower threshold, the four exceptions are likely to due to measurement error in the test. A higher or lower than expected value for one, or both, of the two monocular measurements would be enough to place the point below the line y = x.

With the support of the result of the paired sample *t*-tests and the 82% success rate for classifying the dominant eye, the eye with the higher FMT (least sensitive eye) has been plotted as a function of the lower FMT (most sensitive eye) separately for the on and off-axis stimuli and two background test conditions in Figure 3-24. A first order polynomial, Equation 22, was fitted to each set of data.

$$y = m\,x + c$$

Equation 22: First order polynomial

Based upon the distribution of the data and knowledge of the two quantities being plotted, it has been possible to define lower limits for the values of this polynomial's coefficients. The least sensitive eye's FMT values will be greater than or equal to the values for the most sensitive eye, such that we can state that $y \geq x$. On this basis, it is possible to define the following lower bounds when fitting the data to Equation 22 as: c = 0, and m = 1.

The resulting lines of best fit are plotted for each combination of stimulus condition and location in the subplots of Figure 3-24. The results can be separated into two relationships based upon stimulus location and test conditions.

For the on-axis stimuli the difference in FMTs for the two eyes increases as the FMTs of the most sensitivity eye increases. The rate of increase and the initial offset are different for the two stimulus conditions. The RCS-R condition has the greater offset but the lower rate of increase. When the two sets of data are combined into a single plot for on-axis stimuli, Figure 3-25, there appears to be agreement for a common relationship, as indicated by the R^2 value of > 0.91, with the gradient being the determining factor and only a small offset in FMTs of ~0.05%.

For the off-axis stimuli for both test conditions, there is a common relationship defined by a fixed offset having a broadly equivalent amplitude of ~0.6%. Combing the off-axis data for both stimulus conditions results in a higher R^2 value whilst the line of best fit is effectively unchanged, as illustrated in the right-hand graph of Figure 3-25. This joint result suggests that the off-axis ocular dominance offset is independent of stimulus condition.

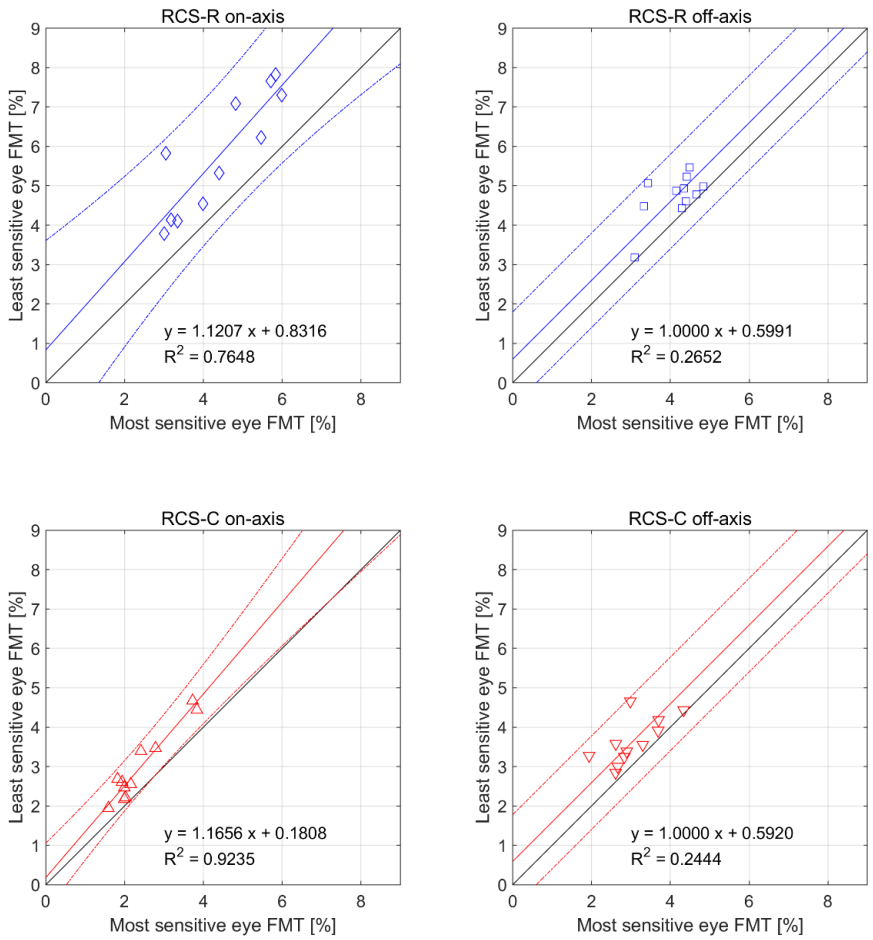

Figure 3-24: FMT values for the least sensitive eye plotted as a function of the FMT values for the most sensitive eye for the four combinations of test condition and stimulus location. Lines of best fit and R^2 values provided for each graph.

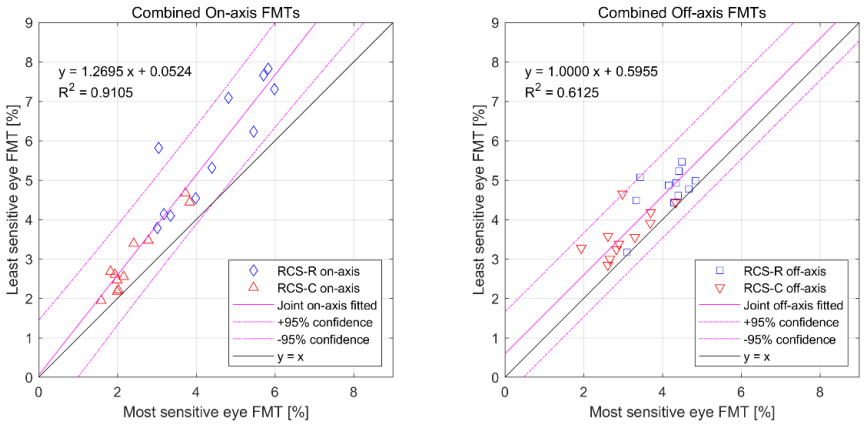

Figure 3-25: FMT values for the least sensitive eye plotted as a function of the FMTs for the most sensitive eye for the on-axis stimulus location (left) and the off-axis stimuli (right) for both test conditions. Lines of best fit based upon the combined set of data for both RCS-R and RCS-C test conditions.

3.3.6 Experiment 6 – Definition of RCS test Standard Normal Observer (SNO)

The primary aim of this experiment was to characterise the RCS test for a larger cohort with the objective of defining a SNO. The amendment to the RCS test software has resulted in two sets of data, which have been treated separately, but with the same analysis techniques applied, so that comparisons can be made. The two data sets are defined as:

- Cohort A corresponding to software version v0.102.4 (n = 78);
- Cohort B corresponding to software version v0.104.7 (n = 43).

It is assumed that the two cohorts were recruited randomly from the same population. Differences between the results for the two cohorts are either due to the cohorts being from different populations or due to the different test software or a function of both.

The initial analysis of the data has followed a similar methodology to that applied in section 3.3.5 with the aim of identifying and excluding outliers prior to the definition of the mean FMT as a function of stimulus location and test condition for the two cohorts.

The raw data for both cohorts are plotted in Figure 3-26 and Figure 3-27 as a function of stimulus location, respectively, for the two test conditions. In addition to the data, the mean value ± 2.5 standard deviations have been plotted for each stimulus as a reference bound between which 98.8% of the data should lie for a normal distribution.

To account for the different sizes of the two cohorts, the number of participants has been normalised to allow comparison of the two datasets on a common basis. From Figure 3-26 the differences between the two cohorts can be seen in the on-axis RCS-R FMT values, with cohort B having the greater range in values. The medians for the RCS-R on-axis condition are similar with values of 2.85% and 2.81% for cohorts A and B respectively. For the off-axis stimuli the difference is greater, with cohort B having a greater spread between the individual stimulus locations. The range of the off-axis FMT values are greater for cohort B by at least 0.60%.

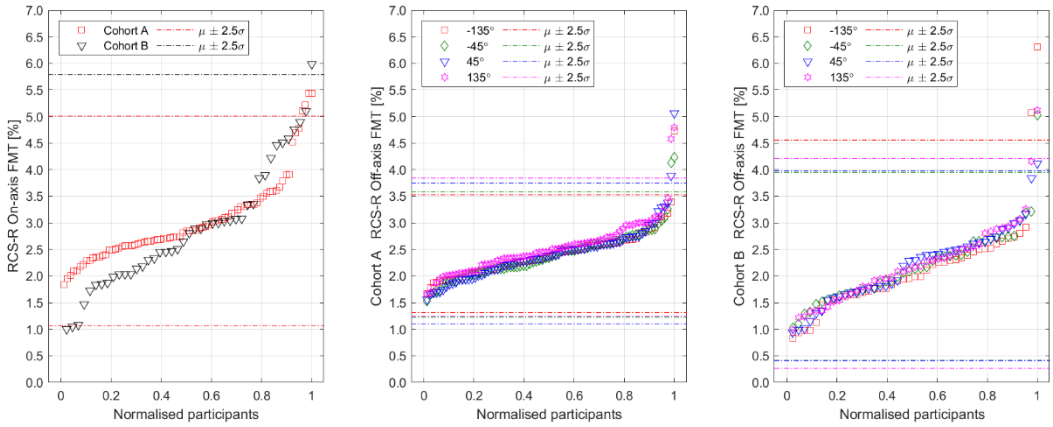

Figure 3-26: The RCS-R raw data for the two cohorts plotted based upon stimulus location. Comparison of on-axis RCS-R FMT values for both cohorts (left); RCS-R off-axis FMT values for cohort A (middle); and RCS-R off-axis FMT values for cohort B (right).

For the RCS-C test condition, Figure 3-27, there is greater agreement between the two cohorts, with the difference between the median values for the two cohorts being less than or equal to 0.10% for the off-axis stimulus locations. For the on-axis stimulus, the difference between the two cohorts is 0.11%, but there is close agreement between the ranges of the two sets of data. Similarly, the range of values for the off-axis RCS-C stimuli are closely matched.

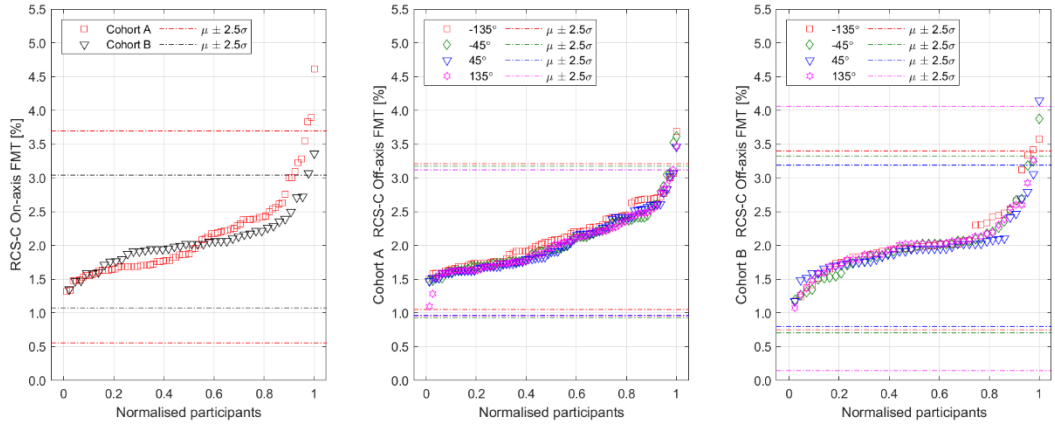

Figure 3-27: The RCS-C raw data for the two cohorts plotted based upon stimulus location. Comparison of on-axis RCS-C FMT values for both cohorts (left); RCS-C off-axis FMT values for cohort A (middle); and RCS-C off-axis FMT values for cohort B (right).

Those participants whose FMT values were beyond the initial bound of the mean $\pm$ 2.5 standard deviations were excluded. This resulted in the exclusion of seven and five participants from cohorts A and B respectively. The data were replotted to determine if any participants fell outside the revised mean $\pm$ 3.5 standard deviations. No further outliers were identified. The resulting in the sizes of cohorts A and B were 71 and 38, respectively.

Comparing the mean RCS test results for the two cohorts after exclusion of outliers, plotted in Figure 3-28, there are similarities between the two cohorts in the FMTs measured for the RCS-C test condition. The RCS-C off-axis FMT values for cohort A have a mean of 2.01%, whilst those for cohort B equate to 1.92%. The on-axis RCS-C FMT values are 2.00% and 1.99% for cohorts A and B.

In contrast, the RCS-R threshold values are different for the off-axis stimuli, with cohort A having the higher mean off-axis RCS-R FMT value of 2.38% compared to 2.03% for cohort B. The on-axis RCS-R FMT values were 2.90% and 2.83% respectively for cohorts A and B.

The error bars for the RCS-R on-axis FMTs are larger for cohort B when compared to cohort A. These comparative properties are also observed in Figure 3-14 in section 3.3.4.

Relating these results back to the software version, although the initial indication from Experiment 4, section 3.3.4, defined that there was not a significant difference between the results for the two software versions, there is some variation in the test results for the RCS-R stimulus condition. The increased S/P value of the RCS-R stimulus condition has resulted in lower off-axis FMT values, whilst the variance of the on-axis RCS-R stimulus has increased. Overall, the RCS-C results are comparable but the subtle change in the RCS-C stimulus condition, i.e. the decreased S/P value, has resulted in a lower FMT being recorded.

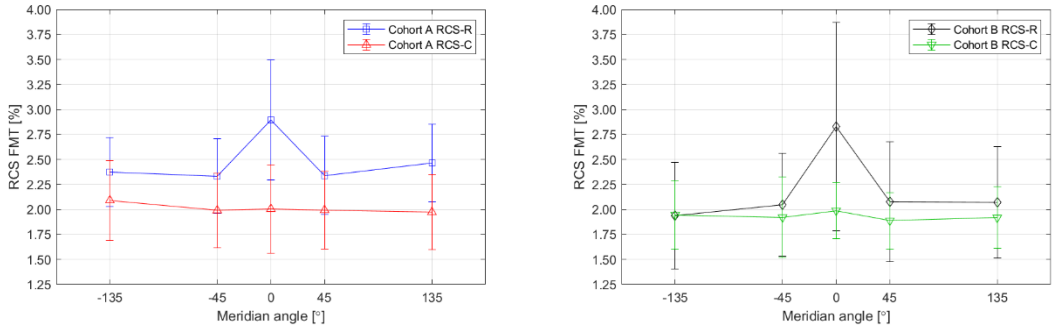

Figure 3-28: Summary plot of the FMT values for the two cohorts showing the mean FMT for each stimulus location with error bars equal to 1 standard deviation.

3.3.6.1 Do the data conform to a normal distribution?

The off-axis RCS-R data for cohort A do conform to a normal distribution, as indicated by the results of undertaking an AD test for each stimulus location, as shown in Table 3-8. The RCS-R on-axis data for cohort A conforms to a lognormal distribution as indicated by an AD test (p=0.2403). The data for the RCS-C at all stimulus locations, for cohort A, does not conform to a normal distribution, even when transformed by a log or square root transformation, see Table 3-9 and Table 3-10.

The RCS-R data for cohort B does conform to a normal distribution, for all test locations, as indicated by the application of an AD test. For the RCS-C stimulus locations, only the on-axis and -135° stimulus locations were indicated to conform to a normal distribution. The other stimulus locations for the RCS-C condition for this cohort did not conform, even when alternative transformations were applied, see Table 3-9 and Table 3-10.

Cohort	Test Condition	Stimulus location				
		-135°	-45°	On-axis	45°	135°
A	RCS-R	0.4282	0.4158	*0.0017	0.5074	0.4353
	RCS-C	*0.0005	*0.0005	*0.0005	*0.0005	*0.0020
B	RCS-R	0.3512	0.4331	0.0763	0.1255	0.6338
	RCS-C	0.0609	*0.0198	0.2201	*0.0144	*0.0154

*Table 3-8: Results of applying the AD test for the null hypothesis that the data is from a normal distribution. (*P-values correspond to where the null hypothesis has been rejected at the 5% significance level.)*

Cohort	Test Condition	Stimulus location				
		-135°	-45°	On-axis	45°	135°
A	RCS-R	-	-	0.2403	-	-
A	RCS-C	*0.0048	*0.0042	*0.0014	*0.0005	*0.0155
B	RCS-R	-	-	0.5878	-	-
B	RCS-C	-	*0.0248	-	*0.0303	*0.0011

*Table 3-9: Results of applying the AD test for the null hypothesis that the data is from a log normal distribution. (*P-values correspond to where the null hypothesis has been rejected at the 5% significance level.) Blank entries correspond to stimuli where the AD test has indicated that the data conforms to a normal distribution.*

Cohort	Test Condition	Stimulus location				
		-135°	-45°	On-axis	45°	135°
A	RCS-C	*0.0015	*0.0012	*0.0005	*0.0005	*0.0069
B	RCS-C	-	*0.0347	-	*0.0265	*0.0051

*Table 3-10: Results of applying the AD test for the null hypothesis that the data once transformed by a square root transformation is from a normal distribution. (*P-values in bold correspond to where the null hypothesis has been rejected at the 5% significance level.) Blank entries correspond to stimuli where the AD test has previously indicated that the data conforms to a normal distribution.*

Box plots of the data give an indication as to the reason why the RCS-C test condition for both cohorts do not conform to a normal distribution as determined by the AD test results. The distributions of the FMT values for the RCS-C stimuli are skewed, which is evident in spread of the data in Figure 3-27 and Figure 3-29. This is most evident for the box plot of the RCS-C data for cohort A. The result for cohort A is also seen in cohort B by the number of points defined as outliers by MATLAB's box plot function, shown as red +'s in the box plots. These points correspond to the data that fall outside the whiskers at ± 1.5 times the interquartile range given by the blue boxes in the plots.

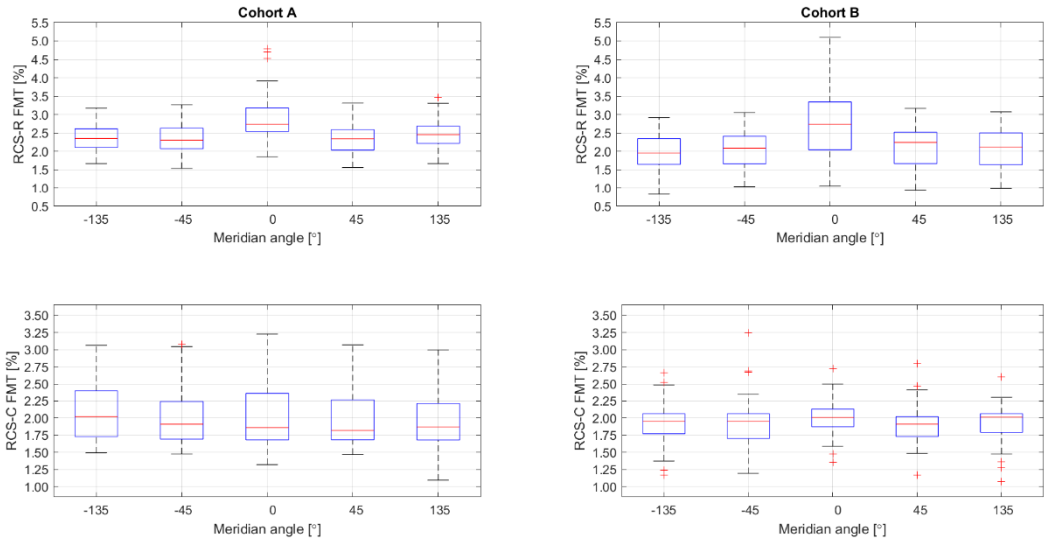

Figure 3-29: Box plots for the RCS-R (top row) and RCS-C (bottom row) test conditions and the two cohorts A (left) and B (right).

The positive skewness of the FMT values is likely to be due limits defined by physics and biology of the visual system. These limits will contribute to the definition of a minimum value for the corresponding FMTs. Confounding influences such as fatigue, inattention and lack of training can result in higher thresholds being measured by the test.

3.3.6.2 Do the data support the generation of a single off-axis FMT value?

With the increased power of the larger cohorts, it is feasible to retest the hypothesis that it is justifiable to combine the off-axis FMT values into a single off-axis FMT value equivalent to the mean off-axis FMT, for each test condition, for the two cohorts.

To test this hypothesis a one-way ANOVA was undertaken for the two test conditions. The results of these analyses are provided in Table 3-11. For each test location the overall result is that no off-axis stimulus location had means that were significantly different. The lack of a significant difference between off-axis stimulus locations reinforces the appearance of the data presented in Figure 3-29 and the results from the other experiments, see section 3.3.5.2. So for young, normal participants the off-axis FMT values for both the RCS-R and RCS-C test conditions can each be summarised by a single off-axis value. The implication is that each peripheral retinal test location exhibits the same sensitivity to these stimuli.

Cohort	Test condition	F	P value
A	RCS-R off-axis	1.75	0.16
A	RCS-C off-axis	1.37	0.25
B	RCS-R off-axis	0.52	0.67
B	RCS-C off-axis	0.19	0.90

Table 3-11: One-way ANOVA for the off-axis FMT values for both test conditions and cohorts.

3.3.6.3 *Evaluate RCS FMT as a function of age for the two cohorts*

The analysis of RCS test FMT values as a function of age is limited by the age distribution of the two cohorts, illustrated in Figure 3-30, and can be summarised by the mean and standard deviation of the two cohorts provided below:

A. 20.76 ± 2.36 years.

B. 19.59 ± 1.85 years.

The age distribution of participants for the two cohorts are a sample of the demographic of SHS students which is naturally biased towards the age group from 18 to 21 years. As a result, the age distribution of the two cohorts limits the validity of fitting of a linear function to model the variation of FMTs, as a function of age, due to the small number of participants above 21 years old. Based upon the histogram, the age distribution of cohort B is more tightly constrained than cohort A.

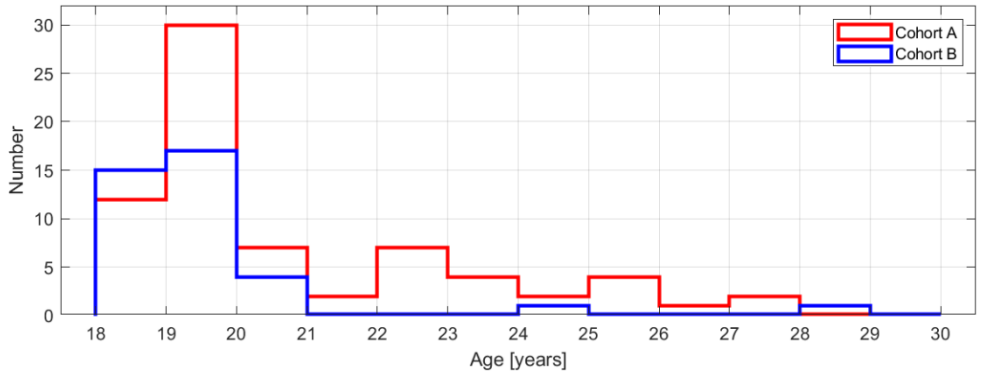

Figure 3-30: Histogram of the age distribution for the two cohorts: cohort A n=71; cohort B n = 38.

As a result of the age distributions of the two cohorts, the FMTs for the two test conditions must be viewed in the knowledge that the variation in threshold will be biased by the few older observers, who may not be representative of all older viewers.

For cohort A, plotted in Figure 3-31, the RCS-R data indicates both the on and off-axis FMTs increase as a function of age, with a greater increase predicted for the on-axis stimulus location. There is a smaller increase with age predicted to be 0.17% over 10 years for the off-axis stimuli based upon this young cohort. The lines of best fit for the RCS-C data both indicate FMTs decrease as a function of age which is a result of the lower thresholds of the older participants. As predicted, the decreasing number of participants as a function of age, for cohort A, has influenced the direction of the fitted trendline. There is an increase in FMT values for the RCS-R test condition, while RCS-C FMTs values are lower for the three participants above 26 years old resulting in the downward bias to the trendline.

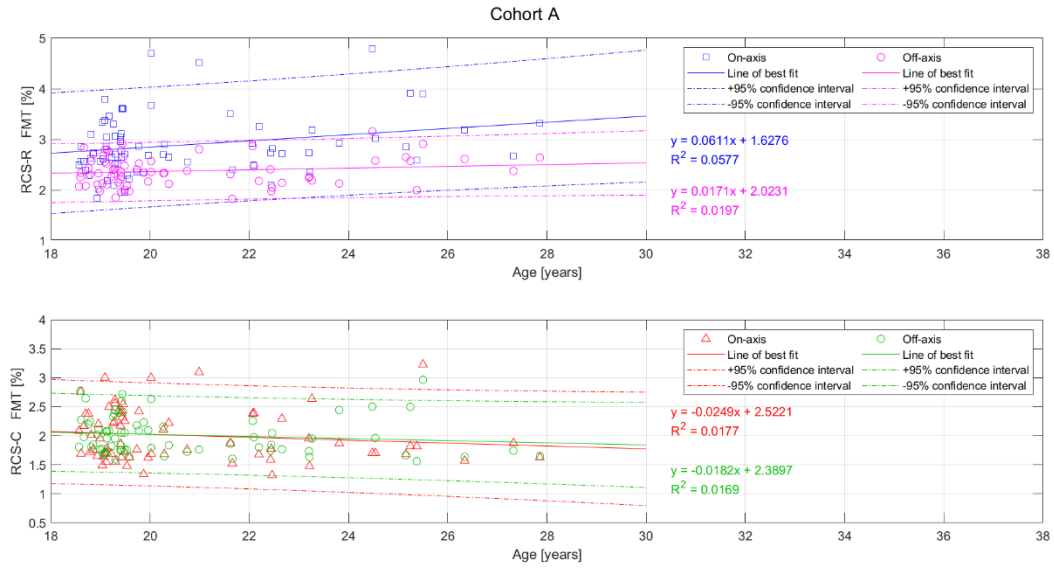

Figure 3-31: RCS FMTs as a function of age for cohort A for the on-axis and mean off-axis FMTs.

Cohort B's RCS FMT values as a function of age, plotted in Figure 3-32, are more biased by the FMTs for the two participants above the age of 24 years old. The on-axis RCS-R FMTs increase with a prediction of 0.39% over 10 years whilst the off-axis FMTs effectively do not change as a function of age. In contrast, the RCS-C results show an increase of 0.40% over 10 years which is biased by the two individuals aged above 24 years. As predicted, the skewed age distribution of cohort B prevents a reliable model for RCS FMTs as a function of age to be formulated.

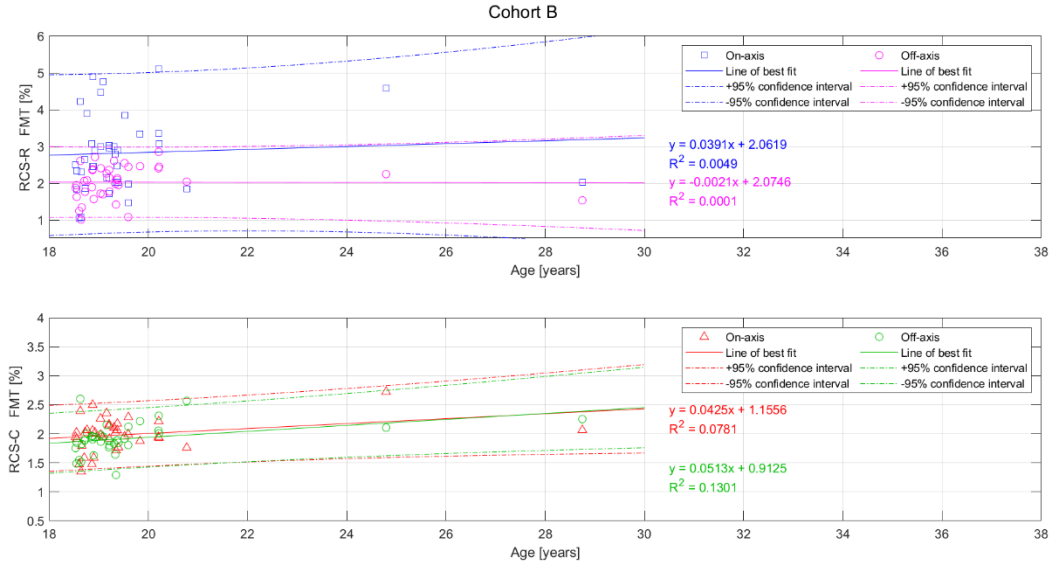

Figure 3-32: RCS FMTs as a function of age for cohort B for the on-axis and mean off-axis FMTs.

Given that the test protocols, defined by the two versions of the RCS tests software, are effectively measuring the same quantity, albeit with different participants, there should be a similar trend to the two sets of results. However, there are too few older participants for meaningful conclusions to be made.

The expected outcome, based upon outcomes of a similar study (Hathibelagal *et al* 2020), is that RCS thresholds are largely age invariant below 45 years of age, increasing rapidly above this age.

3.3.6.4 Standard Normal Observer (SNO)

The RCS-R data were normally distributed in both cohorts, and thus for both versions of the software. The parameters that describe the normal distribution in terms of the mean and lower and upper bounds equal to the mean ± 2 standard deviations ($\mu \pm 2\sigma$) are provided for the on-axis and off-axis FMTs in Table 3-12.

However, the results for the RCS-C test condition need to be considered in terms of the median and a percentile range, which aligns with the method used by Rodriguez-Carmona *et al*. (2005) and Barbur *et al*. (2006) when specifying the SNO for the CAD test. The CAD test SNO is centred on the median value, with limits set at 2.5% and 97.5% of the overall population. Applying this methodology to the RCS-C test results, the RCS-C SNO for the two cohorts are defined in Table 3-13. These values for the RCS test SNO for both versions of the software are based upon the assumption that all participants in the two cohorts are representative of normal observers.

Software version	Cohort	RCS-R Stimulus	Normal distribution		
			$\mu - 2\sigma$	μ	$\mu + 2\sigma$
v0.102.4	A	On-axis	0.40	2.84	5.27
		Off-axis	1.80	2.38	2.95
v0.102.7	B	On-axis	0.75	2.83	4.91
		Off-axis	1.12	2.03	2.95

Table 3-12: Definition of the RCS-R SNO for the two versions of the RCS test software (v0.102.4 and v0.102.7) based upon the results for cohorts A and B.

Software version	Cohort	RCS-C Stimulus	Percentiles		
			2.5^{th}	50^{th}	97.5^{th}
v0.102.4	A	On-axis	1.38	1.86	3.07
		Off-axis	1.59	1.95	2.76
v0.102.7	B	On-axis	1.41	2.01	2.62
		Off-axis	1.38	1.89	2.59

Table 3-13: Definition of the RCS-C SNO for the two versions of the RCS test software (v0.102.4 and v0.102.7) based upon the results for cohorts A and B.

The underlying distributions for the two versions of the test protocol, that define these two SNOs, have been compared using paired *t*-tests for the RCS-R condition and a Wilcoxon signed-rank test for the RCS-C condition. The results of these statistical tests are summarised in Table 3-14. The on-axis RCS-R condition was transformed to a log normal distribution for both protocols based upon the results of the AD tests in Table 3-9. The results of these tests show that there is a statically significant difference between the RCS-R off-axis FMTs for the two test protocols. There is no statistically significant difference between the FMTs for the on-axis RCS-R test protocol, nor is there between the two variants of the RCS-C condition.

Stimulus condition	Stimulus location (meridian angle)				
	-135°	-45°	0°	45°	135°
RCS-R	*<0.0001	*0.0012	0.1967	*0.0070	*<0.0001
RCS-C	0.2394	0.5735	0.5693	0.5104	0.8164

*Table 3-14: Summary of the significance tests applied to the data for the two test protocols. (*P-values correspond to where the null hypothesis has been rejected at the 5% significance level.)*

The result of this analysis is that the RCS-R test FMT results for the two versions of the test software cannot be combined into a single cohort, but it is possible to combine the FMTs for the RCS-C condition into a single cohort. This demonstrates the nature of the differences in the two test protocols and how they differentially affect the measured FMTs. Whilst the RCS-C condition has not been significantly affected, the RCS-R condition has resulted in a change in the magnitude of the response to the revised chromaticity.

3.4 Discussion

3.4.1 Test protocol

A new test protocol has been defined and applied to characterise monocular and binocular FMTs. Using a pre-test adaptation time of 2 minutes, it has been possible to measure FMTs of a rod-mediated response when the test is undertaken in a darkened room with ambient illumination of 100mlux. The ability of the test to instigate a rod-mediated response has been assessed by measuring the FMTs of a rod monochromat and a tritanope.

The diameter and background luminance of the stimuli were defined by locating the point at which a small change in stimulus size had an increased effect on measured FMT for the stimulus condition. This minimised the variance of the FMTs whilst providing a test that should be suitably challenging for participants whose vision does not align to that of a SNO. Whilst data have been gathered to define the basis for a SNO, future experimentation should support the definition of the variation of the SNO as a function of age. Although initial work has been undertaken on this task using the latest version of the test protocol (Hathibelagal *et al* 2020), further work is required.

The similarity of the FMT values recorded for both off-axis and on-axis RCS-C stimuli is attributed to the diameter of the two stimuli being matched to the change in cone photoreceptor density as a function of eccentricity (Curcio *et al* 1990).

The results of the experiments undertaken confirmed the hypothesis that the RCS test enables quantitative assessment of rod and cone-mediated vision. These experiments have also demonstrated the functionality of the RCS test for assessing the sensitivity of both monocular and binocular vision.

3.4.2 RCS-R FMTs are mediated by rods

Comparing the RCS-R FMT values of the rod monochromat, tritanope and normal trichromats all contain a rod-mediated response, however there are also contributions jointly from L and M cones as well as S cones to the perception of the flickering stimuli as visual function increases for the participants. When comparing to the trichromats, the tritanope's lack of S cones appears to compromise sensitivity, although

there has been no accounting for reduction in sensitivity as a function of age (Hathibelagal *et al* 2020). The results of the rod monochromat to both tests conditions demonstrate the RCS-R condition stimulates a greater rod-mediated response than the RCS-C test. This is attributed to the chromaticity of the stimulus and its increased S/P ratio. Likewise, it is evident that the RCS-C condition primarily instigates a cone-mediated response. The results for the rod monochromat for the RCS-C condition indicate that there is some small contribution from rod-mediated vision to the perception of the flickering stimulus albeit not very sensitive.

The higher FMTs for the RCS-R on-axis stimulus, compared to those of the four off-axis stimuli located at 5° eccentricity, is attributed to the lack of rod photoreceptors in the very central region of the fovea (Curcio *et al* 1990) and the reduced sensitivity of cones to the RCS-R stimulus condition with its higher S/P ratio. The data suggest that the RCS-R on-axis stimulus is detected, at least in part, by rods since the stimulus size exceeds the rod free region when fixation instabilities are considered. The result is further supported by the greater variance observed for the RCS-R on-axis FMT values for the revised test compared to the original protocol. As demonstrated in Figure 3-14 and Figure 3-28, the higher S/P ratio of the revised test protocol, defined in Table 3-2, results in greater stimulation of rods. This gives rise to a wider, flatter distribution of on-axis FMT values for the revised test protocol. The effect of increasing the S/P ratio results in a higher scotopic luminance for the same photopic luminance with the change in the spectral properties of the light increasing the likelihood of a rod-mediated compared to a cone-mediated response. The smaller diameter of the on-axis stimulus, half that of the off-axis stimulus will also result in a higher threshold for a rod-mediated response at the on-axis stimulus location due to the reduced corneal flux compared to the larger off-axis stimuli.

Reflecting on the results, a simple test that could be undertaken would be to use the chromaticity values of the RCS-C condition whilst retaining the dimensions of the RCS-R protocol's stimuli at the background luminance of 0.5cd.m^{-2}. Using the RCS-C condition chromaticity at 0.5cd.m^{-2} corrects for the bias of the higher S/P value for the RCS-R condition. This would help to provide further evidence for a rod-mediated response to the RCS-R condition as the expectation is that the FMT values for all stimuli should be higher than those measured for the corresponding RCS-R condition. It would also help to quantify the cone-mediated contribution to the FMT values.

The increase in S/P for the revised test protocol results in lower rod-mediated thresholds as the effective scotopic (Sc) luminance is higher, i.e. 4.5Sc cd.m^{-2} compared to 4.0Sc cd.m^{-2} for the original test protocol based upon the photopic luminance of 0.5cd.m^{-2}.

Additionally, if a pure cone mediated response had been instigated for the RCS-R on-axis stimulus, then it would be expected that the results of the binocular summation metrics for the two on-axis stimulus conditions would have shown greater agreement. Instead, the metric results were either aligned with or greater than the RCS-R off-axis metric values.

The results from Experiment 2, section 3.3.2, and the observed changes in the FMT recorded for the two versions of the RCS test protocol, section 3.3.6, indicate that the hypothesis that the RCS-R test condition

excites a rod-mediated response is true. The response is not wholly rod-mediated but is augmented by a contribution from cones.

To confirm that the hypothesis is true and determine the contribution of cones to the perception of the RCS-R stimulus, a study has been devised which uses the autonomic nature of the pupil light response to characterise the primary photoreceptor mediating the response. This proposed study forms the basis of Experiment 8, the results of which are reported in section 4.3.2.

3.4.3 Changes in test protocol

Although this study had to be reactive to the change in the software, and the associated change in the test protocol, the resulting evaluations have characterised and compared the effects of these changes on the FMT values recorded. As a result, it has been possible to demonstrate for the cohorts tested that the two protocols give similar mean binocular FMT values for the RCS-C condition, which remained largely unchanged. This is not surprising given that the main change to the RCS-C condition was a 2 $cd.m^{-2}$ reduction in RCS-C background luminance and a small change in its chromaticity to reduce the scotopic component from a S/P value of 1 to 0.9.

Whilst there are overlaps in the definition of the SNO for the two protocols for cone-mediated vision, there are differences between the two protocols that preclude the data for rod-mediated vision being combined into a single data set. These differences in protocol relate to the chromaticity and S/P ratio of the background condition that have been attributed to the statistically significant differences for the RCS-R off-axis stimulus locations. The revised RCS-R protocol's higher S/P resulted in the reduction in the mean FMT and a wider spread to the distribution of the data. In contrast, the relatively small shift in the colorimetry of the RCS-C stimulus for the revised protocol has had negligible effect on the RCS-C FMT values recorded.

The result is that the software update has altered the sensitivity to the RCS-R test stimuli and the associated hypothesis, that the unavoidable changes in the definition of the test protocol did not significantly influence FMT values, is not supported for the RCS-R condition. For the RCS-C condition, the hypothesis is supported by the results of the summarised in Table 3-14 showing there is not a statistically significant difference.

Further work, potentially with a larger cohort, would be required to develop a mapping function which can transform the results for software version v0.102.4 to those of version v0.102.7 if version v0.102.4 is to be used in future studies. However, given the reason for the software update was driven by changes made by the monitor manufacturer, it is likely that v0.102.7 will be used for future studies.

3.4.4 Definition of a Standard Normal Observer (SNO)

To facilitate future studies using the RCS test, a SNO has been defined for both test protocols. Although there are similarities in the values, there are differences in the distributions of the results between protocols and stimulus conditions such that:

a) RCS-R off-axis FMTs conform to a normal distribution;
b) RCS-R on-axis FMTs conform to a log normal distribution;

c) RCS-C on and off-axis FMTs do not conform to a normal distribution and a suitable transform has not been identified that will enable the values to be mapped to a normal distribution;
d) As a result, RCS-C FMTs have been defined in terms of median and 5^{th} and 95^{th} percentiles.

The fact that the FMTs for cone-mediated vision need to be described in non-parametric terms agrees with the basis of the model used by the CAD test used to determine chromatic thresholds (Rodriguez-Carmona *et al* 2005, Barbur *et al* 2006). The agreement with another test used to measure a similar effect in the same photoreceptor type gives support to the validation of the function of the RCS-C condition and the RCS test itself. This is not a surprising outcome as the two tests have used a similar methodology when defining their test protocols (Rodriguez-Carmona 2006).

The differences in the statistical properties of the RCS-R on- and off-axis stimuli is thought to be related to the method by which the two stimuli are detected. For the on-axis stimulus, the contribution of cones is likely to be significant. As the stimulus eccentricity increases the contribution of rod-mediate response is thought to be greater as cone density decreases and rod density increases. This is demonstrated by comparing the off-axis FMTs for the rod monochromat, tritanope and the normal trichromats to their on-axis FMT values. There is less of a differential between the off-axis FMTs when compared to the on-axis FMTs for these three levels of visual function.

For the small sample size, and limited age range investigated in this study, there is no significant difference in FMTs, measured using the RCS test, for a cohort of young normals. Defining the effect of age using the RCS test in this study has been addressed separately as part of a separate study (Hathibelagal *et al* 2020) that demonstrated a change in rod-mediated FMTs, measured using the RCS test, above the age of 45 years in agreement with previous studies (Jackson *et al* 1999, Curcio *et al* 1993).

3.4.5 Binocular summation and ocular dominance

The revised protocol, v0.104.7 of the RCS test, was used to evaluate how FMT values measured monocularly and binocularly correspond by evaluating three different metrics for binocular summation. The results have been used to determine the MBTR for cone and rod-mediated vision and on-axis and off-axis visual function. The outcome of the analysis is that whilst FMTs for both rod and cone-mediated vision can be modelled by quadratic summation of monocular thresholds, in agreement with probability summation, the MBTR is different depending on stimulus location.

The cohort's mean MBTR values were $\sqrt{2}$ for cone-mediated on-axis (foveal) FMTs. The on-axis value directly matches the value reported in the literature (Legge 1984, Baker *et al* 2018, Barrett *et al* 2013). For off-axis (parafoveal) stimuli, the mean MBTR increased ~1.77 or $1.25\sqrt{2}$. This off-axis results also aligns with the literature for similarly sized stimuli (Wood *et al* 1992). The 1° and 1.5° stimulus diameters for the RCS-C and RCS-R conditions are between the size III (0.431°) and V (1.724°) targets used by Woods.

Whilst the spread of results across the cohort have been quite wide, for the RCS-R on-axis metric values this appears to be mainly due to the nature of the results for the test condition and stimulus location. Off-axis summation metric values for the RCS-C and RCS-R conditions show less variance yet were recorded by the same individuals.

The results of the QSI model have demonstrated the closest agreement across the small cohort (n=11) of young normals as a method of combining monocular FMTs to predict the binocular FMT value for the off-axis RCS-R and both on and off-axis RCS-C stimulus locations. Based upon these results, the indications are that the hypothesis is correct and monocular RCS FMTs can be used to predict binocular FMTs.

The ASI metric provided an additional metric by which to assess the variation in binocular summation across the fovea and parafoveal regions of the retina. However, the metric did not show the same level of agreement that the QSI demonstrated. This indicates that the pixel capacitance-based model of binocular summation, proposed by the author, does not directly fit the results.

The BSR metric was higher for parafoveal, off-axis, stimuli compared to the foveal, on-axis stimulus, which is in agreement with the findings of Gillespie-Gallery *et al* (2013). However, the BSR values measured in this study for the parafoveal stimuli are higher than those reported by Gillespie-Gallery *et al*, but this could be due to the different tests employed. Gillespie-Gallery *et al* used the AVOT Function Contrast Sensitivity test that was designed to assess spatial vision (i.e., visual acuity and functional contrast sensitivity).

Additionally, there is the statistically significant result that the lower monocular FMT value is aligned to the dominant eye for the RCS-C on-axis and RCS-R off-axis test stimuli. This supports the hypothesis that monocular FMTs can be used to predict ocular dominance and agrees with the wider literature.

From analysis of the thresholds for the less sensitive (non-dominant) eye as a function of those of the more sensitive (dominant) eye, the results indicate two mechanism by which thresholds can be predicted for on-axis and off-axis stimuli. For on-axis stimuli, the FMTs for the less sensitive eye can be described by a scalar multiple of the FMTs for the most sensitive eye. In contrast, for the RCS test's off-axis stimuli, the FMTs of the less sensitive eye can be predicted by a shift or offset of ~0.6% applied to the FMTs of the more sensitive eye. The offset distribution of the off-axis FMT data, shown in Figure 3-24 and Figure 3-25 mimics the form of the relationship reported by Suttle *et al* (2009) for contrast sensitivity.

The apparent dependency on the region of the retina being stimulated, coupled with the differences in MBTR, suggest that there are different summation processes occurring in the fovea and parafoveal areas. The results suggest that signals from the central retina agree better with probability summation, whilst those from the periphery have an additional neural component.

Binocular summation is a complex field, and as this study has highlighted, there are many questions yet to be answered with regards to the underlying mechanisms and the involvement of neural components in addition to the underlying probability-based models.

3.4.6 A single metric for parafoveal photoreceptor sensitivity

Although there is expected to be some variation in the values of the off-axis FMTs for both test conditions for a single participant, as demonstrated in Figure 3-14, statistical analysis of the results for the three main cohorts within the study confirm that there is not a statistically significant difference in the FMTs for the off-axis stimuli. This has allowed the pooling of the off-axis FMTs into a single off-axis FMT metric with the aim of simplifying the reporting of FMTs for the RCS test.

The findings of this study are consistent with the topography of the human retina being reasonably symmetrical for both rods and cones to beyond the parafovea. The asymmetric differences between nasal and temporal, and inferior and superior sections of the retina (Curcio *et al* 1990) primarily relate to eccentricities beyond those assessed in this study. Any variation in sensitivity as a function of stimulus eccentricity is likely to have more of an impact for the monocular FMTs from Experiment 5, section 3.3.5, where both monocular and binocular FMTs were recorded. It would then be expected that the variation in topography would be visible in the mean results of the cohort. This is not the case. There is some variation between stimulus locations, but this appears to be as a function of the spread of the FMTs for each stimulus location.

Test sensitivity can potentially be improved by increasing the number of presentations whilst restricting the number of reversals from which the threshold is calculated, such that the variation between reversal points is minimised. The disadvantage of this approach is that it could make for a lengthy test with an increased risk of test fatigue.

In Figure 3-14 it has been shown that with multiple repetitions of the test, a more accurate measure of a participant's thresholds can be obtained, but this again requires time to undertake the tests. As ever, there is a balance that needs to be maintained between time and effort. It has been shown that pooling of the off-axis FMT values for the four stimuli at 5° eccentricity located at meridian angles of ±45° and ±135° can be achieved and that the four stimulus locations have similar statistical properties. The hypothesis that the RCS FMTs for the four (off-axis) stimuli at 5° eccentricity can be combined into a single metric of parafoveal photoreceptor sensitivity is supported by the outcomes of this study.

3.4.7 Pre-test adaptation time

Focusing on the FMT values for the off-axis RCS-R condition, increasing the pre-test adaptation time does not lead to a decrease in the measured thresholds. Unlike tests which seek to determine the sensitivity of rod-mediated scotopic vision, this test is undertaken at light levels that are equivalent to upper mesopic visual function. As a result, the degree of adaptation to the light level is minimised and once adapted, it is not expected that there would be any further change in FMTs recorded.

If repeating the RCS-R test at a lower luminance, for example 0.05cd.m^{-2}, the pre-test adaptation time takes on greater importance in achieving stable FMTs. At lower adaptation luminance values, the FMTs and associated variability would both be higher as indicated by the initial testing undertaken to define the properties of the stimulus conditions.

3.4.8 Exclusion methodology

The method of excluding outlier data was reliant upon the data conforming to a normal distribution, which has been demonstrated through application of the AD test for the off-axis RCS-R test condition. The main aim of the exclusion methodology was to remove outliers without significantly affecting the overall population. This has been demonstrated in Figure 3-17 and Figure 3-18. As demonstrated in Figure 3-29, the technique is broadly equivalent to the limits in terms of median and inter-quartile ranges. Where there is a difference, the applied exclusion limits allow outliers that are beyond the whiskers of MATLAB's

box-plot function. This mainly occurred for data associated with the revised RCS-C test protocol, where the AD test has demonstrated that the distribution does not conform to a normal distribution even when log and square root transformations are applied. On this basis, the exclusion technique provides a good basis for defining RCS test data that is outside expected limits for the test.

3.4.9 Test reproducibility

Apart from Experiment 4, the study has not directly considered the reproducibility of the test and the effect on its results. Given that the assessment in Experiment 4 was undertaken by the same individual, who was experienced at undertaking the test, the results indicate that both versions of the protocol have a similar variation in FMTs across the five test locations. The value of the standard error is ~0.1% for both sets of 16 measurements across all stimulus locations, as illustrated in Figure 3-14. As shown in Figure 3-33, the expected range of thresholds for an individual measurement, given by the standard deviation for a single assessment ~0.4%, are four times higher than the standard error of the mean based upon the 16 measurements. It also gives an indication of the accuracy to which results should be reported, i.e. to one decimal place.

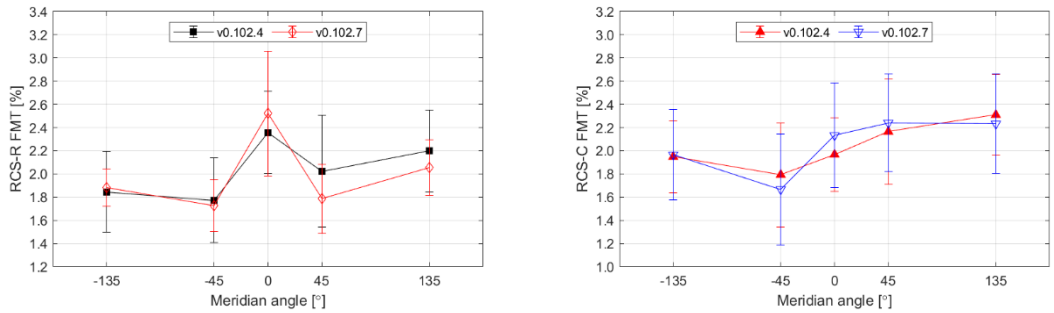

Figure 3-33: Mean RCS test results for 16 repetitions of the test plotted with error bars equivalent to ±1 standard deviation.

The variation in the off-axis FMTs for both test conditions is a function of the participant undertaking the test. After 16 repetitions, this is a genuine asymmetry in sensitivity. Whilst this provides an argument for not combining parafoveal, off-axis FMT values, the previous discussion of combining off-axis FMTs was for group rather individual data. The establishment of the group norm allows assessment of what is abnormal.

3.4.10 Limitations

As ever with trials reliant upon human participants, recruiting an adequate cohort to allow the study to have scientific merit and statistical power can be a limiting factor. Coupling this with the change in the software version, the ability of the last experiment to generate the basis for a SNO for 100 participants was impeded. However, it has been possible to better define the effects of the revised protocol allowing a good first approximation for a SNO to be achieved for both versions of the test software for a cohort of young normal participants. The age range of the cohorts have been biased towards a narrow demographic, which has limited the ability for the study to define any effect of age on the RCS test results.

3.4.11 Confounding factors

The ambient illumination and wider environment may have influenced the thresholds measured. Whilst in some locations, the test environment can be carefully controlled and light leaks from blinds minimised, there were occasions where noise, e.g. other students and both internal and external building works, and light pollution may have affected the results. These have hopefully been minimised by the application of the exclusion criteria that have removed those participants whose results appear as outliers.

Learning from the experience of undertaking this study, the use of closed-back circumaural headphones connected to the laptop computer would assist in acoustically isolating the participant from the external environment whilst allowing them to still hear the beep signifying the end of the stimulus presentation.

3.5 Conclusions and future work

3.5.1 Conclusions

The RCS test protocol has been developed enabling the quantitative assessment of FMTs of both rod and cone-mediated vision to be characterised after only 2 minutes adapting to the respective test condition thus negating the need for long adaptation times.

Although the RCS-R condition FMT values are reliant upon both rod and cone-mediated vision, the chromaticity and temporal properties of the stimulus do enable rod-mediated visual function to be measured objectively.

The RCS test has subsequently been used to characterise monocular and binocular FMTs demonstrating the foveal cone-mediated vision is consistent with probability summation with a binocular summation ratio equal to $\sqrt{2}$.

In addition, the results have also demonstrated that at 5° eccentricity the binocular summation ratio increases to ~$1.25\sqrt{2}$. This value for binocular summation in the parafoveal region has been demonstrated to be independent of photoreceptor type, with a similar value calculated for both rod and cone-mediated vision. This result indicates the involvement of a neural component in the summation process resulting in the increased gain applied to the monocular inputs to binocular vision.

The study has demonstrated that sighting eye dominance can be predicted using the RCS test protocol from monocular responses for both eyes for the RCS-R off-axis and RCS-C on-axis test stimuli. It has also indicated that, for the later version of the RCS test (v0.102.7), the difference in monocular dominance is ~0.59% and that this offset is independent of photoreceptor type for off-axis stimuli. For on-axis stimuli, the indications are that a monocular dominance can be predicted by a scale factor of ~1.27.

For the small sample sizes, and limited age range (18 to 30 years) investigated in this study, there is no significant difference in FMTs as a function of age, measured using the RCS test, for a cohort of young normals.

Analysis of the statistical properties of the results for the two cohorts demonstrates that rod-mediated FMTs conform to a normal distribution, however the cone-mediated FMTs are best represented in terms

of a non-parametric distribution, i.e. defining the distribution in terms of its median and 5th and 95th percentile values.

For young normal participants, it has been shown that the off-axis FMT values can be combined into a single off-axis FMT value for both the RCS-R and RCS-C conditions of the test.

3.5.2 Future Work

There are three studies that would assist in confirming and developing the results of this study.

3.5.2.1 RCS Project 1: Definition of the RCS SNO as a function of age

Future work should be directed towards defining changes in normal healthy participants as a function of age. Given the limited age range of the cohorts used in this study, there are benefits to measuring the FMTs using the RCS test of a wider age distribution. The age distribution of future studies should be expanded to least five decades and the assessment should be undertaken using software version v0.102.7 of the RCS test. This will provide a base dataset that can be used to define the FMTs as a function of age in terms of the SNO defined in this study.

The nature of the RCS test enables the detection of any departure from normal aging both in terms of optics, photoreceptor function, the retina and visual pathways.

3.5.2.2 RCS Project 2: Verification of a rod-mediated response

Using the RSC-C condition chromaticity and the stimulus dimensions of the RCS-R condition, evaluate the FMTs for a background luminance at 0.5cd.m^{-2}. The hypothesis to be tested is that FMT values will be higher than those recorded for the corresponding RCS-R condition due to the lower S/P value of the RCS-C stimulus.

This would assist in determining the contribution of cone-mediated vision at high mesopic light levels and enabling a better understanding of the FMT values recorded for a background luminance at 0.5cd.m^{-2}.

3.5.2.3 RCS Project 3: Use of pupilometry to verify that the RCS-R condition initiates a rod-mediated response

Using the chromaticity of the RCS-R and RCS-C conditions, evaluate the contributions of rod and cone photoreceptors to the transient response to a 100% contrast, large field, stimulus over a 4 log range of background luminance values.

This would provide an insight into the relative contributions of rod and cone-mediated vision across the mesopic range of light levels using an autonomic response.

4 The transient response of the pupil at mesopic light levels

4.1 Introduction

Acting on one of the recommendations from the previous study, section 3.5.2.3, the primary purpose of this exploratory study was to establish that the RCS-R test condition instigated a rod-mediated response by analysing the transient response of the pupil to a fixed contrast positive stimulus. This was compared to the transient response to the RCS-C test condition. Given the limited age range of Experiment 6, the scope of this study was expanded to include an analysis of how the steady state pupil diameter pre-stimulus and transient pupil response to the stimulus varied as a function of age for the two stimuli.

Due to variations in the colour gamut and display technology used to present stimuli, it was not possible to replicate an absolute match to the RCS test conditions. As a result, two stimulus conditions R and C were defined as metameric matches respectively to the RCS-R and RCS-C conditions of the RCS test.

4.1.1 Background

The Pupil Light Reflex (PLR) is mediated by intrinsically photosensitive Retinal Ganglion Cells (ipRGCs) that receive inputs from both rods and cones over 6 log units of illumination (Lucas *et al* 2003, Allen *et al* 2011, Lucas *et al* 2001, Hattar *et al* 2003). At high illumination levels, corresponding to photopic light levels, melanopsin contained within the ipRGCs mediates the long term, sustained constriction of the pupil post stimulus offset, characterised by the Post Illumination Pupil Response (PIPR) (Lucas *et al* 2003, Panda *et al* 2002, Joyce *et al* 2015). This is supported by the static pupillary sensitivity curve at photopic light levels recorded by Bouma (1962), although Bouma did not wholly realise that he had measured melanopsin's luminosity curve at the time.

The evidence in support of pupil response being mediated by rods is provided by the action spectrum of the pupil which was shown to closely match the scotopic spectral sensitivity curve (Alpern and Campbell 1962). Alpern and Campbell also reported that both L and M cones contribute to the transient response to stimulus onset. More recent studies seeking to characterise the influence of ipRGCs on the dynamics of the PLR have demonstrated the changing balance between rod and cone mediation with increasing intensity (McDougal and Gamlin 2010). McDougal and Gamlin's study modelled the relative contributions from all three photosensitive cell types mediating the pupil: rods, cones and melanopsin containing ipRGCs. These showed that rods were the primary photoreceptor mediating the PLR for a 3.16s stimulus, which was below the threshold of melanopsin. As stimulus duration was increased beyond 10s, there was a contribution from melanopsin containing ipRGCs.

Further evidence that rods mediate the PLR at light intensities below the onset of melanopsin containing ipRGCs is provided in a study using mice with different photoreceptors knocked-out (Keenan *et al* 2016). This is not to say that the rod input to the transient response is not influenced by cones, but that rod is the predominant photoreceptor at low to moderate illumination levels (up to 10lux).

These studies provide a good basis for using pupillometry as a method of demonstrating, by experimentation, that stimulus R affects a rod mediated response both in terms of the pre-stimulus diameter and the transient response to stimulus onset.

4.1.1.1 Validation of stimulus R and the RCS-R test condition

The investigation of rod and cone thresholds undertaken in section 3 was based partly on the assumption that, after a short adaptation time, it was possible to stimulate a rod-mediated response to a mean modulated flickering stimulus. Although the results suggested that a rod-mediated response is present, further evidence to validate this assumption assists in providing a strong basis for the RCS-R test protocol. To provide this additional evidence, a visual function primarily mediated by rods was sought, that could be used to characterise the primary photoreceptor mediating the response to the RCS-R test stimulus.

The autonomic nature of the PLR removes the potential for a conscious bias being introduced during a vision test, however other confounding effects can also influence the measured pupil response, e.g. intake of stimulants and depressants (Hou *et al* 2006, Wilhelm *et al* 2014), fatigue (Różanowski *et al* 2015), cognitive load (Piquado *et al* 2010) and emotion (Partala and Surakka 2003).

4.1.1.2 Why use the transient response?

The PLR to an increase in retinal illumination can be separated into two parts. The initial transient response results in an initial constriction before the secondary, sustained response, where the pupil diameter stabilises following the initial exposure of the photoreceptors to the new light level. The pupil diameter for the sustained response is between that of the pre-stimulus diameter and that of the peak constriction of the transient response.

The focus of this study on the transient response comes from the desire to understand the photoreceptors mediating the response to the flickering stimulus of the RCS test. The duration of the stimuli and frequency of the flicker used in the RCS test are such that a sustained response is not entirely evoked. The transient response to the step increase in luminance better represents the onset of the flickering stimulus.

4.1.1.3 Quantitative characterisation of the transient pupil response

Quantitative techniques previously used to characterise the PLR have included measuring the action spectrum and equal energy spectrum of the PLR (Alpern and Campbell 1962). The action spectrum relates to the amount of energy required to instigate a defined change in pupil diameter. Conversely, the equal energy spectrum characterises the change in pupil size to a stimulus of equal energy as a function of wavelength.

Similarly, the magnitude and latency of the transient response to the onset of a stimulus, with a defined contrast relative to the background, can be used to provide an insight to the photoreceptors that are mediating the constriction. In terms of visual function, shorter latencies are associated with cone-mediated vision, excited for example by a red coloured stimulus, whilst longer latencies have been attributed to rod-mediated vision and the use of a blue coloured stimulus (Barbur 1982). The reason for the specific focus on the transient response, in contrast to the sustained response, is that the transient response results from an increase in parasympathetic tone, observed as a constriction of the iris sphincter. In addition, the characteristics of the transient response have been used in the past to understand visual processing levels (Barbur *et al* 1998b). The transient response can be separated into two components:

- Constriction amplitude is proportional to the luminance increment of the stimulus (Young and Kennish 1993) and the spectral content as shown by equal energy spectra.

- Constriction latency is dependent upon the stimulus intensity, decreasing as stimulus intensity increases (Ellis 1981). Values quoted in the literature are dependent on the spectral content of the light but are in the order of 350ms to 200ms for the dark adapted case (Fan *et al* 2009).

4.1.1.4 Effect of age on pupil diameter and the transient response

The effects of age on pupil diameter have been characterised previously (Winn *et al* 1994) and were subsequently utilised to construct a unified model for defining pupil diameter as a function of corneal flux (Watson and Yellott 2012). The reduction in pupil size was modelled as a linear function of age, with the rate of reduction decreasing as a function of illuminance.

The reduction in steady state pupil diameter as a function of age is a combination of pupil miosis, from a reduction in sympathetic tone (Korczyn *et al* 1976), and an increase in the optical density of the crystalline lens for shorter wavelengths, with the latter observed as a yellowing of the lens. The average lens density increased linearly 0.12 density units per decade, at 400nm, between the age of 20 and 60 years, with this rate doubling above 60 years old (Pokorny *et al* 1987).

The effect of both pupil miosis and changes in the lens transmittance reduce the retinal illuminance incident upon photosensitive cells within both the inner and outer retina. The effects of aging are not just limited to the amount of light reaching the retina. The density of rods has been shown to decrease as a function of age (Curcio *et al* 1993), with the decrement being more pronounced in the peripheral retina (Gao and Hollyfield 1992). Whilst coverage is maintained, it is at a lower density as the space left by dying rods is filled by rods with larger inner segments. There is also a reduction in the Retinal Ganglion Cells (RGCs) (Owsley 2011), but there is no specific mention as to whether this includes ipRGCs that are already sparsely distributed.

If the transient PLR is primarily mediated by rods at mesopic light levels, then it stands to reason that as well as steady state pupil diameter, changes in lens transmittance and reduction in rod density may also affect the transient response.

Based upon this background knowledge, is it possible, using a pair of stimuli that preferentially stimulate either a rod or cone mediated response, to understand more about the contribution of the rod and cone photoreceptors to the mediation of the PLR and any changes that may result as a function of age?

4.1.2 Hypotheses

The following hypotheses will be tested within the scope of this study:

a) The rod-enriched stimulus from the RCS test (stimulus R) instigates a rod mediated response.
b) For mesopic light levels, rod photoreceptors mediate the steady state pupil diameter.
c) For mesopic light levels, rod photoreceptors mediate the transient response to a positive stimulus of a fixed contrast with respect to the background luminance.
d) If stimulus R and C affect responses primarily mediated by rod and cone photoreceptors respectively, then can the stimuli be used to characterise age dependent changes in the transient pupil response.

4.1.3 Experimental design

The design of this study has centred on determining the steady state pre-stimulus pupil diameter, and the transient pupil response to a pair of stimuli across a broad range of mesopic light levels from 0.001cd.m^{-2} to 10cd.m^{-2}. It is understood that this range of luminance values is below the threshold of melanopsin (McDougal and Gamlin 2010). The two stimuli used, stimuli R and C, were based respectively upon the chromaticity of RCS-R and RCS-C test conditions from the RCS test protocol (v0.102.4). The age range of the study cohort ranged from 20 years to 65 years, providing an indication of how the pupil response to the two stimulus conditions may varies as a function of age.

4.2 Materials and Methods

4.2.1 Participants

The study cohort of seven participants ranged in age from 21 to 64 years. Participants were recruited from supervising staff and students at City University. All participants gave informed consent, and the study was undertaken in accordance with the tenets of the declaration of Helsinki.

Experiment 7 was undertaken by the author to define the stimulus duration to be used for Experiment 8 undertaken by the full cohort.

4.2.2 Equipment

The test stimuli were presented to the participant using the P-SCAN system (Barbur *et al* 1987, Alexandridis *et al* 1991, Barbur *et al* 1999) using a display which was viewed binocularly from 0.6 m, as illustrated in Figure 2-7. The P-SCAN system can measure the pupil diameter to an accuracy of better than 0.02mm (Bi *et al* 2016).

The luminance and emission spectra of the display had been previously calibrated enabling backgrounds with specific colour co-ordinates, scotopic/photopic ratio (S/P) and luminance values to be reproduced, as described in section 1.4.1. The transient response of each eye to the displayed stimuli was measured at a sampling rate of 50Hz. The stimuli were presented on a background field subtending 33° x 26°. Spectrally calibrated neutral density filters were used to attenuate the screen luminance to produce discrete luminance values at the eye of between 0.001cd.m^{-2} and 50cd.m^{-2}.

4.2.3 Experimental procedure

The measurements were undertaken in a laboratory with blackout blinds over the windows and overhead room lights turned off. The participant was separated from the Principal Investigator (PI) and the monitoring equipment by a curtain. The ambient illumination in the room was 0.100lux.

For each stimulus and luminance condition, the mean PLR was calculated for a sequence of consecutive presentations. The pre-stimulus period for each 10s recording was fixed at 1s. The remaining 9s consisted of the stimulus presentation and the response post-stimulus offset. The specific conditions for each experiment are defined in Table 4-1 with additional explanation in section 4.2.4.

Prior to the first presentation of each stimulus condition, the participant was given two minutes adaptation time to adjust to the test's background luminance condition. Stimulus presentations were

instigated by the PI at an interval of between 20s to 25s which allowed the participant to undertake several blinks to refresh the tear film across their eyes. During each presentation, participants were instructed to try to maintain fixation on the centre of the screen and try not to blink.

4.2.4 Testing

4.2.4.1 Experiment 7 – Definition of stimulus duration

A short initial study was undertaken to determine how stimulus duration would impact on the ability to fully characterise the pupil's transient response. The testing consisted of 32 presentations of a rectangular stimulus centred on the optical axis of the P-SCAN system for each stimulus duration. The stimulus duration was varied from 1s to 4s in 1s increments. The colorimetry of the stimulus used, stimulus D defined in Table 4-1, closely approximated the D65 illuminant.

4.2.4.2 Experiment 8 – Rod and Cone stimulus validation

An experiment was undertaken to evaluate the PLR in response to the rod enriched stimulus (R) and cone enriched stimulus (C) based upon the test conditions used in the RCS test with the aim of validating that the rod stimulus instigated a rod mediated response.

In total twelve background luminance values (0.001cd.m^{-2}, 0.005cd.m^{-2}, 0.01cd.m^{-2}, 0.02cd.m^{-2}, 0.06cd.m^{-2}, 0.15cd.m^{-2}, 0.25cd.m^{-2}, 0.5cd.m^{-2}, 1cd.m^{-2}, 2cd.m^{-2}, 4cd.m^{-2}, 9cd.m^{-2}) were used to assess the pre-stimulus diameter and transient response across the mesopic range of light levels.

For each background luminance value, the sequence of repeated presentations for stimulus R was undertaken first, followed by those for stimulus C. The testing started at the lowest luminance level and was completed over a series of days to minimise the effect of measurement fatigue. There was one exception, participant 6, (P6), who completed their set of measurements in a day.

4.2.5 Conditions

The stimulus conditions used for both experiments are defined in Table 4-1. Each of the stimuli was presented centrally with respect to the screen dimensions. The relationship between the three stimuli in terms of colorimetry is illustrated in Figure 4-1.

Experiment	Stimulus ID	Scotopic/Photopic ratio (S/P)	CIE x	CIE y	Background luminance range [cd.m^{-2}]	Stimulus size [degrees]	Stimulus area [degrees^2]
Experiment 7 - Determine stimulus duration	D	N/A	0.305	0.323	5	30 x 24	720
Experiment 8 – Validation of stimulus condition	R	8	0.18	0.0899	0.001 to 9		
	C	0.7	0.58	0.37			

Table 4-1: Summary of stimulus conditions used for Experiments 7 and 8.

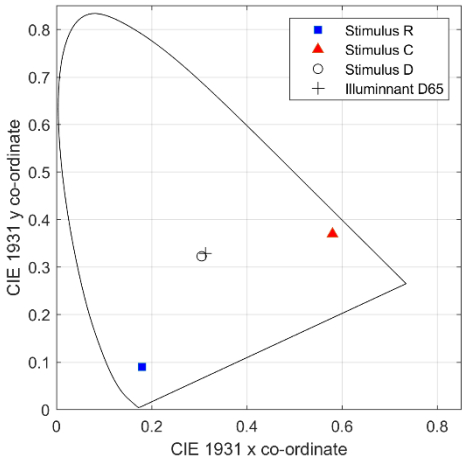

Figure 4-1: The CIE 1931 (x, y) co-ordinates of the stimuli used in this study relative to the D65 illuminant.

4.2.6 Analysis

4.2.6.1 Experiment 7

The mean pupil trace was calculated for each eye and combined to give a single response for each stimulus duration. The resulting traces were normalised with respect to the stimulus diameter at stimulus onset and compared based upon the relative transient and sustained response as a function of stimulus duration.

4.2.6.2 Experiments 8

The raw data were reviewed for each stimulus presentation and recordings that had been significantly affected by eye blinks, or prolonged partial or complete closure of the eye lid, were discarded. The mean pupil trace was calculated for each eye and combined to give a single response to the stimulus condition. The following metrics, illustrated in Figure 4-2, were used for the quantitative analysis of the resulting data:

- Pre-stimulus diameter defined as the mean pupil diameter for the 1s period prior to stimulus onset.
- Peak constriction defined as the minimum pupil diameter after stimulus onset.
- The constriction amplitude defined as the difference between the pre-stimulus diameter and the peak constriction.
- Constriction latency defined as time between stimulus onset and the peak in acceleration post stimulus onset.

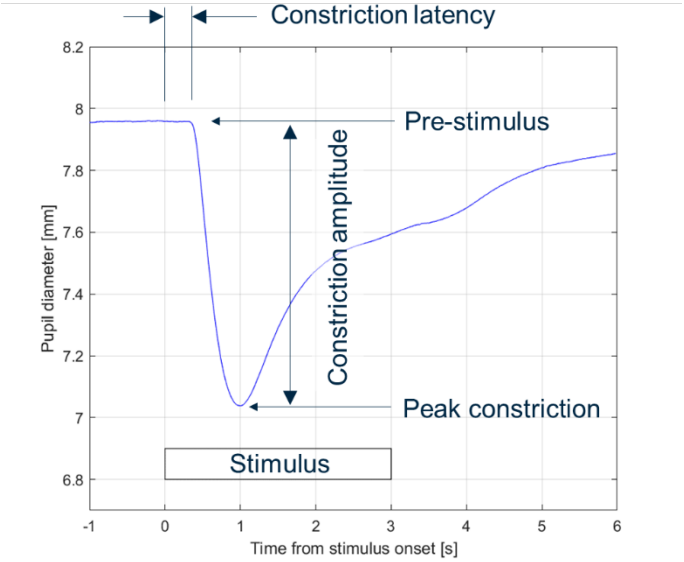

Figure 4-2: Definition of key metrics used in the assessment of the transient response of the pupil to a stimulus.

Analysis was undertaken using a combination of Microsoft Excel and MATLAB R2018b to perform linear regression and additional analyses.

The use of peak acceleration to determine the onset of constriction is drawn through from the physics of a simple harmonic oscillator where the greatest force, and thus acceleration, is applied when a body changes direction or is released from rest. The use of the peak acceleration to determine the onset latency has been proposed as a reliable method (Kardon *et al* 1991, Bergamin and Kardon 2003).

Working on the assumption that the rod and cone conditions do instigate a response that is mediated respectively by rods and cones, the retinal illuminance for the two conditions can be calculated. The scotopic retinal illuminance (E_{Sc}), given by Equation 23, includes a consideration of: the scotopic/photopic ratio (S/P) of the stimulus; its photopic luminance (L); and the area of the pupil as a function of diameter (ϕ).

$$E_{Sc} = (S/P).L\pi\left(\frac{\emptyset}{2}\right)^2$$

Equation 23: Scotopic retinal illuminance

As photopic vision is mediated by cones, an apodisation factor, $\rho(\phi)$, has been included in the calculation of the photopic retinal illuminance (E_{Ph}), given by Equation 24, to account for the directional sensitivity of cones due to the Stiles Crawford effect (Stiles and Crawford 1933).

$$E_{Ph} = \rho(\emptyset).L\pi\left(\frac{\emptyset}{2}\right)^2$$

Equation 24: Photopic retinal illuminance

Similarly, where corneal flux has been considered, it has been calculated with the respective scaling factors applied to account for the condition's S/P value or the directional sensitivity of cones as a function of pupil diameter.

Equation 25 was used to fit pupil diameter as a function of retinal illuminance instead of as a function of corneal flux, as proposed by Stanley and Davies (1995) and adopted by Watson and Yellot (2012) in their unified model.

$$f(x) = c_1 - c_2\left(\frac{(x/c_3)^{c_4}}{(x/c_3)^{c_4} + c_5}\right)$$

Equation 25: Pupil diameter as a function of light flux or retinal illuminance

4.3 Results

4.3.1 Experiment 7 - Definition of stimulus duration

As shown in Figure 4-3, increasing the duration of the stimulus results in the ability to identify more components of the PLR with greater clarity. Peak constriction is achieved just before 1s from stimulus onset. Immediately after peak constriction there is rapid dilation, the rate of which subsequently reduces at ~1.5s post stimulus onset. For the PLR in response to the 3s and 4s stimuli, there is sustained dilation prior to the rapid dilation at ~0.3s post stimulus offset. The sustained dilation prior to stimulus offset is slower than the initial constriction. The transient response of the 2s stimulus is not clearly separable from the reaction to stimulus offset. However, the transient response of the 3s and 4s stimuli can be separated from stimulus offset by the sustained dilation. Ensuring that the transient response has been completed in full is important if it is to be fully characterised quantitatively, and as a result a stimulus duration greater than 2s should be used. The results indicate a 3s stimulus duration will enable the transient response to be fully characterised whilst allowing for some variation between participants.

Post-stimulus offset, the pupil diameter returns to within 95% of the pre-stimulus diameter. The latency of the post-stimulus dilation appears to be equivalent for stimulus durations ≥2s. The rate of post-stimulus dilation is slower than the initial constriction at onset.

The pupil diameter beyond 6s from stimulus onset is more variable due to the participant starting to blink and the associated natural variation in pupil size.

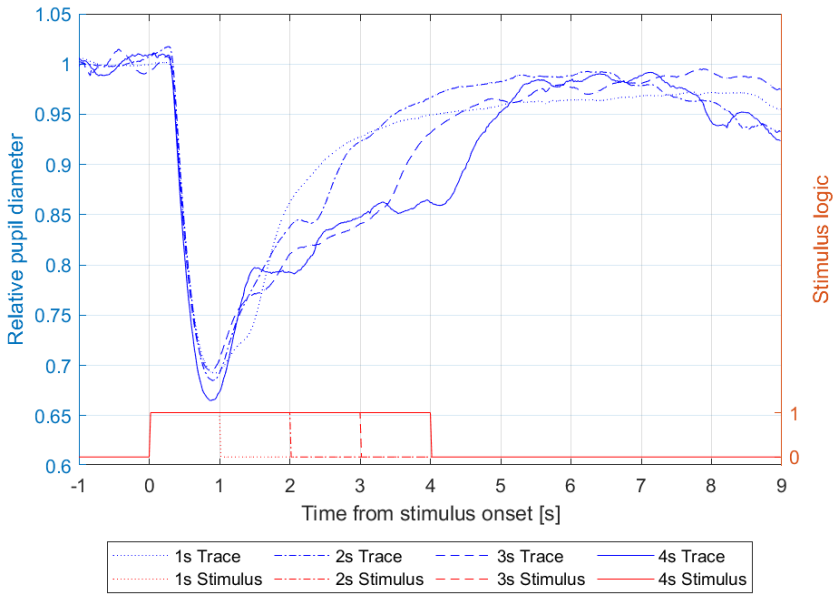

Figure 4-3: Relative pupil diameter as a function of time and the relationship with stimulus duration.

4.3.2 Experiment 8 – Does the RCS-R condition produce a rod mediated response?

4.3.2.1 Pre-stimulus diameter

The pre-stimulus diameters for stimuli R and C for participant 3 (P3) are plotted in Figure 4-4 as a function of photopic and scotopic retinal illuminance. As a function of photopic retinal illuminance, the two stimuli result in two separate functions that diverge as retinal illumination increases. When the pre-stimulus diameter is plotted as a function of the scotopic retinal illuminance, the two curves appear to follow a similar trend, with overlapping confidence bounds at 95%. Based upon this, the two sets of data have been combined to generate a single graph of pre-stimulus diameter as a function of scotopic retinal illuminance for this participant, right-hand plot of Figure 4-4. The result is a single function whose confidence interval at 95% bound most of the data points. The resulting coefficient of determination of 0.9530 also demonstrates that there is a high level of agreement to the data being represented by a single function.

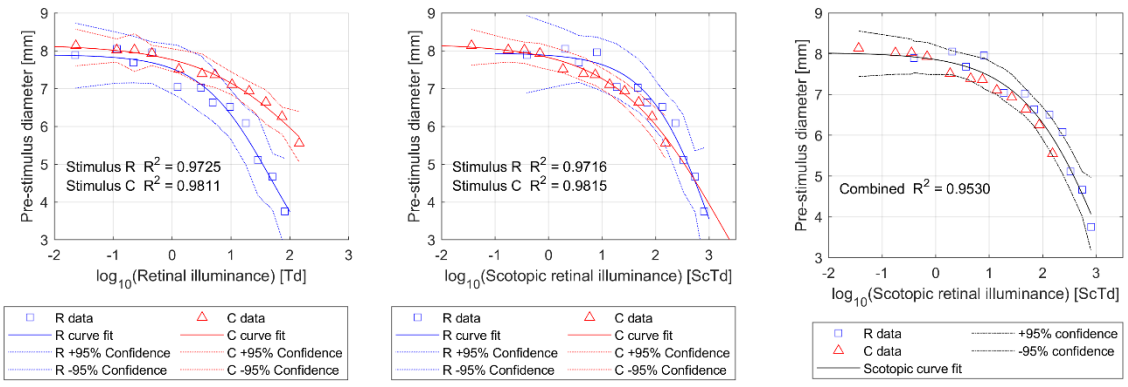

Figure 4-4: Pre-stimulus diameters for both stimulus R and C as a function of photopic (left), and scotopic (middle) retinal illuminance for participant P3. The data for stimulus R and C are combined into a single function of scotopic retinal illuminance (right). The plotted upper and lower confidence intervals are at 95%.

This analysis has been replicated for all participants, as illustrated in Figure 4-5, with a similar behaviour being observed. The coefficients of determination are above 0.9 for four of the seven participants with two more having values above 0.8. For participant P2, there is greater variation in the pre-stimulus diameter at lower retinal illuminance values where the fitted function has its upper asymptote at 6.3mm. The upper asymptotes of the fitted functions for participants P5 to P7 align at ~5.5mm. The cause of the observed variation is either representative of the range of pupil diameters, i.e. normal behaviour, or the interaction of a confounding influence (possible distraction due to noise external to the laboratory building).

The results for P7 could be interpreted as not fully agreeing with the proposed model. From 1ScTd, it might be argued that the data for the two stimuli diverge. Alternatively, this could be attributed to variance in the results, with all points still within the 95% confidence intervals of the fitted function.

Comparing the group's results, see Figure 4-6, indicates that the pre-stimulus diameter converges on a lower asymptote. However further data at higher scotopic retinal illuminance values is required to confirm that this is the case. The dynamic range of the P-SCAN system prevents higher luminance values being achieved for the two stimulus conditions.

The general trend observed for all participants is that the results for both stimulus R and C align as a function of scotopic retinal illuminance.

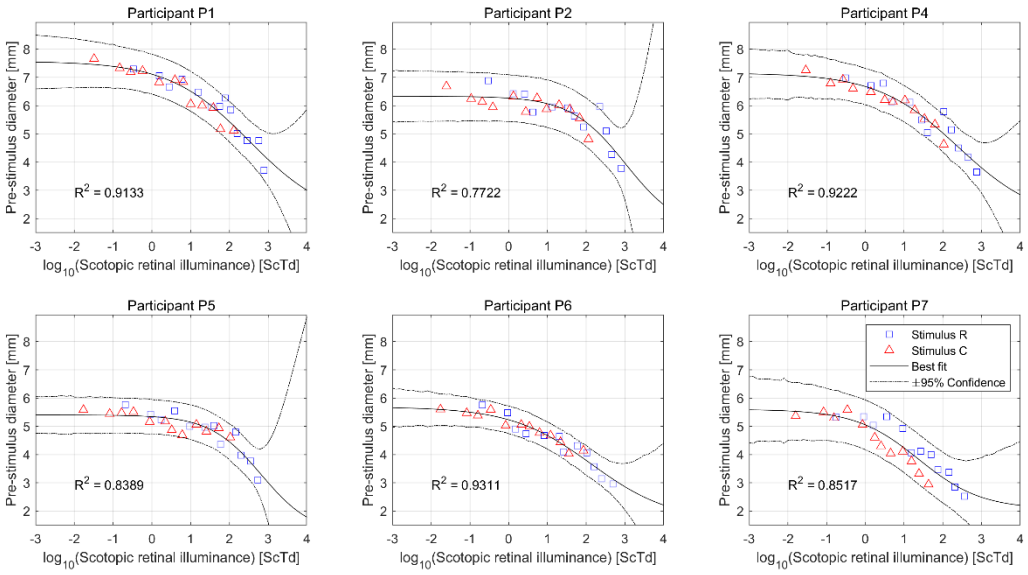

Figure 4-5: Pre-stimulus diameter as a function of scotopic retinal illuminance for each participant for the two stimuli, line of best fit and ±95% confidence intervals.

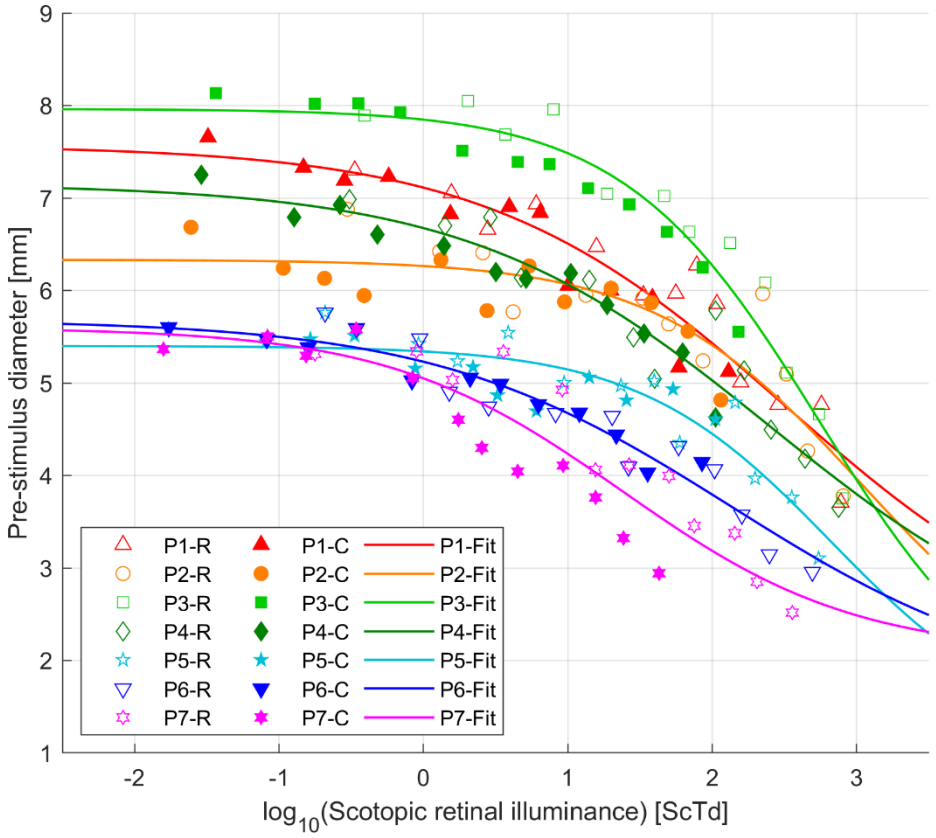

Figure 4-6: Comparison of the pre-stimulus diameter as a function of scotopic retinal illuminance for the cohort.

To illustrate the variation in pre-stimulus pupil diameter at a given scotopic retinal illuminance across the cohort, the pre-stimulus diameter has been calculated at -1 log ScTd and +2 log ScTd using the lines of best fit for each participant. These two scotopic retinal illuminance values are within the range of values for which measurements were made. Based upon Figure 4-6, these two values of retinal illuminance align respectively with the pre-stimulus diameter's upper asymptote and the region where pupil diameter can be described as a linear function of the log of scotopic retinal illuminance. Furthermore, these two points correspond to scotopic and mesopic illumination conditions, respectively. The resulting linear relationships, shown in Figure 4-7, provide an indication of how retinal illumination affects steady state pupil diameter as a function of age.

The overall relationship, demonstrated in Figure 4-7, is a reduction in pre-stimulus pupil diameter as age increases for both retinal illuminance values selected. The data corresponding to the higher retinal illuminance value has the steeper gradient. There is greater variance in pre-stimulus diameter as a function of age for the -1 log ScTd data when compared to the +2 log ScTd data for this small cohort, as indicated by the R^2 values.

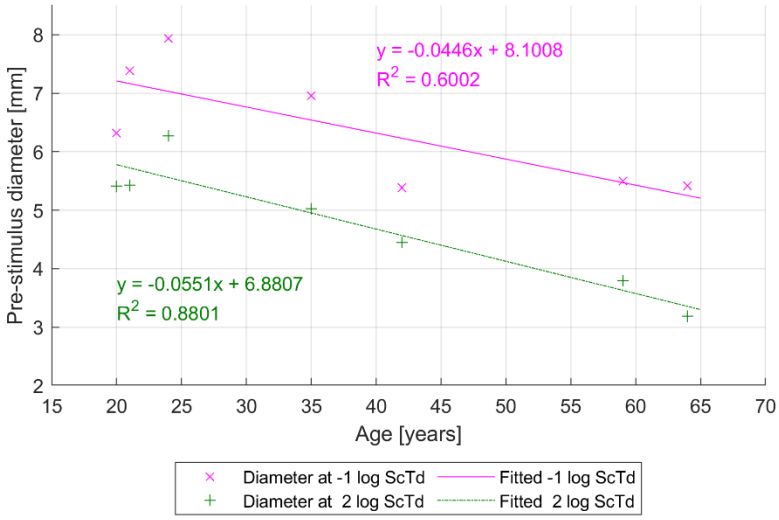

Figure 4-7: Pre-stimulus diameter as a function of age assessed at -1 log ScTd and +2 log ScTd

Utilising the common luminance value, 9cd.m^{-2}, used as a test point for this study and that undertaken by Winn *et al* (1994), a direct comparison is provided in Figure 4-8. The 10° circular stimulus used by Winn *et al* was smaller than the stimuli used in this study and as a result the corneal flux will be higher for this study. This results in a smaller pupil diameter being recorded for the 9cd.m^{-2} stimuli of this study. Despite the differences in corneal flux, the trend observed does align with the findings of Winn *et al*.

Although for this analysis stimuli R and C have the same photopic luminance, they result in different pre-stimulus pupil diameters. This is an illustration of the pupil diameter being driven by the scotopic content of the stimulus. In scotopic luminance terms, the luminance of stimulus C corresponds to 6.3Sc cd.m^{-2} and stimulus R equates to 72Sc cd.m^{-2}, an effective ratio of 11.42. This demonstrates that the pre-stimulus pupil diameter is dependent upon both the corneal flux and the scotopic content of the stimulus. It also demonstrates that the colorimetry of stimulus R instigates a rod-mediated response.

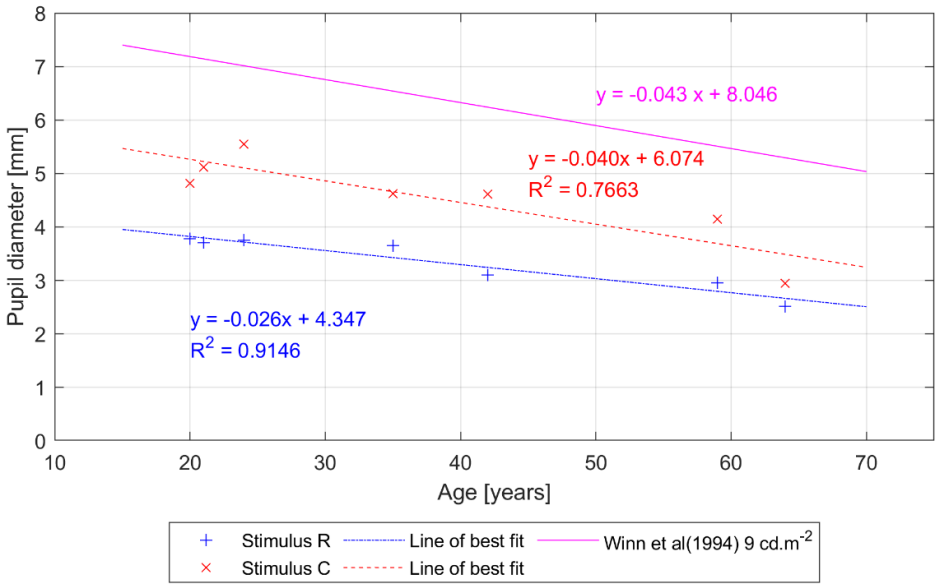

Figure 4-8: Pre-stimulus diameter as a function of age for both stimulus R and C at a luminance of 9 cd.m^{-2}. For comparison the line of best fit for a 9 cd.m^{-2}, 10° diameter circular field (Winn et al 1994).

4.3.2.2 Constriction amplitude

In a similar manner to the pre-stimulus diameter, the constriction amplitudes for participant 3 have been plotted as a function of both photopic and scotopic retinal illuminance in Figure 4-9. When plotted as a function of photopic retinal illuminance, the constriction amplitudes for the two stimuli are two separate functions. However, when the constriction amplitude is plotted as a function of scotopic retinal illuminance, the two sets of data align. The shift in retinal illuminance between the two graphs is ~1.058 log units. This broadly corresponds to the ratio of the S/P values for stimuli R and C, i.e. $\log_{10}(8.0/0.7)$.

There is a clear peak in constriction amplitude at ~2 log ScTd for stimulus R. There is potentially a peak in the constriction amplitude for stimulus C at ~2 log ScTd but without more data points this cannot be confirmed. The significance of the 2 log ScTd value is that at this retinal illuminance the sensitivity of rods begins to rapidly decrease as rod responses start to saturate (Aguilar and Stiles 1954).

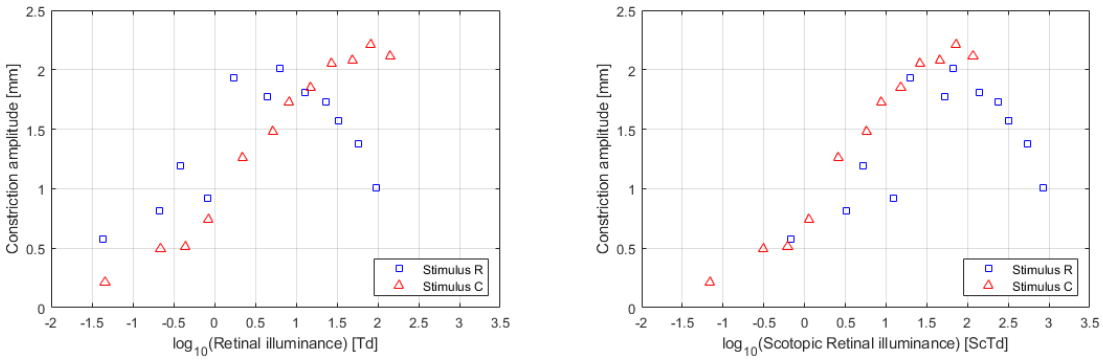

Figure 4-9: Constriction amplitude as a function of (photopic) retinal illuminance (left) and scotopic retinal illuminance (right) for participant P3.

Assuming that constriction amplitude is a function of scotopic retinal illuminance, the appearance of the results suggest that constriction amplitude can be modelled by a Gaussian function with a pedestal, see Equation 26. Coefficient A accounts for any constriction for regions where pupil diameter is independent of the change in retinal illuminance. Coefficient C is the illumination level at peak constriction.

$$y = A + B \exp\left(-\left(\frac{(x - C)}{D}\right)^2\right)$$

Equation 26: Gaussian function with a pedestal.

The following analysis considers the validity of the proposed model for constriction amplitude across the whole cohort. The analysis then considers the variation in values of the model's coefficients across the cohort.

Evidence to support this model is provided in Figure 4-10, where the difference between the pre-stimulus and peak constricted pupil diameters, for the combined set of values for participant 4, are plotted as a function of scotopic retinal illuminance. A generalised form of the constriction amplitude, independent of stimulus type, is plotted as a function of scotopic retinal illuminance. The agreement between the difference of the two fitted functions in the left hand graph of Figure 4-10 and the result of fitting Equation

26 to this data is given by the R^2 value of 0.9922 for the Gaussian model with a pedestal. The pedestal accounts for the constriction amplitude for the asymptotes of the Stanley and Davies model.

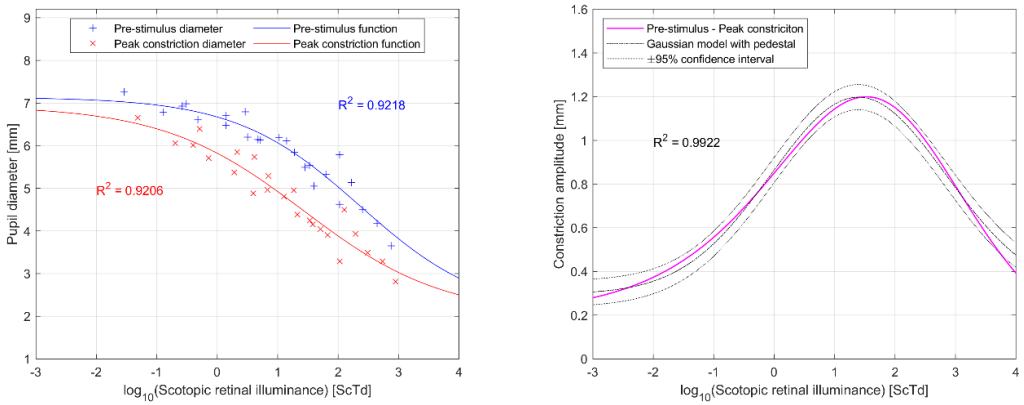

Figure 4-10: Graphs supporting the use of a Gaussian function with a pedestal to describe the constriction amplitude of the pupil in response to a stimulus of fixed contrast with respect to the background condition. (Left) Data for participant 4's pre-stimulus and peak constricted pupil diameters fitted as a function of scotopic retinal illuminance using Equation 25. Results of both stimuli have been combined into a single data set. (Right) The peak constriction calculated as the difference between the two fitted functions plotted along with the result of fitting Equation 26 to the data.

The validity of this model is confirmed by the coefficients of determination shown within the legends of the individual plots in Figure 4-11. The model for constriction amplitude as a function of both photopic and scotopic retinal illuminance has been fitted separately to data for the two stimulus conditions in Figure 4-11.

The constriction amplitude as a function of photopic retinal illuminance results in a pair of functions with an offset between the peaks for stimulus R and C, as illustrated in the top row of Figure 4-11. When constriction amplitude is plotted as a function of scotopic retinal illuminance, accounting for the S/P values of the stimuli, these Gaussian functions appear to align for the younger participants. For the oldest participant, the function describing the constriction amplitude in response to stimulus C appears to shift towards lower retinal illuminance values.

In addition to the shift in the peak of the Gaussian functions, the amplitude of the function decreases as a function of age. Given that the pre-stimulus diameter has been shown to decrease as a function of age and assuming that the minimum pupil diameter remains independent of age, it makes sense that constriction amplitude will also decrease as a function of age.

Not all the data fitted the Gaussian model for constriction amplitude based upon an initial set of seed coefficients. The three cases that did not fit the model are illustrated in Figure 4-12. The non-conformance was attributed to artefacts in the averaged response to at least one of the two stimuli. With knowledge of the general behaviour of the model, the data for all participants was refitted using the bounding criteria given in Table 4-2. This achieved a better solution for participants 2 and 6 with minimal change for the other participants. Using the revised set of Gaussian functions, the difference in the location of the peak values for both stimuli is plotted as a function of scotopic retinal illuminance in Figure 4-13.

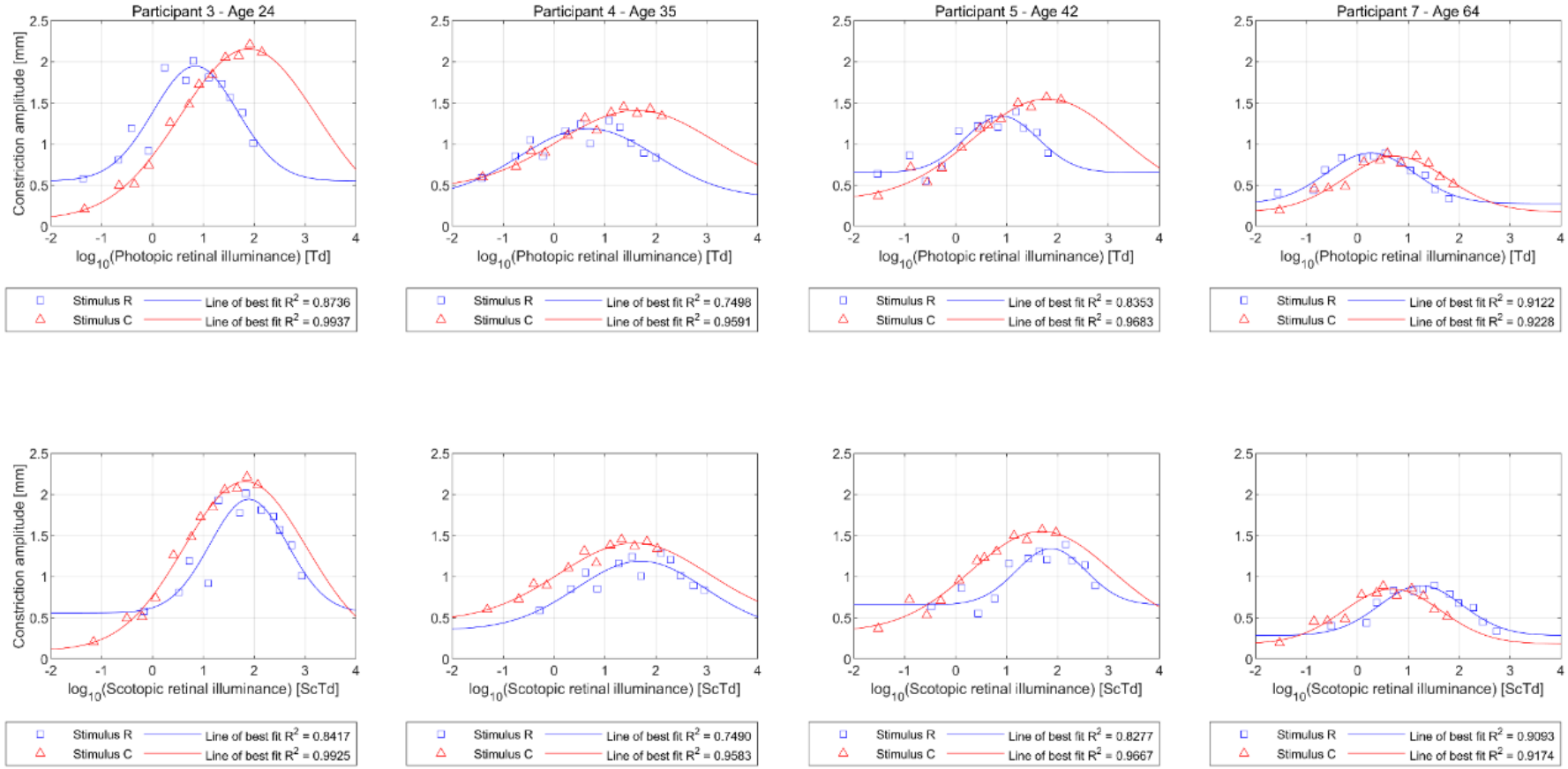

Figure 4-11: Constriction amplitude as a function of photopic (top) and scotopic (bottom) retinal illuminance for four individuals whose age spans four decades. Participant's age given at the head of each column.

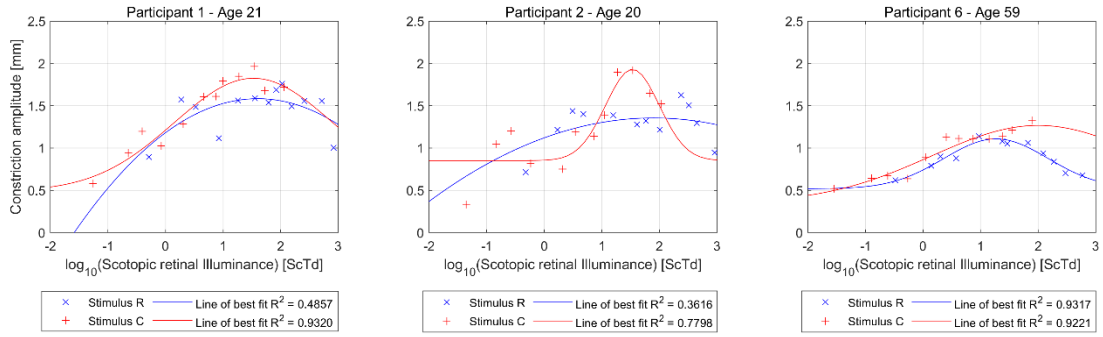

Figure 4-12: Constriction amplitude as a function of scotopic retinal illuminance for the remaining three participants not shown in Figure 4-11. The fitting of the Gaussian curves to the constriction amplitude data for each stimulus was undertaken without any constraints but a starting point was provided.

Coefficient	A (pedestal)	B (amplitude)	C (peak location)	D (spread)
Upper limit	0.75	2.50	2.00	2.00
Lower limit	0	0	0	0.50

Table 4-2: Bounding criteria used to fit the Gaussian function, Equation 26, to the constriction amplitude data for both stimuli.

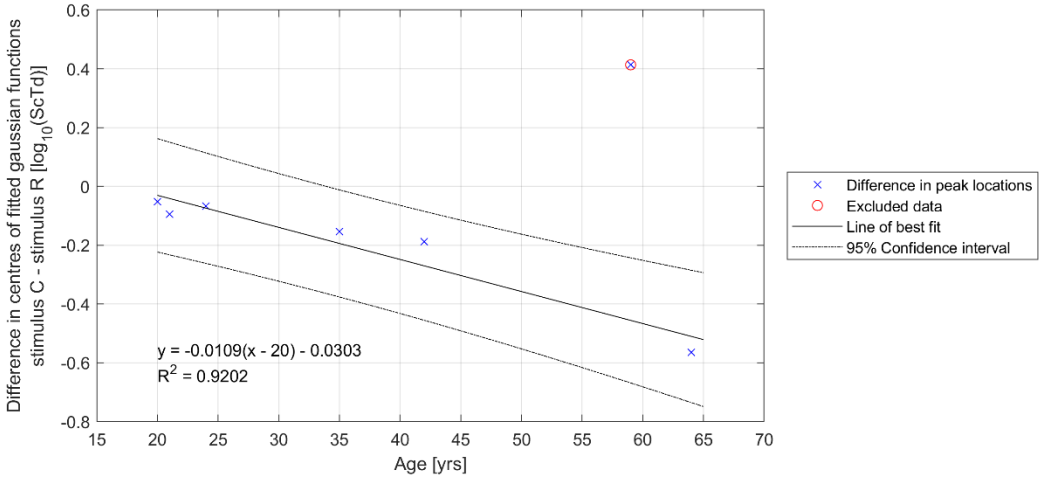

Figure 4-13: The offset between the centres of the Gaussian function fitted to the constriction amplitude data, expressed in photopic retinal illuminance, as a function of participant's age.

The data for participant 6 was excluded from the fitting of the line of best fit in Figure 4-13 that confirms the shift in the two peaks as a function of age. The magnitude of the difference in the Gaussian centres for participant 6 was considered too large to be representative of the global behaviour based upon the confidence intervals of the plotted solution. To assess whether this hypothesis was well founded, participant 6's data was re-evaluated, as illustrated in Figure 4-14.

The process of re-evaluating participant 6's data has been based on assuming that the data supports the proposed model. The process started with fitting the pre-stimulus diameter data for both stimuli to a single function given by Equation 25. In addition, the pupil diameter at peak constriction for the two stimuli were fitted separately using the same equation, as shown in the left-hand graph of Figure 4-14. From these three functions, the (model) constriction amplitudes for the two stimuli were calculated and

plotted alongside the actual data, as shown in the top right graph of Figure 4-14. The R^2 values of 0.7190 and 0.8704 respectively for stimulus R and C confirm the good level of agreement of the raw data with the model. Lastly, the difference in Gaussian function centres were plotted as a function of age with the revised estimate for participant 6 (highlighted) as shown in the bottom right-hand corner of Figure 4-14. The calculation of the line of best fit includes the revised data for participant 6, which now lies within the confidence intervals at 95%. Although the R^2 value is lower than when participant 6 was excluded, there is good agreement for all participants below the age of 45 years.

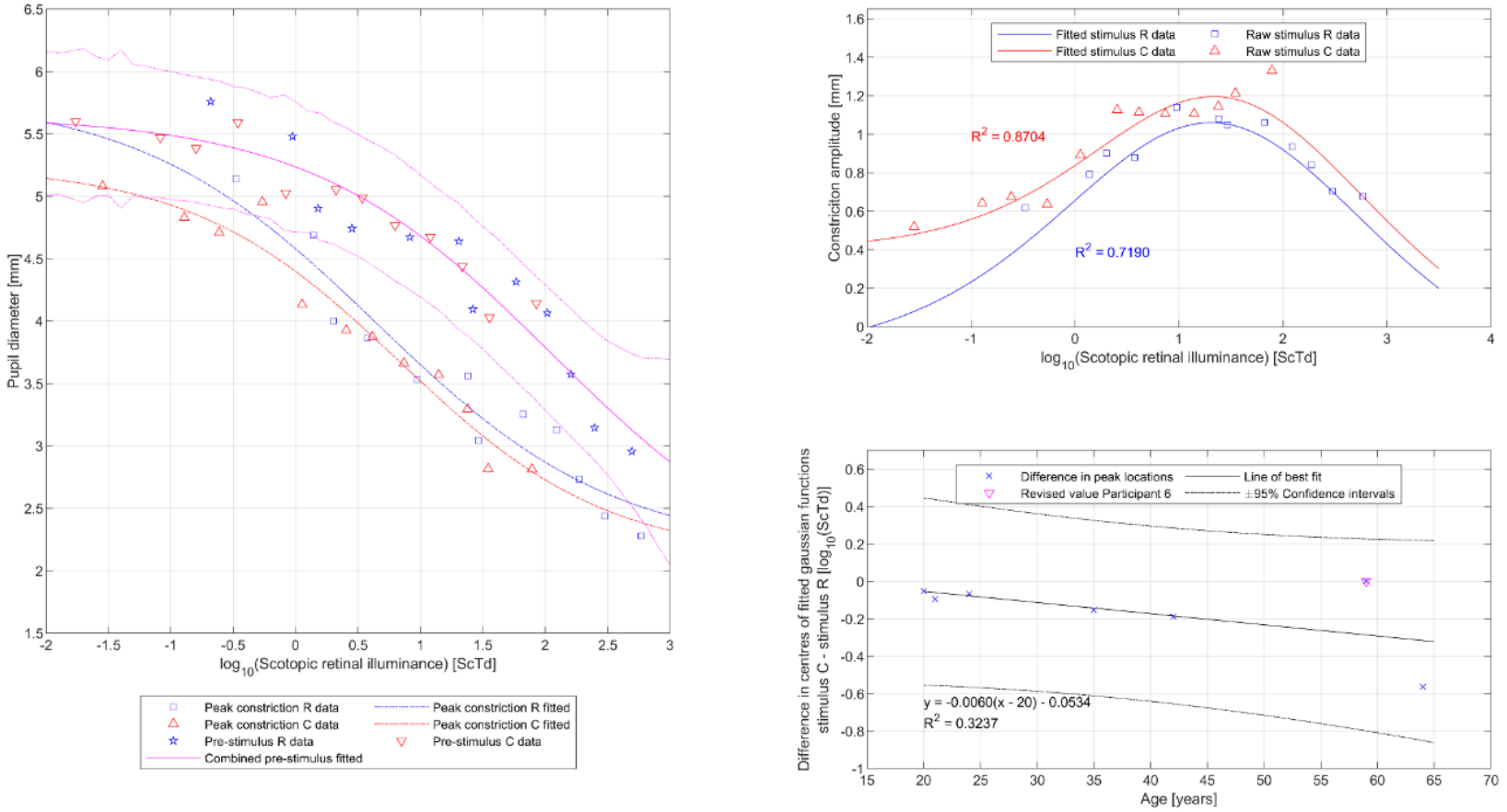

Figure 4-14: Re-evaluation of the data for participant 6. (Left) Model pre-stimulus diameter under scotopic conditions plotted along with fitted curves for peak constricted diameter for the two stimuli. (Top right) The modelled constriction amplitude Gaussian functions plotted alongside raw constriction amplitude values. (Bottom right) Updated graph of the difference in the peak value of the two Gaussian functions as a function of age for all participants.

Having formulated a model for constriction amplitude as a function of scotopic retinal illuminance, the results when expressed as a function of photopic retinal illuminance were evaluated using the same methodology as described above. The two sets of data are presented in Figure 4-15 with resulting lines of best fit. These lines of best fit define the relationship in terms of scotopic and photopic retinal illuminance. The photopic function is effectively the scotopic function shifted by the ratio of the S/P values for the two stimuli.

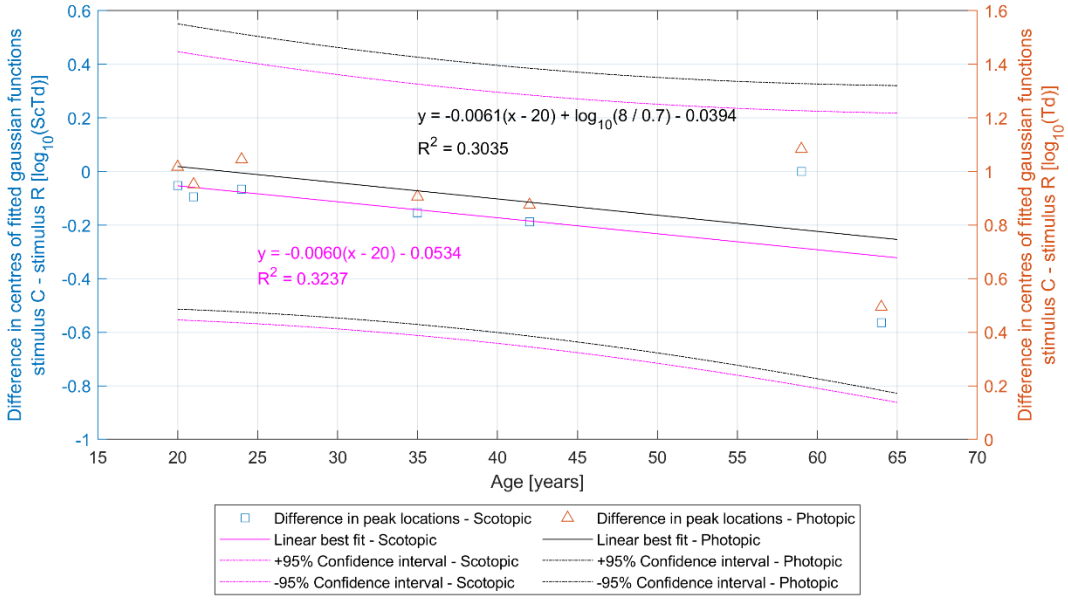

Figure 4-15: The difference between the Gaussian function centres describing the constriction amplitudes for the two stimuli in terms of scotopic retinal illuminance (left hand axis) and photopic retinal illuminance (right hand axis) as a function of age.

The underlying effect demonstrated in Figure 4-15 is that the retinal illuminance at which the peak in constriction amplitude occurs decreases by 0.27 log Td between 20 and 65 years for this small cohort. The observed shift is independent of whether the retinal illuminance is expressed in scotopic or photopic units, as expected. The reasons for this shift are discussed in section 4.4.2.

The relationship shown in Figure 4-16 is based upon the location of the centre of the gaussians describing the constriction amplitude for the two stimuli as a function of retinal illuminance. This data, plotted as a function of age, is presented in Figure 4-16. The trend, shown by the lines of best fit, is a reduction in the scotopic retinal illuminance at which the peak constriction occurs. The magnitude of the shift is greater for stimulus C than for stimulus R. The difference between these two lines of best fit is the metric plotted in Figure 4-15. The indication is that the larger change occurs in the response to stimulus C as identified from the appearance of Figure 4-16, where the constriction amplitude function for stimulus C shifts towards lower retinal illuminance values with increasing age.

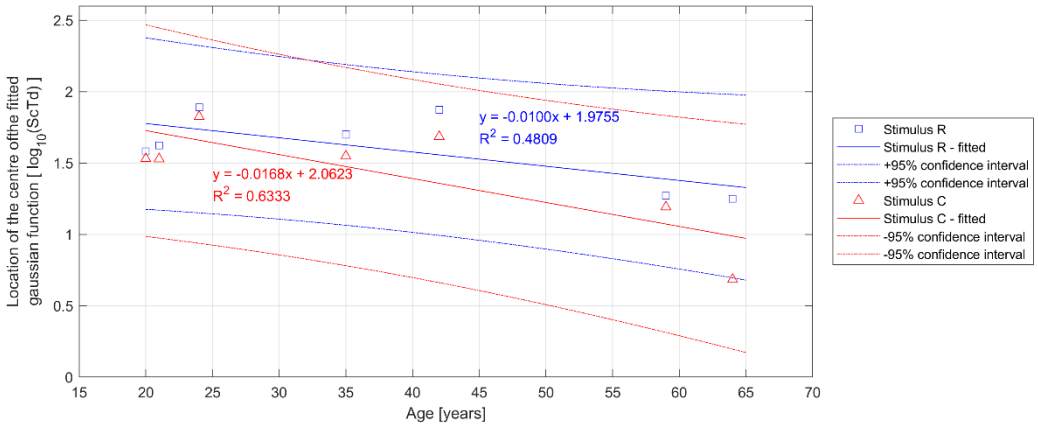

Figure 4-16: Centres of the fitted Gaussian functions as a function of participant age.

The variation in the magnitude of the peak constriction amplitude as a function of age is plotted Figure 4-17. This shows the reduction in overall amplitude of the fitted Gaussian functions with a greater rate of reduction observed for the stimulus C. Based upon the lines of best fit, by the age of ~70 years the peak constriction amplitude for the two stimuli will be equivalent. The graphs indicate that for a 20 year old, the difference in the peak constriction amplitudes is ~0.30mm.

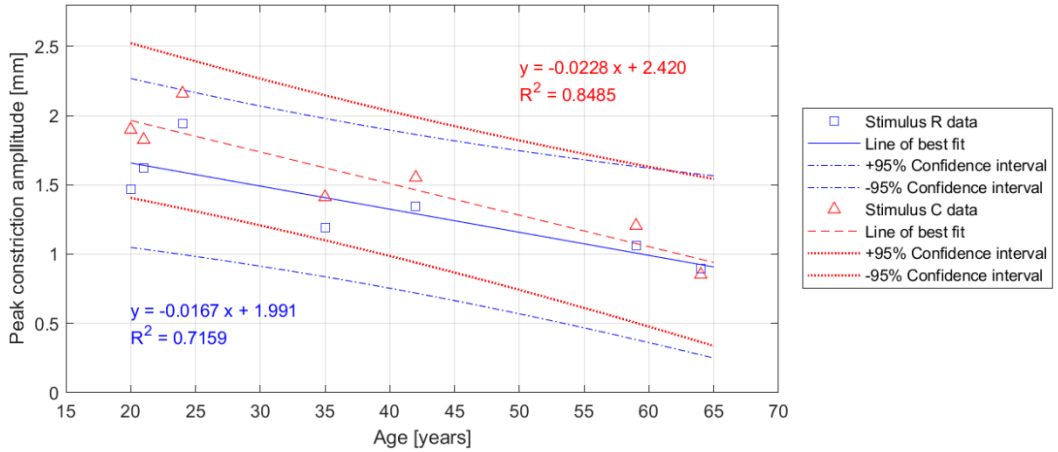

Figure 4-17: The variation in peak constriction amplitude as a function of age for both stimulus R and C.

The result of this analysis indicates a change in the amplitude of the transient PLR as a function of age with an additional dependency on the S/P of the stimulus.

4.3.2.3 Constriction Latency

The temporal properties of the transient response, described by the constriction latency, have been plotted as a function of both photopic and scotopic retinal illuminance for participants 2, 5, 6, and 7 in Figure 4-18. The data have been fitted with a line of best fit based upon Equation 25 to describe constriction latency as a function of retinal illuminance. This has been successful with all R^2 values above 0.88, and 20 of the 28 values being above 0.95.

The application of this model for describing constriction latency as a function of retinal illuminance allows for an upper asymptote that appears to coincide with the upper asymptote observed for the pre-stimulus diameter. A linear relationship, as a function of log retinal illuminance, would not allow for the observed

upper asymptote. For participants 6 and 7, there also appears to be a lower asymptote to the constriction latency where the response to stimulus R and C converge. When plotted in terms of photopic retinal illuminance, the latency is shorter for stimulus R. However, when plotted as a function of scotopic retinal illuminance, the two functions intercept. For retinal illuminance values to the right of the intercept, the constriction latency of stimulus C is shorter than that for stimulus R. Unlike the pre-stimulus pupil diameter and constriction amplitude, constriction latency does not appear to converge on a single function when plotted in terms of scotopic retinal illuminance.

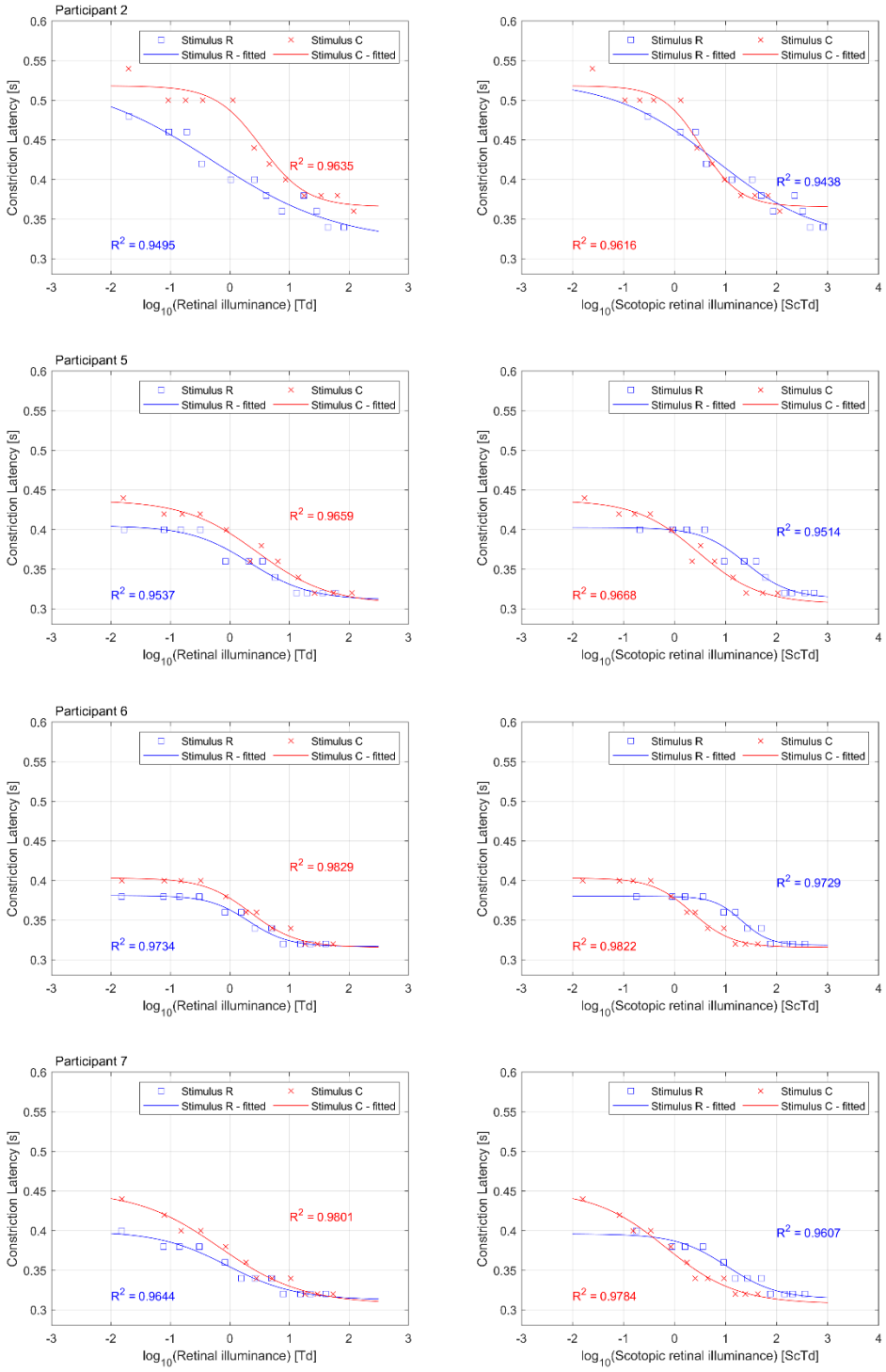

Figure 4-18: Constriction amplitude as a function of photopic (left hand side) and scotopic (right hand side) retinal illuminance for participants 2, 5, 6, and 7 (top to bottom).

The second interception point at 2ScTd for participant 2's data is thought to be a result of the lack of data for stimulus C above a scotopic retinal illuminance of 2.2 logScTd. The lack of an upper asymptote for participant 2's constriction latency data for stimulus R suggests that the pre-stimulus diameter for Participant 2 at low retinal illuminance values had not reached its lower asymptotic value as the latency values would appear to be increasing as retinal illuminance is reduced. Looking back at Figure 4-6, participant 2 had a smaller pupil diameter at lower light levels compared to participants 1 and 3.

From the graphs of constriction latency as a function of retinal illuminance (Figure 4-18), there appears to be a general trend of constriction latency decreasing as a function of age. This is supported by Figure 4-19 where the constriction latencies at a retinal illuminance of -1 logTd and +1 logTd have been plotted as a function of age. These retinal illuminance values correspond to the region where, for all participants, the constriction latencies for both stimuli appear to vary linearly as a function of log retinal illuminance. Within this region the gradients of the lines of best fit are broadly equivalent for the two stimulus conditions. The reduction in constriction latency as a function of age appears to be dependent on retinal illuminance and the S/P ratio of the stimulus.

The cause of the lower value for the coefficient of determination appears to be the results for participants 1 and 2. These two data points appear to have had little effect on the overall trend as a function of age for either of the retinal illuminance levels.

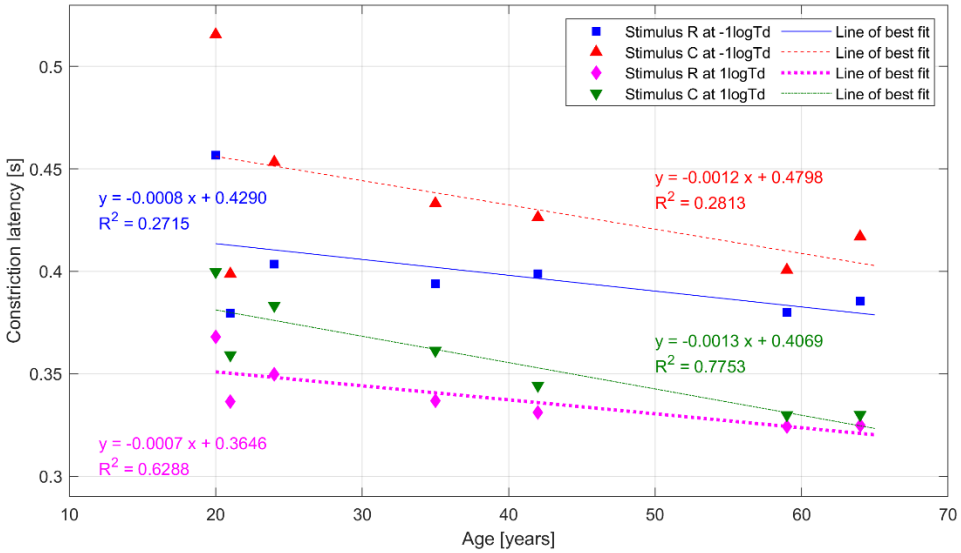

Figure 4-19: Constriction latency evaluated at a retinal illuminance of ±1 log Td as a function of participant age.

Based upon the previous observation, the intersection point between the constriction latency for stimulus R and C in scotopic retinal illuminance as a function of participant's age has been plotted in Figure 4-20. This graph indicates that there is a linear relationship with the intersection point shifting towards lower scotopic retinal illuminance values as participant's age increases. The magnitude of the effect is ~1 log ScTd over the age range of the participants.

As previously demonstrated in Figure 4-18, the result of the translation from photopic to scotopic retinal illuminance is the intersection of the two functions defining constriction latency as a function of scotopic

retinal illuminance for the two stimuli. The log of the scotopic retinal illuminance at which the functions intersect appears to vary linearly as a function of age as demonstrated in Figure 4-20. The coefficient of determination indicates a good fit to the data which fall within the 95% confidence intervals. Subsequent analysis calculated Pearson's linear correlation coefficient as having a value of -0.9422 with an associated p-value of 0.0015, indicating that the correlation is significantly different from zero.

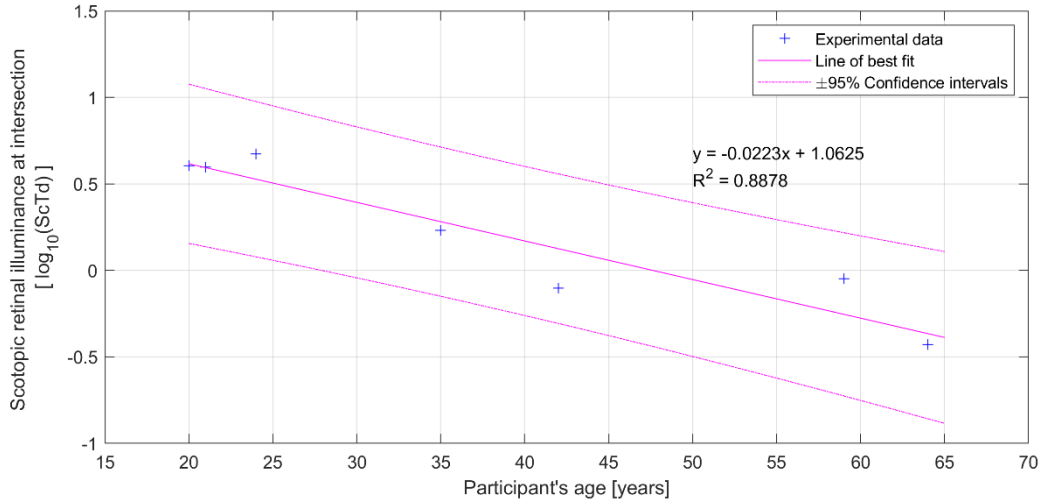

Figure 4-20: Variation of the intersection point between the constriction latency for stimulus R and C in scotopic retinal illuminance as a function of participant's age.

Together with the results for the constriction amplitude, these results indicate a change in the dynamic between rod and cone mediated inputs to the transient pupil response as a function of both scotopic retinal illuminance and age.

These changes are summarised in the following points:

- For young participants, the peak in constriction amplitude occurs at ~2ScTd.
- The peak constriction shifts to lower retinal illuminance values as a function of age.
- Constriction amplitude decreases as age increases.
- Constriction latency decreases as retinal illuminance increases.
- Constriction latency decreases as S/P ratio increases for the same photopic retinal illuminance.
- Constriction latency decreases as age increases.

4.4 Discussion

The sub-sections that follow initially discuss the key findings with respect to the three metrics used to describe the pre-stimulus diameter and the transient component of the PLR to a 100% positive contrast stimulus. From this discussion, theories are developed describing the mediation of both the steady state, pre-stimulus pupil diameter and the transient response to stimulus onset. This is followed by a consideration of the limitations of the study and confounding factors that may have influenced the outcomes of the study as well as lessons learnt for future work.

4.4.1 Pre-stimulus pupil diameter

For all participants, it has been demonstrated that the steady state, pre-stimulus pupil diameter is primarily mediated by rod photoreceptors for stimuli with luminance values between 0.001cd.m^{-2} and 9cd.m^{-2}. When plotted as a function of photopic retinal illuminance, the pre-stimulus diameters for the two stimuli chromaticities resulted in two separate curves of the form proposed by Stanley and Davies (1995) given in Equation 25. When plotted as a function of scotopic retinal illuminance, the pre-stimulus diameters for the two stimuli aligned and were fitted by a single function, described by Equation 25, with R^2 values close to unity. This observation agrees with the literature considered in section 4.1.1.1 and confirms the hypothesis that the rod enriched stimulus R used by the RCS test instigates a rod mediated response.

The involvement of cones in the steady state pupil diameter is limited. If there was a luminance (L + M) based cone response, then it would be expected that the curves for stimulus R and C would be the other way round in Figure 4-4. As it is, there is greater constriction as a function of photopic retinal illuminance for stimulus R. Alternatively this could be an S cone response, given the similarities in the two sensitivity functions. However the literature provides support to a rod mediated response based upon the action spectrum of the PLR (Alpern and Campbell 1962).

The steady state pupil diameter starts to constrict for retinal illuminance values between –0.5 and 0.5 log ScTd. By the point at which the rods are starting to saturate, at 2ScTd (Aguilar and Stiles 1954), the pre-stimulus pupil diameter is already between ~33% and ~50% of its constriction range, i.e. the difference between the upper and lower diameter asymptotes. The constriction continues as retinal illuminance increases to the point where rods are fully saturated, projected to be between 3.0 and 4.0 log ScTd. Controlling the retinal illumination by reducing the pupil diameter has benefits for the rods, as it ensures their contribution to wider visual function. The results support the hypothesis that for mesopic light levels, rod photoreceptors mediate steady state pupil diameter.

Evaluating the pre-stimulus pupil diameter at fixed scotopic retinal illuminance values demonstrated that pupil size declines more steeply as a function of age at 2 log ScTd than at -1 log ScTd. These two retinal illuminance values span firstly, the range where initially the pupil diameter is close to the upper asymptote of Equation 25, and secondly, the region where the pupil has constricted to control the illumination on the retina as rods start to saturate.

A comparison with the results of Winn *et al* (1994) indicated that for the same stimulus luminance there was a similar reduction in pupil diameter as a function of the participant's age for stimulus C. The pupil diameters for this study at 9cd.m^{-2} were smaller than those of Winn *et al* due to the larger corneal flux of the stimuli used in this study.

The identified variation of pre-stimulus pupil diameter as a function of age is in agreement with similar studies (Bitsios *et al* 1996). The reduction in pupil diameter has been linked to losses in sympathetic tone causing a shift in the equilibrium between the pupil dilator and sphincter muscles (Bitsios *et al* 1996). In addition, the agreement between the results for this study and that of Winn *et* al gives confidence that the results for this study's small cohort (n=7) are representative of the wider population in terms of age.

Winn *et al* did not evaluate the contributions of the effects of aging they identified on the reduction in pupil diameter as a function of age.

4.4.2 Constriction amplitude

Plotting the constriction amplitudes for the two stimulus conditions as a function of photopic retinal illuminance resulted in two separate functions. When the S/P value of each stimulus was accounted for and the data plotted as a function of scotopic retinal illuminance, the peaks of the two curves aligned. This further supports the hypotheses that stimulus R instigates a rod mediated response and that the underlying reference frame for the transient response to a positive contrast stimulus is rod mediated.

The peak constriction for the cohort generally aligned between 1.5 to 2.0 log ScTd, however the peak constriction amplitude was 0.2 to 0.3mm higher for stimulus C, compared to stimulus R. This suggests that a greater contribution from L and M cones, based upon the colorimetry of stimulus C, results in a larger constriction when compared to that from stimulus R at an equivalent scotopic retinal illuminance. The luminance values of the stimuli were sufficient for the stimulation of cones as the colour of the stimuli was perceived by participants. If rods are starting to saturate between 1.5 to 2.0 log ScTd, the cones will potentially have the greater sensitivity to changes in illumination as the background luminance increases.

Taking a generalised case, the peak value of the constriction amplitude plotted as a function of scotopic retinal illuminance broadly aligns to ~1.7 log ScTd with the right-hand tail of the Gaussian model approaching the pedestal by ~3.5 log ScTd. These values align with those of Aguilar and Stiles (1954) in their study of the saturation of the rod mechanism. Their conclusion was that rod sensitivity started to reduce at 2 log ScTd and becomes saturated between 3.3 to 3.7 log ScTd. This then provides an explanation for the shape of the constriction amplitude function. The pupil constricts whilst the rods are sensitive to the change in retinal illumination. Once the rods start to saturate, the amplitude of any further constriction is likely to be bounded by the physical limits of how much the iris sphincter muscle can constrict. The reduction in constriction amplitude at higher retinal illuminance values aligns with the transition to the lower asymptote as steady state pupil diameter approaches ~2mm, i.e. the limit to which the iris sphincter muscle can constrict.

The ~0.3mm difference between the peak constriction amplitude for the two stimulus conditions is thought to be a real effect. There was no additional manipulation of the raw data to generate the original sets of graphs apart from the removal of responses which were affected by eye blinks or prolonged closures. This happened during both stimulus conditions to a similar degree so is unlikely to have confounded the data.

The analysis demonstrated that the constriction amplitude could be modelled as a Gaussian function with a pedestal, see Equation 26, with the use of appropriate upper and lower bounding conditions, given in Table 4-2. The bounding conditions were based upon the properties of the constriction amplitude data for most of the group. Whilst the main Gaussian function accounted for the constriction amplitude as a function of retinal illuminance, the pedestal accounts for any small constrictions that may occur in the asymptotic regions of the steady state pupil function, which would cause an offset in the constriction amplitude. The level of fit achieved is demonstrated by the high R^2 values.

The analysis also applied the proposed Gaussian model to the data for participant 6 enabling a reasonable level of fit to be obtained.

Comparing the proposed constriction amplitude model with the study by Ellis (1981) provides a method of assessing the similarities of the measurements made and effects being characterised. Ellis fitted a quadratic to the relationship between direct light reflex amplitude (constriction amplitude) and stimulus intensity, but as demonstrated in Figure 4-21 this could equally be fitted by the proposed Gaussian function. The fitted solution resulted in a zero pedestal, hence the first term has been dropped from the equation shown in the graph.

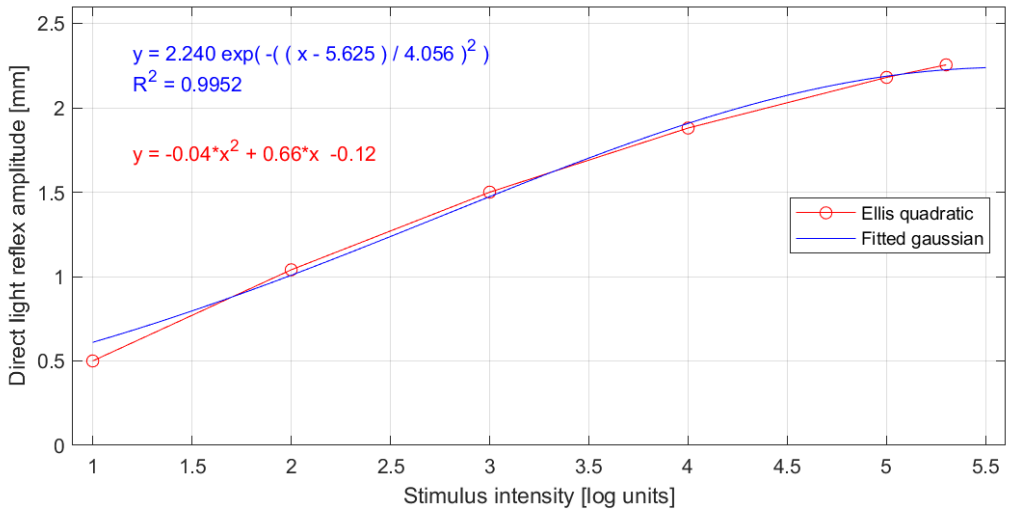

Figure 4-21: Comparison of Ellis' model for direct reflex amplitude with the proposed Gaussian model.

The result of fitting the Gaussian model to the data has indicated two potential age-based variations in constriction amplitude. Firstly, the results indicate a shift in the peak of the Gaussian function for both stimuli to lower scotopic retinal illuminance values as a function of age. The shift observed for stimulus C is greater than that for stimulus R, as shown in Figure 4-15 and Figure 4-16. Secondly, the amplitude of the peak constriction reduces as a function of age, as illustrated in Figure 4-17, with the rate of decline in the peak amplitude being greater for stimulus C.

Whilst the first is harder to explain, the second observation could be the effect of senile miosis reducing the pupil diameter as a function of age, which subsequently reduces the available range over which the pupil can constrict. The physical limit of how much space muscle fibres occupy when fully constricted imposes the lower limit on the amplitude of constriction. Although this lower limit of constriction amplitude was not evaluated within this study, it is expected that this lies at ~2mm based upon the consensus in the literature and is the same for both young and older participants.

Alternatively, or jointly, there could be a change in the balance in the mediation of the transient response, which is a function of increasing age. If it were purely due to an increasing effect of senile miosis, the reduction in amplitude would be similar for both stimulus conditions as a function of age. This would result in a simple fixed offset in the range of the pupil size across all light levels and the value of the upper asymptote would be reduced by the same amount. This is not the case, with the change in the response

amplitude to stimulus C being greater than that for stimulus R. This indicates a change in the mediation of the transient response as a function of age. In terms of visual function, it has been established that there are age related changes in flicker thresholds that have been measured using stimuli with similar/equivalent chromaticities (Hathibelagal *et al* 2020).

The increasing separation between the peaks of the constriction amplitudes for stimulus R and C in terms of scotopic retinal illuminance resulted in a change of ~0.27 log ScTd over the 45 year age range of the participants. This result indicates a change in the dynamic of the transient response and the contributions of the mediating photoreceptors to the increment in retinal illuminance. It also correlates with the change observed in the steady state pre-stimulus pupil diameter.

The attribution of this effect to a single cause is not possible. The attenuation of shorter wavelengths by the lens will cause a reduction in the stimulation of rods and S-cones and impact the signal received at the ipRGCs. The retinal illuminance values evaluated by this study are below the threshold of melanopsin contained within the ipRGCs. The ipRGCs can thus be considered as acting purely as RGCs for the PLR. Jackson *et al* (1999) suggest that scotopic thresholds are elevated as a result of slower rhodopsin regeneration as a function of age. The impact of changes in lens spectral transmittance and age-related changes in rod density cannot be fully resolved without additional measurements of lens transmission or knowledge of a participant's retinal topography. Any future study should, as a minimum, include characterising the transmission spectra of the lens and the degree of senile miosis in addition to the measurement of the PLR to stimuli with differing S/P.

The result of these age-related changes on the balance between rod and cone mediated responses entering the ipRGCs will be an imbalance in favour of cones. The imbalance would be observed as lower thresholds for cone mediated responses relative to those mediated by rods. This explanation is supported by a separate study, undertaken using the RCS test, that demonstrated rod mediated FMTs increase more than cone FMTs as a function of age for participants over the age of ~45 years (Hathibelagal *et al* 2020).

Based upon this, whilst it may be concluded that the rods mediate the underlying response, contributions from L and M cones affect the amplitude of the transient response to a positive stimulus of a fixed contrast with respect to the background luminance for mesopic light levels. The effects of age on the eye appear to result in a shift in the dynamic of the transient PLR in the favour of a cone-mediated response, which should still be viewed in the scotopic reference frame.

4.4.3 Constriction latency

The result that constriction latency reduces as a function of increasing stimulus intensity is in agreement with other studies (Feinberg and Podolak 1965, Fan *et al* 2009, Ellis 1981, Bergamin and Kardon 2003). However, none of these studies attempted to describe the change in constriction latency as a function of retinal illuminance. (It is noted that Ellis fits a second order polynomial to express latency as a function of stimulus intensity in log units.) Although limited in statistical power, the results of the current study suggest that constriction latency can be represented by a sigmoid like function, like that used to describe the pupil diameter as a function of corneal flux or retinal illuminance (Watson and Yellott 2012, Stanley and Davies 1995).

This model has shown good agreement with the data but may have been compromised by the quantisation of the latency data by the frame rate of the video acquisition system. The sigmoid function enables the model to account for the apparently asymptotic behaviour of the latency data for stimuli at the lower and upper ranges of luminance values tested. Both the quadratic of Ellis (1981) and data of Bergamin and Kardon (2003) can be approximated by the sigmoid function. The ~3 log unit range of stimulus intensities (quoted as 0.319cd.m^{-2} to 31.9cd.m^{-2}) used by Bergamin and Kardon (2003) aligns to the transition from mesopic to photopic vision. It is in part because of Bergamin and Kardon's study, that there is confidence in the definition that the constriction latency has a lower asymptote as stimulus luminance increases. In figure 3 of their journal paper the transition is clear and in terms of the proposed model, would align with the transition from the linear region to the lower asymptote. In comparison, this current study has concentrated on the high scotopic (0.001cd.m^{-2}) to boundary between the mesopic and photopic visual ranges (9cd.m^{-2}).

When constriction latency is plotted as a function of photopic retinal illuminance, it appears that rods mediate the faster response. For the young participants, the data for stimulus R appears to correspond to the region between the sigmoid function's asymptotes. For stimulus C, the function suggests an asymptote at one or both ends of the data. Plotting constriction latency as a function of scotopic retinal illuminance, the two functions intersect but do not co-align like the pre-stimulus diameter data. The indication is that in terms of scotopic retinal illuminance, there comes a point when constriction latency appears to be primarily mediated by cones rather than rods. Figure 4-20 predicts this intersection point shifts by 1 log ScTd from 0.6 to -0.4 log ScTd towards lower retinal illuminance values over the 45 year age range of the participants. This shift is like that observed for constriction amplitude both in terms of favouring a cone-mediated response as well as the magnitude of the shift in terms of scotopic retinal illuminance. The rate of reduction in the latency is between 1.5 and 2 times greater for stimulus C compared to that for stimulus R. This indicates a change in the balance between rods and cones, in favour of cones mediating the pupil's transient response as a function of age.

This may initially seem to go against the conclusions of other studies (Lobato-Rincón *et al* 2014), but this may be a question of stimulus duration, units and accounting for equivalency at the retina. Lobato-Rincón *et al* used a 200ms stimulus duration compared to the 3s used for this study to ensure the full transient response of the pupil was recorded. The reason why this current study has been based around retinal illuminance is so that the response of photoreceptors can be evaluated based upon the same amount of light being incident upon both rods and cones.

It is already understood that cone mediated vision has a faster response than rod mediated vision, as demonstrated by the temporal sensitivity function (Kelly 1961). The duality of the rod pathway, with its slow and fast pathways, coupled with the change from purely rod mediated to rod-cone mediated vision (Stockman *et al* 1991, Sharpe *et al* 1989, Conner 1982) affects how the temporal modulations of luminance are processed. Coupling the temporal properties of the photoreceptors to the step function of the stimulus onset, which consists of high, medium, and low frequency components, the increasing luminance of the background and stimulus results in shorter latencies to stimulus onset as retinal illuminance increases.

The intersection of the constriction latency function for stimulus R and C would suggest a link to a point where cone-mediated signals dominate the rod-mediated response, i.e. the point where cones start to contribute to the mediation of the transient response. The faster transmission pathway, without the delays of the two rod pathways, results in the shorter constriction latencies as retinal illuminance increases beyond the cone threshold. Beyond the initial intersection point, both curves co-align to an asymptote where constriction latency is independent of any further increase in (scotopic) retinal illuminance. The occasions where there is a second intersection point at the upper limit of the measurement range are due to the lack of data to enable the lower asymptote to be fitted/predicted accurately. The wider literature suggest that the lower latency value should be around 200ms for a young normal (Fan *et al* 2009, Lowenstein and Freidman 1942).

4.4.4 Summary of transient PLR dynamics

To understand the dynamics of the PLR, as indicated by the results of this study, there is a need to consider the PLR in terms of scotopic units. When plotted as a function of photopic retinal illuminance the metrics used to characterise the PLR do not align. Photopically the response latency to stimulus R was shorter than that for stimulus C. However, once the stimulus conditions are converted to scotopic units, the onset of the cone contribution to the underlying rod mediated response is observed. This effective transition from rod to cone mediation of the transient PLR occurs at the point of intersection between the constriction latencies for the two stimuli used in this study, i.e. ~0.5 log ScTd for the young participants. The results indicate that as the participant's age increases the retinal illuminance of this intersection point decreases.

Together the joint response of the rod-cone interaction results in the constriction of the pupil as retinal illuminance increases. The peak constriction amplitude is reached when the rods start to saturate. Beyond this point it is thought that the constriction amplitude is limited by a combination of continued rod saturation and the physical limitations of the iris sphincter resulting in a reduction in constriction amplitude.

Whilst the rods mediate the steady state, pre-stimulus diameter of the pupil, the mediation of the transient response at mesopic illumination levels is reliant upon the rod-cone pathway illustrated schematically by Lucas *et al* (2014), which determines the amplitude and latency of the response. This is equivalent to the mediation of visual function across the same range of illumination and supports the concept of a shared architecture for visual and pupillary functions.

This theory agrees in part with the results that McDougal and Gamlin (2010) obtained for the relative contributions of the three photosensitive cells that drive the PLR. Their results showed that the shorter the stimulus duration, the higher the relative contribution from cones compared to rods. In terms of the transient response, the rod-cone pathway is responding to the initial change in light intensity, which as Alpern *et al* (1963) demonstrated is a product of flash duration and intensity.

From the metrics applied to characterise the PLR, there is evidence that the PLR transitions from being purely rod-mediated under scotopic conditions. Under mesopic conditions the PLR is mediated by both rods and cones with the contributions varying as a function retinal illumination. The indications are that

the photopic PLR is mediated by cones with melanopsin containing ipRGCs providing additional protection to the retina under high illumination conditions, observed as the sustained constriction post stimulus offset.

4.4.5 Proposed theory

The indications are that the observed differences in pre-stimulus and transient PLR as a function of participant age are real. There is agreement between the age dependency of the pupil diameter reported by Winn *et al* (1994) and the results of this study for stimulus C at 9cd.m^{-2}, with a similar rate of decline reported. The offset between the results of Winn *et al* and those of this study have been explained by the larger corneal flux used for this study resulting in smaller pupil diameters.

Age related changes in the spectral transmittance of the crystalline lens result in a reduction in the rod mediated response. Additionally, there are age related changes in retinal topography. Studies of the effects of age on the human retina conclude that the density of rods decreases as a function of age, whilst there is only a small reduction in cones (Curcio *et al* 1993, Gao and Hollyfield 1992). Gao and Hollyfield reported that the rate of equatorial rod cell loss is faster between the ages of 17 to 44 (970 cells/mm^2/yr) than between the ages of 57 to 95 (570 cells/mm^2/yr). The rate of equatorial cone cell loss occurs at a uniform rate of 16 cells/mm^2/yr. The different rates of loss should be viewed with the knowledge that rods have a much higher density than cones in the peripheral regions of the retina.

The impact of the reduced regeneration rates of rhodopsin as a function of age (Jackson *et al* 1999) will also affect the transient response leading to greater weight placed on the cone mediated response as illumination levels increase. This could be enough to cause the shifts in the constriction amplitude and latency for the two stimulus conditions as a function of age.

The optical properties of the lens change as a function of age, giving it a yellow appearance. The effect of this is to attenuate the amount of blue light reaching the retina with the lens acting as a low (frequency) pass filter. At 400nm the average density of the lens increases by 0.12 density units/decade between 20 and 60 years. This rate increases to 0.40 density units/decade above 60 years (Pokorny *et al* 1987). The attenuation of blue light will reduce the stimulation of rods and S-cones at mesopic light levels.

Senile miosis attenuates the illumination incident upon the retina at lower retinal illuminance levels, as demonstrated by the pre-stimulus diameters across the study cohort. Senile miosis limits the pupil's size by reducing the range over which it dilates. This constrains the peak constriction amplitude achieved leading to a reduction as a function of increasing age. This effect has been demonstrated in this study with a reduction from 2mm to 1mm across the study cohort. These peak constriction amplitudes may seem low, but this study only used a 100% contrast stimulus based upon the luminance of the background scene. This should be viewed in the context of other studies that have demonstrated the relationship between the contrast (Gamlin *et al* 1998) or intensity (Alpern *et al* 1963) of the stimulus and constriction amplitude.

It is hypothesised that the combination of these effects will result in a reduction in the magnitude of the rod response reaching the ipRGC compared to that from the cones at mesopic light levels (for a young

normal). These light levels are below the threshold of melanopsin within the ipRGCs, so the contribution of melanopsin has not been included in the proposed theory.

The two graphs in Figure 4-22 seek to illustrate the effects of aging in the context of the results of this study. The two sets of relative weighting functions for the young and older participants are based upon the generalised result for a 20 year-old and a 65 year-old participant respectively. The proposed model does not describe all the observed changes in the PLR as a function of age, but it does provide a basis for illustrating the proposed mechanisms behind them.

As shown in the top graph of Figure 4-22, when retinal illuminance is low, rods dominate visual function whilst cones are below their threshold. For the reference case of the 20 year-old normal, rods and cones are fully functioning, i.e. 0 when fully saturated (rods) or below threshold (cones), and 1 when primarily mediating vision. For the second test case (~65 year-old), the combined effect of the increased attenuation of shorter wavelengths, and the relative reduction in density of rod photoreceptors, compared to cones, has been modelled as an overall reduction in the strength of the rod response compared to that from the cones. For the basis of the model, it is assumed that the change in cone function with age is negligible and so the same cone function is used for both test cases. The scotopic retinal illumination values where the rod and cone functions intersect for the two test cases are calculated from the line of best fit in Figure 4-20. This defines the intersection point for the constriction latencies for stimulus R and C as a function of age.

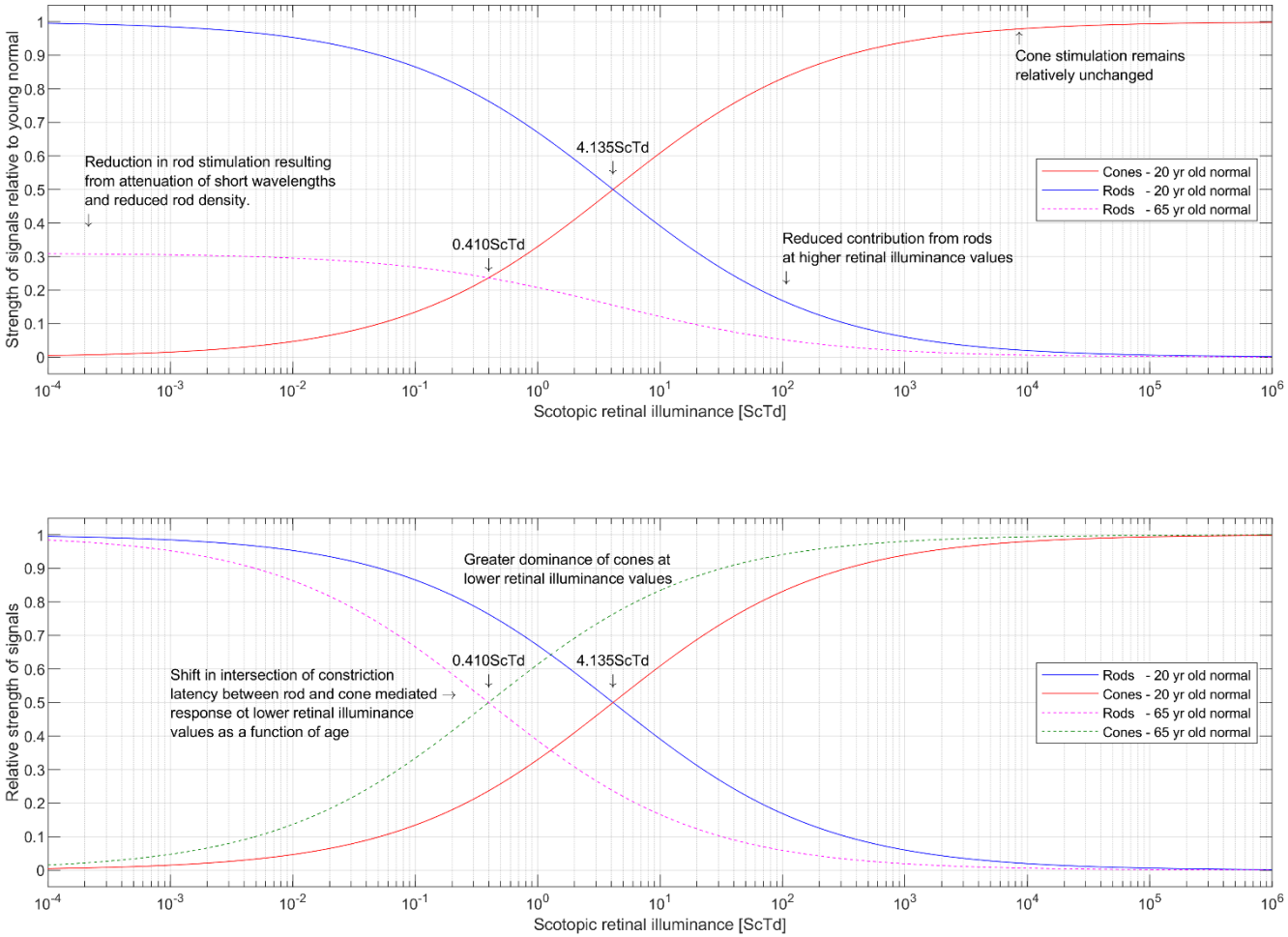

Figure 4-22: Illustration of the effect of age on the PLR in terms of signal strength of rod and cone photoreceptors (top) and relative strength to photoreceptor signals (bottom) as a function of scotopic retinal illuminance.

The coefficients for the three curves based upon the Stanley Davies equation, Equation 25, are provided in Table 4-3.

The graph of the cone signal strength is acknowledged not to be true representation on the onset of a cone -mediated response. In reality, the cone signals have more of an abrupt threshold, equivalent to 1TdSc at 8mm pupil diameter for a -2.7 log cd.m^{-2} stimulus (Barrionuevo *et al* 2014), instead of the gradual increase between -4 and -1 log ScTd.

To align the curves to achieve an intersection at 0.41ScTd for the 65 year-old test case, only the amplitude of the rod curve has been changed, i.e. coefficients C_1 and C_2 defined in Table 4-3. The reason why only the initial amplitude is modified is that an age-based reduction in rod density, rhodopsin regeneration rates and the light incident upon the retina due to increased attenuation of blue light by the lens, will reduce the signal reaching the ipRGCs. Senile miosis will further reduce the retinal illuminance by constraining the pupil's ability to dilate.

Curve	Coefficient				
	C_1	C_2	C_3	C_4	C_5
Cone – 20 year-old	0	-1	4.135	0.5	1
Rods – 20 year-old	1	1	4.135	0.5	1
Rods – 65 year-old	0.31	0.31	4.135	0.5	1

Table 4-3: Table of coefficients for the curves in the top graph of Figure 4-22. The form of the function is given by the Stanley-Davies equation (Equation 25).

Compared to the young normal, this change in rod response/function relative to retinal illuminance is consistent with the shift in retinal illuminance at which the peak constriction amplitude occurs for stimulus R illustrated in Figure 4-17.

Considering the lower graph in Figure 4-22, the two pairs of curves for the young and older participant have been generated by considering the relative contribution of the rods and cones to the stimulation of the ipRGC. The equations used to calculate these contributions are given in Equation 27 and Equation 28.

$$f_{Rod}(E) = \frac{R(E)}{R(E) + C(E)}$$

Equation 27: Relative contribution to ipRGC stimulation for rod photoreceptors.

$$f_{Cone}(E) = \frac{C(E)}{R(E) + C(E)}$$

Equation 28: Relative contribution to ipRGC stimulation for cone photoreceptors.

The resulting graphs show how the change in rod stimulation gives rise to a change in the dynamic between the rod and cone photoreceptors. In relative terms, the main difference in mesopic vision appears to be a greater contribution of cone-mediated vision at lower retinal illuminances for older participants. This aligns with a reduction in sensitivity of rod-mediated vision. The evidence for this shift is provided by the changes as a function of age observed in the magnitude and latency of the transient PLR. These changes in mesopic visual function are in addition to the limitation that senile miosis imposes on pupil dilation, limiting the illumination reaching the retina at scotopic illumination levels.

The outcome of this model suggests that mesopic visual function needs to be redefined with an age component to take account of the apparent shift in the weights of the scotopic and photopic luminous efficiencies. The CIE modelled the transition between scotopic and photopic vision as a weighted average. The results of this study suggest that the CIE weighting function should also be adjusted to account for age.

Associated with the change in the relative contributions from the rods and cones, there is also an associated shift in the effective S/P value. The reduction in the scotopic component gives greater prominence to the photopic component even though there is little change in the underlying cone mediated function. The rate of cone loss as a function of age is less and the luminance (L+M cone) response is less affected by the attenuation of shorter wavelengths by the lens.

Returning to the final hypothesis to be evaluated by this study, it has been demonstrated that the two stimuli, R and C, can be used to characterise age dependent changes in the transient pupil response.

Testing the proposed model experimentally could be undertaken by repeating this study with younger participants wearing blue blocking lenses of decreasing spectral transmittances. This would simulate the effect of the yellowing of the lens as a function of age. The results would be independent of changes in photoreceptor topography or senile miosis,

4.4.6 Stimulus duration

The duration of the stimulus selected enabled the dynamic of the afferent and efferent components of the transient response to be characterised for the 100% contrast stimulus. Increasing the duration of the stimulus did not have any effect on the latency of the response. The adoption of the 3s stimulus duration ensured that the measurement of the transient response was not influenced by:

- The sympathetic nervous system's response to the stimulus offset
- The sustained response at ~1.5s post stimulus onset to the increment in corneal flux at stimulus onset.

Whereas the amplitude of the response to the stimulus post peak constriction is dependent upon the duration of the stimulus, the initial constriction appears to be independent. It could be that a stimulus with a duration less than the constriction latency may not invoke the full amplitude of constriction, but this was outside the limits of stimuli used for this study. Based upon the set of results presented in Figure 4-3, the duration of the constriction is 0.6s, so potentially stimuli with a duration shorter than this will not provide a true reflection of the transient response to the stimulus.

The observed variation in PLR with stimulus duration agrees with similar experiments (Alpern *et al* 1963) where stimulus duration was increased. The longer the stimulus duration, the greater clarity achieved in defining the different elements of the PLR and more specifically for this study, the transient response.

4.4.7 Limitations

4.4.7.1 Measurements

The properties of the CRT display, in terms of its luminance and colour gamut, limited the ability to fully explore pupil diameter as a function of retinal illuminance. The upper stimulus luminance values for

stimuli R and C were dictated by the display, which limited the ability to explore the lower asymptote of the PLR at photopic light levels. Despite these limitations, the P-SCAN system has enabled the PLR to be assessed over a range of light levels spanning 5 $\log_{10}$ units.

Whilst the P-SCAN system is a capable system, its temporal resolution is limited by the frame rate of the cameras used to acquire the image of the pupil. A frame rate higher than 50Hz would have enabled greater temporal resolution of the constriction latency. Although it was a limitation of the evaluation of constriction latency, by using a broad range of luminance conditions, spanning five orders of magnitude, the impact has been minimised.

External factors, out of the control of the principal investigator, may have affected some of the measurements made. Construction noise external to the laboratory building throughout the data gathering for the study could have resulted in pupil dilation (Zekveld *et al* 2018), reducing the magnitude of the pupil constrictions recorded. Whilst the noise attenuating headphones would have attenuated the building work, they would also have had the unwanted effect of attenuating the audio cue at the end of a stimulus presentation. This cue is used by participants to blink and ready themselves for the next measurement.

4.4.7.2 Statistical power

The study itself was designed as an exploratory study, to firstly determine the majority photoreceptor response to the two stimulus conditions used in the RCS test, see section 3.4.2. The secondary aim was to provide a basis for studying the amplitude and latency of the transient response enabling the identification of potential age-related variations in the transient PLR to be assessed. The aims of the study have been achieved.

The number of participants and their distribution across the five-decade age range limited the scope of the scope of the statistical analysis when comparing the transient PLR between two cohorts: young versus old. However, the distribution/spread of the participants' ages did provide the basis for comparing trends across the cohort. The coefficients of determination for the relationships plotted have in many cases indicated a strong agreement to the fitted functions.

To improve the statistical power of future studies, it is recommended that two cohorts of 5 participants be used from the age group of 20 to 25 years and 55 to 65 years. This would allow a more robust statistical analysis of the trends indicated by this study at a significance level of α=0.05.

4.4.8 Confounding factors

Across the whole study, it was assumed that there was minimal contribution from melanopsin as the luminance of the test stimuli were below the activation point of melanopsin. Studies seeking to characterise the PIPR like that of Munch *et al* (2012) utilise stimuli with luminance values of 15cd.m^{-2} and 34cd.m^{-2} for blue and red light respectively. In addition, the colorimetry of stimulus R was aligned to promote a rod response and not one from melanopsin containing ipRGCs. Secondly, and more importantly, the contribution of melanopsin to the PLR is primarily observed as a post-stimulus offset

whereas this study has focussed specifically on the transient response to the onset of a positive contrast stimulus.

To minimise the effect of fatigue as confounding factor, participants were instructed to arrive rested having achieved a minimum of eight hours sleep. In addition to fatigue, a participant's cognitive load can affect their pupil size with an increased cognitive load leading to pupil dilation (Daniels *et al* 2012, Kahneman and Beatty 1966, Kang *et al* 2014). Factors that could affect this are aspects of their life outside the control of the experiment, which were unknown at the time of undertaking the measurements and could potentially have varied from day to day. Accounting for these factors could have been achieved by using a lifestyle questionnaire to record the participant's subjective opinion of their emotional state and any stress factors. Although a qualitative assessment could have been made, applying a quantitative correction is considered impracticable.

The effect of external factors was minimised within each measurement by recording data for 32 presentations of each test condition. Additionally, the use of 12 test points covering a ~4 log cd.m^{-2} range of the background luminance values for the two stimulus conditions provided a basis for determining the overall trend or behaviour of the PLR across the range of mesopic light levels. This reduced the impact of the confounding factors of one measurement on the overall result.

4.4.9 Learning from experience

Pupillometry is a powerful method of investigating photoreceptor function. Although in terms of considering the effects of age on mediation of the PLR, the study was limited by the size and demographic of the cohort, it has highlighted that lens transmission data should be gather in conjunction with pupillometry data. This will allow this aspect of aging to be accounted for enabling better estimates for the effects of changes in photoreceptor topography and sensitivity to be derived. The effect of senile miosis is captured through the measurement of the pre-stimulus diameter at low retinal illuminance values.

4.5 Conclusions and future work

4.5.1 Conclusions

This study has demonstrated that stimulus R, which is based upon the RCS-R stimulus condition, instigates a response primarily mediated by rods. As scotopic retinal illuminance increases beyond the cone threshold, the response to stimulus R results in an increasing cone component which contributes to the PLR.

Across the range of scotopic retinal illuminance values tested, from 10^{-2} to 10^{3} ScTd, the pre-stimulus diameter is primarily defined by the scotopic component of the stimulus. Above ~10^{0} ScTd, the pupil starts to constrict until rods fully saturate. For a young normal, constriction amplitude peaks as the rod photoreceptors start to saturate at 2 log ScTd. Above this retinal illuminance, the constriction amplitude reduces due to the physical limitations of sphincter constriction.

The study has characterised the result of the combined effects of age on the transient PLR in terms of the constriction amplitude and latency. The properties of these two components have been demonstrated to reduce linearly as a function of age. As a function of increasing age:

- Pre-stimulus diameter decreases for backgrounds of -1 and 2 log ScTd.
- The peak amplitude of the constriction amplitude reduces.
- The scotopic retinal illuminance at which peak constriction amplitude occurs decreases.
- Constriction latency decreases.
- The scotopic retinal illuminance of the intersection of the constriction latency for the two stimuli, R and C, decreases.

The effects of age have been attributed to a combination of senile miosis; attenuation of shorter wavelengths as the lens ages; and changes in photoreceptor topography and rhodopsin regeneration rates.

The combined effects of age result in a reduction in relative weight of the rod contribution to the PLR, compared to that from cones, which is manifest as a reduction of the effective S/P ratio and a shift to lower illuminance levels of the mesopic region as a function of age.

The steady state pre-stimulus and transient peak constriction diameters, and the constriction latency have been fitted as a function of scotopic retinal illuminance using the model proposed by Stanley and Davies (1995). In addition, the transient constriction amplitude has been modelled based upon a Gaussian function combined with a fixed pedestal.

4.5.2 Further work

There are three studies that would assist in confirming the results of Experiment 8 and provide additional evidence to support the explanations of the observations made.

For all the proposed projects, measuring the transmission spectrum of the participants' lenses would assist in resolving some of the effects of age on the PLR.

4.5.2.1 Project 1: Effect of age

Given the small cohort of participants for this study, there are benefits to expanding the cohort of a future study to either:

1. Include more participants within each age group, e.g. participants under 35 years old and participants above 55 years old.
2. Achieve a more even distribution of participants across the age range between 20 and 65 years old.

This would provide increased power to the study through larger cohorts as well as allowing age related changes in the transient response to be more consistently defined.

4.5.2.2 Project 2: Luminance extremes

Although this study covered a 5 log variation in stimulus luminance, this still leaves scope to explore the transient response for light levels above and below this range. Of particular interest are light levels above the current range as this would inform the model for the constriction amplitude and whether it can be

defined as a Gaussian function. Additionally, it would assist in confirming that there is a lower asymptote to the constriction latency as a function of retinal illuminance. A study to consider stimuli with luminance values below 10^{-3}cd.m^{-2} would inform the shape of the constriction latency function and whether it has an upper asymptote, confirming if it follows a sigmoid function as indicated by this study.

4.5.2.3 Project 3: Stimulus/background interaction

Repeat the current study using:

- A stimulus with a S/P value between 0.7 and 8, e.g. 2 or 4 to confirm the conclusions as to which photoreceptor type is mediating the steady state and transient PLR.
- A lower/higher contrast stimulus, e.g. 50% or 200%, to predict the amplitude of constriction as a function of background luminance.

5 The effects of altitude and oxygen concentration on visual function

5.1 Introduction

The purpose of the study was to investigate the effect of mild hypoxia at 3048 m, equivalent to an altitude of 10,000 ft, on a participant's ability to process visual information presented in their peripheral vision. The study also sought to determine if a concentration of supplementary oxygen lower than 100% can improve visual sensitivity at altitude.

5.1.1 Background

The effects of hypoxia on visual function include a reduction in the sensitivity of rod photoreceptors and associated increase in dark adaptation time (Ernest and Krill 1971, Connolly and Hosking 2006); an impairment to mesopic vision resulting in elevated mesopic contrast acuity thresholds and a reduction of dynamic contrast sensitivity (Connolly 2011). In addition to increased rod thresholds, hypoxia has also been shown to raise cone thresholds (Ernest and Krill 1971) with a corresponding change in chromatic sensitivity (Connolly *et al* 2008, Hovis *et al* 2013). The effects of hypoxia increase as a function of altitude, or reducing fraction of inspired oxygen (Kobrick and Dusek 1970), and have been shown to have greater effect at increased eccentricity (Ernest and Krill 1971). Exposure to acute hypoxia has been linked to an increase in intersaccadic drift velocity resulting in diminished eye stability (Di Stasi *et al* 2014).

In contrast hyperoxia, arising from breathing 100% oxygen at ground level, has been demonstrated to reverse the effects of hypoxia on visual function leading to shorter dark adaptation times (Connolly 2011, Connolly and Hosking 2006) and increased photoreceptor sensitivity.

A confounding effect in studies of hypoxia is hyperventilation which results in alkalosis and a reduction in thresholds, whilst acidosis (breathing 7% CO_2 in ample oxygen) causes increments in thresholds (Alpern and Hendley 1952). Alpern and Hendley go on to conclude that the changes in metabolic state, i.e. blood pH, are not enough to instigate a significant change in thresholds, and it is the change in respiratory state that affects visual function at the level of the photoreceptor rather than cortically.

The outcomes of this previous work have helped to inform the requirement for the use of supplementary oxygen by military rotary wing pilots as a countermeasure to the effects of mild hypoxia for night-time operations at altitude.

What is apparent from reviewing the literature is that whilst there has been significant focus on changes in visual function at altitude and the effect of hyperoxia at ground level, there appears to be limited number of studies, if any, directed at the use of an inspired fraction of oxygen (F_IO_2) between 21% and 100%.

The physiological response to hypoxia is dominated by changes in respiratory and cardiovascular response; and the neurological effects of hypoxia combined with cardiorespiratory response. In addition to these physiological responses are changes in psychomotor function and cognitive function as well as the changes in visual function (Harding 2001). The degree to which an individual is affected is a consequence of their respiratory response to hypoxia. By an altitude of 3048 m, without the use of supplementary oxygen, aircrew are likely to be suffering from impaired hand-eye co-ordination with

memory function becoming increasingly impaired. At higher altitudes, greater than 4752 m, muscular coordination decreases. Combining the reported changes in visual thresholds, which primarily affect peripheral visual function, with the potential reduction in muscle co-ordination, gives rise to the situation where it potentially becomes harder to process visual cues presented peripherally. This is of interest with the increasing dependence on the use of Helmet Mounted Displays (HMDs) to provide visual cues and primary flight information to military pilots. With this shift from the use of head down displays and cockpit instruments to a heads up and heads out approach, the ability to process visual cues across the full HMD field of view gains importance.

So the development of a new psychophysical test, the Eye Movement And Integrated Latency (EMAIL) test (Llapashtica 2019, Barbur 2017), is of interest as it provides a novel method of characterising the time required to process stimuli located at eccentricities up to around 11°. More specifically, it provides a method of assessing whether this particular aspect of visual function is affected by altitude and inspired fraction of oxygen. The interest in using the EMAIL test is that it combines both on-axis and off-axis visual function to complete the task of detecting and identifying the orientation of a Landolt C optotype. In addition, the RCS test, reported in section 3, provides a new method to characterise the effects of mild hypoxia and the use of supplementary oxygen on visual function for stimuli located on-axis and at 5° eccentricity.

5.1.2 Aims

There were two main aims of this study. The first aim was to validate the utility of the RCS and EMAIL vision tests in quantifying changes in visual function due to hypobaric hypoxia equivalent to an altitude of 3048 m (10,000 ft) and normobaric hyperoxia enabling comparison with earlier work using similar test conditions (Connolly *et al* 2008).

Using the RCS and EMAIL vision tests, the aim of the second phase of the study was to evaluate the use of a lower concentration of supplementary oxygen as an effective countermeasure to the effects of mild hypoxia at 3048 m relative to the control condition of normobaric normoxia.

In addition to the primary aims of the study, a short investigation was undertaken with the aim of determining the configuration of the EMAIL test stimulus to be used in the study's two phases described above.

5.1.3 Hypothesis

5.1.3.1 Phase 1

Hypothesis A – The sensitivity of photoreceptors in the peripheral retina is reduced with oxygen deficiency.

Hypothesis B – The time required to detect, saccade to and correctly identify a target presented in the peripheral visual field will increase as a function of oxygen deficiency within the retina.

5.1.3.2 Phase 2

Hypothesis C – Peripheral visual function, quantified in terms of photoreceptor sensitivity, computation of saccadic eye movements and the time to correctly detect and identify a target, can be improved with supplementary oxygen.

5.1.4 Experimental design

The trial was split into two phases. Phase 1 collected data to validate the results of previous tests (Connolly 2011, Connolly *et al* 2008, Connolly and Hosking 2008), and extend current understanding of the effects of hypoxia on peripheral visual function. The testing sought to determine the effect of hypoxia at 10,000 ft (condition B in Table 5-1) on the sensitivity of both rod and cone photoreceptors to two flickering stimuli presented centrally, where cone photoreceptors dominate vision, and peripherally, where rod photoreceptors' contribution is increased. This was undertaken using the rod and cone test protocols of the Rod Cone Sensitivity test, referred to as RCS-R and RCS-C respectively. The EMAIL vision test was used to assess the effect of hypoxia on the time required to detect and subsequently correctly identify a target presented peripherally. These results were compared to those gathered when the participant was breathing air, the control (condition A), and 100% oxygen at ground level (condition C), the latter was anticipated to enhance photoreceptor sensitivity and speed of visual processing, validating the hypothesis that the retina is functionally hypoxic in dim light at sea level when breathing air. The exposure conditions for phase 1 are summarised in Table 5-1.

Condition	Breathing Gas	Altitude	Oxygen concentration (F_IO_2)	Lung Alveolar Partial Pressure (P_AO_2)
A – Normobaric Normoxia (NN)	Air	Ground Level	21 %	~110mmHg
B – Hypobaric Hypoxia (HH)	Air	10,000 ft (3048 m)	21 %	~55mmHg
C – Normobaric Hyperoxia (100)	Supplementary Oxygen	Ground Level	100 %	~670mmHg

Table 5-1: Exposure conditions for phase 1 – validation of previous results.

For phase 2 the same three vision tests, EMAIL, RCS-R and RCS-C, were performed using the same test procedure in terms of adaptation to the ambient atmospheric and illumination conditions. The key difference with respect to phase 1 was that the test exposure conditions varied the inspired concentration of oxygen at ground level and at altitude, as set out in Table 5-2, with aim of informing the minimum supplementary oxygen concentration required to improve visual performance at ground level and at 10,000 ft. The control in phase 2 was breathing air normally at ground level (condition D). It was anticipated that 29% oxygen at ground level (condition E) would optimise twilight visual performance and that this would be matched at 10,000 ft when breathing 43% oxygen (condition F).

The order of the test exposures for each phase was pseudo-randomised and balanced to address any ordering effects. As set out in Table 5-3, the first 15 minutes for a given test exposure established the

altitude/oxygen concentration for the exposure and enabled the participant's respiratory system to acclimatise to the conditions. The order of the vision tests was the same for all exposure conditions to minimise the effect on each vision test of the acclimatisation time to the environmental conditions.

An example of the testing structure, based upon the ordering given in Table 5-1 and Table 5-2 and the sequencing within a test exposure, as outlined in Table 5-3, is provided graphically in Figure 5-1 and Figure 5-2 respectively for phase 1 and 2.

Condition	**Breathing Gas**	**Altitude**	**Oxygen concentration (F_IO_2)**	**Lung Alveolar Partial Pressure (P_AO_2)**
D – Normobaric Normoxia (NN)	Air	Ground level	21 %	~110mmHg
E – Normobaric Hyperoxia (29)	Supplementary Oxygen	Ground level	29 %	~160mmHg
F – Hypobaric Hyperoxia (43)	Supplementary Oxygen	10,000 ft	43 %	~160mmHg

Table 5-2: Exposure conditions for phase 2 – optimising sensitivity trial.

Time from initiation of test exposure	**Condition at ground level**	**Condition at altitude**
0:00 hrs	Connect participant to gas supply for condition and initiate respiratory acclimatisation.	
0:01 hrs	Acclimatisation	Initiate ascent to altitude at 2,000 ft/min
0:06 hrs		Arrive at 10,000 ft
0:13 hrs	Pre-test adaptation to stimulus condition in darkened chamber.	
0:15 hrs	Undertake EMAIL vision test, typically 5 min. Once test is complete, undertake a set of linearity checks on the mass spectrometer.	
0:28 hrs	Start 2 min pre-test adaptation to stimulus condition in darkened chamber.	
0:30 hrs	Undertake RCS-R vision test, typically 5 min.	
0:43 hrs	Start 2 min pre-test adaptation to stimulus condition in darkened chamber.	
0:45 hrs	Undertake RCS-C vision test, typically 5 min.	
After conclusion of RCS-C vision test.	Exposure concluded.	Exposure concluded with descent to ground level at 2,000 ft/min.

Table 5-3: Timeline for the exposure conditions at ground level and altitude and the commonality in the administration of the vision tests for each exposure condition.

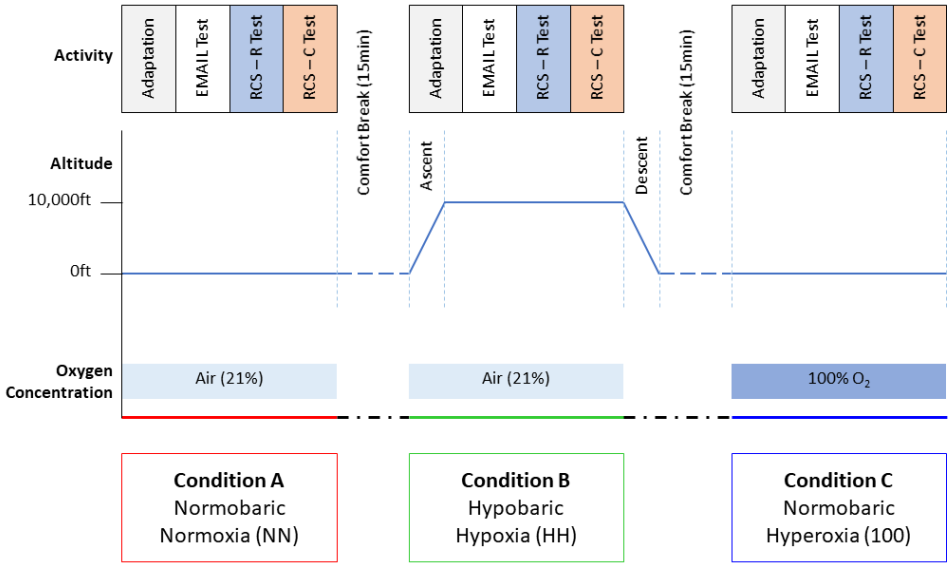

Figure 5-1: Example structure and exposure conditions for phase 1.

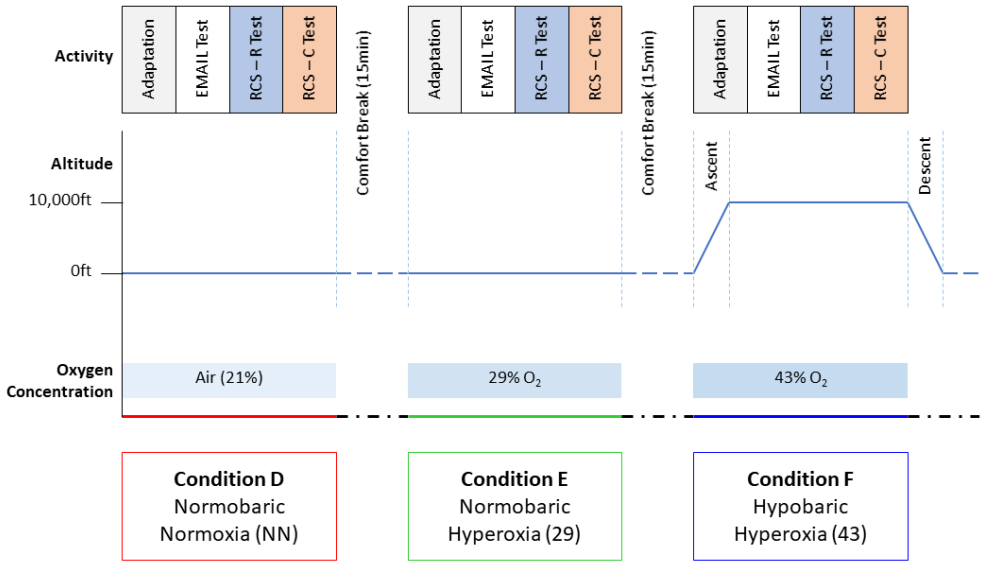

Figure 5-2: Example structure and exposure conditions for phase 2.

5.2 Materials and Methods

5.2.1 Participants

The 12 participants (28.9 ± 5.9 years [$\mu \pm \sigma$]), comprising ten males and two females, were recruited from employees at QinetiQ's Farnborough and Boscombe Down sites. All participants had no colour vision deficiency, as measured using the CAD test, and achieved Snellen visual acuity of at least 6/6 in each eye, corrected if necessary, using either spectacles or contact lenses (two males). None reported any issues with their visual function.

Participants were recruited for phase 1 with the intention that they would also participate in phase 2. There was a gap of at least 1 week between a participant completing the two phases.

The participants acted as their own controls for both phases. Whilst they were not directly aware of the exposure order of the respiratory conditions, they were aware of which condition was undertaken at altitude due to the additional checks and controls that were made to ensure their safety.

One participant was withdrawn from the study part way through their second exposure condition of phase 1 due to discomfort; a comfortable fit for the P/Q mask could not be achieved due to a previously broken nose. They were subsequently replaced, in agreement with the trial's protocol, with another participant who completed both phases of the trial.

5.2.2 Equipment

Details of the equipment used are given in 2.1.2 and 2.3.

As a result of lessons learnt from previous studies, the luminance of the background conditions for the three vision tests were measured using a Bentham DMc 150F+252 spectro-radiometer and corrections applied to ensure they met the test protocol for each test defined in Table 5-4 and Table 5-5.

Setting	Value	Stimulus	Value
Luminance	8 $cd.m^{-2}$	Eccentricity	8°
Chromaticity CIE 1931 (x, y)	(0.305, 0.323)	Meridian	0
Contrast Polarity	Negative	Max Rotation	5°
Contrast Level	30%	Bilobed	Yes
Initial Stimulus Duration	600ms	Gap Size [arcmin]	4

Table 5-4: Test configuration for the EMAIL test (Software version 0.97)

Parameter	ROD	CONE
Luminance	0.5 $cd.m^{-2}$ (As viewed using the Oakley Holbrook sunglasses S/N 5718.)	24 $cd.m^{-2}$
S/P	8	1
CIE 1931 (x, y)	(0.18, 0.0828)	(0.58, 0.3456)

Table 5-5: Test configuration for the Rod Cone Sensitivity test protocols (Software version 0.102.4)

5.2.3 Respiratory conditions

There was no sustained loss of pressure within the mask, i.e. greater 2 mmHg for more than 50 ms, for any participant during the trial. There was some fluctuation in argon levels for some participants, but these were less than 2 mmHg and were attributed to transient variations in the seal due to facial movements whilst completing the test. A prolonged presence of argon within the mask cavity would signify a loss of mask seal and the risk that the participant was no longer 'on' condition.

The ascent to altitude was initiated within 1 min of the participant breathing the appropriate gas mixture for the test condition. The ascent to altitude took 5 minutes resulting in at least 9 minutes to stabilise on condition prior to the commencement of the first vision test.

The larger of the two masks (Type P/Q mask) was changed due to a stiff expiratory valve which increased the breathing resistance. This only affected the participant using the larger mask (P mask) in both phases of the trial (participant 2). There were no issues with the smaller Q mask used by the other participants.

5.2.4 Experimental procedure

The three vision tests were administered using a standalone computer system. The participant used a numeric keypad with raised buttons to record the location or orientation of the target on screen. The wearing of the P/Q mask prevented the use of a chin rest to standardise head position during each test. Instead, participants were instructed to sit with their head resting against the seat's head rest, as shown in Figure 5-3.

Figure 5-3: Participant seated in the large compartment of the hypobaric chamber. The mass spectrometer is not connected in this photograph but the port in the side of the mask is visible. The Participant's mask is connected to a pressure demand regulator (to the left of the photograph) by the green anti-kink hose.

With the exception of Experiment 9, all testing was undertaken within the hypobaric chamber at MOD Boscombe Down. The light level inside the chamber was controlled by covering the windows to reduce ambient illumination within the chamber to mesopic levels (70 mlux) for the duration of the vision testing and the periods of pre-test adaptation to the test conditions. Otherwise, artificial lights were turned on for the safety of occupants of the chamber.

During each exposure, the participant remained seated at rest in the hypobaric chamber and was accompanied by the Principal Investigator (PI), who breathed air. Participants were not required to move about inside the chamber. The occupants of the chamber were in constant communication with staff outside the chamber.

5.2.5 Physiological monitoring

Physiological monitoring was undertaken continuously throughout all exposures. The start and end of each vision test was noted alongside the physiological data. Appropriately calibrated data was analysed in detail to determine the participant's respiratory state during each vision test. Heart rate, blood oxygen saturation (SpO_2), inspired partial pressure of oxygen (P_IO_2), end tidal partial pressure of oxygen ($P_{ET}O_2$), and carbon dioxide ($P_{ET}CO_2$) were measured repeatedly for each vision test. This produced over 1000 sets of data (5 physiological parameters x 3 vision tests x 3 respiratory conditions x 12 subjects for 2 experiments). The mean respiratory rate was calculated from the time interval between breaths.

5.2.6 Variations from experimental procedure

There were a few occasions when specific vision experiments were repeated on the day either within the condition, or repeating part of the exposure and having undertaken a period of adaptation. In each instance, listed below, the repeated set of results were used in the analysis.

- Participant 4 Phase 1 condition B

  RCS-C test repeated as it was realised that the participant had not removed the sunglasses after the RCS-R test. The repeated test was undertaken whilst still on condition at altitude.

- Participant 6 Phase 1 condition A

  RCS-R and RCS-C tests repeated after suspected problems with the sequencing of the target presentations – last set of presentations were all at the same location negating in part the 'random' order of the presentation as the participant identifies the repeated presentation at the same stimulus location.

- Participant 1 Phase 2 condition F

  The RCS-C test was repeated because the original test was undertaken with a 1 Hz temporal modulation of stimulus' luminance instead of 15 Hz. As the discovery was made during the descent to ground after all other tests had been completed, the decision was made to return to 10,000 ft and stabilise for 5 min prior to repeating the test.

- Participant 3 Phase 2 condition E

  EMAIL test was repeated between the RCS-R and RCS-C test as it was suspected that the participant was suffering from drowsiness. This resulted in a loss of attention and an inability to maintain fixation on the stimuli or fixation markers as observed by the principal investigator monitoring the test remotely.

- Participant 10 Phase 2 condition D

  The RCS-C test was repeated due to a technical error in the test selection by the PI.

In addition, there was a failure of the mass spectrometer 45 s into the RCS-C test for condition F (42% oxygen at 10,000 ft) for participant 2. At the time of the failure the participant was 'on condition' prior to the failure, i.e. there had not been any loss in mask seal and a subsequent loss of mask seal was unlikely to have occurred during the test as the participant was seated and focused on the task of completing the final vision test of the condition. Additionally, there was a safety limit on the maximum duration, of an hour, that the participant could remain at altitude.

With the agreement of the QEC Chairperson, participants 10 and 12 were permitted, following consultation with the Supervising Medical Officer, to be included while taking non-sedating medication for hay fever.

5.2.7 Analysis

The analysis of the experimental data has centred on firstly determining whether the participants were on condition for each of the vision tests. Having established that to be true, Analysis Of Variance (ANOVA),

or an equivalent non-parametric test when required, were utilised to determine whether a statistically significant change in visual function occurred due to the test conditions for each phase.

The EMAIL tests undertaken in Experiment 9, to define the test protocol for the EMAIL test used for Experiments 10 and 11, were completed by participants with prior experience of the test, so learning effects were not considered an issue. However, the participants undertaking Experiments 10 and 11 had no prior experience of the test. To ensure that the participants for these two experiments were performing at their best, the number of reversals used to calculate the ISL values for each test condition were reduced from 18 to 6. This corresponded to a maximum range of less than ± 20 ms compared to a variation greater than ±40 ms for 18 reversals for some participants, as illustrated in Figure 5-4.

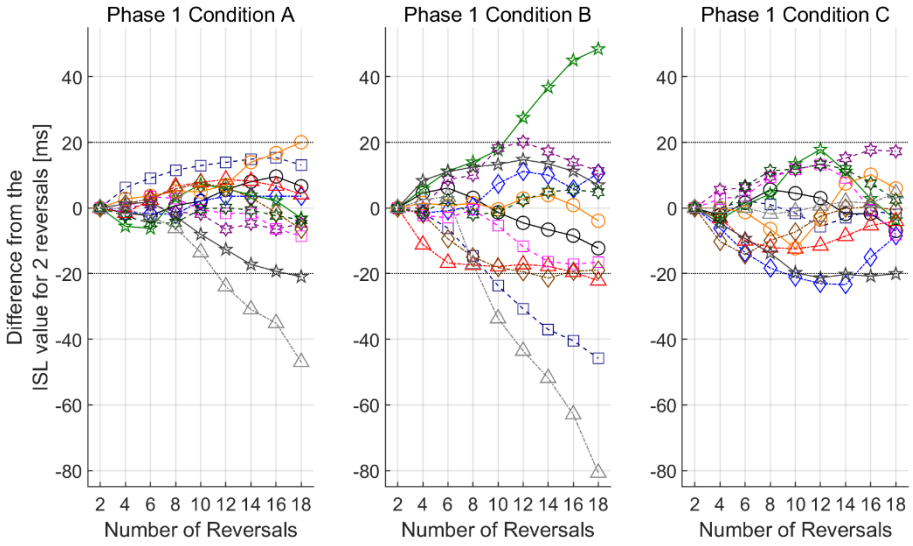

Figure 5-4: Plot of variation in ISL value as the number of reversals increases from the minimum number of 2 reversals. Lines at ±20 ms provided as a reference.

5.3 Results

5.3.1 Experiment 9 – EMAIL test parameter optimisation

The results of this initial experiment, presented in Figure 5-5 and Figure 5-6, formed the basis for defining the test stimulus used for the EMAIL test. It also provided an ability to assess any limitations of the test that may negatively impact the implementation of the EMAIL test during the subsequent phases of the study.

An Integrated Saccade Latency (ISL) of 7ms was recorded for a 100% negative contrast stimulus presented on-axis, as shown in the left-hand graph within Figure 5-5. This time corresponds to the Visual Processing Time (VPT) as the requirement to detect and saccade to the stimulus location are negated by stimulus location. The VPT increases as the contrast of the stimulus decreases below 50%. For stimuli located at eccentricities greater than 5°, the ISL values increase as contrast is reduced below 50%. Above 5° eccentricity there is proportionally a smaller increment in ISL as eccentricity is increased. This is either a function of the saccade amplitude or the time to detect the stimulus or a combination of both, however without supporting eye tracker data the true cause cannot be defined.

The large difference between the on-axis and off-axis values, for eccentricities greater than 5°, suggests that photoreceptor density and corresponding visual acuity are key factors in determining the ISL. The spatial extent of the stimulus was not increased to expose the reduction in spatial acuity as a function of eccentricity.

The interesting relationship is the effect of contrast for a stimulus at 2° eccentricity. Here the reduction in contrast leads to an increase in ISL which, once the contrast drops below 35%, appears to correspond to the relationship defined for stimuli with an eccentricity of at least 5°. This suggests a transition between being able to resolve the location of the gap in the Landolt C with minimal eye movement for high contrast stimuli to the stimulus needing to be imaged onto the fovea before its orientation can be identified. This introduces a delay whilst the eye saccades to the target. Alternatively, this could be an anomaly characteristic of the single participant for this group of measurements. Repeating this experiment with eye tracking and a larger cohort would have resolved this point.

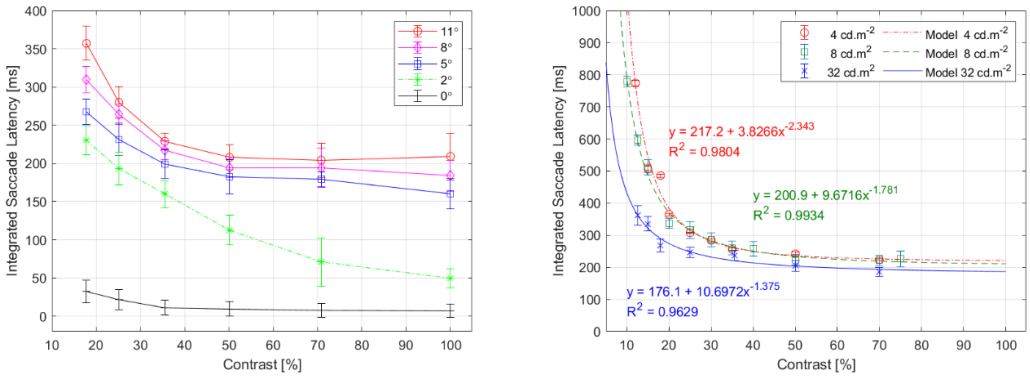

Figure 5-5: Variation of ISL as a function of stimulus contrast and eccentricity when presented on a 32 cd.m^{-2} white background (left). Variation in ISL as a function of stimulus contrast and background luminance for a stimulus presented at 8° eccentricity (right). Tests undertaken by the author. The error bars equal one standard deviation.

The relationship between ISL as a function of both background luminance and stimulus contrast is shown in the right-hand graph of Figure 5-5. The higher background luminance of 32 cd.m^{-2} corresponds to shorter ISL values for each contrast setting but there is only a small difference between the results for a background of 4 cd.m^{-2} and 8 cd.m^{-2}. This indicates that the flux of photons incident upon the retina influences the ISL both in terms of the initial detection of stimulus location and subsequent identification of the stimulus orientation.

To ensure that the behaviours observed in Figure 5-5 where not unique to the author, the results for the stimulus at 8° eccentricity on an 8 cd.m^{-2} white background were compared to measurements for a second, young normal, participant. The results for both participants, presented in Figure 5-6, show close agreement.

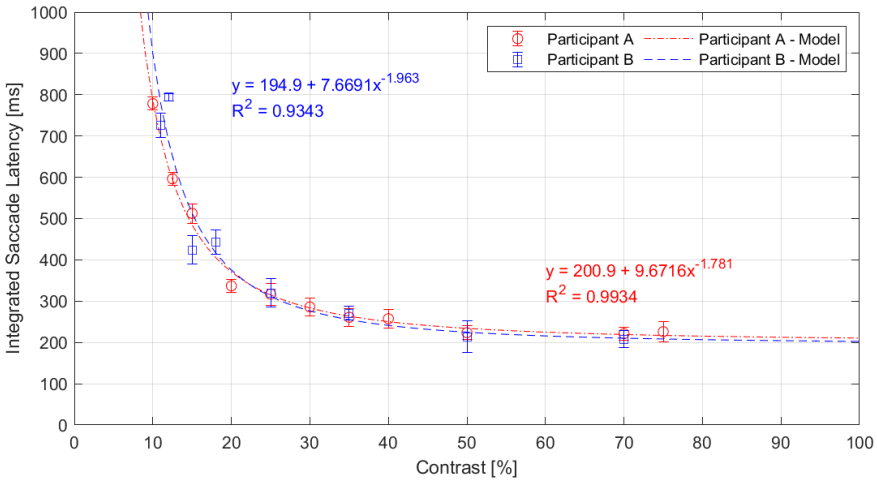

Figure 5-6: Variation of ISL as a function of stimulus contrast for an 8 cd.m^{-2} white background, CIE 1931 (0.305, 0.323). Stimulus was presented at 8° eccentricity. The error bars equate to one standard deviation.

The model, based on a power function, that has been used to generalise the ISL as a function of contrast appears to show good agreement with R^2 values greater than 0.93 for both participants.

While analysing the results of these experiments, it was observed that the EMAIL test software has an upper limit on the stimulus duration of 800 ms. This could significantly limit the results obtained when the participant is hypoxic. As a result, it was decided that the value of stimulus contrast used for the subsequent study should be greater than 20%. This provided for a margin of variation between participants reducing the risk of the stimulus being repeatedly presented with a duration of 800 ms.

The upper limit for the value of stimulus contrast used for the subsequent study should also be less than 50% to provide a stimulus that will potentially elicit a change in ISL as a function of respiratory condition. Above 50%, the ISL is independent of stimulus contrast with the expectation that there would be negligible change in ISL value as a function of respiratory condition.

5.3.2 Experiment 10 – Phase 1 - Validation of previous results

5.3.2.1 Physiological status of participants

The full physiological data describing the respiratory state of each participant are provided in Appendix C.1. Based upon the $P_{ET}O_2$ and SpO_2 values, it might be concluded that all participants were on condition. However, consideration of the $P_{ET}CO_2$ values would suggest that two participants, 2 and 5, were experiencing hypocapnia with $P_{ET}CO_2$ values below 30 mmHg for all three conditions. Consequently, the vision test results of these two participants have not been included in the calculation of the group test results. Participant 6 was excluded from the analysis of the RCS tests as their $P_{ET}CO_2$ values were below 30 mmHg for the last two vision tests of condition A. The exclusion of participants also had implications for the planned statistical analysis of the vision test results as it was no longer possible to apply the Repeated Measures ANOVA technique. Instead, alternative parametric and non-parametric ANOVA analyses have been performed as appropriate.

The $P_{ET}CO_2$ values recorded for participants 3 and 10 also fell below the 30 mmHg for condition C. There are potentially two factors that could be contributing to these results. The first is that for both these naïve

participants, condition C was their first test point and hence their first time breathing using a mask. This could have resulted in a tendency to over-breathe to overcome the safety pressure being applied to mitigate mask leaks, which in turn may have resulted in mild hyperventilation. The second factor can be attributed to the Haldane effect (Christiansen *et al* 1914), a consequence of breathing an increased concentration of oxygen, that results in decreased CO_2 being carried from the tissues to the lungs by haemoglobin. The subsequent retention of cerebral CO_2 promotes increased ventilation to eliminate it more quickly. This effect was also observed to a lesser degree for other participants and only for condition C. For participants 3 and 10, reduced $P_{ET}CO_2$ values were not recorded for conditions A and B and hence these two participants have been included in the study.

For the remaining nine participants, their $P_{ET}O_2$ values are reflected in their SpO_2 values with the effects of hypobaric hypoxia reducing the oxygen tension and haemoglobin saturation. In contrast, breathing 100% oxygen at ground level saturated the blood with oxygen, shown by the mean SpO_2 of 98.3%. The $P_{ET}CO_2$ values for condition B, hypobaric hypoxia, are not significantly different when compared to the control condition A, normobaric normoxia. With the changes in SpO_2 value, the heart rate and breathing rate adapts as the respiratory and circulatory system does not have to work as hard to ensure tissues and organs get sufficient oxygenated blood to function for condition C, whereas for condition B the values are slightly elevated. There may have been an elevation in heart rate due to condition B being the first time many of the participants will have experienced being in an altitude chamber. These results were replicated for all three vision tests. The was a variation in the atmospheric pressure at ground level for each of the conditions but this variation is linked to changes in the weather and the movement of weather systems during each participant's attendance; approximately 4 hours from the start of the first condition to completion of the last. The variation in the pressure at altitude is attributed to the slight variation in manually maintaining the chamber at an atmospheric pressure equivalent to 3048 m, i.e. 523 mmHg (ICAO 1993).

A summary of the group's physiological data, once exclusions have been applied, is provided in Table 5-6 to Table 5-8 for the three vision tests.

Metric	End tidal oxygen ($P_{ET}O_2$) [mmHg]			Oxygen saturation (SpO_2) [%]			End tidal carbon dioxide ($P_{ET}CO_2$) [mmHg]		
Condition	A	B	C	A	B	C	A	B	C
Mean	110.2	63.2	697.2	95.3	87.4	98.5	34.9	36.3	32.8
Standard Deviation	8.0	3.9	10.3	1.3	2.3	0.4	3.6	2.4	3.1
Standard Error	2.5	1.2	3.3	0.4	0.7	0.1	1.1	0.8	1.0
Min	95.2	56.9	675.6	93.5	83.4	97.9	30.3	32.1	27.4
Max	120.3	69.6	713.4	97.8	90.3	99.0	40.1	41.8	38.2
Range	25.2	12.7	37.8	4.2	6.9	1.1	9.8	9.6	10.7

Table 5-6: Summary of the phase 1 physiological data describing the respiratory condition of the group for the EMAIL test.

Metric	End tidal oxygen ($P_{ET}O_2$) [mmHg]			Oxygen saturation (SpO_2) [%]			End tidal carbon dioxide ($P_{ET}CO_2$) [mmHg]		
Condition	A	B	C	A	B	C	A	B	C
Mean	105.8	61.5	686.6	95.0	86.4	98.6	35.5	36.2	32.7
Standard Deviation	8.1	4.7	15.0	1.5	2.8	0.3	3.5	2.7	2.9
Standard Error	2.7	1.6	5.0	0.5	0.9	0.1	1.2	0.9	1.0
Min	93.1	56.0	654.1	92.8	83.1	98.2	30.4	30.0	28.0
Max	118.4	72.3	704.3	97.0	91.6	99.2	39.4	39.0	36.2
Range	25.3	16.2	50.2	4.2	8.5	1.0	9.0	8.9	8.2

Table 5-7: Summary of the phase 1 physiological data describing the respiratory condition of the group for the RCS-R test.

Metric	End tidal oxygen ($P_{ET}O_2$) [mmHg]			Oxygen saturation (SpO_2) [%]			End tidal carbon dioxide ($P_{ET}CO_2$) [mmHg]		
Condition	A	B	C	A	B	C	A	B	C
Mean	106.5	62.7	688.8	94.7	87.0	98.6	35.1	35.1	32.3
Standard Deviation	6.8	4.9	7.9	1.3	3.2	0.4	3.8	3.5	2.6
Standard Error	2.1	1.6	2.5	0.4	1.0	0.1	1.2	1.1	0.8
Min	97.2	55.8	676.6	92.9	82.4	98.0	29.5	27.9	29.0
Max	118.4	73.6	699.9	96.5	93.1	99.2	39.2	38.7	36.0
Range	21.2	17.8	23.3	3.6	10.7	1.2	9.7	10.8	7.1

Table 5-8: Summary of the phase 1 physiological data describing the respiratory condition of the group for the RCS-C test.

5.3.2.1.1 EMAIL ISL vision test

The mean ISL values for the group and the within participant variation for the three test conditions are plotted in Figure 5-7. The group results indicate that ISL values for the three test conditions are not meaningfully different with similar mean values and variances. The within participant variation indicates that there is no consistent trend between the respiratory conditions.

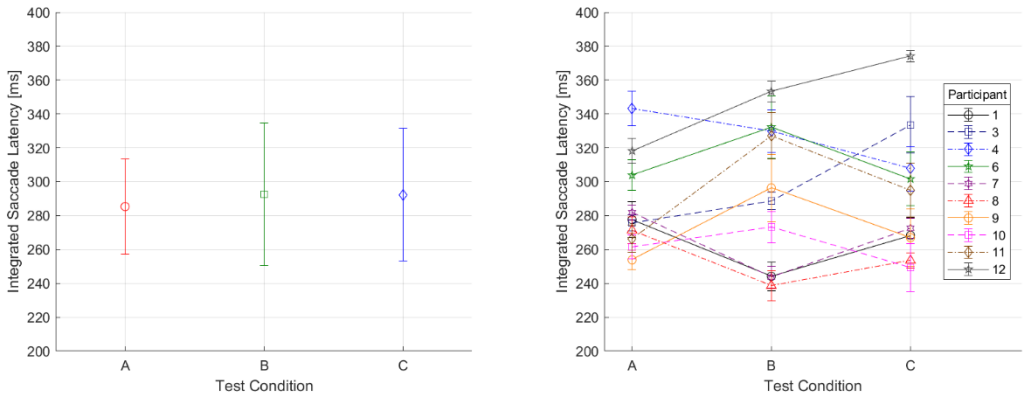

Figure 5-7: Summary of the EMAIL test results for phase 1. (Left) Mean results for each condition plotted with error bars equal to ±1 standard deviation. (Right) ISL value for each participant for each condition showing the within participant variation across the three test conditions.

The result of undertaking an Anderson Darling (AD) test for normality on the ISL data for control condition A indicates that it conforms to a normal distribution (p = 0.1541). Based upon this result, a two-way ANOVA was performed on the phase 1 EMAIL test ISL values with results given in Table 5-9. These indicate that none of the test conditions have mean values statistically significantly different from each other. There was, as expected, a significant variation between participants. There was no apparent within participant variation as illustrated by the trend shown in the right-hand graph of Figure 5-7.

Source	SS	Df	MS	F	Prob>F
Conditions	345	2	172.52	0.33	0.7213
Participants	27290.5	9	3032.28	5.85	**0.0007
Error	9331.8	18	518.44		
Total	36967.4	29			

*Table 5-9: Two-way ANOVA analysis results performed on the phase 1 EMAIL test results. (** Indicates statistical significance at $\alpha = 0.01$.)*

Plotting the mean ISL values for each condition as a linear function of mean $P_{ET}O_2$ and SpO_2, as shown in Figure 5-8, further illustrates the variance between participants in the test results. Lines of best fit have been calculated to determine the ISL as a function of oxygen tension in the choroid and oxygenation of the blood in the retinal artery that correspond respectively to the $P_{ET}O_2$ and SpO_2 values. The gradient of the line of best fit in both graphs indicates that for a 30% contrast stimulus, a decrement in PO_2 will have negligible effect on the ability to identify the stimulus.

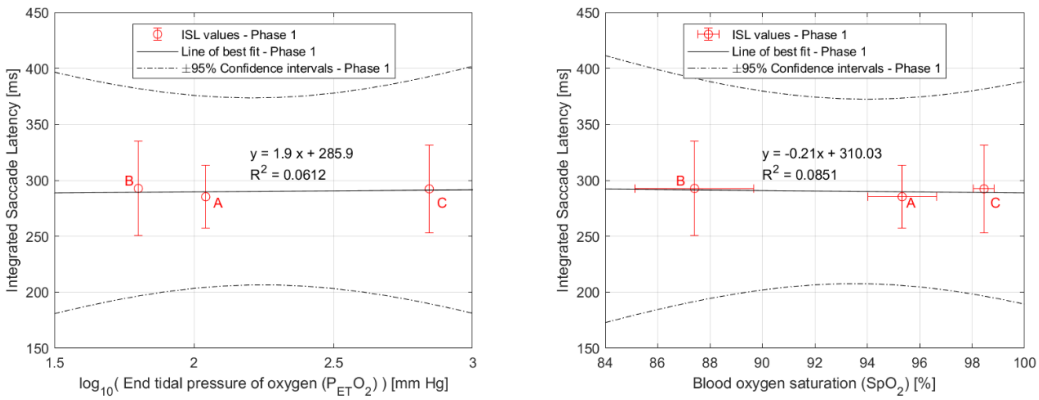

Figure 5-8: EMAIL test ISL values as a function of mean PETO2 (left) and mean SpO2 (right) for conditions A, B and C. Error bars are equivalent to ±1 standard deviation.

5.3.2.1.2 RCS-R vision test

The phase 1 RCS-R results for the three conditions for all stimulus locations are presented in Figure 5-9. The results for the control condition, A, demonstrate a similar variation in FMT value as a function of stimulus location/meridian angle as observed in the results from Chapter 3. The results for the test conditions, B and C, also follow the same pattern of a higher on-axis FMT compared to the values for the four off-axis stimuli at 5° eccentricity. The thresholds for the centre, on-axis, stimulus have been considered independently from the FMTs for the four stimuli at 5° eccentricity. The mean threshold for these four outer stimuli is referred to as the mean off-axis threshold in the subsequent analysis. The box plots for the RCS-R, shown in Figure 5-10, have been plotted using this method of classifying thresholds based upon test stimulus location.

Both the summary plot, Figure 5-9, and the box plots, Figure 5-10, illustrate the variation in RCS-R thresholds with test condition and stimulus location. For the on-axis stimulus, the threshold values for condition B, hypobaric hypoxia, have an Inter-Quartile Range (IQR) that is double that of the control condition A, shown in the left-hand box plot of Figure 5-10. The IQR for condition C is just over a third that of condition A. Comparison of the mean and median values in Table 5-10, indicates they are broadly equivalent.

For the mean off-axis RCS-R thresholds, there is an increase in both the mean and median FMT value between condition A and B and only a minor reduction between condition A and C with a reduction in the range being observed. The IQR values are broadly the same across the conditions but there is a reduction in the range observed for condition C, as noted for the on-axis RCS-R results.

MATLAB's box plot function has classified one of the results as an outlier. This outlier, should have minimal effect on the overall result apart from increasing the standard deviation of the on-axis data for condition C. This is illustrated in the size of the on-axis error bars in Figure 5-9. Considering the off-axis results, no outliers are identified and hence the on-axis outlier has been included.

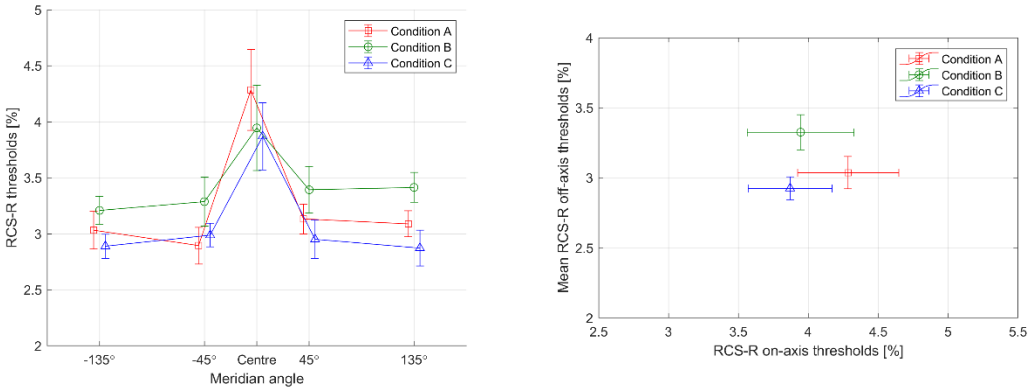

Figure 5-9: Summary of the phase 1 RCS-R results for the three test conditions as a function of on-screen stimulus location with conditions A and C offset by -5°/+5° from the meridian angle (left) and mean off-axis threshold plotted against on-axis threshold (right). Error bars equate to 1 standard error.

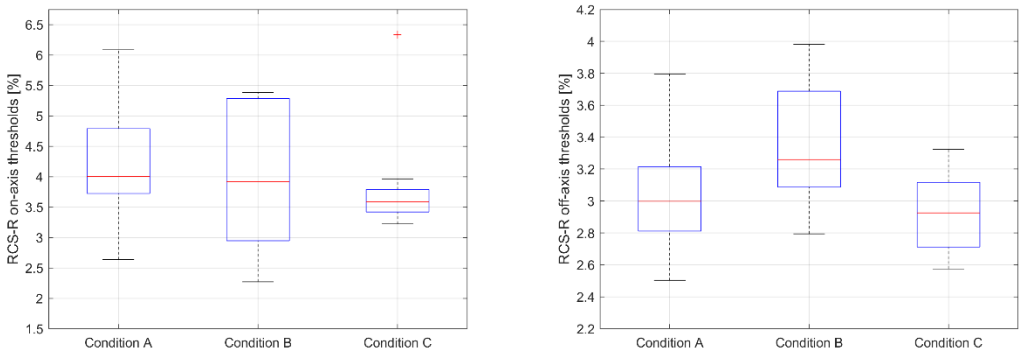

Figure 5-10: Box plot of the RCS-R test results for the on-axis (left) and off-axis (right) stimulus locations following the exclusion of participants 2, 5 and 6.

Metric	RCS-R on-axis			RCS-R off-axis		
	A	B	C	A	B	C
Mean	4.29	3.94	3.87	3.04	3.33	2.92
Standard Deviation	1.14	1.21	0.95	0.37	0.40	0.26
Standard Error	0.36	0.38	0.3	0.12	0.13	0.08
Median	4.01	3.92	3.58	3.00	3.26	2.93
Inter-Quartile Range	1.07	2.34	0.37	0.40	0.60	0.41
Range Minimum	2.64	2.27	3.22	2.50	2.79	2.58
Range Maximum	6.09	5.39	6.33	3.80	3.98	3.32
Range	3.45	3.11	3.11	1.29	1.19	0.75

Table 5-10: Summary statistics for the RCS-R test results for the on- and off-axis test stimuli. The RCS-R off-axis statistic are based upon each participant's mean threshold for the four stimuli located at 5° eccentricity.

The observed increase and variability in the FMT values with the onset of mild hypoxia, condition B, is as expected. The data suggests that the severity of the effects of hypoxia may vary as a function of retinal eccentricity indicated by the observed changes in both mean and median value with condition. Not all participants have been affected in the same way by the onset of hypoxia leading to the increased variability for condition B. Increasing F_IO_2 has resulted in a reduction in the variation and only a small lowering of thresholds. This corresponds to participants reaching maximum sensitivity in response to breathing 100% oxygen.

An AD test applied to both RCS-R on-axis and mean off-axis data confirmed that both distributions conform to a normal distribution with *p*-values of 0.125 and 0.744 respectively. The results of a two-way ANOVA of the on-axis RCS-R data, see Table 5-11, indicates that no condition had means that were significantly different (p = 0.4753). There was a significant interaction arising from the participants which can be attributed to the variation in individual sensitivity to the changing respiratory conditions.

Source	SS	Df	MS	F	Prob>F
Conditions	0.8824	2	0.4412	0.78	0.4753
Participants	20.2434	8	2.5304	4.77	**0.0053
Error	9.0565	16	0.5660		
Total	30.1823	26			

*Table 5-11: Two-way ANOVA analysis performed on the RCS-R test on-axis data for phase 1. (** The interaction is statistically significant at $\alpha = 0.01$.)*

A two-way ANOVA was performed on the RCS-R off-axis data for phase 1 utilising the four off-axis thresholds values for the three test conditions for each participant, see Table 5-12. This provided four repetitions per participant. The result of the two-way ANOVA for the off-axis stimuli indicates that there was a statistically significant difference between conditions. A post hoc analysis was undertaken to understand between which conditions the significant difference occurred. The results of the post hoc analysis, provided in Table 5-13, indicate that the difference in rod mediated thresholds for an off-axis stimulus at 5° eccentricity are statistically significant for: conditions A and B (p = 0.0060) and conditions B and C (p = 0.0001). There was no significant difference between conditions A and C (p = 0.4397), which suggests that there is only small difference between the functionality of the visual system under normobaric normoxia and normobaric hyperoxia as measured by the RCS-R test configuration.

These results indicate that the thresholds were elevated when participants were mildly hypoxic at 3048 m. The differences in FMTs between mild hypoxia at 3048 m and normobaric hyperoxia from breathing 100% O_2 emphasise the loss of sensitivity in the outer retina from the onset of hypoxia. The lack of a significant difference between normobaric normoxia and hyperoxia does not mean that there is not some benefit to be derived from the increased F_IO_2, it is just that it is small compared to the effect of the onset of hypoxia. The measured change in FMTs is consistent with concept that the outer retina is functionally mildly hypoxic at ground level.

The statistical significance of the variation between participants in the two-way ANOVA indicates that the baseline measures on the test varied widely between participants, which can be attributed to natural variation in the study cohort. The highly significant result for the interaction term (p = 0.0005) between conditions and participants indicates the variability of the responses to the respiratory conditions between individuals, which can also be attributed to natural variation between participants.

Source	SS	dF	MS	F	Prob>F
Conditions	3.0842	2	1.5421	10.31	**0.0001
Participants	4.1777	8	0.5185	3.47	**<0.0018
Interaction	7.3327	16	0.4583	3.06	**0.0005
Error	12.1196	81	0.1496		
Total	26.6841	107			

*Table 5-12: Summary of the application of a Two-way ANOVA to the RCS-R off-axis data for phase 1. (** The interaction is statistically significant at an $\alpha = 0.01$.)*

Group 1	Group 2	P value
A	B	**0.0060
A	C	0.4397
B	C	**0.0001

*Table 5-13: Post hoc analysis of RCS-R off-axis thresholds using pairwise t-tests to assess the difference between conditions. (** The interaction is statistically significant at an $\alpha = 0.01$.)*

Considering the results as a function of $P_{ET}O_2$ and SpO_2, enables them to be placed in perspective respectively with regards to the oxygenation of the outer retina, Figure 5-11, and the inner retina and visual cortex, Figure 5-12.

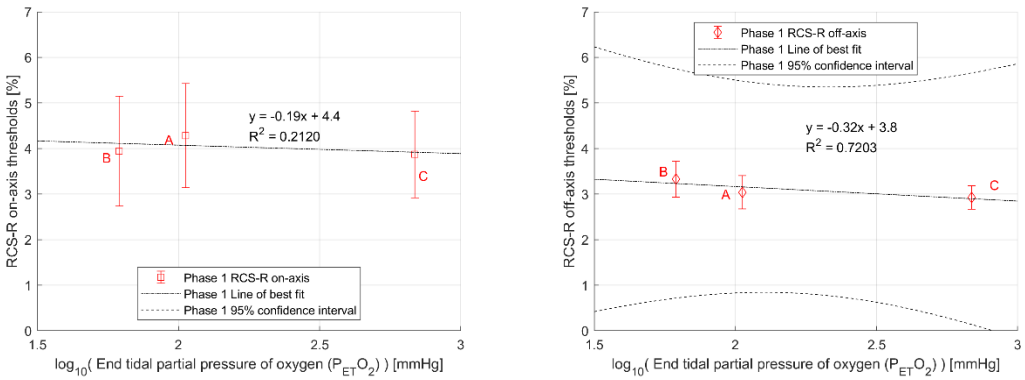

Figure 5-11: RCS-R thresholds as a function of $PETO_2$ for the on-axis stimulus (left) and the off-axis stimuli (right). These RCS-R off-axis thresholds plotted are the mean thresholds with error bars of 1 standard deviation .

The minimal variation in the mean off-axis thresholds for conditions A and C as a function of both $P_{ET}O2$ and SpO_2 suggest that there will be minimal change in RCS-R off-axis thresholds for the test conditions E and F assessed within phase 2 of the study. The lack of statistical significance for the RCS-R on-axis thresholds is supported by the independence of RCS-R on-axis thresholds when plotted as a function of SpO_2, Figure 5-12. Conversely there appears to be a strong relationship between RCS-R off-axis thresholds as a function of SpO_2. This indicates a dependence of FMTs on the oxygenation of the inner retina and visual cortex.

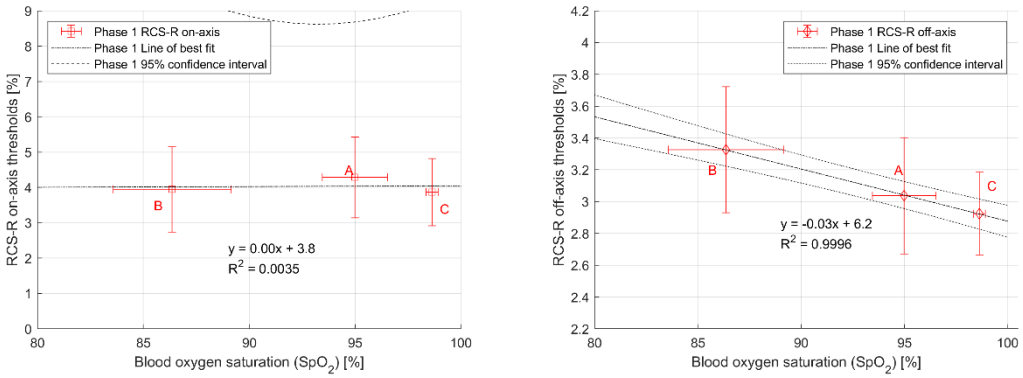

Figure 5-12: RCS-R thresholds as a function of SpO_2 for the on-axis stimulus (left) and the off-axis stimuli (right). These RCS-R off-axis thresholds plotted are the mean thresholds with error bars of 1 standard deviation.

5.3.2.1.3 RCS-C vision test

The RCS-C results for the five stimulus locations are presented in Figure 5-13. The higher value for the on-axis RCS-C threshold was not unexpected as the on-axis stimulus has a diameter half that of the off-axis stimuli located at 5° eccentricity. The apparent lower mean off-axis threshold with increasing meridian angle was unexpected but appears to be reproduced for all test conditions. Both the on-axis and off-axis thresholds have lower values for condition C, corresponding to hyperoxia, than those for the other test conditions. A greater shift from the control condition A was observed in the on-axis threshold for condition C than for the shift observed between condition A and B. The variation in the RCS-C on-axis FMT values is greater for condition B, hypobaric hypoxia, which is consistent with the RCS-R on-axis results for the same condition.

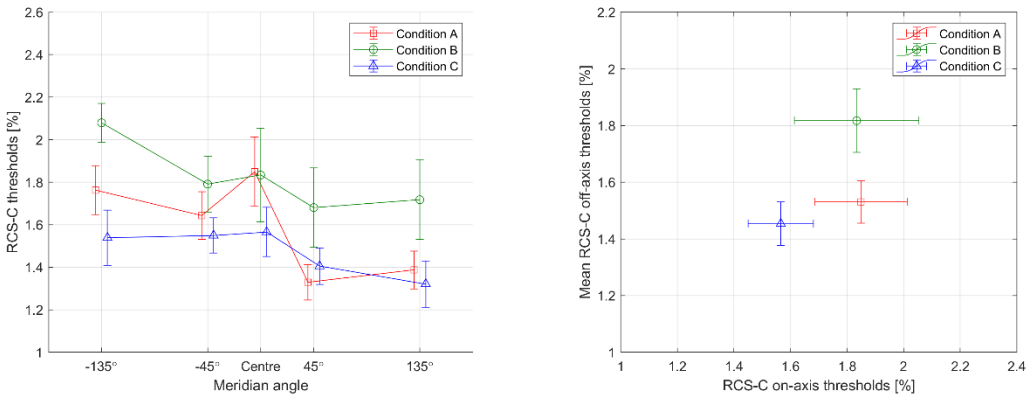

Figure 5-13: Summary of the phase 1 RCS-C results for the three test conditions as a function of on-screen stimulus location with conditions A and C offset by -5°/+5° from the meridian angle (left) and mean off-axis threshold plotted against on-axis threshold (right). Error bars equate to 1 standard error.

As with the RCS-R results, increasing the inspired oxygen concentration has resulted in lower off-axis thresholds. Similarly, an elevation in off-axis threshold is observed when the participants experienced hypobaric hypoxia at 3048 m. This difference in the mean off-axis threshold is greater between condition A and B than that between A and C.

The box plots, shown in Figure 5-14 for both the RCS-C on-axis and mean off-axis thresholds for each respiratory condition, provide confirmation that the observed effect is not limited to the mean value of the group but is also observed for the group median and IQRs, see the summary statistics provided in

Table 5-14. These plots indicate condition B results in a higher range of on-axis threshold values whilst condition C appears to result in a reduction in the range of on-axis values. The median off-axis thresholds follow a similar pattern to that observed for the RCS-R off-axis thresholds with a lower value for condition C compared to condition A. The median RCS-C off-axis thresholds were elevated for condition B, corresponding to hypobaric hypoxia.

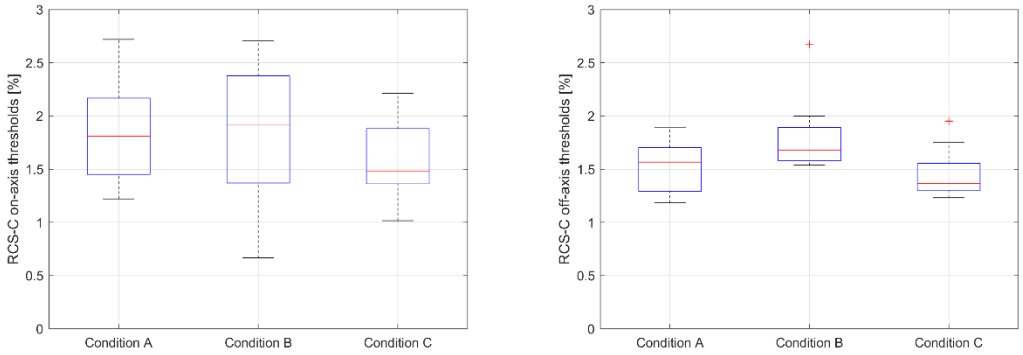

Figure 5-14: Box plot of the RCS-C test results for the on-axis (left) and off-axis (right) stimulus locations following the exclusion of participants 2, 5 and 6.

Metric	RCS-C on-axis			RCS-C off-axis		
	A	B	C	A	B	C
Mean	1.85	1.83	1.57	1.53	1.82	1.45
Standard Deviation	0.51	0.7	0.37	0.24	0.36	0.24
Standard Error	0.16	0.22	0.12	0.07	0.11	0.08
Median	1.81	1.91	1.48	1.57	1.68	1.37
Inter-Quartile Range	0.72	1.01	0.52	0.41	0.31	0.26
Range Minimum	1.22	0.67	1.02	1.18	1.54	1.23
Range Maximum	2.72	2.71	2.21	1.89	2.67	1.95
Range	1.5	2.04	1.2	0.71	1.14	0.72

Table 5-14: Summary statistics for the RCS-C test results for the on-axis and off-axis test stimuli.

Application of an AD test for normality to the on-axis data for the control condition indicated it conformed to a normal distribution with a *p*-value of 0.617. For the RCS-C off-axis data, the AD test indicated that the data also conformed to a normal distribution (p = 0.148).

The results of a two-way ANOVA applied to the RCS-C on-axis thresholds, see Table 5-15, indicated that there was not a statistically significant difference between the on-axis results for the three respiratory conditions (p = 0.435). These results indicate that the effect of either hypobaric hypoxia or normobaric hyperoxia do not cause a significant change in visual thresholds as characterised by the on-axis stimulus of the RCS-C test.

Source	SS	dF	MS	F	Prob>F
Conditions	0.4577	2	0.2289	0.88	0.4347
Participants	2.89752	8	0.3622	1.39	0.2733
Error	4.171	16	0.2607		
Total	7.52624	26			

Table 5-15: Summary of the application of a two-way ANOVA to the RCS-C on-axis data for phase 1.

The results of the two-way ANOVA performed on the RCS-C off-axis data, see Table 5-16, and the post hoc pairwise *t*-tests, Table 5-17, indicated a statistically significant difference between the two test conditions,

hyperbaric hypoxia at 3048 m and normobaric hyperoxia (p = 0.0001) as well as the control condition, normobaric normoxia and hypobaric hypoxia (p = 0.0040) . There was not a significant difference between the control condition and normobaric hyperoxia condition.

Source	SS	dF	MS	F	Prob>F
Conditions	0.8660	2	0.4330	10.12	**0.0001
Participants	0.5048	8	0.0631	1.47	0.1793
Interactions	2.04994	16	0.1281	2.99	**0.0006
Error	3.4649	81	0.04278		
Total	6.8851	107			

Table 5-16: Summary of the application of a two way ANOVA to the phase 1 RCS-C off-axis data after transformation to account for lognormal distribution for all results. (The interaction is statistically significant at an $\alpha = 0.05$. ** The interaction is statistically significant at an $\alpha = 0.01$.)*

Group 1	Group 2	P value
A	B	**0.0040
A	C	0.5516
B	C	**0.0001

Table 5-17: The significance of the interaction between the pairs of conditions. (The interaction is statistically significant at an $\alpha = 0.05$.)*

The consistent statistically significant difference between the hypobaric hypoxic condition and the other two conditions for both the off-axis RCS test results indicates that photoreceptors at 5° eccentricity are both being deleteriously affected by the reduced oxygen tension in the choroid resulting from the onset of hypoxia. The provision of supplementary oxygen at 100% acts as a countermeasure reversing the effect and additionally enhancing the sensitivity of this section of the retina. The lack of a significant effect when the results for normobaric normoxia and hyperoxia are compared could be due to the magnitude of the enhancement and the variability of the participants to the respiratory conditions, which is to be expected, as indicated by statistically significant p-values for the interaction.

The variation of RCS-C thresholds as a function of $P_{ET}O_2$ is like that for RCS-R thresholds with a small increase in threshold value as $P_{ET}O_2$ is reduced. There is also a similar difference in the R^2 values for the on and off RCS-C thresholds when modelled as a function of SpO_2, with the effect on off-axis data again having an R^2 value close to unity. These changes in cone mediated vison reflect observation from previous studies (Connolly and Hosking 2008, Ernest and Krill 1971). The decrement in sensitivity between the control condition, normobaric normoxia, and condition B, hypobaric hypoxia, is predicted to become more significant as altitude and severity of hypoxia increases. This result also appears to confirm that cone and rod-mediated visual thresholds are consistently oxygen-dependent at 5° eccentricity at these background luminance levels.

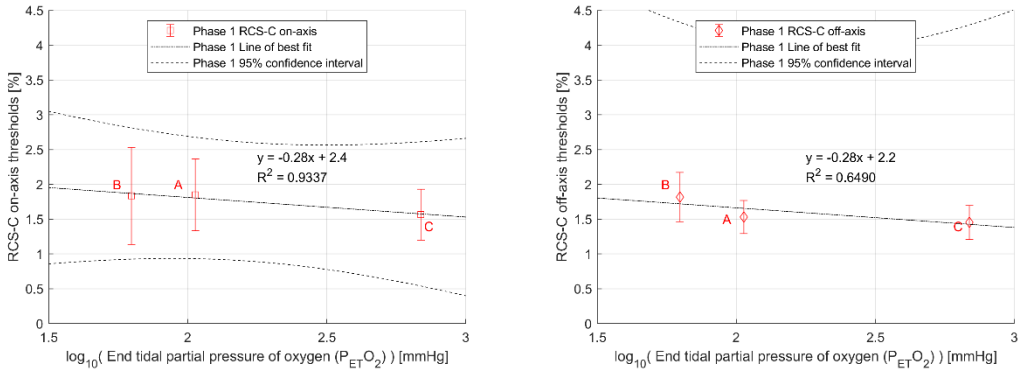

Figure 5-15: RCS-C on-axis (left) and off-axis (right) thresholds as a function of $P_{ET}O_2$. Error bars equal 1 standard deviation.

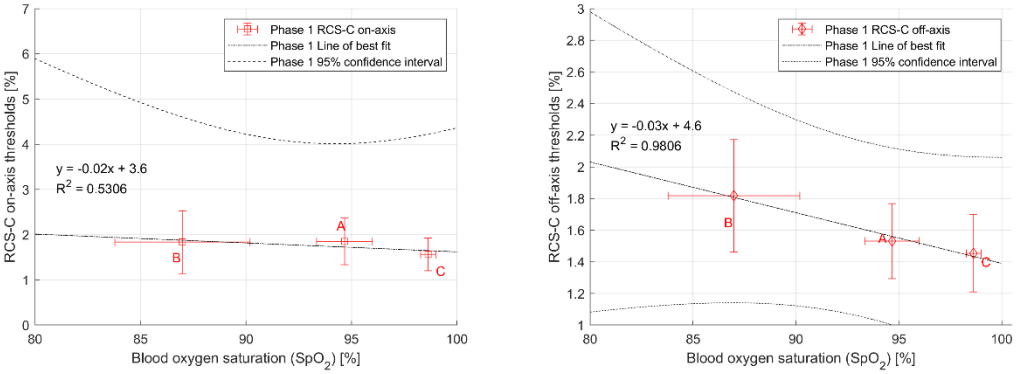

Figure 5-16: RCS-C on-axis (left) and off-axis (right) thresholds as a function of arterial blood oxygen saturation. Error bars equate to 1 standard deviation.

5.3.3 Experiment 11 – Phase 2 - Optimising sensitivity using supplementary oxygen

5.3.3.1 Physiological status of participants

The increased concentration of oxygen, coupled with the effect of the reduced ambient pressure, for condition F was designed to produce a comparable respiratory condition to the small (8%) increment in F_IO_2 at ground level for condition E. The achievement of this respiratory condition is illustrated by the equivalent values for the $P_{ET}O_2$ and SpO_2 measured across the EMAIL, RCS-R and RCS-C vision tests in the respective summary statistics tables: Table 5-18, Table 5-19 and Table 5-20.

Analysis of the physiological data for each participant indicated that participant 2 was affected by the faulty expiratory valve on his mask and as a result was excluded from further analysis within phase 2 of the study. Participant 2 had lower $P_{ET}CO_2$ values than the rest of the cohort indicating that hypocapnia may have been induced, which would skew the results of the vision tests.

For the other participants, the $P_{ET}CO_2$ values were stable between the vision tests and broadly equivalent within each exposure condition. There was a variation with test condition, but this is expected as F_IO_2 and altitude were varied.

Condition	End Tidal Oxygen ($PETO_2$) [mmHg]			Oxygen saturation (SpO_2) [%]			End tidal carbon dioxide ($PETCO_2$) [mmHg]		
	D	E	F	D	E	F	D	E	F
Mean	112.5	171.8	171.0	95.8	97.4	96.5	33.8	32.4	35.3
Standard Deviation	40.8	62.9	63.6	36.9	37.4	36.4	11.1	10.9	12.1
Standard Error	12.3	19.0	19.2	11.1	11.3	11.0	3.3	3.3	3.7
Min	104.6	157.5	159.3	93.7	94.3	90.2	30.8	25.2	20.3
Max	123.3	186.1	181.1	97.5	98.6	98.3	37.6	41.0	42.4
Range	18.7	28.6	21.8	3.8	4.2	8.1	6.8	15.8	22.2

Table 5-18: Summary of the phase 2 physiological data describing the respiratory condition of the group for the EMAIL test.

Condition	End tidal oxygen ($PETO_2$) [mmHg]			Oxygen saturation (SpO_2) [%]			End tidal carbon dioxide ($PETCO_2$) [mmHg]		
	D	E	F	D	E	F	D	E	F
Mean	108.7	168.7	168.7	95.6	97.5	97.0	34.8	32.8	35.0
Standard Deviation	4.3	7.5	5.3	1.1	1.4	0.8	2.5	5.9	6.2
Standard Error	1.4	2.4	1.7	0.3	0.4	0.2	0.8	1.9	2.0
Min	103.8	156.7	162.8	94.2	94.3	95.5	29.8	24.6	19.8
Max	116.8	180.0	179.3	97.3	98.9	98.3	39.2	43.1	42.4
Range	13.0	23.2	16.5	3.1	4.6	2.8	9.4	18.6	22.5

Table 5-19: Summary of the phase 2 physiological data describing the respiratory condition of the group for the RCS-R test.

Condition	End tidal oxygen ($PETO_2$) [mmHg]			Oxygen saturation (SpO_2) [%]			End tidal carbon dioxide ($PETCO_2$) [mmHg]		
	D	E	F	D	E	F	D	E	F
Mean	110.0	168.8	169.1	95.8	97.5	97.2	33.8	31.7	34.6
Standard Deviation	6.2	6.4	4.4	1.2	1.3	0.8	3.7	5.3	5.7
Standard Error	1.9	1.9	1.3	0.3	0.4	0.2	1.1	1.6	1.7
Min	100.7	158.0	160.8	94.0	94.5	96.0	27.0	26.2	20.6
Max	120.0	177.7	176.7	97.3	98.9	98.7	39.8	43.7	41.6
Range	19.4	19.8	16.0	3.3	4.4	2.8	12.8	17.5	21.0

Table 5-20: Summary of the phase 2 physiological data describing the respiratory condition of the group for the RCS-C test.

5.3.3.2 EMAIL ISL vision test

Like the results for phase 1, the group mean ISL values are similar across the three test conditions, as shown in Figure 5-17, and vary by less than one standard deviation. The variance in data reduces as F_IO_2 increases from condition D to F but the variation for conditions E and F is within the error bars, equal to $\pm$1 standard deviation of the mean value, for condition D. Similarly, there is not an overall trend within the results for each participant, as shown in the right-hand graph of Figure 5-17.

The increased standard deviation for condition D can be attributed to the result for participant 10 that has the additional effect of causing an upward shift in the group mean value for the condition. The higher ISL values for participant 10 appear to be characteristic of their performance at the test for this phase of the study. Removing participant 10 from the cohort would reduce the group mean by 16 ms and the standard deviation of the group by 24 ms. This would more closely align the group results for condition D to those of the other conditions providing further support for the lack of variation in ISL as a function of the test conditions.

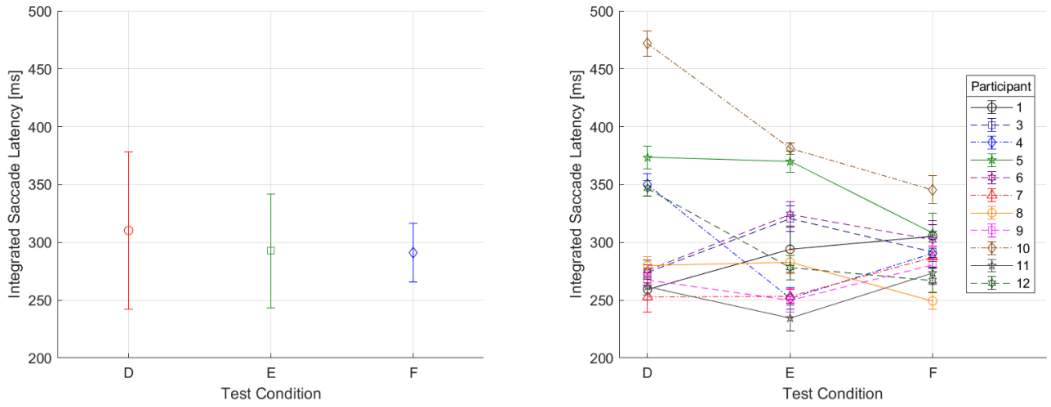

Figure 5-17: Summary of the EMAIL test results for phase 2. (*Left*) Mean results for each condition. (*Right*) ISL value for each participant for each condition.

An AD test indicated that the control condition did not conform to a normal distribution ($p = 0.001$). Subsequent tests to determine if the data conformed to a normal distribution when transformed using a natural log, or a square-root function, provided similar results ($p = 0.021$ and $p = 0.015$ respectively). On this basis a Kruskal Wallis ANOVA was performed, see Table 5-21, which showed that the test conditions, E and F, were not significantly different from the control condition D. There was no apparent within participant variation as illustrated by the trend shown in the right-hand graph of Figure 5-17.

Source	SS	df	MS	Chi-q	Prob>Chi-sq
Conditions	8.73	2	4.3636	0.09	0.9544
Error	2983.27	30	99.4424		
Total	2992	32			

Table 5-21: Kruskal Wallis ANOVA analysis results performed on the phase 2 EMAIL test results.

Although phase 1 and 2 were undertaken on separate days, with at least 7 days between exposures, the same cohort of participants undertook both phases. On this basis, if the two sets of results for the control conditions A and D are statistically from the same population, i.e. the null hypothesis is true, the data from the two phases of the study may be combined to give an overview of how altitude and inspired oxygen concentration affect visual function. As one of the two sets of data has been shown not to conform to a normal distribution, a non-parametric method was applied that also accounted for the different sizes of the two populations after exclusions. The result of applying a Wilcoxon rank sum test indicated that the data for the two conditions are samples from a continuous distribution with equal medians ($p = 0.6985$). On this basis the ISL values for both phases of the study have been jointly plotted as a function of $P_{ET}O_2$ and SpO_2 respectively in Figure 5-18.

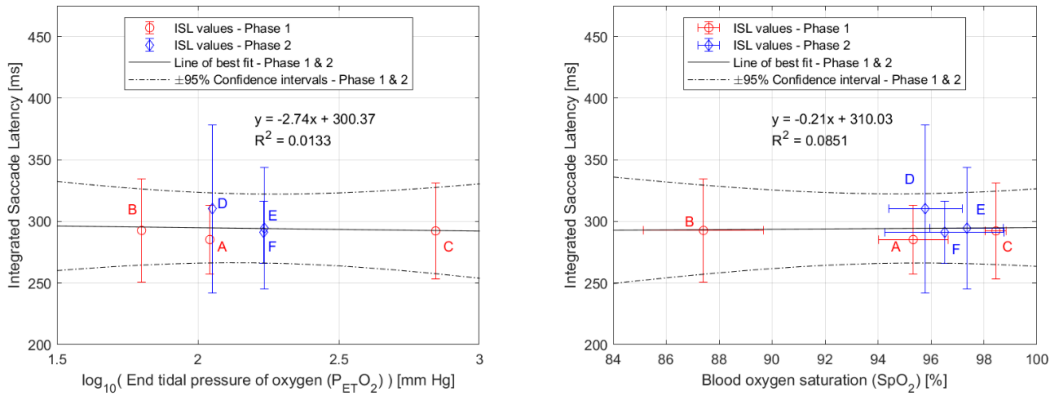

Figure 5-18: Summary of results for both phases of the study showing the ISL values as a function of PETO2 (*left*) and SpO2 (*right*).

The combination of the two sets of data, corresponding to an increased set of respiratory conditions, further confirms the result that for a 30% contrast stimulus changes in $P_{ET}O_2$ and SpO_2 have no effect on the time required to detect and identify the stimulus. The greater variability in the ISL values for the control conditions A and D can be explained by the inconsistent data for one participant, participant 10.

5.3.3.3 RCS-R vision test

Based upon the results from phase 1, and the wider literature, the expectation was that there will be a small reduction in the RCS-R off-axis thresholds as F_IO_2 was increased to be equivalent to 29% at ground level.

The box plots, in Figure 5-19, of the RCS-R on-axis and mean off-axis FMTs for the three respiratory conditions used in phase 2 partly support this hypothesis. If the outliers, denoted by red crosses, are excluded, the median RCS-R off-axis FMT value for condition E are broadly equivalent to the control condition D. For off-axis stimulus locations, the median thresholds for condition F are lower than the control condition with a corresponding shift in the data's range. These outliers for both the on-axis and mean off-axis thresholds for condition E, defined by MATLAB's box plot function, correspond to participants 10 and 12 for the on-axis stimulus and participant 12 for the mean off-axis thresholds.

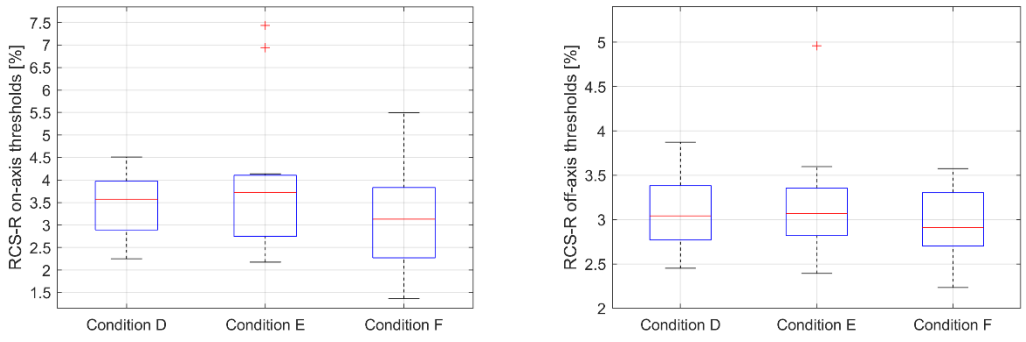

Figure 5-19: Box plots for the RCS-R on-axis (left) and mean off-axis (right) thresholds for phase 2 experimental conditions. The red crosses correspond to the points excluded by the MATLAB boxplot function.

The thresholds for the identified outliers are plotted alongside their own results, and those of the whole cohort is provided in Figure 5-20. Although participant 12's on-axis results are widely distributed, there is a common individual trait that their on-axis thresholds are higher than their off-axis thresholds. This

behaviour was replicated in their results for phase 1, see Appendix C.2.2. Although high, these values have been included as they appear to be a true result.

Participant 10's on-axis and off-axis thresholds are higher for condition E than the rest of the group. Whilst this individual appears to have consistently higher thresholds than the rest of the cohort for the other test conditions, the wide disparity in participant 10's off-axis thresholds for condition E supports their exclusion.

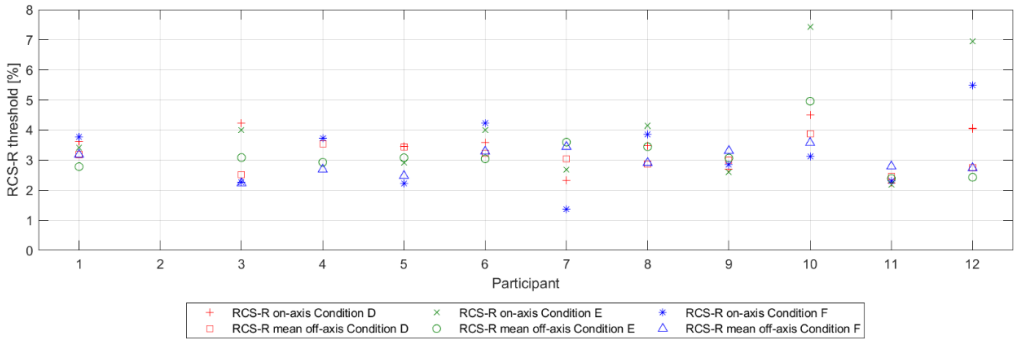

Figure 5-20: Summary of the RCS-R test results by participant for all conditions for phase 2. Participant 2 excluded as they were classed as suffering from hypocapnia for all test conditions.

In Figure 5-21 the apparent independence of the RCS-R mean off-axis threshold value to the changes in test condition is demonstrated by the alignment of the results for the three test conditions to a mean threshold of ~3%. There is more variation in the RCS-R on-axis threshold value, but this is within the error bars, equivalent to ±1 standard error. The indications are that there is not a significant difference in RCS-R thresholds between the conditions. This was confirmed by undertaking two-way ANOVA analyses for the on-axis and off-axis stimulus locations, provided in Table 5-22 and Table 5-23. Prior to undertaking these analyses, it was confirmed, by the application of AD tests that both data distributions conformed to a normal distribution. The AD test p-values for the RCS-R on-axis and off-axis thresholds were 0.150 and 0.382, respectively.

Based upon the analysis of the RCS-R thresholds for both on- and off-axis stimuli, the relatively small increase in F_IO_2 did not have a significant effect on visual function.

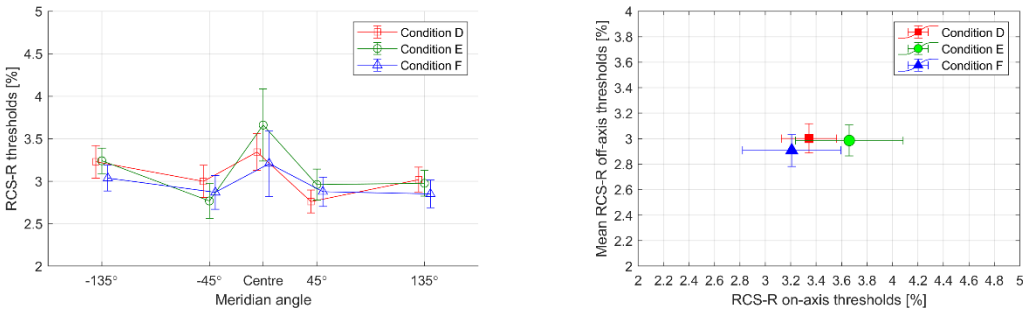

Figure 5-21: Summary of the phase 2 RCS-R results for the three test conditions as a function of on-screen stimulus location with conditions D and F offset by -5°/+5° from the meridian angle (left) and mean off-axis threshold plotted against on-axis threshold (right). Error bars equate to 1 standard error.

Source	SS	dF	MS	F	Prob>F
Conditions	1.0777	2	0.53885	1.26	0.3073
Participants	26.1703	9	2.90781	6.8	**0.0003
Error	7.6942	18	0.42745		
Total	34.9422	29			

*Table 5-22: Two-way ANOVA analysis performed on the RCS-R test on-axis data for phase 2. (** Statistically significance at $\alpha = 0.01$.)*

Source	SS	dF	MS	F	Prob>F
Conditions	0.2025	2	0.10124	0.50	0.6095
Participants	8.0061	9	0.88957	4.37	**0.0001
Interaction	7.6173	18	0.42318	2.08	*0.0127
Error	18.3047	90	0.20339		
Total	34.1306	119			

Table 5-23: Two-way ANOVA analysis performed on the RCS-R test off-axis data for phase 2. (Statistical significance at $\alpha = 0.05$ ** Statistical significance at $\alpha = 0.01$.)*

Combining the RCS-R results of phase 2 with those from phase 1 provides a greater insight into the ability of supplementary oxygen to overcome the effects of hypoxia at 3048 m.

The RCS-R on-axis thresholds potentially vary as a linear function of the $\log_{10}$ of $P_{ET}O_2$, as shown in Figure 5-22, but the R^2 value for the fitted line is low, <0.1. The confidence bounds at 95% align with the error bars of ± 1 standard deviation for each of the data points.

The more interesting result, in terms of visual function, is the variation of RCS-R off-axis thresholds as a function of $P_{ET}O_2$, shown in the right-hand graph of Figure 5-22. Comparing the RCS-R off-axis thresholds for both phases with the linear model of RCS threshold as a function of $P_{ET}O_2$ suggests that the model could be improved. This comparison is supported by the result of a *t*-test applied to the off-axis data for the control conditions, A and D, for the two phases demonstrates that the null hypothesis that the two data share a common mean is valid (p = 0.7572). For $P_{ET}O_2$ values greater than 100 mmHg, corresponding to the normoxic or hyperoxic conditions, the RCS-R off-axis thresholds appear to be largely invariant to increases in $P_{ET}O_2$. This is supported by the lack of statistical significance reported for the two-way ANOVA when applied to the phase 2 data. In contrast, the onset of hypoxia results in an increase in RCS-R off-axis thresholds. A better model could be an exponential function as demonstrated in Figure 5-23. Although this alternative model gives a higher R^2 value, indicating a better fit to all thresholds, the true form of this function cannot be defined without data for lower $P_{ET}O_2$ values corresponding to higher altitudes. This alternative model does capture the small reduction in visual thresholds with the use of supplementary oxygen and supports the concept that the outer retina is functionally hypoxic under normal conditions.

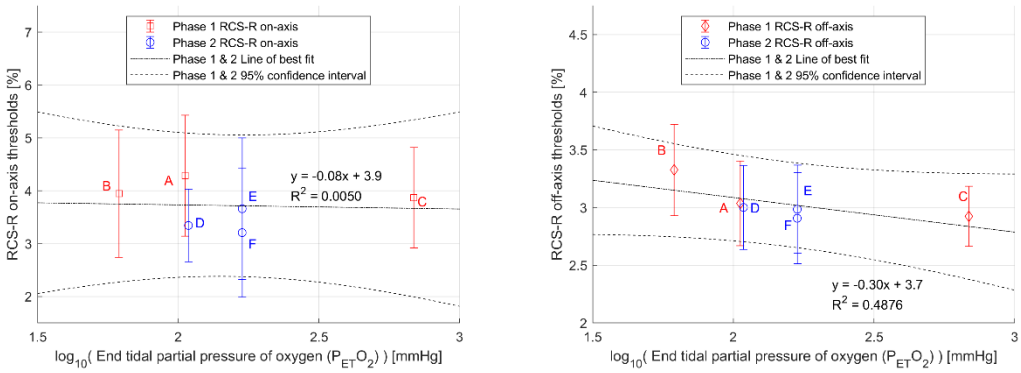

Figure 5-22: RCS-R on-axis and mean off-axis thresholds as a function of $P_{ET}O_2$ for the conditions from both phase 1 and 2 of the study. Error bars equate to 1 standard deviation.

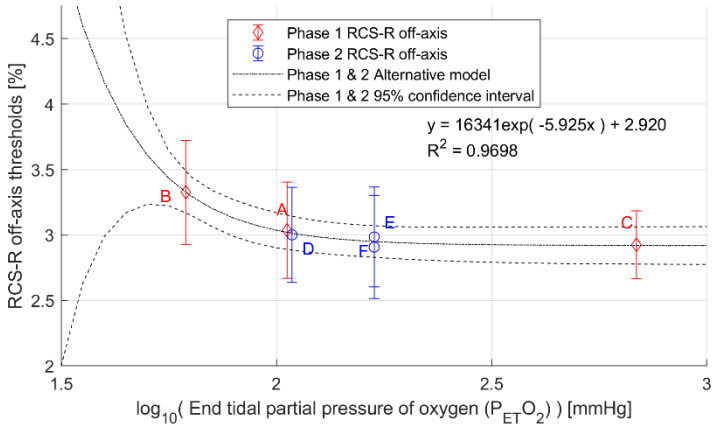

Figure 5-23: An alternative model for fitting RCS-R off-axis thresholds as a function of $P_{ET}O_2$ for the conditions from both phase 1 and 2 of the study. Error bars equate to 1 standard deviation.

Finally, assuming that conditions B and F were undertaken at an equivalent altitude, both the right hand graph in Figure 5-22 and again in Figure 5-23 shows a 0.4% reduction in the RCS-R off-axis threshold that can be attributed to the use of supplementary oxygen. This indicates that the countermeasure of breathing an F_IO_2 of 43% has been effective in mitigating the effects of hypobaric hypoxia at 3048 m on visual thresholds.

Whilst there is no overt awareness of the loss of visual information due to the onset of hypoxia, when a direct comparison is made, based upon modelling the effects of hypoxia and hyperoxia at similar altitudes, the additional textural cues arising from the reduction in thresholds were found to be more apparent (Moorhead *et al* 2016). Although the magnitude of the effect observed in the current study is small, the effects of acute hypoxia on visual function are known to increase with altitude and so the difference of 0.4% at 3048 m between the thresholds for hypobaric hypoxia and hypobaric hyperoxia may well increase significantly at higher altitudes. The impact of a 0.4% reduction in thresholds, i.e. gain in sensitivity, may well have some impact on the helicopter pilot's ability to make full use of visual cues, particularly at higher altitudes.

Whilst the case for a relationship between RCS-R on-axis thresholds and SpO_2, shown in Figure 5-24, appears to have a higher coefficient of determination than that as a function of $P_{ET}O_2$, there is still variation in the on-axis thresholds for a given SpO_2 value. The RCS-R off-axis thresholds show a stronger

linear relationship with SpO_2, with off-axis FMT values increasing as the blood becomes less saturated with oxygen. The indication is that decreased blood oxygen saturation may predict likely decrement in peripheral visual function with hypoxia. The caution with this relationship is that lowering of blood oxygen saturation and loss of visual sensitivity are effects of hypoxia and not the other way round.

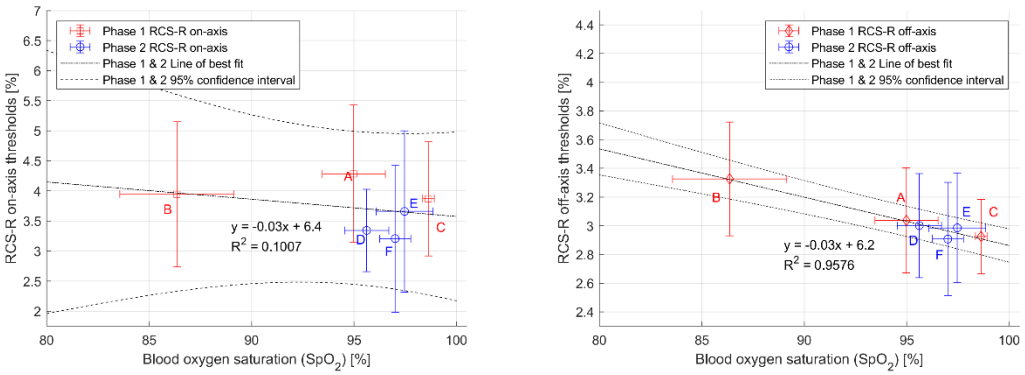

Figure 5-24: RCS-R on-axis and mean off-axis thresholds as a function of SpO_2 for the conditions from both phase 1 and 2 of the study. Error bars equate to 1 standard deviation.

5.3.3.4 RCS-C vision test

The box plot in Figure 5-25 provides an overview of the spread of the data, and when considered with the summary graph in Figure 5-26, it can be seen that the MATLAB boxplot function has identified that RCS-C thresholds for participant 10 under condition F as outliers. Further inspection of Figure 5-26 suggests that this participant has generally higher thresholds that are not as widely spread as some other participants, such as participants 5 or 6, and consequently the data for participant 10 has been included in the following analysis.

Considering the box plot in combination with the mean thresholds for both the on-axis and off-axis stimuli, see Figure 5-25 and Figure 5-27 respectively, the thresholds are lower with the increased F_IO_2. The effects of hypoxia at altitude have been more than compensated for by use of 43% oxygen with both the on-axis and off-axis thresholds lower than the complementary condition E. Between conditions D and F there is a shift in mean FMT values for all stimulus locations of ~0.43%. This effect appears to be more pronounced for the off-axis thresholds supporting the findings from phase 1 that the off-axis thresholds are affected more by changes in oxygen tension than the thresholds for foveal based vision. Like the phase 1 results, there also appears to be the reduction in thresholds for the control condition with increasing meridian angle.

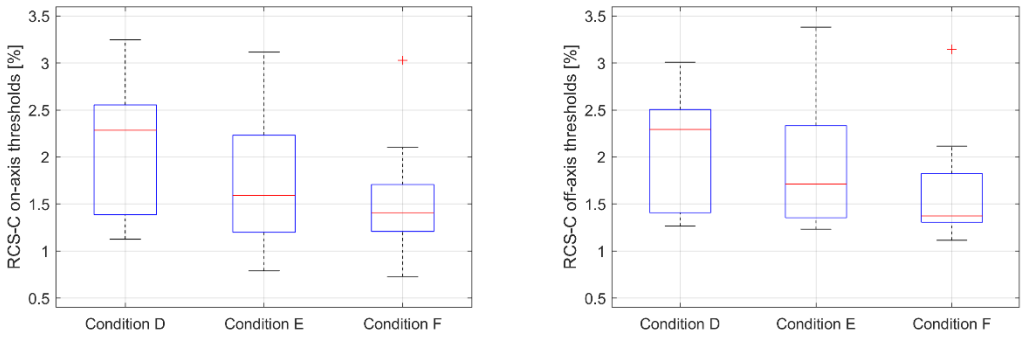

Figure 5-25: Box plots for the RCS-C on-axis (left) and mean off-axis (right) thresholds for phase 2 experimental conditions. The red crosses correspond to the points excluded by the MATLAB boxplot function.

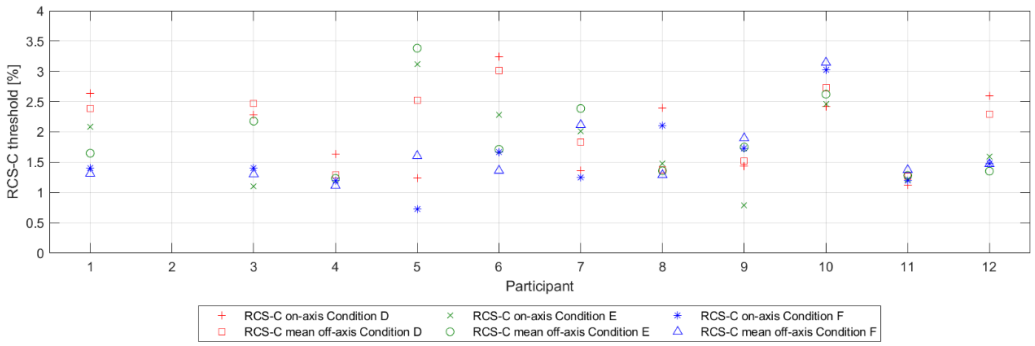

Figure 5-26: Summary of the individual results for each participant based upon their on-axis and mean off-axis RCS-C thresholds with participant 2 excluded.

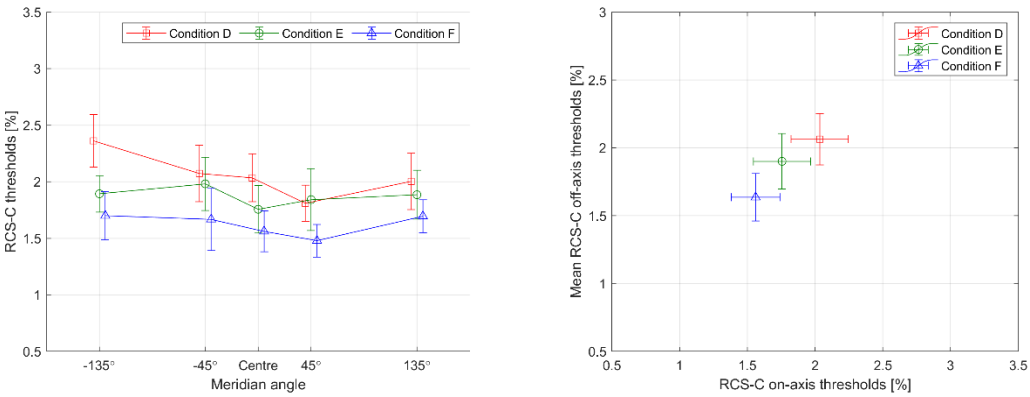

Figure 5-27: Phase 2 RCS-C thresholds when plotted as a function of stimulus location with conditions D and F offset by -5°/+5° from the meridian angle (left) and when mean off-axis thresholds are plotted against on-axis thresholds (right) for the test conditions. Error bars equate to 1 standard error.

The application of AD tests confirmed that the RCS-C threshold values for the on-axis stimuli conformed to a normal distribution ($p = 0.239$) however the RCS-C off-axis threshold values were found to conform to a log normal distribution ($p = 0.083$).

Metric	RCS-C on-axis			RCS-C off-axis		
	D	E	F	D	E	F
Mean	2.03	1.76	1.56	2.06	1.90	1.64
Standard Deviation	0.70	0.70	0.60	0.63	0.68	0.58
Standard Error	0.21	0.21	0.18	0.19	0.20	0.17
Median	2.29	1.59	1.41	2.29	1.71	1.37
IQR	1.17	1.03	0.50	1.10	0.98	0.52
Min	1.13	0.79	0.73	1.26	1.23	1.11
Max	3.25	3.12	3.03	3.01	3.38	3.15
Range	2.12	2.33	2.30	1.74	2.15	2.03

Table 5-24: Summary statistics for RCS-C

The subsequent application of ANOVA demonstrated that there was no significant difference between the RCS-C on-axis threshold for each condition (p = 0.1979), see Table 5-25. The results of the two-way ANOVA provided in Table 5-26 and subsequent post hoc analysis, see Table 5-27, confirm that there is a statistically significant difference between the RCS-C off-axis thresholds for conditions D and F (p < 0.0001), and E and F (p = 0.0040). There was not a statistically significant difference between conditions D and E. The strong statistically significant difference between the participants for the RCS-C off-axis FMTs and similarly the p-values for the interaction term in Table 5-26 demonstrate the variability in the response of participants to changes in environmental and physiological conditions.

Source	SS	dF	MS	F	Prob>F
Conditions	1.2426	2	0.62131	1.76	0.1979
Participants	6.3062	10	0.63062	1.78	0.1297
Error	7.0665	20	0.35332		
Total	14.6153	32			

Table 5-25: Summary of the application of a two-way ANOVA to the RCS-C on-axis data for phase 2.

Source	SS	dF	MS	F	Prob>F
Conditions	1.1914	2	0.59571	13.63	**<0.0001
Participants	7.7518	10	0.77518	17.74	**<0.0001
Interaction	3.9999	20	0.2	4.58	**<0.0001
Error	4.3253	99	0.04369		
Total	17.2684	131			

*Table 5-26: Summary of the application of a two-way ANOVA to the RCS-C off-axis data for phase 2. (** Statistical significance at $\alpha = 0.01$.)*

Condition 1	Condition 2	p-value
D	E	0.1526
D	F	**<0.0001
E	F	**0.0040

Table 5-27: Post hoc analysis of RCS-C off-axis results.

A comparison between these results and those from the previous experiment, conditions A to C, needs to be tempered by the difference between the thresholds for the control conditions, A and D, for the two phases of the study. The application of a *t*-test to test the null hypothesis that the means of the two sets of off-axis RCS-C FMTs are equal demonstrated that there is a statistically significant difference (p = 0.0003) between the results for the two experiments' control conditions. (Both data sets were

transformed to account for them belonging to a lognormal distribution, as indicated by the AD tests previously applied.) In contrast, the application of a *t*-test to test the null hypothesis that the RCS-C on-axis results have equal means confirmed that this is the case (p = 0.5193). These two results are supported by the two graphs plotted in Figure 5-28 and Figure 5-29 where RCS-C on-axis and off-axis thresholds have been plotted as a function of $P_{ET}O_2$ and SpO_2 respectively for all test conditions (A to F).

For the both RCS-C on and off-axis thresholds as a function of $P_{ET}O_2$, the linear relationship is still valid with a loss RCS-C sensitivity as $P_{ET}O_2$ is reduced. The comparison also suggests that there may be equivalency between the on-axis thresholds recorded for conditions C, E and F. The same may be true for the off-axis RCS-C thresholds but the statistically significant difference in the thresholds for the two control conditions limits the scope of the comparisons. Had the thresholds of the control conditions for the two phases been better aligned, the case could have been made for an exponential relationship as per the joint RCS-R off-axis results for both phases.

The variation in the SpO_2 values for conditions E and F, Figure 5-29, is negligible and is within measurement error, as is likely to be the case for conditions A and D. The result of the variation in the RCS-C off-axis thresholds for the two control conditions can be observed by the flattening of the line of best fit, from -0.020 to -0.013, suggesting that there is little effect of blood oxygen saturation on cone sensitivity. There is also a large reduction in the coefficient of determination because of the variation between the results of the two phases of the study.

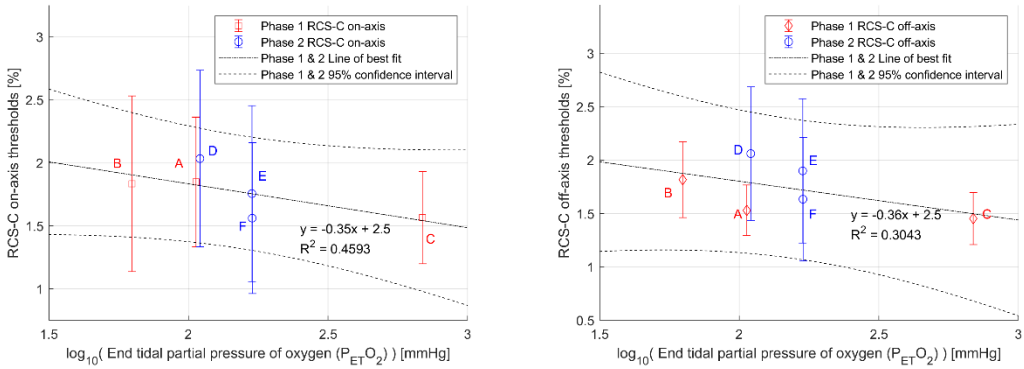

Figure 5-28: RCS-C on-axis (left) and off-axis (right) thresholds as a function $P_{ET}O_2$ for all conditions. Error bars equate to 1 standard deviation.

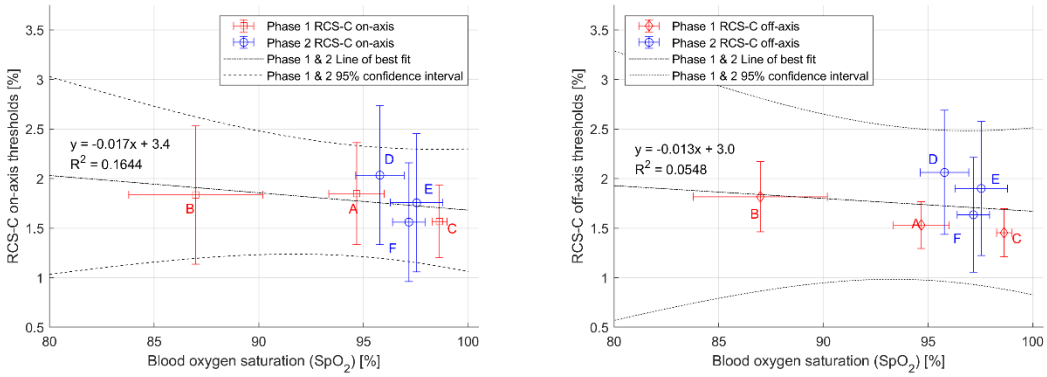

Figure 5-29: RCS-C on-axis (left) and off-axis (right) thresholds as a function SpO_2 for all conditions. Error bars equate to 1 standard deviation.

5.4 Discussion

5.4.1 Review of respiratory conditions

The level of hypoxia achieved in the first phase of the trial corresponded to a P_AO_2 of 63.2 mmHg which is above the theoretical prediction of 54 mmHg assuming a P_ACO_2 of 40 mmHg. The P_AO_2 values for the condition in the second phase of the study undertaken at altitude were similarly around 10 mmHg higher than the theoretical values. Viewed in isolation, the impact on first phase was that the effect of hypobaric hypoxia would have been slightly less. For the second phase of the trial, the participants were not hypoxic for condition F but instead experienced hypobaric hyperoxia. The respiratory condition experienced would have corresponded to atmospheric pressures between 565 and 550 mmHg corresponding to an altitude of around 2438 m to 2645 m, below the desired altitude of 3048 m.

In practice the average $P_{ET}CO_2$ values for the control and hypoxic conditions were between 34 mmHg and 37 mmHg suggesting that the results may be confounded by mild hypocapnia potentially arising from a lack of experience breathing using the Type P/Q aircrew mask. The hyperoxic condition did result in lower $P_{ET}CO_2$ values, ~33 mmHg, as expected.

The influence of hyperventilation was mitigated by considering the respiratory state of the participants in the analysis and excluding those that had $P_{ET}CO_2$ values below 25 mmHg. If the participants were hyperventilating, this would have resulted in a slight increase in sensitivity (Connolly and Hosking 2006) reducing the magnitude of differences between flicker modulation thresholds measured using the RCS test for the different conditions. In isolation the effect of the higher P_AO_2 values on their own would have reduced the magnitude of the effect of the respiratory condition on the results of the vision tests.

5.4.2 Key findings

Notwithstanding the comments above, the key results of the study were a statistically significant elevation of both rod and cone thresholds at 5° eccentricity, as measured by the RCS test, when the participants experienced hypobaric hypoxia at an altitude of 3048 m compared to the normobaric hyperoxic condition when breathing 100% oxygen. There was also a statistically significant difference in rod thresholds at 5° eccentricity between the hypobaric hypoxic condition and the normobaric normoxic condition.

The use of supplementary oxygen also resulted in statistically significant difference between RCS-C off-axis thresholds at 5° eccentricity between hypobaric hyperoxia and both normobaric normoxia and normobaric hyperoxia. These demonstrate the benefits of using supplementary oxygen as a countermeasure to the loss of visual sensitivity arising from hypobaric hypoxia. The interesting result is that it is the off-axis stimuli where the significant effect is observed indicating that this region of the retina, at 5° eccentricity, is more affected by changes in P_AO_2 than the fovea, based upon the stimuli used for the both the RCS-R and RCS-C tests.

The luminance of the different stimuli corresponds to high mesopic for the RCS-R test and low photopic for the RCS-C test condition. This variation in luminance levels correspond to the transition experienced at dawn and dusk. The RCS test results for phase 1 partly overlap with Connolly's assessment of acuity at 2438 m at 5° eccentricity but at slightly higher luminance levels for both test conditions (Connolly 2011).

This is not surprising given the psychophysical tests employed. The extension to consider the effect of hypoxia on suprathreshold peripheral visual function at 8° aligns with the response time studies undertaken by Kobrick and Dusek (1970) but they utilised higher altitudes and thus invoked greater levels of hypoxia with corresponding increase in the effect size observed. The greater susceptibility of rods, compared to cones, to changes in respiratory conditions is highlighted by the results of the RCS test. The results for phase 1 also show a change due to the use of supplementary oxygen at 100% as a countermeasure to mitigate the effects of hypoxia.

Plotting the thresholds as a function of both SpO_2 and $P_{ET}O_2$ highlights that at least for rods, the change in sensitivity is primarily due to changes in the outer retina and choroidal oxygen tension rather than the changes in blood oxygen saturation in the inner retina and visual cortex. This is illustrated by the exponential relationship between RCS-R off-axis thresholds and $P_{ET}O_2$ compared to the linear relationship as a function of SpO_2. The RCS-C off-axis data shows a similar behaviour for the first phase of the study but results for phase 2 slightly confound the fitting of RCS-C off-axis thresholds as an exponential function of $P_{ET}O_2$. Consequently, the results of the study support the hypothesis that the sensitivity of photoreceptors in peripheral retina is reduced with oxygen deficiency.

The on-axis thresholds do not appear to be as affected by the onset of hypoxia. This can be attributed to the density and type of photoreceptors responding to the two test stimuli. It has been previously proposed that when hypoxic, the rod photoreceptors have a greater metabolic demand than cones under mesopic conditions (Connolly 2011, Wangsa-Wirawan and Linsenmeier 2003, Linsenmeier 1986). As a result, cone sensitivity is reduced due to the greater oxygen consumption by the rods. The lack of rods within the fovea will have meant that the cones would be less likely to be affected by the increase in oxygen consumption by rods at the lower light level. This agrees with the results that show little difference between the thresholds for the control and hypoxic conditions.

In contrast, the results indicate the benefits of hyperoxia are apparent in the change in off-axis sensitivity of cone-mediated vision under low photopic conditions. A statistically significant difference was not observed for the RCS-R off-axis thresholds for the phase 2 test conditions. This might suggest a form of hysteresis in the demand for oxygen by rods and the cones response to increased choroidal oxygen levels resulting from hypoxia and hyperoxia, respectively. However, this does not completely align with the model of increased oxygen consumption by rods causing a reduction in cone sensitivity. An alternative explanation, and probably the more realistic, is that the statistically significant differences between participants ($p = 0.0001$) and the associated interaction ($p = 0.0127$) characterised by the two-way ANOVA, are masking the underlying changes in FMTs at high mesopic luminance values. The box plot in Figure 5-19 would suggest that there is a difference between the median RCS-R thresholds for condition F (hypobaric hyperoxia), and conditions E (normobaric hyperoxia) and D (normobaric normoxia).

The level of hypoxia induced by Feigl *et al* (2011) corresponded to a higher altitude than that simulated in this study; their participants were breathing 12% oxygen compared to around 14% for this study. In agreement with the study by Feigl *et al*, who also used flickering stimuli, the change in photopic sensitivities between the hypoxic or normoxic condition were not significant. Previously flickering stimuli

have been associated with a higher metabolic demand and changes in blood flow (Garhöfer *et al* 2004, Felder *et al* 2017, Kiryu *et al* 1995), but these studies have all used flickering stimuli with a duration of at least a minute. Although the RCS tests took between 5 to 10 minutes to complete, each stimulus presentation was limited to 333 ms (RCS-C) or 500 ms (RCS-R). Whilst there may a temporary increase in the metabolic demand of the photoreceptors, there may not be the same change in blood supply as observed in these other studies. Additionally the vasculature of the choroid provides a blood flow ~20 times greater than that of the inner retina and cannot increase any further (Wangsa-Wirawan and Linsenmeier 2003) which accounts for why the effects of hypoxia are correlated with the oxygen tension of the choroid and outer retina.

The results for the EMAIL test do not show a statistically significant variation with test condition. The ISL values appear to conform to a linear function of both $P_{ET}O_2$ and SpO_2 but sensitivity of the test, i.e. large standard deviation of the test results, across the cohort impacts the ability draw any further conclusions about the nature of the relationship. Given these results, the hypothesis that the time required to detect and identify a stimulus increases as a function of oxygen deficiency is not proven. Given the apparent invariance to changes in test conditions, it could be concluded that at 30% contrast the time to detect and identify the stimulus is independent of oxygen deficiency for the test conditions.

Considering the statistics of the ISL values for the phase 1 conditions, places the result of the Kruskal Wallis test result in context. The mean and the standard deviation of the ISL values for each condition do not vary by more than the bounds set by the mean and standard deviation for the control condition, or the median and the inter-quartile range (IQR). There is effectively equivalency leading to the inference that an increment or decrement of the inspired oxygen concentration has very little effect on ISL value for the test conditions used. It must be remembered that the EMAIL test used a supra-threshold stimulus with 30% contrast so any change in test result was likely to be small when compared to the effect of altitude and oxygen concentration on visual thresholds.

The results from phase 2 of the study partly support the hypothesis that peripheral visual function is improved by supplementary oxygen. The caveat with this statement is that supplementary oxygen, when used to mitigate the effects of hypoxia does improve peripheral visual function. This was demonstrated for both the RCS and EMAIL tests results for condition F when compared to the other conditions for phase 2. In the context of the wider question of whether there is a statistically significant difference in visual thresholds when F_IO_2 is increased at ground level, giving rise to an increased P_AO_2, the measured change in thresholds or ISL do not support the hypothesis. This is because the changes are so small, given the test conditions used in the study. For a 0.7 log change in $P_{ET}O_2$, there is only a 0.05% change in RCS-R off-axis thresholds, using the model illustrated in Figure 5-23. Further development and validation of this model relies on gathering more off-axis threshold data at respiratory conditions equivalent to altitudes above 3048 m.

There was broad equivalence between the results for conditions E and F for both RCS and EMAIL tests. Furthermore, the results for condition F had a reduced standard deviation when compared to the other test results.

The results for the vision tests undertaken when the participant was hyperoxic had decreased variance suggesting the visual sensitivity was being optimised across the cohort, converging on a small set of values. The optimal threshold corresponds to a biophysical limit defined by the limits of phototransduction and the subsequent cellular and neural connections. The effect of hypoxia was the opposite, with increased variance for the on-axis, foveal, responses observed for condition B across the three tests, as the role of oxygen in these cellular and neural connections is exposed.

The results of the study demonstrated that the RSC test can measure statistically significant differences in peripheral visual thresholds with only 2 minutes dark adaptation time.

The key result from phase 2 of the study was the demonstration of the use of a reduced concentration (43%) of supplemental oxygen to mitigate the effects of altitude equivalent to condition B in phase 1. The results from the vision tests were broadly equivalent to an F_IO_2 of 29% at ground level. Depending on the operational requirement, there could be an argument made for reducing the concentration of supplementary oxygen from 100% to 43% whilst still being able to provide an excess of oxygen to counteract the effects of hypoxia at 3048 m or higher, e.g. 4572 m (15,000 ft). At an altitude of 4572 m, the F_IO_2 of 43% equates to a P_AO_2 of 100 mmHg, equivalent to normobaric normoxia.

5.4.3 Evaluation of EMAIL test

The selection of the contrast and eccentricity of the EMAIL test stimulus was a balance between defining a stimulus that provided a visual challenge without introducing confounding effects of the variation of acuity and contrast sensitivity as a function of hypoxia. Reducing the contrast of a supra-threshold stimulus under normobaric normoxic conditions may have resulted in the stimulus being at or below threshold for the hypobaric hypoxic exposure. This would have confounded the results as the test's outcome would then be reliant upon the sensitivity of individual participants. The reason for including the EMAIL test was to determine if there was an effect on the participant's ability to detect and process information displayed at an eccentricity where typically alpha-numeric data are in some symbology sets used with augmented reality devices. For this information to be visible, the symbology needs to have sufficient contrast against the background scene, and hence the requirement for a supra-threshold stimulus.

Had the EMAIL test's upper limit on the test stimulus duration, set at 800 ms, not been found, it could have limited the benefits of the combination of the 4 AFC methodology used with the adaptive 2 down, 1 up staircase in providing a method of determining the ISL for a test condition. Without the ability to undertake a pilot test in the hypobaric chamber at altitude, an estimate was made of the effect size that might be observed and the between subject variation across the cohort. Given the results of this study, the stimulus contrast could have been reduced to 15%, which would have resulted in ISL values of around 450 ms based upon the preliminary lab tests. As demonstrated by the RCS test results, this is a supra-threshold contrast level but offers sufficient challenge to test if there is an effect from the change in altitude and inspired oxygen concentration but at the risk of an increase in variance across the cohort.

Comparing the EMAIL test results with the contrast acuity thresholds for a 12 $cd.m^{-2}$ background at 2438 m, the target contrast for maintenance of gap orientation discrimination under photopic conditions is

around 11% at 5° eccentricity, with the hyperoxia condition around 9.5% (Connolly 2011). These results are for hypoxia at a lower altitude than those used in this study, so it is likely that the stimulus contrast thresholds would be higher given the increased eccentricity and reduced background luminance condition based upon the results in Figure 5-5 and Figure 5-6.

The lack of any statistically significant results for the variation in ISL with changes in altitude or F_IO_2 for the test stimulus conditions is informative. Whereas previous studies have addressed the effects of hypoxia on visual thresholds, this result for a supra-threshold stimulus informs our understanding from an operational perspective. Visual information presented in NVGs and in the outside world is not wholly based on what is visible at visual threshold. Whilst texture can be inferred by visual information at threshold, the stronger visual cues relating to shape and form are abstracted from edge features that are often supra-threshold as exemplified by the Pelli-Robson chart (Pelli *et al* 1988).

For the EMAIL test, which is initially reliant upon peripheral vision at 8° eccentricity to enable detection of the stimulus, the increased stimulus contrast and consequently higher flux of photons incident upon the retina provided sufficient stimulation to overcome any loss of sensitivity due to the reduction in oxygen tension in the choroid. Table 5-28 demonstrates this point with the increment in luminance of the EMAIL stimulus more than six times that of the RCS-C stimulus.

Test	EMAIL	RCS-R	RCS-C
Background luminance [cd.m^{-2}]	8.0	0.5	24.0
Stimulus contrast [%]	30.0	3.0	1.6
Stimulus luminance [cd.m^{-2}]	10.4	0.515	24.38
Luminance increment [cd.m^{-2}]	2.4	0.015	0.38

Table 5-28: Comparison of the luminance increment for the vision test stimuli used in this study.

Without supporting eye tracker data, no firm conclusions can be made as to whether the small variations in ISL as a function of test condition can be attributed directly to, or are a combination of:

- Changes in peripheral (off-axis) sensitivity leading to variation in saccade latency;
- Changes in oculomotor function (saccade duration) as a result of hypoxia;
- Changes in oculomotor function (corrective glissade) as a result of hypoxia;
- Changes in foveal (on-axis) sensitivity leading to variation in visual processing time.

Based upon the results from this study, it is hypothesised that variation in oculomotor function is negligible at 3048 m. It is not an effect that has been reported in connection with mild hypoxia (Harding 2001) However, with more severe hypoxia, equivalent to ~6096 m, ocular muscle function is compromised (Wilmer and Berens 1918). In contrast, the evidence for changes in visual thresholds as a function of mild hypoxia are more compelling. It is therefore hypothesised that any change in ISL is because of an increment in the saccade latency due to hypoxia, based upon the observed changes in peripheral thresholds for both rod and cone mediated vision and evidence from other studies (Kobrick and Dusek 1970). This increment should be greater if the contrast of stimulus is reduced.

5.4.4 Test repeatability

Trials involving human participants are complex. Although studies can be designed to minimise confounding effects, variation in the participant's performance on the day of the test can affect test repeatability. This appears to have been the cause of the differences between the two control conditions for the two phases of the study, conditions A and D, and the repeatability of the RCS test for some individuals.

The use of the hypobaric chamber provided a guarantee that the participant should be experiencing mild hypoxia for the hypobaric hypoxic condition and that the effect of supplementary oxygen at a fractional inspired oxygen of 43% as a counter measure to mild hypoxia could be assessed. Whilst studies undertaken at ground level using defined concentrations of oxygen, which are balanced with nitrogen, can provide an idealised response to the respiratory condition by simulating being at altitude, the hypobaric chamber provides the physical change in pressure which guarantees hypobaric representation of the operational environment and imposition of the consequent hypoxic challenge breathing ambient air.

The use of safety pressure for all exposures would not have affected the overall results of the study as it only introduces a small positive pressure, of ~3 mmHg, ensuring that any leaks from the mask were outwards, from the mask to the ambient atmosphere. This will not have affected the atmospheric pressure experienced for each test condition as the magnitude of the pressure difference is less than the variance in the atmospheric pressure.

5.4.5 Limitations

The absence of meaningful differences between conditions A and C of phase 1 of the study effectively meant that phase 2 of the study would be unlikely to produce any statistically significant results. This might have been different if the RCS tests had a smaller variance associated with their measurements. This could be achieved by increasing the number of reversals before concluding the test and extending the initial period where reversals are excluded. Alternatively, a larger cohort could have been defined increasing the number of participants, but this brings its own problems with increasing the cost of the study and being able to recruit enough participants. However there appears to be an underlying limitation in that there is only a small difference in visual function for conditions A and C, i.e. normoxia and hyperoxia for a F_IO_2 of 100%. The potential benefit of supplementary oxygen to enhance sensitivity to the test stimuli is slight, however it has been demonstrated in phase 2 that its use can improve off-axis sensitivity, even at an F_IO_2 of 43%.

5.4.6 Confounding factors

The variation in the performance between the control conditions for phase 1 and 2 of the study is likely to be a combination of a series of confounding factors, e.g. day to day variability of the participant, and novelty of the study. For most of the participants, this was their first experience of undertaking trials in the hypobaric chamber or using the mask and regulator. Whilst attempts were made to minimise the influence of external factors, such as caffeine intake and sleep, others were out of the control of the author, e.g. workload arising from their role within QinetiQ.

5.4.7 Learning from experience

The cause of the hypocapnia recorded for participant 2 has been attributed to the P mask's faulty expiratory valve. The effect of the faulty valve would have caused a flow of gas through the mask such that the mass spectrometer would not have reliably measured the total partial pressure of CO_2 present in the expired breath. There was no CO_2 in the composition of the inspired gas as the oxygen content is balanced by nitrogen. The participant themselves would have felt that they needed to breath harder, akin to pressure breathing, which was reported at the end of the session but was attributed to inexperience breathing using the mask. A Mask Cavity Pressure sensor could have detected this event and is something worth considering for future trials.

5.5 Conclusions and future work

5.5.1 Conclusions

The utility of the RCS test has been demonstrated in the characterising the reduction in visual sensitivity at 5° to flickering stimuli arising from the effects of mild hypoxia. The RCS test has also characterised the benefits of using supplementary oxygen to overcome the effects of mild hypoxia. Statistically significant changes in flicker modulation thresholds were recorded for rod photoreceptors when participants were mildly hypoxic at 3048m (10,000 ft) compared with normobaric normoxia ($p = 0.006$). Statistically significant differences in flicker modulation thresholds at 5° eccentricity were also measured for rods and cone photoreceptors when participants were experiencing mild hypoxia compared with hyperoxia resulting from breathing 100% oxygen ($p = 0.0001$).

These results indicate the sensitivity of the photoreceptors located in the peripheral retina are affected by the oxygen tension in the choroid. Although a statistically significant relationship has not been established when comparing normobaric normoxia and normobaric hyperoxia at an inspired fraction of either 29% or 100%, the results do show that choroidal oxygen tension has a part in maintaining photoreceptor sensitivity. Even if these results do not explicitly prove it, the enhanced results at hyperoxic conditions lend support to the agreed theory that the outer retina, used for peripheral vision, is functionally hypoxic in dim light. This arises from demand for oxygen from the larger number rods being greater than that for the lower density of cones as illumination levels decrease. The result is that cones are deprived of oxygen despite an individual cone having a higher metabolic demand than one rod. At the fovea, cones are the only photoreceptor dependent on choroidal oxygenation levels.

There was not a significant difference in the time required to detect and identify an off-axis, 8° eccentric, optotype with a contrast of 30%. This was attributed to the contrast of the stimulus being sufficient to overcome the loss of sensitivity resulting from mild hypoxia.

Finally, the study demonstrated that the effects of mild hypoxia at 3048m can be overcome using supplementary oxygen with a concentration of 43% and that the resulting visual performance at high mesopic light levels is broadly comparable to an inspired fraction of 29% at ground level, whilst at low photopic it is significantly different to normobaric normoxia and hyperoxia at an inspired fraction of 29%.

5.5.2 Further work

There are three studies that have been identified that would further enhance the results of this study and wider understanding of visual function. These are described in the following subsections.

5.5.2.1 Project 1: Effects of hypobaric hypoxia on ability to process peripheral stimuli

What seems to be apparent from the results across both phases of the study is that the visual challenge was not enough to stimulate a significant change in ISL as a function of respiratory condition, i.e. both hypoxia and hyperoxia. To address this, the contrast of the EMAIL stimulus could be reduced further, e.g. to 15% or lower. Similarly, the luminance of the background condition for the RCS-R test could be reduced further using additional neutral density filters to position the stimulus more centrally within the mesopic range where the effects of mild hypoxia have been shown to be more evident.

5.5.2.2 Project 2: Effects of hypobaric hypoxia at 3658m and 4572m on visual function

Repeating the phase 1 of the study using respiratory conditions equivalent to higher altitudes, e.g. 3658 m (12,000 ft) or 4572 m (15,000 ft), would provide additional test points that would enable the models for RCS-R off-axis thresholds as a function of $P_{ET}O_2$ and SpO_2 to be extended. Although studies have been undertaken across a range of altitude/respiratory conditions, using a variety of vision tests, there does not appear to be a defined set of functions which enable the prediction of the effects of hypoxia at a given altitude on visual function.

5.5.2.3 Project 3: Effect of stimulus eccentricity on Integrated Saccade Latency

The variation of ISL with stimulus contrast and eccentricity, illustrated in the left-hand graph of Figure 5-5, are based upon the responses for one participant. Whilst there is confidence that these results illustrate a real effect, based upon similar measurements (Llapashtica 2019), there is a requirement to verify the effect is real and repeatable.

6 Discussion

6.1 Research project aims

The aim of this research project was to learn more about visual function under mesopic lighting conditions, enabling the development of vision tests that can characterise mesopic visual function and informing the development of new technologies or systems to optimise aircrew performance. The vision tests undertaken within the scope of this research project and the outcomes of the three studies are reviewed in the following sections with respect to this central aim.

6.2 Advanced vision tests

6.2.1 Rod Cone Sensitivity (RCS) test

The RCS test was used to provide an assessment of visual function in terms of FMTs at high mesopic (0.5cd.m^{-2}) and low photopic (24cd.m^{-2})[12] light levels. The chromaticities of the backgrounds had different S/P values to preferentially stimulate either rod or cone-mediated responses, respectively. FMTs were measured at five stimulus locations enabling characterisation of foveal visual sensitivity as well as peripherally at 5° eccentricity. The luminance of the background condition and the diameters of the stimuli were defined based upon the outcomes of initial experimentation. The benefit of the test was that it did not require extended periods of dark adaptation. The test for the high mesopic, RCS-R condition was initiated after 2 minutes adaptation to the background stimulus condition in a darkened environment.

The RCS test was used to investigate the relationship between monocular and binocular FMTs at the stimulus locations for the two background luminance/chromaticity conditions. This enabled an assessment of binocular summation and the relationship between FMTs values of the dominant and non-dominant sighting eye. The results of the RCS test were recorded for a cohort of young, normal participants with the aim of establishing the set of FMTs values that describe the Standard Normal Observer (SNO) for the two versions of the test protocol. Lastly, the test was used to characterise the effects of altitude and inspired oxygen concentration on FMTs at high mesopic and low photopic luminance values corresponding to the period between sunset/sunrise and civil twilight[13].

The initial test results, used to define the test protocol, provided a useful method of understanding the variation of FMTs as a function of eccentricity and stimulus diameter for the two test conditions. As the stimulus diameter was decreased, the FMTs increased in agreement with a power function.

Whilst the luminance and chromaticity of the RCS-C test condition instigates a cone mediated response, the mediation of the response to the RCS-R condition is not purely mediated by rods at 0.5cd.m^{-2}. The increase of the S/P for the RCS-R condition necessitated by the change in software version, showed there was an associated statistically significant ($p<0.01$) change in the four off-axis, peripheral thresholds

[12] Luminance quoted for software version v0.102.4. This value is or 22cd.m^{-2} for software version v0.102.7.

[13] Assuming a reflectance of between 33% and 50% and an illumination level of between 200 to 100lux reducing to 1lux at civil twilight.

recorded for the RCS-R condition. This demonstrates the involvement of rods in the mediation of the response to the chromatic and temporal properties of the stimulus condition. Although the chromaticity of the background and 5Hz flicker frequency are biased towards stimulating a rod-mediated response, the luminance of the condition does result in a cone-mediated component to the overall response. The participant is aware of the colour of both stimulus conditions, although the perception of the stimulus' flicker is purely based upon the modulation of the luminance rather than any change in chromaticity. The RCS-R test condition is a useful method of assessing visual function in the form of FMTs at mesopic luminance levels.

The test has benefits both as a research tool and as a test method for assessing visual function of applicants. As a research tool, its utility has been demonstrated in characterising the effects of altitude and oxygen concentration on visual function. Similarly, it has been used as a method to characterise differences between monocular and binocular thresholds of foveal and peripheral vision for both RCS test conditions.

Whilst the test does not replace a visual fields test, it could act as a complementary test within the clinical environment. As more data is gathered as part of research projects undertaken in parallel to this one, the variation in FMTs as a function of age and ocular health can be characterised and 'normal' behaviour can be better established. The results of Experiment 6 provide the basis for defining this normal behaviour. The utility of the test was demonstrated in characterising the visual function of an individual with the results reproducible for both versions of the test protocol software. When evaluating the FMTs for a large cohort, a baseline has been established in terms of a SNO. It has also been demonstrated that off-axis FMTs may be evaluated using the mean data from all quadrants of the visual field, thus simplifying the analysis of RCS test results.

The modification to the chromaticity of the stimuli, necessitated by the change in the display hardware part way through the study resulted in two different test protocols/software versions. In response, the results for Experiment 6 were separated based upon software version. Subsequent statistical analysis indicated that the differences in the RCS-R off-axis FMT values of the two cohorts were statistically significant ($p < 0.01$) preventing these results being combined into a single dataset. There is no statistically significant difference between the FMTs for the on-axis RCS-R test protocol, nor was there between the two variants of the RCS-C condition. The results from Experiment 6, for both versions of the test protocol, provide a reference point for future studies.

The test is engaging, and the learning mode assists in familiarising the participant with the test procedure. However, with hindsight there were occasions when participants might have benefited from a longer familiarisation period. This may have resolved the observed differences in RCS test values between the two control conditions of Experiments 10 and 11. The effectiveness of the learning mode could, and probably should, have been evaluated by undertaking a study to consider the variation in FMTs as a function of number of tests completed. Experiment 4 was undertaken by an experienced observer and as such their data does not assist in resolving this issue for naïve observers.

Reflecting on the decisions made in defining the test protocol, namely the size of the stimuli used, there is an argument that can be made for reducing the size of the stimuli further. This would have the effect of increasing the FMT values recorded with the drawback of increasing the variance in measurement. The potential benefit would be to make the test more sensitive either to variations in physiological conditions, e.g. hypobaric hypoxia or normobaric hyperoxia, or changes in ocular health. Whilst the v0.102.4 test protocol enabled statistically significant differences in off-axis FMTs between hypobaric hypoxia equivalent to 3048m and normobaric normoxia ($p<0.01$) and normobaric hyperoxia (100%) ($p=0.0001$) to be measured for both test conditions in Experiment 10, the test was not sensitive enough to detect a significant change in off-axis FMTs between and normobaric normoxia and normobaric hyperoxia (100%). This is either because there is no difference or that the test could not detect the difference.

6.2.2 Pupillometry

Pupillometry was used as a method to verify that the chromaticity of the RCS-R test stimulus instigated a rod-mediated response. This developed into a wider study of the amplitude and latency of the transient PLR using the chromaticities of the RCS test.

The results of the study have demonstrated the shift in mediation of the transient PLR across the mesopic range of light levels from rods to cones as luminance increases. Furthermore, there are indications that their relative contributions change as a function of age. Over the range of light levels tested (0.001 to 9 $cd.m^{-2}$), the results indicate the pre-stimulus diameter is mediated by rods with pupil diameter reducing as rods approach saturation.

Although commercial handheld pupillometers are available, their use is often related to monitoring or assessment of neurological conditions and critical care (National Institute for Health and Care Excellence 2020). In contrast, the P-SCAN system used for Experiments 7 and 8 is a research tool and as such allows greater flexibility with the spatial extent, luminance, and chromaticity of the stimulus. In terms of optimising aircrew performance, the use of pupillometry is most likely to be restricted to research studies. The autonomic nature of the PLR and the properties of the consensual response make it is possible to probe cortical functions both to gain a greater understanding of the visual system (Barbur *et al* 1998a, 1998b) and its application in a clinical setting (Hall and Chilcott 2018).

The measurements made within the context of Experiment 8 were time consuming; a set of measurements took up to six hours per participant. However, by obtaining repeated results for each test point it was possible to characterise the mean response to a stimulus. This had the benefit of reducing the within measurement variation and some of the effects of external confounding influences, e.g. noise from building work and day to day variations in emotional state and fatigue.

Whilst tests like the CAD test have a specific requirement that they address, the outstanding question for pupillometry is what requirement does it fulfil? Research has been undertaken using pupillometry as a method of characterising fatigue by measuring the Post Illumination Pupil Response (PIPR) (Münch *et al* 2012) or the instability of the pupil characterised by the Pupillary Unrest Index (PUI) (Różanowski *et al* 2015) or similar metrics (Lowenstein *et al* 1963). This has resulted in commercial pupillometers designed specifically to characterise the PIPR. Indeed, the use of pupillometry as a method of characterising fatigue

was originally considered as a line of enquiry for this research project. Apart from this, there is not a clear requirement that directly links to its use in the selection of aircrew at this moment in time. Its strength however is as a research tool to gain a clearer insight into both non-imaging and imaging visual functions at mesopic and photopic illumination levels.

6.2.3 Eye Movement And Integrated Latency (EMAIL) test

The EMAIL test was used to assist in characterising the effects of altitude and oxygen concentration on visual function. The test provides a mechanism by which to assess how stimulus contrast and eccentricity affect the time to process visual information. As a research tool, this is useful in understanding why some visual cues are seen and others are missed or require a longer look. When the results of Experiment 9 are viewed in conjunction with similar studies (Barbur and Chisholm 2001), minimum luminance contrast requirements for HMDs can be defined based around the values of 40% to 50%. For contrast values below this range, the time taken to detect, saccade to and identify the stimulus increases, as shown in Figure 5-5.

Used in isolation, without an eye tracker, the structured nature of the testing undertaken in Experiment 9 enabled the EMAIL test to indicate that the time required to identify a stimulus when presented on-axis was ~20 ms. Increasing the eccentricity adds a delay whilst it is initially detected and the necessity to saccade to the stimulus' location before identification occurs. Varying the eccentricity of the stimulus highlights eccentricity-based variations in visual function that are considered later in section 6.3.1. When used in conjunction with an eye-tracker, the ability to separate out the three elements of detection, saccade to and identification provides an additional insight into visual function (Llapashtica 2019). However, as identified in the lessons learnt from Experiments 10 and 11, its use with an eye tracker requires the head to be stabilised which may restrict some applications.

The test did have a limitation arising from its implementation. The upper limit of the stimulus duration either needs to be removed or increased from 800 ms to at least 2 seconds. This would enable the use of lower contrast stimuli in determining the participant's ability to process peripherally located cues without being time constrained.

6.2.4 Summary

Whilst clinical tests can provide an indication of ocular health, the RCS and EMAIL tests have provided a more detailed characterisation of specific visual functions relating to visually challenging illumination conditions between sunset/sunrise and twilight. Both tests provide a measure of how peripheral information is processed that could have future applications, either in characterising the impact of pilot aids or the effects of environmental stressors on visual function. Both tests have demonstrated their utility as part of an applied research study, see section 5.

Although a powerful tool for investigating visual function, pupillometry is and will probably remain primarily a research tool in the context of optimising aircrew performance.

6.3 Visual function

6.3.1 Differences in foveal and peripheral visual function

There are several outcomes from the first study, which when viewed in combination with those from the second and third study, have implications for our understanding of peripheral visual function at mesopic and photopic light levels.

Whilst the assessment of binocular summation for on-axis, foveal vision was consistent with probability summation, off-axis parafoveal visual function has an increased summation ratio ~1.25 times that at the fovea for both the low photopic and high mesopic light levels characterised by the RCS test conditions. The increased weight given to the visual field away from the fovea indicates links to wider cortical functions corresponding to features in the periphery used to gauge motion and depth, given the greater angular disparities between the two monocular views of the world. From an image forming perspective, these disparities could be mitigated by the greater degree of spatial summation resulting in a coarser sampling of the visual scene.

The similar values for the summation ratio recorded for the off-axis stimuli for both stimulus conditions indicates a commonality in the architecture of the retinal at this 5° eccentricity for both photoreceptor types. This could be a coincidence or a factor of the cone involvement with mediating the response to the RCS-R stimulus.

Additional differences were observed between the most and least sensitive eye in terms of the FMTs for the on-axis and off-axis stimuli across the cohort of Experiment 5. The results shown in Figure 3-25 suggest two different behaviours of how the monocular FMTs are related. For the on-axis stimulus, the line of best fit aligns to a constant gain value of 1.27 between the FMTs for the most and least sensitive eye. However, for the off-axis, peripheral FMTs the line of best fit indicates a fixed offset of 0.60% in the FMTs. The reasons for these differences have not been determined other than to speculate they appear to be related to organisation of the retina at each location. The greater cortical magnification associated with foveal vision may give rise to a gain or an amplification based relationship. Spatial summation in the periphery and the need to process data from a much larger retinal area with a proportionally smaller region of the visual cortex may lead to the offset nature reported. The monocular FMT values were able to predict the ocular dominance with a success rate of 82%.

The differences highlighted by the RCS test between foveal and peripheral visual function are expanded further by its use in evaluating changes in visual function due to altitude and oxygen concentration. Statistically significant results were not obtained for the on-axis condition, but they were for the off-axis stimuli when comparing the extremes of the conditions tested, i.e. hypobaric hypoxia compared to normobaric hyperoxia (100%) ($p=0.001$).

The peripheral retina demonstrates a greater susceptibility to changes in oxygen tension in the choroid. The exponential model illustrated in Figure 5-23 indicates that as end tidal partial pressure of oxygen reduces, so RCS-R off-axis thresholds will increase, indicating a loss of sensitivity as altitude is increased. The exponential model also assists in explaining the lack of statistically significant RCS results between

the normobaric normoxic and normobaric hyperoxic conditions. Although the gains in sensitivity as the inspired fraction of oxygen is increased are small, gains are predicted even if they are not statistically significant. In support of this argument, when the participants were hyperoxic (100%) the range of the thresholds were smaller than the normoxic condition.

The initial exploration of the variation of ISL as a function of contrast and eccentricity highlights an interesting transition in visual function between the fovea and the peripheral retina. The transition appears to be dependent upon the stimulus' contrast. The transition from the on-axis processing architecture to the off-axis architecture must occur at some point between the fovea and the 5° eccentricity. Beyond 5° eccentricity the increment in ISL is small, <50ms as eccentricity increases from 5° to 11°. This should be compared to the difference of ~150ms between 0° and 5° eccentricity and a difference of ~100ms between 2° and 5° for a 100% contrast stimulus. The ~50 ms difference can be explained by the saccade duration (Llapashtica 2019, Barbur 2017, Barbur *et al* 2017). As the contrast is reduced, visual function associated with 2° eccentricity approaches that of 5° eccentricity. This has been explained in part by the longer time required to detect the lower contrast stimuli in the peripheral retina.

These results demonstrate that visual function is more than just considering the properties of foveal visual function. Peripheral visual function plays a key role in the perception of detail providing cues to the foveal visual sub-system to identify the nature of the stimulus.

6.3.2 Transient PLR response at mesopic light levels

The outcomes of the study of the transient mesopic PLR suggest that linear models for pupil constriction amplitude and latency need to be updated.

The indications are that the constriction amplitude can best be modelled by a Gaussian function whose peak aligns with the point at which rods start to saturate at ~2 log ScTd (Aguilar and Stiles 1954). The evidence for this function is provided by fitting of the experimental data, Figure 4-11 as well as considering the differences between the models adopted for the pre-stimulus and peak constriction diameter of the pupil, Figure 4-10.

Similarly, the wider applicability of a sigmoid function to model the variation of constriction latency as a function of log (scotopic) retinal illuminance adds to our understanding of how the PLR is mediated. The sigmoid function used in this study has been based upon that proposed by Stanley and Davies (1995) and subsequently utilised by Watson and Yellot (2012) in their unified model for pupil size.

The implications of the variation in constriction latency to the wider response to peripherally presented stimuli corresponds to the photoreceptor type that acts as the majority mediator of visual response at a given light level. The restriction to peripheral stimuli reflects the distribution of the ipRGCs across the retina, and their absence from the fovea. It is known that rods have a slower response to cones, so there will be a difference between latencies for scotopic and photopic vision (Barbur 1982). Mesopic light levels correspond to the transition from rod to cone mediated vision and thus latencies vary accordingly (Barbur and Stockman 2010). An output from the study considering the transient PLR is a set of data that shows

how latency varies not only for young participants but also an initial indication of a potential variation as a function of age.

The proposed model/explanation presented in section 4.4.5 seeks to address these changes in terms of both the amplitude and latency of the transient response. To validate this model, a similar study should be undertaken with a larger cohort of young and older participants, as described in section 4.5.2.1.

6.3.3 Variation in mesopic sensitivity as a function age

It is not new that visual function changes with age. One of the reasons for the upper age limit of 40 years for the altitude study was to reduce the effect of presbyopia on the results and mitigate the onset of changes in visual thresholds (Bi *et al* 2016). The observed changes in the PLR as a function of age provides additional evidence to support changes in rod mediated vision. The resulting inference is that together changes in rod topography, lens transmission and rhodopsin regeneration rates (Owsley 2011, Curcio *et al* 1993), result in a change in the balance of signals from rods and cones driving the transient PLR. As the eye changes with age, so the relative strength of the rod signal is reduced compared to that of cones. This results in the observed shift in the crossover point between the rod and cone mediation of the transient PLR to lower retinal illuminance values as a function of age. This reduction in the dominance of rod mediation of visual function is of interest given the demographic of commercial aircrew, which is biased towards those in their 50's and 60's (CAA 2018). If image formation at mesopic light levels follows a similar transition, then it is likely that older aircrew will suffer a loss of visual function exhibited as a reduced ability to detect and/or identify low luminance, low contrast features in the external environment between sunset and sunrise. This reduction in sensitivity is supported by the increase in time to dark adapt (Domey *et al* 1960) illustrated in Figure 1-14. This loss of functionality could be evaluated using the EMAIL test using appropriate test conditions, e.g. a background luminance equivalent to moonlight/starlight (~0.01cd.m^{-2}) and an achromatic Landolt C test stimulus with a 4 arcmin gap, located at 8° eccentricity. These test conditions would enable comparisons to be made with measurements made in this and other studies.

6.3.4 Effects of altitude and oxygen concentration on visual function

The results of this study complement the conclusions of previous studies (Connolly 2011, Connolly and Hosking 2008, 2006) that have considered the effects of altitude and oxygen concentration on visual performance at low light levels. Whilst these previous studies defined the effects of hypoxia on visual function, the current study provides evidence that supplementary oxygen at an inspired fraction of 43% acts a countermeasure to the effects of hypoxia at 3048m. The study has also provided additional understanding to what degree visual function is affected by changes in altitude and oxygen concentration. The results of the EMAIL test demonstrate that at a contrast of 30%, supra-threshold visual function at low photopic light levels (8cd.m^{-2}) is not significantly affected by hypobaric hypoxia at 3048m or the use of supplementary oxygen.

Changes in altitude and oxygen concentration did not cause a significant difference in on-axis FMTs measured using the RCS-R and RCS-C test stimuli. However, off-axis at 5° eccentricity the photoreceptors were more affected, with significant differences between hypobaric hypoxia at 3048m compared to the

control condition of normobaric normoxia ($p<0.01$). These differences were demonstrated for both test conditions/chromaticities. The lack of a statistically significant difference between the control condition and normobaric hyperoxia (100%) demonstrates the way the retina has evolved to optimise to life on the Earth's surface. There were statistically significant differences observed when hypobaric hypoxia at 3048 m is compared to normobaric hyperoxia (100%) for the off-axis stimuli of both test conditions ($p=0.0001$).

The inability to demonstrate statistically significant differences between normobaric normoxia and hyperoxia (100% and 29%) is indicative of the small changes in photoreceptor sensitivity involved and the sensitivity of the RCS test to these potentially subtle variations. This is not to say that changes were not observed, it is just the effect size was not enough to achieve statistical significance. The reduced range of the on-axis RCS thresholds recorded for the hyperoxic (100%) when compared to the normoxic (21%) condition indicate that FMTs are optimal when oxygen tension at the choroid is maximised. These results do not detract from the theory that the peripheral retina is functionally hypoxic.

The lack of a statistically significant change in the time required to process a 30% contrast stimulus (8° eccentricity presented against an 8 $cd.m^{-2}$ background) provides a functional test of retinal and cognitive performance within the context of a detection and identification task that is primarily mediated by cones. Although the effect of changing the respiratory conditions did not result in statistically significant changes in the ISL, it does provide a useful reference point for determining the effects of altitude and inspired oxygen concentration on visual functions of peripheral detection and foveal identification. The result provides an upper bound for stimulus contrast to be defined for when the visual processing function(s) associated with the detection of peripheral stimuli are no longer significantly affected by the effects of mild hypoxia equivalent to 3048m. The lack of statistically significant differences for the FMTs of on-axis stimuli for both RCS test conditions, in contrast to the significant differences observed for the off-axis RCS test stimuli at 5° suggest that it is the detection of the peripheral cues that will be primarily affected by changes in altitude and oxygen concentration.

Repeating the EMAIL assessment at lower contrast values for the same background luminance would assist in further defining the effects of mild hypoxia on the ability to process peripheral stimuli. A repeat of the assessment should be mindful of the confounding effect of the visual threshold on the ability detect and identify the stimulus. To mitigate this, it is recommended that an assessment of the achromatic thresholds using the same background conditions as the EMAIL test be undertaken to provide a baseline for comparison for each participant, and the group.

6.3.5 The combined effect of environmental conditions and age on visual function

The cohort of participants for the study investigating the effects of altitude and oxygen concentration were all aged less than 40 years. Based upon the indications from the Experiment 8 and the age-related loss of sensitivity associated with rod-mediated vision (Hathibelagal *et al* 2020, Bi *et al* 2016), it is hypothesised that the effects of altitude and oxygen concentration are likely to become more exaggerated as participant's age increases.

The results of Experiment 8 suggest a reduction in the amplitude of the rod response compared to that of cones as participant's age increased. The effect of this was the observed shift to lower retinal illuminance

values of the point at which cones start to become the majority mediator of the PLR, and it is hypothesised the same is true for visual function. Whilst there are reports that the RGC mediating the PLR is intrinsically photosensitive (Douglas 2018, Lucas *et al* 2001, Hattar *et al* 2002, 2003), the literature review in section 1 or section 4.1.1 did not highlight a separate class of rods or cones that specifically mediated the PLR.

Combining the proposed shift in mediation of visual function with the knowledge that dark adaptation takes longer when the participant is subject to mild hypoxia(Connolly and Hosking 2006), the sensitivity of the aging retina is likely to be affected more by the reduced oxygen tension within the choroid than that of young participants. Additionally, as shown in Figure 1-14, dark adaptation is already affected by age under normoxic conditions. The reasoning behind this assertion is that photoreceptors require more oxygen in dark adapted conditions due to the increased metabolic processes (Linsenmeier 1986, Feigl *et al* 2011). Under mesopic conditions, the greater metabolic demand of rods for oxygen compromises the oxygenation state of cones and as a result cone function. This results in a degradation in the chromatic and luminance contrast sensitivity of cones because of the inhibitory effect of the oxygen starved rods. Although rod density may be decreased, their inner segments expand to maintain coverage (Curcio *et al* 1993) and as a results it is thought there would not necessarily be a reduction in the metabolic demand of rods.

6.3.6 Wider implications of research

The benefits of this research project and the outcomes of the study into the effects of altitude and oxygen concentration on visual function are not just limited to aircrew. The effects of diabetic retinopathy have been linked to retinal hypoxia (Arden *et al* 1998). The ability of the RCS test to characterise the effects of mild hypoxia, equivalent to 3048m, provides the basis for its use as test to characterise the effects of diabetic retinopathy.

There may be a requirement to tailor the protocol to ensure that the test has the desired sensitivity to characterise the effects of the disease, but the body of work reported in section 3 should provide a good starting point.

In addition to being able to characterise the condition, this study also provides evidence for a therapeutic approach using supplementary oxygen as a countermeasure as suggested by Arden and Tsang (1998).

6.4 Optimising aircrew performance

In terms of aircrew performance, and how it can be optimised, the research project has assisted in developing a greater understanding of factors that could contribute to affect task performance both in terms of visual sensitivity, due to changes in ambient illumination, and long-term variations in visual function as aircrew age. Gaining greater understanding of changes in rod and cone mediated vision across mesopic light levels will provide a basis for understanding variations in operational capability in the periods around dusk and dawn, i.e. between sunset/sunrise and civil and nautical twilight.

The discussion of the EMAIL test results has already highlighted the minimum contrast below which the time to process an off-axis visual cue is degraded. This sets up an ideal minimum requirement for the contrast of symbology presented in HMDs. It also assists in understanding why some visual cues are

missed and why at night, pilots tend to dwell longer on some features compared to daytime flying. The longer the time needed to process a peripheral cue, the greater the chance the aircraft could be drift in its attitude. If undetected, then this can start a series of errors which may result, at worst, in a loss of the aircraft and/or loss of life.

The outcomes of the third study, section 5, have the greatest direct relevance to aircrew. There are three potential implications for aircrew performance and methods for maintaining visual function equivalent to that at ground level and under photopic conditions.

The first arises from the demonstration of the changes in peripheral FMTs resulting from the effects of hypobaric hypoxia equivalent to 3048m. These were found to be statistically significant when compared to FMTs under conditions of normobaric normoxia for both RCS-R and RCS-C test conditions, respectively corresponding to high mesopic and low photopic visual function.

The second arises from the statistically significant result that peripheral low photopic visual FMTs where improved when RCS-C FMT values were compared between normobaric normoxia and hypobaric hyperoxia (42% F_IO_2) ($p<0.0001$). This has implications for the concentration of oxygen used as a countermeasure, reducing the requirement from 100% to 42% oxygen, with the potential for cost savings.

Whilst the results of this study are applicable to 3048m, they do not directly represent the effect of altitude and different concentrations of supplementary oxygen at higher altitudes, e.g. 3658 m (12,000 ft). It can be inferred from the results of the study that the required concentration of the supplementary oxygen should be sufficient to be equivalent to breathing ~30% oxygen at sea level. (At 3048m, the alveolar partial pressure of oxygen resulting from breathing an inspired concentration of 43% is broadly equivalent to breathing ~30% oxygen at sea level.) This should provide optimal sensitivity as the indications were that there was no statistically significant difference between the normobaric normoxic conditions and those where the participants were subject to normobaric hyperoxic conditions at both 29% and 100% inspired fractions of oxygen.

Before changes are made operationally, supporting evidence will be needed to substantiate the benefits to visual function at higher altitudes corresponding to the full operational altitude range of the respective aircraft type(s). Gathering this supporting evidence may require further hypobaric studies of visual function, like those undertaken within the context of this research project.

Thirdly, the indication that the ability to detect, saccade to and identify a 30% contrast stimulus located at 8° eccentricity is unaffected by mild hypoxia, equivalent to 3048 m, provides an upper bound on the effects of mild hypoxia on visual function.

Compared to the benign environment of the laboratory, the aircraft cockpit is often a workload intensive setting associated with high physical and mental workload. In addition to responding to external visual stimuli associated with the control, navigation, and guidance of the aircraft they must also instruments within the cockpit providing information about the platform's speed, bearing and height. There are additional stressors associated with thermal burden, vibration and fatigue that may affect overall task performance. Whilst laboratory tests can help inform the problem space by providing a prediction of the

effect size, the effect of these additional stressors needs to be considered in terms of the overall effect on aircrew performance and ultimately flight safety.

6.5 Lessons learnt

Whilst the limitations of individual experiments have been discussed previously within the context of each of the three studies, the following discussion focusses on the lessons learnt and limitations arising from consideration of the wider research project.

With hindsight, there are some aspects that could have been explored in more detail that were at the time overlooked. The results of Experiment 9, and more specifically the variation in both contrast and eccentricity of the ISL, shown in Figure 5-5, warrant further investigation. What drives the transition as a function of contrast between being able to perceive a stimulus with minimal eye movements to needing to saccade to identify the orientation of the stimulus? As ambient illumination levels decrease at the end of the day, so scene luminance is reduced, and prominent features change in appearance potentially reducing in contrast. The result is the need to dwell longer to abstract visual cues from the scene. Often these cues are selected so that they are located peripherally to provide the spatial references to maintain the desired aircraft attitude. For example, helicopter pilots use sets of orthogonal cues to maintain a stable hover by visually assessing their relative motion to two orthogonal reference points. In this way motion in all six degrees of freedom can be resolved and corrective action applied.

Further study of the region from the fovea out to ~5° eccentricity to determine how visual function changes between foveal on-axis to peripheral off-axis vision would potentially assist in understanding the differences in the relationship between monocular FMTs plotted in Figure 3-25. Studying this region would also assist in quantifying the differences in binocular summation resulting in the greater gain observed for off-axis summation compared to on-axis visual function. Are the observed changes purely due to changes in photoreceptor topography and the switch from a processing architecture based upon a cone to bipolar to RGC ratio of ~1:1:1 compared to one defined by spatial summation of multiple photoreceptors connected to an RGC via horizontal and bipolar cells?

In analysing the data after the completion of all experiments, a greater appreciation of statistical techniques has been developed. The result is that there should have been a greater emphasis in the initial study, section 3, to understanding the limits of the RCS test in terms of repeatability and reproducibility. The results of the investigation undertaken within Experiment 4 could have been made more powerful by increasing the number of participants. By ensuring that they were naïve, learning effects and test repeatability could have been characterised. This would have assisted in mitigating the potential for training effects as a confounding influence in Experiments 10 and 11. Potentially this may have reduced the variation in FMTs recorded for the RCS-C test between the two phases of the study.

The results of several experiments have been limited by the size, and in some cases the age distribution, of the cohort. Although within the context of Experiment 6, the original hope had been to establish a wider age distribution to the cohort, the issues surrounding the change in test protocol dictated a different approach. Despite assurances that nothing had changed, no quantitative data was provided to support the claim. From the author's perspective, there was a need to assess the null hypothesis that the two

protocols were equivalent. Instead of broadening the age distribution, the focus switched to establishing a new standard normal for a young cohort using the revised test protocol v0.102.7. In addition, Experiment 4 was undertaken as an initial investigation into this issue. The results of Experiment 4, for one individual, supported null hypothesis whilst in Experiment 6, the analysis indicates a statistically significant difference between the RCS-R off-axis thresholds for the two test conditions ($p<0.01$). The results of the statistical analysis suggest that it was right and correct to be critical of the effects in the change in test protocol between v0.102.4 and v0.102.7.

The definition of the variation in FMTs as a function of age, measured using v0.102.7 of the RCS test, was answered by a separate sister study undertaken by the LV Prasad Eye Institute (Hathibelagal *et al* 2020) recording data monocularly compared to the binocular thresholds reported in section 3.3.6. This sister study is the result of a parallel research project seeking to develop the initial outcomes of this study, i.e. the definition of the RCS test protocol and the outcomes of Experiments 1 to 3 and the results of Experiment 5.

Unlike Experiment 6, Experiment 8 capitalised on an opportunity to compare PLR responses to the chromaticity of the two RCS stimulus conditions across a ~45 year age group. The significance of the results was limited by the size of the cohort however that does not prevent some of the observations being relevant and furthering the collective understanding of the transient PLR. The recording of data corresponding to the transmittance of each participant's lens was not considered at the time. However, with hindsight, this data would have assisted in interpreting the results and the development of the model of why the shifts in the balance between rod and cone mediated response appear to vary with age. The strength of Experiment 8 was the number and distribution of the luminance values used that almost spanned the entire mesopic range (0.001 to 9 $cd.m^{-2}$).

6.6 Future research directions

The future work proposed at the end of each study has been based primarily on the assumption of binocular visual function and the provision of results to support the binocular data already gathered. The reasoning for this binocular approach is that pilots primarily use binocular vision to abstract visual cues from their surroundings.

However, the variation in monocular and binocular FMT values for both on- and off-axis stimulus locations was explored within the scope of a small study (n=12) with some interesting observations. It would be of interest to see if the identified relationships are replicated in a larger cohort. The benefit would be to gain an understanding of how monocular visual function both at the fovea and peripherally maps to binocular vision. This would provide an understanding of how visual cues are processed monocularly and binocularly. If there are two independent mechanisms for motion in depth (Nefs *et al* 2010), then could there be more than one mechanism by which monocular cues are processed either within the within the retina, i.e. on-axis versus off-axis, or between participants? This would assist in validating some of the relationships proposed in section 3.3.5.4 and if there really is a difference in the FMTs for the least sensitive eye compared to the most sensitive eye as a function stimulus location.

7 Conclusions

This research project has not necessarily been about a making a massive leap forwards in our understanding of visual function. It has instead provided a revised perspective on relationships previously reported and confirmed results using different vision test methodologies. In addition, it has provided the foundation for research undertaken jointly with LV Prasad Eye Institute (Hathibelagal *et al* 2020).

The RCS test has enabled quantitative assessment of the sensitivity monocular and binocular vision at low photopic and high mesopic light levels with a short two minute pre-test adapting period. This negates the need for lengthy adaptation times before assessing rod-mediated visual function. The RCS rod-enriched test condition (RCS-R) produces a rod-mediated response as indicated by the comparison of the two test protocols assessed. There was a statistically significant difference between the two RCS-R off-axis FMTs values for the two test protocols ($p<0.01$). It has been demonstrated that the RCS FMTs for the four peripheral, off-axis stimuli can be combined into a single metric of parafoveal photoreceptor sensitivity. The indications are that monocular RCS FMTs can be used to predict binocular FMTs and in addition can predict ocular dominance.

Across the mesopic/photopic light levels tested (0.001 to 9 $cd.m^{-2}$) it was demonstrated that the PLR is based on a rod-mediated background response. To appreciate the dynamics of the transient response of the pupil to a positive fixed contrast stimulus, the constriction amplitude and latency should be expressed in terms of scotopic retinal illuminance. The sigmoid model of pupil diameter as a function of corneal flux proposed by Stanley and Davies (1995) can be used to describe the variation in pre-stimulus diameter and constriction latency as a function of scotopic retinal illuminance. The constriction amplitude to the positive contrast stimulus has been modelled as a pedestalled Gaussian function of log scotopic retinal illuminance. The dynamics of the transient PLR change as a function of increasing age. These variations in constriction latency align to changes in the dynamic of between rods and cones. The indications are that retinal illuminance of intersection where cones become the major mediator reduces as a function of age.

The results of the EMAIL test when viewed in conjunction with previous work (Barbur and Chisholm 2001) have demonstrated that above 50%, the ISL is independent of stimulus luminance contrast.

The effects of mild hypobaric hypoxia, equivalent to 3048m, on FMTs have been assessed using the RCS and EMAIL tests. The sensitivity of photoreceptors in the peripheral retina is reduced for hypobaric hypoxia compared to normobaric normoxia and normobaric hyperoxia. There was no significant change in the time to detect, saccade to and correctly identify a target presented in the peripheral visual field as a function of changes in P_AO_2. The effects of mild hypoxia at 3,048m can be overcome by breathing supplementary oxygen with a concentration of 43% and that the resulting visual performance is broadly comparable to an inspired fraction of 29% at ground level.

The vision tests undertaken in this research project have provided a greater understanding of both on-axis and off-axis visual function at photopic and mesopic lighting conditions. Whilst the study on the effects of altitude and oxygen concentration on visual function directly addressed the optimisation of aircrew performance, it is likely that outcomes from the other studies may have a role in future research targeted at optimising aircrew performance.

A Medical Screening Questionnaire Form – Altitude trial

Medical Screening Questionnaire

Name ..... Date of birth ...../...../.....

Age ..... Sex: Male / Female

General Questions

Please delete as appropriate:

1. Have you ever been told that you have high blood pressure? YES / NO

   If YES, please give details

   .....

2. Have you had any history of heart trouble or lung disease? YES / NO

   If YES give details

   .....

3. Have you a family history of heart disease/stroke? YES / NO

   If YES give details

   .....

4. Have you ever been told by a doctor that you have asthma? YES / NO

5. Do you suffer from a wheezy chest? YES / NO

6. Do you ever have pains in your heart or chest? YES / NO

7. Have you ever suffered fits, seizures or repeated faints or dizzy spells? YES / NO

8. Has a doctor told you that you have a bone or joint problem which could be made worse by exercise? YES / NO

9. Do you suffer from diabetes? YES / NO

10. Have you been in hospital at all in the last 2 years? YES / NO

    If YES give reason and outcome

    .....

11. Have you had any operations or major illness in the last 6 months? YES / NO

If YES give details

.....

12. Are you undergoing treatment or having any regular medication at the moment? YES / NO

If YES, please give details

.....

13. Are you taking any pills or other medicines, including inhalers or injections? YES / NO

If YES give full details (from bottle labels)

.....

14. Do you have any physical disabilities of any kind? YES / NO

If YES, please give details

.....

15. For this trial, with respect to your eyes and your vision, do you have a history of any of the following:

- Any past or present eye disease, abnormality or need for eye surgery? YES/NO
- Any past or recent history of strabismus (squint) or double vision? YES/NO
- Any past or current requirement for spectacles or contact lenses? YES/NO
- Any history of significant eye injury, especially penetrating injury? YES/NO
- Any need for medication (including eye drops) for an eye condition? YES/NO
- Any family history of significant eye disease? YES/NO
- Any impairment of vision in either eye (including abnormal colour vision) YES/NO
- Any other condition that affects your eyes or vision (e.g. hay fever)? YES/NO

If YES to any then please give details ……

……

16. For this trial, do you have, or have you ever had any anxiety over exposure to darkness or confined spaces? YES/NO

For work in the altitude chamber: Do you have a history of any of the following;

A. Ear or sinus problems, surgery or barotrauma? YES / NO

B. Any problem performing normal 'ear clearing' manoeuvres? YES / NO

C. Recent dental treatment i.e. anything other than a check-up? YES / NO

D. Any recreational exposure to increased pressures (e.g. SCUBA diving)? YES / NO

E. Have you ever suffered any complications from previous trials or treatment? YES / NO

If YES give details

……

F. Do you suffer from any allergies? YES / NO

If YES give details

.....

G. Do you suffer from any neurological or psychiatric illness requiring treatment? YES / NO

H. Do you smoke? YES / NO

I. Have you ever suffered from any form of anaemia? YES / NO

J. Do you have a personal or family history of sickle cell disease or trait or ancestry that means you might carry the sickle cell gene? (If unsure, please discuss with the examining medical officer)

YES / NO / UNSURE

FOR WOMEN:

Is there any possibility that you may be pregnant at the moment? YES / NO

B Participant Lifestyle Proforma

To be complete on the day of the study

Short notice exclusions		
Any use of drugs or medication (prescribed or non-prescribed, with the exception of paracetamol or oral contraceptive, in the last 24 hrs?	Yes	No
Any exposure to hypobaric or hyperbaric environments in the last 24 hrs?	Yes	No
Have you had any dental procedures performed in the last 48 hours?	Yes	No
Have you any intercurrent illness, i.e. have you any illness that intervenes during the course of another illness? (An example would be a fever or vomiting if you have diabetes.)	Yes	No

Lifestyle		
Are you well rested?	Yes	No
Have you missed any meals in the last 24hrs?	Yes	No
Have you had any alcohol in the last 24hrs?	Yes	No
Have you had any caffeine today?	Yes	No

Pregnancy test (female participants only)		
Pregnancy test result.	**+**	**-**

Participant Name
Participant Signature
Date

C Altitude trials data – Phase 1

C.1 Physiological data

C.1.1 EMAIL test

Participant	Atmospheric pressure [mmHg]			End tidal oxygen ($P_{ET}O_2$) [mmHg]			Oxygen saturation (SpO_2) [%]			End tidal carbon dioxide ($P_{ET}CO_2$) [mmHg]			Heart Rate [bpm]			Breathing rate [min^{-1}]		
	A	B	C	A	B	C	A	B	C	A	B	C	A	B	C	A	B	C
1	756	527	756	114.0	61.1	695.5	94.7	89.4	97.9	40.1	37.3	35.5	60	64	61	11	10	10
2	760	523	761	134.4	60.3	723.8	96.8	90.1	98.2	21.5	27.2	16.0	61	53	62	9	8	9
3	731	519	731	95.2	60.2	695.2	95.2	83.4	98.1	37.8	34.5	29.4	52	55	55	12	13	12
4	747	524	764	102.2	61.7	696.4	93.5	84.7	98.3	38.4	37.1	38.2	60	72	50	9	10	6
5	739	524	738	119.0	70.5	705.2	98.1	96.2	96.6	25.8	27.4	25.2	55	51	54	16	14	11
6	755	524	754	112.2	56.9	701.0	95.5	88.1	97.9	30.3	41.8	33.1	51	49	38	12	15	11
7	753	524	753	113.9	64.3	701.8	96.3	90.3	98.8	33.3	35.7	32.4	54	56	54	18	18	17
8	754	525	754	117.8	63.2	705.6	97.8	86.2	98.5	34.1	36.8	33.9	50	55	51	17	18	16
9	753	524	752	120.3	69.6	700.5	94.7	88.3	98.7	30.4	35.6	34.1	52	51	54	11	13	11
10	760	524	759	111.4	62.4	713.4	95.8	88.2	98.4	34.4	35.7	27.4	39	39	38	16	19	16
11	743	524	743	114.2	69.6	686.7	96.4	89.6	99.0	31.8	32.1	30.6	42	46	38	19	19	17
12	753	524	752	101.1	62.6	675.6	93.5	85.8	98.9	38.3	36.7	33.2	55	57	55	10	16	13

Phase 1 physiological data for each participant and test condition for the EMAIL test.

C.1.2 RCS-R test

Participant	Atmospheric pressure [mmHg]			End tidal oxygen ($P_{ET}O_2$) [mmHg]			Oxygen saturation (SpO_2) [%]			End tidal carbon dioxide ($P_{ET}CO_2$) [mmHg]			Heart Rate [bpm]			Breathing rate [min^{-1}]		
	A	B	C	A	B	C	A	B	C	A	B	C	A	B	C	A	B	C
1	756	527	756	104.7	58.4	685.5	95.2	87.6	98.3	39.2	38.6	35.8	61	65	58	9	10	10
2	760	523	761	132.1	71.1	718.6	96.4	92.6	98.3	20.7	25.1	15.1	58	55	56	7	8	10
3	731	519	731	93.1	57.2	673.2	94.9	83.3	98.2	38.6	36.8	32.3	57	56	57	10	12	12
4	747	524	764	100.3	56.0	690.9	93.4	83.1	98.7	38.5	36.3	36.2	58	70	51	8	9	6
5	739	524	738	120.8	78.7	690.8	97.9	97.3	96.9	24.7	23.2	22.7	55	52	51	14	14	11
6	755	524	754	111.5	56.5	692.2	96.0	87.2	98.0	30.9	40.2	28.4	47	49	43	11	15	10
7	753	524	753	108.4	62.2	691.0	96.4	88.2	98.8	33.3	34.5	30.0	56	57	51	19	19	17
8	754	525	754	118.4	62.9	699.7	97.0	86.7	98.6	30.4	36.4	31.4	54	57	49	18	17	17
9	753	524	752	109.1	62.2	692.3	92.8	83.8	98.7	34.9	38.3	34.4	50	51	51	11	13	9
10	760	524	759	115.4	62.1	704.3	96.6	87.5	98.5	31.8	36.3	28.0	41	43	36	16	16	15
11	743	524	743	105.4	72.3	654.1	95.3	91.6	99.2	33.4	30.0	30.6	37	40	42	16	21	16
12	753	524	752	97.7	60.6	688.8	93.3	85.4	98.7	39.4	39.0	35.6	54	59	54	9	15	11

Phase 1 physiological data for each participant and test condition for the RCS-R test.

C.1.3 RCS-C test

Participant	Atmospheric pressure [mmHg]			End tidal oxygen ($P_{ET}O_2$) [mmHg]			Oxygen saturation (SpO_2) [%]			End tidal carbon dioxide ($P_{ET}CO_2$) [mmHg]			Heart Rate [bpm]			Breathing rate [min^{-1}]		
	A	B	C	A	B	C	A	B	C	A	B	C	A	B	C	A	B	C
1	756	527	756	105.7	59.2	689.7	94.7	87.6	98.0	38.3	38.3	34.1	63	63	59	9	10	9
2	760	524	761	123.2	78.1	713.0	96.0	95.1	98.1	23.2	19.5	15.4	57	57	56	6	10	7
3	732	519	731	97.2	55.8	678.3	94.9	83.4	98.5	39.0	37.8	33.1	60	56	54	11	10	10
4	747	524	764	100.0	63.8	690.0	93.5	88.7	98.6	38.8	32.3	36.0	56	65	51	8	8	6
5	739	524	738	116.9	74.0	693.1	97.8	96.1	97.2	25.2	23.8	21.0	55	49	51	14	12	12
6	755	524	754	127.1	55.8	690.3	97.2	88.7	97.7	24.0	40.0	29.7	49	54	41	12	11	10
7	753	524	754	106.6	62.6	696.2	96.5	87.4	99.0	34.1	33.4	30.8	55	58	51	17	20	17
8	754	525	754	113.6	62.9	692.4	96.4	86.6	98.9	31.1	36.7	32.0	52	59	49	18	16	16
9	753	524	753	110.3	59.8	693.3	93.0	82.4	98.5	33.9	38.7	29.3	53	53	55	10	15	8
10	760	524	759	118.4	64.7	699.9	94.9	88.8	98.5	29.5	34.7	29.0	42	41	35	17	17	14
11	743	524	743	105.4	73.6	676.6	95.2	93.1	99.2	31.9	27.9	30.6	36	37	41	17	21	17
12	753	524	753	101.1	62.2	683.0	92.9	85.0	98.6	39.2	36.5	35.6	53	59	54	10	12	9

Phase 1 physiological data for each participant and test condition for the RCS-C test.

C.2 Vision test data

C.2.1 EMAIL test

Participant	Condition		
	A	B	C
1	268.6	262.5	276.9
2	247.2	318.2	255.9
3	270.3	277.2	328.5
4	340.0	292.7	312.3
5	305.7	336.9	284.3
6	302.2	337.6	295.7
7	265.4	248.3	265.3
8	283.4	252.2	265.3
9	263.2	305.8	253.3
10	284.3	277.2	260.0
11	265.3	324.6	299.2
12	362.7	437.3	369.7

Phase 1 EMAIL test results for all participants.

C.2.2 RCS-R test

Participant	Condition A					Condition B					Condition C				
	-135°	-45°	0°	45°	135°	-135°	-45°	0°	45°	135°	-135°	-45°	0°	45°	135°
1	2.92	2.99	4.36	3.21	2.86	3.31	4.01	3.92	3.98	3.70	2.81	2.44	3.37	3.61	2.28
2	2.26	2.73	2.89	3.18	2.50	2.44	3.04	3.57	3.32	3.10	2.86	3.42	3.90	3.49	3.88
3	2.83	2.17	3.85	2.91	3.18	3.16	3.44	2.27	2.96	3.04	2.71	2.70	3.97	2.68	2.21
4	3.97	3.68	6.09	3.92	3.61	2.77	4.01	5.29	4.01	3.89	3.24	2.90	3.44	2.66	3.18
5	3.64	3.44	3.56	3.67	3.31	3.64	2.62	3.86	3.04	3.17	3.31	3.22	3.04	2.91	2.21
6	3.61	3.51	1.61	3.71	3.50	3.28	3.61	3.39	3.28	3.56	3.57	3.61	1.10	3.61	3.79
7	3.25	3.09	2.64	3.50	3.31	3.61	2.78	3.14	3.61	3.03	2.95	3.57	3.54	2.83	2.94
8	2.49	2.19	4.01	3.00	3.61	2.56	2.61	3.89	2.84	3.17	2.82	3.17	3.73	3.40	3.61
9	3.34	3.17	4.24	2.92	2.58	3.07	2.04	3.97	3.33	3.17	3.28	2.96	3.22	1.95	2.71
10	3.00	3.38	3.34	3.35	3.03	3.14	3.35	2.36	3.23	3.39	2.85	3.26	3.64	3.61	3.57
11	2.13	2.53	3.97	2.50	2.86	3.44	3.97	5.28	4.31	4.20	2.17	2.82	3.58	3.08	2.61
12	3.34	2.84	6.09	2.87	2.75	3.82	3.39	5.39	2.26	3.14	3.17	3.07	6.33	2.72	2.74

Phase 1 RCS-R test results for all participants.

C.2.3 RCS-C test

Participant	Condition A					Condition B					Condition C				
	-135°	**-45°**	**0°**	**45°**	**135°**	**-135°**	**-45°**	**0°**	**45°**	**135°**	**-135°**	**-45°**	**0°**	**45°**	**135°**
1	1.91	1.65	1.81	1.70	1.48	1.85	1.51	2.13	1.99	1.00	1.00	1.61	1.48	1.59	1.03
2	1.19	1.20	1.20	1.02	1.15	1.74	1.52	2.40	1.24	1.43	1.15	1.51	1.13	1.37	1.13
3	1.57	1.55	1.22	1.68	1.30	1.86	2.01	0.67	1.51	0.83	1.37	1.55	1.87	1.20	1.13
4	1.91	1.52	2.50	1.30	1.53	2.70	1.99	1.91	1.48	1.83	1.24	1.33	1.30	1.13	1.37
5	2.50	1.99	1.59	2.10	1.66	2.53	2.13	2.21	1.87	2.31	2.42	2.06	1.87	1.47	2.24
6	2.42	2.38	2.15	2.16	2.66	1.37	1.13	1.61	1.30	1.22	2.34	1.69	2.00	2.56	2.91
7	2.10	2.49	1.52	1.52	1.47	1.90	1.48	0.92	1.31	1.46	1.63	1.33	1.38	1.76	1.24
8	1.41	1.44	2.72	1.20	1.13	2.20	1.56	2.33	1.59	1.33	1.54	1.56	1.41	1.24	1.13
9	2.19	1.56	2.06	1.29	1.98	1.87	1.55	1.52	1.32	1.98	1.99	2.20	2.21	1.44	2.18
10	1.55	1.36	1.37	1.24	1.00	2.03	1.74	1.79	1.37	2.29	1.48	1.48	1.02	1.33	1.37
11	1.13	1.35	1.97	0.89	1.37	2.35	2.76	2.53	3.15	2.44	1.26	1.41	1.52	1.13	1.13
12	2.10	1.87	1.48	1.15	1.24	1.95	1.53	2.71	1.41	2.31	2.34	1.49	1.90	1.84	1.33

Phase 1 RCS-C test results for all participants.

D Altitude trials data - Phase 2

D.1 Physiological data

D.1.1 EMAIL test

Participant	Atmospheric pressure [mmHg]			End tidal oxygen ($PETO_2$) [mmHg]			Oxygen saturation (SpO_2) [%]			End tidal carbon dioxide ($PETCO_2$) [mmHg]			Heart Rate [bpm]			Breathing rate [min^{-1}]		
	D	E	F	D	E	F	D	E	F	D	E	F	D	E	F	D	E	F
1	746	746	523	115.8	171.0	167.7	97.2	98.4	98.3	32.4	34.7	20.3	55	52	56	11	9	11
2	747	746	523	129.2	187.8	182.0	97.1	96.3	98.6	20.6	18.9	27.4	48	51	46	9	8	14
3	732	732	523	104.6	166.7	159.3	97.5	98.6	98.2	34.7	31.6	36.9	36	36	36	17	14	15
4	735	735	523	104.9	157.5	169.3	95.5	97.4	97.3	36.6	39.2	37.3	54	48	50	8	7	8
5	755	755	524	113.2	178.1	172.2	93.7	94.3	98.1	32.2	28.3	33.7	46	50	51	12	12	16
6	750	749	524	111.5	175.5	173.8	96.6	98.4	97.0	34.8	28.1	36.6	40	42	39	10	9	13
7	740	754	524	109.9	165.9	175.0	95.0	96.6	95.7	32.3	32.0	34.2	51	48	47	18	15	19
8	743	743	524	108.5	169.7	172.5	97.1	98.4	96.4	34.5	32.7	37.1	56	55	57	15	14	16
9	758	758	523	123.3	173.3	170.3	95.7	97.4	96.5	31.4	34.9	37.9	48	44	45	9	7	13
10	754	755	525	112.4	186.1	170.4	97.1	98.5	90.2	34.1	25.2	39.1	36	37	36	13	21	16
11	754	754	524	122.0	182.1	181.1	94.1	95.5	96.9	30.8	29.1	33.4	38	43	41	16	16	17
12	754	754	524	112.0	164.0	169.0	94.4	97.4	97.1	37.6	41.0	42.4	69	69	63	12	10	14

Phase 2 physiological data for each participant and test condition for the EMAIL test.

D.1.2 RCS-R test

Participant	Atmospheric pressure [mmHg]			End tidal oxygen ($PETO_2$) [mmHg]			Oxygen saturation (SpO_2) [%]			End tidal carbon dioxide ($PETCO_2$) [mmHg]			Heart Rate [bpm]			Breathing rate [min^{-1}]		
	D	E	F	D	E	F	D	E	F	D	E	F	D	E	F	D	E	F
1	746	746	523	106.9	166.6	167.2	96.6	98.5	97.9	35.5	35.0	19.8	55	54	59	7	8	11
2	747	746	523	123.9	186.5	182.5	97.1	96.2	98.7	22.9	18.8	26.3	46	49	47	11	9	12
3	732	732	523	106.0	164.1	162.8	96.7	98.4	98.3	34.2	33.7	37.2	37	36	36	13	11	12
4	735	735	523	103.8	158.6	164.3	95.7	97.2	96.9	36.4	39.1	38.5	52	48	53	6	8	9
5	755	755	524	116.8	180.0	167.4	94.4	94.3	97.0	29.8	24.6	32.8	46	51	52	10	12	12
6	750	749	524	104.1	170.3	163.7	96.2	98.3	97.0	35.1	28.8	40.3	38	41	37	10	10	14
7	740	754	524	108.8	173.8	175.2	95.0	96.3	95.5	32.4	26.3	32.8	51	50	51	18	12	20
8	743	743	524	107.6	170.6	170.3	97.3	98.4	96.7	36.5	30.6	36.5	33	56	57	14	12	18
9	758	758	523	111.3	169.0	170.3	94.5	96.9	96.6	34.7	36.9	37.2	48	48	46	9	7	14
10	754	755	525	113.3	179.6	169.4	97.5	98.4	98.7	33.9	24.6	39.5	37	35	37	14	13	16
11	754	754	524	114.6	177.6	179.3	95.6	98.9	97.1	33.8	29.9	32.7	37	37	44	15	14	17
12	754	754	524	107.0	156.7	166.2	94.2	97.5	97.0	39.2	43.1	42.4	73	65	64	9	8	15

Phase 2 physiological data for each participant and test condition for the RCS-R test.

D.1.3 RCS-C test

Participant	Atmospheric pressure [mmHg]			End tidal oxygen ($P_{ET}O_2$) [mmHg]			Oxygen saturation (SpO_2) [%]			End tidal carbon dioxide ($P_{ET}CO_2$) [mmHg]			Heart Rate [bpm]			Breathing rate [min^{-1}]		
	D	E	F	D	E	F	D	E	F	D	E	F	D	E	F	D	E	F
1	746	746	523	113.8	173.8	168.0	97.3	97.8	97.8	32.6	29.0	20.6	54	56	56	9	11	11
2	747	746	523	117.6	185.5	176.5	96.9	96.5	98.4	26.0	19.3	29.0	43	47	45	12	10	13
3	732	732	523	110.4	166.1	160.8	96.7	98.5	98.1	31.5	31.8	37.0	36	37	35	15	12	12
4	735	735	523	100.7	158.0	166.0	95.5	97.5	97.1	38.2	38.5	37.4	52	49	50	9	9	9
5	755	755	524	120.0	172.9	175.8	95.6	94.5	97.1	27.0	28.3	28.7	51	45	54	9	11	14
6	750	750	524	109.8	170.7	170.2	96.4	98.2	97.0	32.7	27.7	37.5	42	39	37	10	8	14
7	740	754	524	110.3	167.0	176.7	94.9	96.4	96.0	31.8	29.0	33.9	51	50	48	18	16	19
8	743	743	524	105.2	166.8	169.2	96.5	98.5	96.7	34.9	32.5	35.4	58	56	57	8	10	18
9	759	758	523	104.8	167.6	168.4	94.0	97.0	96.5	36.8	34.2	38.1	49	49	44	9	7	13
10	754	755	525	110.6	176.8	169.7	97.3	98.3	98.7	35.4	26.2	37.9	40	35	36	15	11	16
11	754	754	524	119.8	177.7	170.2	95.5	98.9	96.8	31.3	27.8	33.0	37	36	42	18	17	18
12	754	754	524	103.9	159.2	165.8	94.0	97.4	97.1	39.8	43.7	41.6	72	65	65	9	9	14

Phase 2 physiological data for each participant and test condition for the RCS-C test.

D.2 Vision test data

D.2.1 EMAIL test

Participant	Condition		
	D	E	F
1	275.2	300.7	311.3
2	275.5	285.4	255.7
3	269.7	319.3	268.8
4	344.5	258.1	267.3
5	348.3	367.8	298.5
6	280.7	335.9	295.3
7	273.2	262.0	276.6
8	273.2	302.7	243.8
9	266.0	259.6	273.8
10	460.0	360.3	310.5
11	262.4	243.2	255.4
12	379.3	284.9	262.3

Phase 2 EMAIL test results for all participants.

D.2.2 RCS-R test

Participant	Condition D					Condition E					Condition F				
	-135°	-45°	0°	45°	135°	-135°	-45°	0°	45°	135°	-135°	-45°	0°	45°	135°
1	3.52	2.97	3.61	2.87	3.34	2.52	2.35	3.41	3.38	2.89	3.16	4.05	3.78	2.68	2.84
2	2.63	2.59	2.60	2.35	2.29	2.62	2.99	3.29	2.80	3.24	2.68	2.19	2.59	2.11	2.64
3	2.30	2.71	4.23	2.23	2.86	2.88	3.21	4.01	3.26	2.99	2.40	1.99	2.26	2.47	2.07
4	4.14	3.58	3.72	3.53	2.96	3.29	2.30	3.72	3.35	2.78	3.09	2.77	3.72	2.38	2.53
5	3.81	3.57	3.46	2.87	3.48	3.44	3.35	2.91	2.12	3.39	2.82	2.42	2.22	2.15	2.52
6	3.45	3.16	3.57	3.06	3.25	3.53	2.89	4.01	2.34	3.42	2.44	3.57	4.23	3.57	3.57
7	2.70	3.28	2.34	2.83	3.36	3.59	3.74	2.69	3.61	3.44	3.34	3.17	1.37	3.66	3.61
8	2.57	2.56	3.48	2.76	3.57	3.57	3.20	4.14	3.61	3.39	2.68	2.37	3.85	3.33	3.27
9	3.57	3.16	2.70	2.85	2.42	3.57	2.55	2.59	3.09	3.06	4.01	2.98	2.84	3.19	3.06
10	4.01	3.61	4.51	3.86	4.02	4.47	3.46	7.43	6.43	5.48	3.69	3.69	3.13	3.43	3.49
11	3.48	1.59	2.25	2.00	2.73	3.62	1.52	2.18	2.35	2.08	3.35	3.02	2.31	2.34	2.48
12	2.74	3.39	4.06	2.61	2.21	2.39	2.56	6.95	2.49	2.29	3.07	2.33	5.49	3.01	2.54

Phase 2 RCS-R test results for all participants.

D.2.3 RCS-C test

Participant	Condition D					Condition E					Condition F				
	-135°	-45°	0°	45°	135°	-135°	-45°	0°	45°	135°	-135°	-45°	0°	45°	135°
1	2.16	1.92	2.64	2.06	3.39	1.41	2.22	2.08	1.64	1.33	1.24	1.08	1.41	1.41	1.52
2	0.78	1.30	1.20	0.96	1.02	2.57	2.09	2.95	2.69	1.97	1.16	1.25	1.24	1.33	1.13
3	3.44	2.82	2.29	1.45	2.17	2.64	2.06	1.11	2.21	1.79	1.13	1.48	1.41	1.22	1.40
4	1.41	1.13	1.63	1.48	1.17	1.59	1.02	1.20	1.10	1.22	1.24	1.20	1.20	1.06	0.96
5	2.90	2.53	1.23	2.26	2.38	2.90	3.09	3.12	4.11	3.42	1.91	1.65	0.73	1.00	1.85
6	3.48	2.33	3.25	2.76	3.47	1.35	2.11	2.28	1.36	2.02	1.04	1.02	1.66	1.41	1.97
7	2.11	2.24	1.37	1.33	1.63	1.95	2.73	2.01	2.37	2.49	2.35	2.77	1.25	1.58	1.76
8	1.59	1.30	2.39	1.30	1.30	1.69	1.26	1.48	1.30	1.19	1.31	1.30	2.10	1.26	1.30
9	1.91	1.13	1.44	1.79	1.26	1.86	1.33	0.79	1.73	2.07	1.95	1.13	1.72	2.20	2.31
10	3.00	3.78	2.42	1.87	2.26	2.40	3.22	2.46	2.34	2.54	3.38	4.00	3.03	2.56	2.64
11	1.39	1.30	1.13	1.13	1.24	1.33	1.15	1.21	1.14	1.51	1.24	1.41	1.20	1.37	1.48
12	2.59	2.34	2.60	2.49	1.76	1.69	1.61	1.59	0.96	1.15	1.91	1.31	1.48	1.20	1.46

Phase 2 RCS-C test results for all participants

References

Adelson E 1982 Saturation and adaptation in the rod system *Vision Res.* **22** 1299–312

Aguilar M and Stiles W S 1954 Saturation of the rod mechanism of the retina at high levels of stimulation *Opt. Acta Int. J. Opt.* **1** 59–65

Alexandridis E, Leendertz J A and Barbur J L 1991 Methods for studying the behaviour of the pupil *J. Psychophysiol.* **5** 223–39

Allen A E, Brown T M and Lucas R J 2011 A distinct contribution of short wavelength sensitive cones to light evoked activity in the mouse pretectal olivary nucleus (PON) *J. Neurosci. Off. J. Soc. Neurosci.* **31** 16833–43

Alpern M and Campbell F W 1962 The spectral sensitivity of the consensual light reflex *J. Physiol.* **164** 478–507

Alpern M and Hendley C D 1952 Visual functions as indices of physiological changes in the acid-base balance of the blood* *Optom. Vis. Sci.* **29** 301–14

Alpern M, McCready D W and Barr L 1963 The dependence of the photopupil response on flash duration and intensity *J. Gen. Physiol.* **47** 265–78

Anderson A J and Vingrys A J 2000a Effect of stimulus duration in flicker perimetry *Clin. Experiment. Ophthalmol.* **28** 223–6

Anderson A J and Vingrys A J 2000b Interactions between flicker thresholds and luminance pedestals *Vision Res.* **40** 2579–88

Anderson A J and Vingrys A J 2001 Multiple processes mediate flicker sensitivity *Vision Res.* **41** 2449–55

Ando S, Yamada Y and Kokubu M 2010 Reaction time to peripheral visual stimuli during exercise under hypoxia *J. Appl. Physiol.* **108** 1210–6

Arden G B, Wolf J E and Tsang Y 1998 Does dark adaptation exacerbate diabetic retinopathy?: Evidence and a linking hypothesis *Vision Res.* **38** 1723–9

Baker D H, Lygo F A, Meese T S and Georgeson M A 2018 Binocular summation revisited: Beyond √2 *Psychol. Bull.* **144** 1186–99

Barbur J L 1995 A study of pupil response components in human vision *Basic and Clinical Perspectives in Vision Research: A Celebration of the Career of Hisako Ikeda* ed J G Robbins, M B A Djamgoz and A Taylor (Boston, MA: Springer US) pp 3–18 Online: https://doi.org/10.1007/978-1-4757-9362-8_1

Barbur J L 1982 Reaction-time determination of the latency between visual signals generated by rods and cones *Ophthalmic Physiol. Opt.* **2** 179–85

Barbur J L 2017 The EMAIL Test - Measurement of integrated saccade latency and visual processing times without eye-tracking

Barbur J L and Chisholm C M 2001 The Contrast Acuity Assessment (CAA) test Online: http://publicapps.caa.co.uk/docs/33/CAPAP200105.PDF

Barbur J L and Connolly D M 2011 Effects of hypoxia on color vision with emphasis on the mesopic range *Expert Rev. Ophthalmol.* **6** 409–20

Barbur J L, Forsyth P M and Findlay J M 1988 Human saccadic eye movements in the absence of the geniculocalcarine projection *Brain* **111** 63–82

Barbur J L, Harlow A J and Plant G T 1994 Insights into the different exploits of colour in the visual cortex *Proc. Biol. Sci.* **258** 327–34

Barbur J L, Harlow A and Sahraie A 1992 Pupillary responses to stimulus structure, colour and movement *Ophthalmic Physiol. Opt.* **12** 137–41

Barbur J L, Llapashtica E, Connolly D and Sadler J 2017 Measurement of oculomotor parameters and visual processing times without eye-tracking *Acta Ophthalmol. (Copenh.)* **95** Online: https://onlinelibrary.wiley.com/doi/abs/10.1111/j.1755-3768.2017.03331

Barbur J L and Rodriguez-Carmona M 2015 Color vision changes in normal aging *Handbook of Color Psychology* ed A J Elliot, M D Fairchild and A Franklin (Cambridge: Cambridge University Press) pp 180–96 Online: https://www.cambridge.org/core/product/identifier/9781107337930%23CN-bp-8/type/book_part

Barbur J L, Rodriguez-Carmona M and Harlow A 2006 Establishing the statistical limits of "normal" chromatic sensitivity *CIE Expert Symp. CIE Proc. 75 Years Stand. Color. Obs.* 5

Barbur J L, Rodriguez-Carmona M L and Morgan M J 2002 Double-blindsight in human vision *Invest. Ophthalmol. Vis. Sci.* **43** 3909–3909

Barbur J L, Sahraie A, Simmons A, Weiskrantz L and Williams S C R 1998a Residual processing of chromatic signals in the absence of a geniculostriate projection *Vision Res.* **38** 3447–53

Barbur J L and Stockman A 2010 Photopic, Mesopic, and Scotopic vision and changes in visual performance. *Encyclopaedia of the Eye* ed D Dartt, J Besharse and R Dana (Academic Press: Oxford) pp 323–31

Barbur J L, Thomson W D and Forsyth P M 1987 A new system for the simultaneous measurement of pupil size and two-dimensional eye movements *Clin. Vis. Sci.* **2** 131–42

Barbur J L, Weiskrantz L and Harlow J A 1999 The unseen color aftereffect of an unseen stimulus: Insight from blindsight into mechanisms of color afterimages *Proc. Natl. Acad. Sci. U. S. A.* **96** 11637–41

Barbur J L, Wolf J and Lennie P 1998b Visual processing levels revealed by response latencies to changes in different visual attributes *Proc. Biol. Sci.* **265** 2321–5

Barlow H B 1957 Increment thresholds at low intensities considered as signal/noise discriminations *J. Physiol.* **136** 469–88

Barlow H B 1958 Temporal and spatial summation in human vision at different background intensities *J. Physiol.* **141** 337–50

Baron W S and Westheimer G 1973 Visual acuity as a function of exposure duration* *JOSA* **63** 212–9

Barrett B T, Panesar G K, Scally A J and Pacey I E 2013 Binocular Summation and Other Forms of Non-Dominant Eye Contribution in Individuals with Strabismic Amblyopia during Habitual Viewing *PLOS ONE* **8** e77871

Barrionuevo P A, Nicandro N, McAnany J J, Zele A J, Gamlin P and Cao D 2014 Assessing rod, cone, and melanopsin contributions to human pupil flicker responses *Invest. Ophthalmol. Vis. Sci.* **55** 719–27

Barten P G J 2003 Formula for the contrast sensitivity of the human eye Electronic Imaging 2004 ed Y Miyake and D R Rasmussen (San Jose, CA) pp 231–8 Online: http://proceedings.spiedigitallibrary.org/proceeding.aspx?articleid=837000

Baylor D A 1987 Photoreceptor signals and vision. Proctor lecture. *Invest. Ophthalmol. Vis. Sci.* **28** 34–49

Baylor D A, Lamb T D and Yau K W 1979 Responses of retinal rods to single photons. *J. Physiol.* **288** 613–34

Bergamin O and Kardon R H 2003 Latency of the pupil light reflex: Sample rate, stimulus intensity, and variation in normal subjects *Invest. Ophthalmol. Vis. Sci.* **44** 1546–54

Berson D M, Dunn F A and Takao M 2002 Phototransduction by retinal ganglion cells that set the circadian clock *Science* **295** 1070–3

Bi W, Gillespie-Gallery H, Binns A and Barbur J L 2016 Flicker sensitivity in normal aging—Monocular tests of retinal function at photopic and mesopic light levels *Invest. Ophthalmol. Vis. Sci.* **57** 387

Bitsios P, Prettyman R and Szabadi E 1996 Changes in autonomic function with age: a study of pupillary kinetics in healthy young and old people *Age Ageing* **25** 432–8

Black A E, Prentice A M and Coward W A 1986 Use of food quotients to predict respiratory quotients for the doubly-labelled water method of measuring energy expenditure *Hum. Nutr. Clin. Nutr.* **40** 381–91

Blackwell H R 1952 Studies of psychophysical methods for measuring visual thresholds *J Opt Soc Am* **42** 606–16

Blackwell H R and Blackwell O M 1980 Population data for 140 normal 20–30 year olds for use in assessing some effects of lighting upon visual performance *J. Illum. Eng. Soc.* **9** 158–74

Blake R and Fox R 1973 The psychophysical inquiry into binocular summation *Percept. Psychophys.* **14** 161–85

Blake R, Sloane M and Fox R 1981 Further developments in binocular summation *Percept. Psychophys.* **30** 266–76

Bossi M, Hamm L M, Dahlmann-Noor A and Dakin S C 2018 A comparison of tests for quantifying sensory eye dominance | Elsevier Enhanced Reader *Vision Res.* **153** 60–9

Bouma H 1962 Size of the static pupil as a function of wavelength and luminosity of the light incident on the human eye *Nature* **193** 690–1

Bradley M M, Miccoli L, Escrig M A and Lang P J 2008 The pupil as a measure of emotional arousal and autonomic activation *Psychophysiology* **45** 602–7

CAA 2018 Pilot licence holders by age and sex 2018.pdf Online: https://www.caa.co.uk/uploadedFiles/CAA/Content/Standard_Content/Data_and_analysis/Datasets/Licence_holders_by_age_and_sex_by_year/Pilot%20licence%20holders%20by%20age%20and%20sex%202018.pdf

Caldwell J A 2005 Fatigue in aviation *Travel Med. Infect. Dis.* **3** 85–96

Callaway E M 2005 Structure and function of parallel pathways in the primate early visual system *J. Physiol.* **566** 13–9

Campbell F W and Green D G 1965 Optical and retinal factors affecting visual resolution. *J. Physiol.* **181** 576–93

Campbell F W and Gubisch R W 1966 Optical quality of the human eye *J. Physiol.* **186** 558–78

Carpenter R H S 2000 The neural control of looking *Curr. Biol.* **10** R291–3

Carroll J, Neitz J and Neitz M 2002 Estimates of L:M cone ratio from ERG flicker photometry and genetics *J. Vis.* **2** 1–1

Chen S-K, Badea T C and Hattar S 2011 Photoentrainment and pupillary light reflex are mediated by distinct populations of ipRGCs *Nat. Lond.* **476** 92–5

Christiansen J, Douglas C G and Haldane J S 1914 The absorption and dissociation of carbon dioxide by human blood *J. Physiol.* **48** 244–71

CIE 2004 CIE 15 Technical Report: Colorimetry

CIE 2015 Technical Report Colorimetry - Part 5: CIE 1976 L*u*v* colour space and u', v' uniform chromaticity scale diagram

Coletta N J and Adams A J 1984 Rod-cone interaction in flicker detection *Vision Res.* **24** 1333–40

Conner J D 1982 The temporal properties of rod vision. *J. Physiol.* **332** 139–55

Connolly D 2008 *Visual effects of respiratory disturbance* (City University of London)

Connolly D M 2011 Oxygenation state and twilight vision at 2438 m *Aviat. Space Environ. Med.* **82** 2–8

Connolly D M 2014 *Sickle cell trait and altitude research at QinetiQ* (QinetiQ)

Connolly D M, Barbur J L, Hosking S L and Moorhead I R 2008 Mild hypoxia impairs chromatic sensitivity in the mesopic range *Invest. Ophthalmol. Vis. Sci.* **49** 820–7

Connolly D M and Hosking S L 2006 Aviation-related respiratory gas disturbances affect dark adaptation: A reappraisal *Vision Res.* **46** 1784–93

Connolly D M and Hosking S L 2008 Oxygenation and gender effects on photopic frequency-doubled contrast sensitivity *Vision Res.* **48** 281–8

Cornsweet T N 1962 The Staircase-method in psychophysics *Am. J. Psychol.* **75** 485–91

Curcio C A, Millican C L, Allen K A and Kalina R E 1993 Aging of the human photoreceptor mosaic: evidence for selective vulnerability of rods in central retina. *Invest. Ophthalmol. Vis. Sci.* **34** 3278–96

Curcio C A, Sloan K R, Kalina R E and Hendrickson A E 1990 Human photoreceptor topography *J. Comp. Neurol.* **292** 497–523

Dacey D M 1996 Circuitry for color coding in the primate retina *Proc. Natl. Acad. Sci. U. S. A.* **93** 582–8

Dacey D M 2000 Parallel pathways for spectral coding in primate retina *Annu. Rev. Neurosci.* **23** 743–75

Dacey D M, Liao H-W, Peterson B B, Robinson F R, Smith V C, Pokorny J, Yau K-W and Gamlin P D 2005 Melanopsin-expressing ganglion cells in primate retina signal colour and irradiance and project to the LGN *Nature* **433** 749–54

Daniels L B, Nichols D F, Seifert M S and Hock H S 2012 Changes in pupil diameter entrained by cortically initiated changes in attention *Vis. Neurosci.* **29** 131–42

Di Stasi L L, Cabestrero R, McCamy M B, Ríos F, Quirós P, Lopez J A, Saez C, Macknik S L and Martinez-Conde S 2014 Intersaccadic drift velocity is sensitive to short-term hypobaric hypoxia *Eur. J. Neurosci.* 1–7

Domey R G, McFarland R A and Chadwick E 1960 Dark adaptation as a function of age and time: II. a Derivation *J. Gerontol.* **15** 267–79

Douglas R H 2018 The pupillary light responses of animals; a review of their distribution, dynamics, mechanisms and functions. *Prog. Retin. Eye Res.* **66** 17–48

Drouyer E, Rieux C, Hut R A and Cooper H M 2007 Responses of Suprachiasmatic Nucleus neurons to light and dark adaptation: Relative contributions of melanopsin and rod–cone inputs *J. Neurosci.* **27** 9623–31

Duncan R O and Boynton G M 2003 Cortical Magnification within Human Primary Visual Cortex Correlates with Acuity Thresholds *Neuron* **38** 659–71

EASA 2020 *EASA Annual Safety Review (ASR) - 2020* (European Union Aviation Safety Agency) Online: https://www.atc-network.com/atc-news/easa-european-aviation-safety-agency-germany/easa-publishes-annual-safety-review-asr-2020

Ecker J L, Dumitrescu O N, Wong K Y, Alam N M, Chen S-K, LeGates T, Renna J M, Prusky G T, Berson D M and Hattar S 2010 Melanopsin-expressing retinal ganglion-cell photoreceptors: cellular diversity and role in pattern vision *Neuron* **67** 49–60

Ellis C J 1981 The pupillary light reflex in normal subjects. *Br. J. Ophthalmol.* **65** 754–9

Ernest J T and Krill A E 1971 The effect of hypoxia on visual function psychophysical studies *Invest. Ophthalmol. Vis. Sci.* **10** 323–8

FAA 2017 Aeronautical Information Manual Online: https://www.faa.gov/air_traffic/publications/media/aim.pdf

Fan X, Hearne L, Lei B, Miles J H, Takahashi N and Yao G 2009 Weak gender effects on transient pupillary light reflex *Auton. Neurosci.* **147** 9–13

Feigl B, Zele A J and Stewart I B 2011 Mild systemic hypoxia and photopic visual field sensitivity *Acta Ophthalmol. (Copenh.)* **89** e199–204

Feinberg R and Podolak E 1965 Latency of pupillary reflex light stimulation and its relationship to aging *Behaviour, Aging and the nervous system* (Charles C Thomas) Online: https://www.faa.gov/data_research/research/med_humanfacs/oamtechreports/1960s/media/AM65-25.pdf

Felder A E, Wanek J, Blair N P and Shahidi M 2017 Retinal vascular and oxygen temporal dynamic responses to light flicker in humans *Invest. Ophthalmol. Vis. Sci.* **58** 5666–72

Ffytche D H, Skidmore B D and Zeki S 1995 Motion-from-hue activates area V5 of human visual cortex *Proc. Biol. Sci.* **260** 353–8

Galloway N, Amoaku W, Galloway P and Browning A 2006 *Common eye diseases and their management* (Springer-Verlag)

Gamlin P D R, McDougal D H, Pokorny J, Smith V C, Yau K-W and Dacey D M 2007 Human and macaque pupil responses driven by melanopsin-containing retinal ganglion cells *Vision Res.* **47** 946–54

Gamlin P D R, Zhang H, Harlow A and Barbur J L 1998 Pupil responses to stimulus color, structure and light flux increments in the rhesus monkey *Vision Res.* **38** 3353–8

Gao H and Hollyfield J G 1992 Aging of the human retina. Differential loss of neurons and retinal pigment epithelial cells. *Invest. Ophthalmol. Vis. Sci.* **33** 1–17

Garhöfer G, Zawinka C, Resch H, Huemer K H, Dorner G T and Schmetterer L 2004 Diffuse luminance flicker increases blood flow in major retinal arteries and veins *Vision Res.* **44** 833–8

Gillespie-Gallery H, Konstantakopoulou E, Harlow J A and Barbur J L 2013 Capturing age-related changes in functional contrast sensitivity with decreasing light levels in monocular and binocular vision *Invest. Ophthalmol. Vis. Sci.* **54** 6093–103

Gipson I K 2013 Age-related changes and diseases of the ocular surface and cornea diseases of the ocular surface and cornea *Invest. Ophthalmol. Vis. Sci.* **54** ORSF48–53

Grill-Spector K and Malach R 2004 The human visual cortex *Annu. Rev. Neurosci.* **27** 649–77

Hall C A and Chilcott R P 2018 Eyeing up the Future of the Pupillary Light Reflex in Neurodiagnostics *Diagnostics* **8** 19

Harding R M 2001 Medical aspects of harsh environments, Volume 2, Chapter 32, Pressure changes and hypoxia in aviation *Medical Aspects of Harsh Environments* vol 2, ed K Pandolf and R Burr (Office of the Surgeon General, United states Army) p 30 Online: https://pdfs.semanticscholar.org/8995/c1867de9100c13821800fca173ae69d90b9c.pdf

Harris J, Nefs H T and Grafton C E 2008 Binocular vision and motion-in-depth *Spat. Vis.* **12** 531–47

Hathibelagal A R, Bharadwaj S R, Yadav A R, Subramanian A, Sadler J R E and Barbur J L 2020 Age-related change in flicker thresholds with rod- and cone-enhanced stimuli *PLOS ONE* **15** e0232784

Hattar S, Liao H-W, Takao M, Berson D M and Yau K-W 2002 Melanopsin-containing retinal ganglion cells: Architecture, projections, and intrinsic photosensitivity *Science* **295** 1065–70

Hattar S, Lucas R J, Mrosovsky N, Thompson S, Douglas R H, Hankins M W, Lem J, Biel M, Hofmann F, Foster R G and Yau K-W 2003 Melanopsin and rod–cone photoreceptive systems account for all major accessory visual functions in mice *Nature* **424** 76–81

Hecht S, Haig C and Chase A M 1937 The influence of light adaptation on subsequent dark adaptation of the eye *J. Gen. Physiol.* **20** 831–50

Hecht S, Haig C and Wald G 1935 The dark adaptation of retinal fields of different size and location *J. Gen. Physiol.* **19** 321–37

Hess E H and Polt J M 1964 Pupil Size in Relation to Mental Activity during Simple Problem-Solving *Science* **143** 1190–2

Hess R F and Nordby K 1986a Spatial and temporal limits of vision in the achromat. *J. Physiol.* **371** 365–85

Hess R F and Nordby K 1986b Spatial and temporal properties of human rod vision in the achromat. *J. Physiol.* **371** 387–406

Hiatt K L, Rash C E, Harris E S and McGilberry W H 2004 *Apache aviator visual experiences with IHASDSS Helmet Mounted Display in operation Iraqi Freedom* (US Army Aeromedical Research Laboratory) Online: https://apps.dtic.mil/dtic/tr/fulltext/u2/a426334.pdf

Home R 1978 Binocular summation: A study of contrast sensitivity, visual acuity and recognition *Vision Res.* **18** 579–85

Hood D C and Finkelstein M A 1986 Chapter 5 Sensitivity to light *Handbook of Perception and Human Performance* vol 1 (John Wiley & Sons, Inc.)

Hou R H, Scaife J, Freeman C, Langley R W, Szabadi E and Bradshaw C M 2006 Relationship between sedation and pupillary function: comparison of diazepam and diphenhydramine *Br. J. Clin. Pharmacol.* **61** 752–60

Hovis J K, Milburn N J and Nesthus T E 2013 *Hypoxia, color vision deficiencies, and blood oxygen saturation* (Office of Aerospace Medicine, Federal Aviation Administration) Online: https://www.faa.gov/data_research/research/med_humanfacs/oamtechreports/2010s/media/201320.pdf

ICAO 1993 *Manual of the ICAO standard atmosphere extended to 80 kilometres (262 5000 feet)* (International Civil Aviation Organisation) Online:

http://www.aviationchief.com/uploads/9/2/0/9/92098238/icao_doc_7488_-_manual_of_icao_standard_atmosphere_-_3rd_edition_-_1994.pdf

Jackson G R, Owsley C and McGwin G 1999 Aging and dark adaptation *Vision Res.* **39** 3975–82

Jäkel F and Wichmann F A 2006 Spatial four-alternative forced-choice method is the preferred psychophysical method for naïve observers *J. Vis.* **6** 13–13

Janáky M, Grósz A, Tóth E, Benedek K and Benedek G 2007 Hypobaric hypoxia reduces the amplitude of oscillatory potentials in the human ERG *Doc. Ophthalmol.* **114** 45–51

Johansson J, Seimyr G Ö and Pansell T 2015 Eye dominance in binocular viewing conditions *J. Vis.* **15** 21

Joyce D S, Feigl B, Cao D and Zele A J 2015 Temporal characteristics of melanopsin inputs to the human pupil light reflex *Vision Res.* **107** 58–66

Jubran A 2015 Pulse oximetry *Crit. Care* **19** Online: https://www.ncbi.nlm.nih.gov/pmc/articles/PMC4504215/

Jubran A 1999 Pulse oximetry *Crit. Care* **3** R11

Judd D B 1951 Report of U.S. secretariat committee on colorimetry and artificial daylight *Proceedings of the twelfth session of the CIE* (Stockholm: Bureau Central de la CIE) p 11

Kahneman D and Beatty J 1966 Pupil diameter and load on memory *Science* **154** 1583–5

Kang O E, Huffer K E and Wheatley T P 2014 Pupil dilation dynamics track attention to high-level information *PLoS ONE* **9** Online: https://www.ncbi.nlm.nih.gov/pmc/articles/PMC4146469/

Kardon R H, Kirkali P A and Thompson H S 1991 Automated pupil perimetry pupil field mapping in patients and normal subjects *Ophthalmology* **98** 485–96

Keenan W T, Rupp A C, Ross R A, Somasundaram P, Hiriyanna S, Wu Z, Badea T C, Robinson P R, Lowell B B and Hattar S S 2016 A visual circuit uses complementary mechanisms to support transient and sustained pupil constriction *eLife* **5** e15392

Kelbsch C, Strasser T, Chen Y, Feigl B, Gamlin P D, Kardon R, Peters T, Roecklein K A, Steinhauer S R, Szabadi E, Zele A J, Wilhelm H and Wilhelm B J 2019 Standards in Pupillography *Front. Neurol.* **10** Online: https://www.frontiersin.org/articles/10.3389/fneur.2019.00129/full

Kelly D H 1961 Visual responses to time-dependent stimuli. I. Amplitude sensitivity measurements *J. Opt. Soc. Am.* **51** 422–9

Kelly D H 1962 Visual responses to time-dependent stimuli.* III. Individual variations *J. Opt. Soc. Am.* **52** 89

Kessel L, Lundeman J H, Herbst K, Andersen T V and Larsen M 2010 Age-related changes in the transmission properties of the human lens and their relevance to circadian entrainment *J. Cataract Refract. Surg.* **36** 308–12

Kim C B Y and Mayer M J 1994 Foveal flicker sensitivity in healthy aging eyes. II. Cross-sectional aging trends from 18 through 77 years of age *JOSA A* **11** 1958–69

Kiryu J, Asrani S, Shahidi M, Mori M and Zeimer R 1995 Local response of the primate retinal microcirculation to increased metabolic demand induced by flicker. *Invest. Ophthalmol. Vis. Sci.* **36** 1240–6

Kobrick J L and Dusek E R 1970 Effects of hypoxia on voluntary response time to peripherally located visual stimuli. *J. Appl. Physiol.* **29** 444–8

Kolb H 2018 Sagittal horizontal section of the adult human eye *Webvision* Online: http://webvision.med.utah.edu/imageswv/draweye.jpeg

Korczyn A D, Laor N and Nemet P 1976 Sympathetic pupillary tone in old age *Arch. Ophthalmol.* **94** 1905–6

Kostic C, Crippa S V, Martin C, Kardon R H, Biel M, Arsenijevic Y and Kawasaki A 2016 Determination of rod and cone influence to the early and late dynamic of the pupillary light response *Invest. Ophthalmol. Vis. Sci.* **57** 2501–8

Lamb T D 2013 Evolution of phototransduction, vertebrate photoreceptors and retina *Prog. Retin. Eye Res.* **36** 52–119

Lamb T D and Pugh E N 2004 Dark adaptation and the retinoid cycle of vision *Prog. Retin. Eye Res.* **23** 307–80

Laycock J 1986 Colour contrast calculations for displays viewed in illumination *J. Inst. Electron. Radio Eng.* **56** 96-

Lee S C S, Martin P R and Grünert U 2019 Topography of neurons in the rod pathway of human retina *Invest. Ophthalmol. Vis. Sci.* **60** 2848–59

Legge G 1984 Binocular contrast summation - II. Quadratic summation *Vision Res.* **24** 385–94

Linsenmeier R A 1986 Effects of light and darkness on oxygen distribution and consumption in the cat retina *J. Gen. Physiol.* **88** 521–42

Llapashtica E 2019 *Eye Movements & the Integrated Saccade Latency Test* (City University of London)

Llapashtica E, Sadler J, Barbur J L, Connolly D M, Sun T and Grattan K T V 2017 Integrated saccade latency as a measure of fatigue *Aerosp. Med. Hum. Perform.* **88** p298

Lobato-Rincón L-L, Cabanillas-Campos M del C, Bonnin-Arias C, Chamorro-Gutiérrez E, Murciano-Cespedosa A and Sánchez-Ramos Roda C 2014 Pupillary behavior in relation to wavelength and age *Front. Hum. Neurosci.* **8** Online: https://www.ncbi.nlm.nih.gov/pmc/articles/PMC4001033/

Loewenfeld I 1999 *The Pupil: Anatomy, Physiology, and Clinical Applications* (Butterworth-Heinemann)

Lowenstein O, Feinberg R and Loewenfeld I E 1963 Pupillary movements during acute and chronic fatigue - A new test for the objective evaluation of tiredness *Invest. Ophthalmol. Vis. Sci.* **2** 138–57

Lowenstein O and Freidman E D 1942 Pupillographic studies: 1 Present state of pupillography, its method and diagnostic significance

Lucas R J, Douglas R H and Foster R G 2001 Characterization of an ocular photopigment capable of driving pupillary constriction in mice *Nat. Neurosci.* **4** 621–6

Lucas R J, Hattar S, Takao M, Berson D M, Foster R G and Yau K-W 2003 Diminished pupillary light reflex at high irradiances in melanopsin-knockout mice *Science* **299** 245–7

Lucas R J, Peirson S, Berson D M, Brown T M, Cooper H M, Czeisler C A, Figueiro M G, Gamlin P D, Lockley S W, O'Hagan J B, Price L L A, Provencio I, Skene D J and Brainard G C 2014 Measuring and using light in the melanopsin age *Trends Neurosci.* **37** 1–9

Lumb A 2017 *Nunn's applied respiratory physiology* (Elsevier)

MacAdam D L 1942 Visual sensitivities to color differences in daylight* *JOSA* **32** 247–74

McDougal D H and Gamlin P D 2015 Autonomic control of the eye *Compr. Physiol.* **5** 439–73

McDougal D H and Gamlin P D 2010 The influence of intrinsically-photosensitive retinal ganglion cells on the spectral sensitivity and response dynamics of the human pupillary light reflex *Vision Res.* **50** 72–87

McFarland R A 1971 Human factors in relation to the development of pressurized cabins Online: https://utmb-ir.tdl.org/handle/2152.3/4199

McIlwain J T 1998 *An introduction to the Biology of Vision* (Cambridge University Press)

MOD 2011 *Defence Standard 00-970* (Ministry of Defence)

MOD 2019 MOD Boscombe Down Defence Aerodrome Manual Issue 5 Online: https://www.raf.mod.uk/our-organisation/stations/mod-boscombe-down/documents/mod-boscombe-down-dam/

Mollon J D 1999 Color vision: Opsins and options *Proc. Natl. Acad. Sci. U. S. A.* **96** 4743–5

Moorhead I R, Connoll D M and Sadler J R E 2016 Demonstration of the effects of hypoxia and benefits of oxygen on unaided twilight viewing and assisted night vision Aerospace Medical Association 87th Annual Scientific Meeting (Atlantic City)

Münch M, Léon L, Crippa S V and Kawasaki A 2012 Circadian and wake-dependent effects on the pupil light reflex in response to narrow-bandwidth light pulses *Invest. Ophthalmol. Vis. Sci.* **53** 4546–55

National Institute for Health and Care Excellence 2020 The technology | NPi-200 for pupillary light reflex in critical care patients | Advice | NICE Online: https://www.nice.org.uk/advice/mib235/chapter/The-technology

Nefs H T, O'Hare L and Harris J M 2010 Two independent mechanisms for Motion-In-Depth perception: Evidence from individual differences *Front. Psychol.* **1** Online: https://www.frontiersin.org/articles/10.3389/fpsyg.2010.00155/full

van Nes F L and Bouman M A 1967 Spatial Modulation Transfer in the Human Eye *J Opt Soc Am* **57** 401–6

Oliva M and Anikin A 2018 Pupil dilation reflects the time course of emotion recognition in human vocalizations *Sci. Rep.* **8** 4871

Osterberg G 1935 Topography of the layer of rods and cones in the human retina *Acta Ophthalmol. (Copenh.)* **13** 1–97

Owsley C 2011 Aging and vision *Vision Res.* **51** 1610–22

Panda S, Sato T K, Castrucci A M, Rollag M D, DeGrip W, Hognesch J B, Provencio I and Kay S A 2002 Melanopsin (Opn4) requirement for normal light-induced circadian phase shifting *Science* **298** 2214–6

Partala T and Surakka V 2003 Pupil size variation as an indication of affective processing *Int. J. Hum.-Comput. Stud.* **59** 185–98

Pelli D G, Robson J G and Wilkins A J 1988 The design of a new letter chart for measuring contrast sensitivity *Clin. Vis. Sci.* **2** 187–99

Piquado T, Isaacowitz D and Wingfield A 2010 Pupillometry as a measure of cognitive effort in younger and older adults *Psychophysiology* **47** 560–9

Pirenne M H 1943 Binocular and uniocular threshold of vision *Nature* **152** 698–9

Pokorny J, Smith V C and Lutze M 1987 Aging of the human lens *Appl. Opt.* **26** 1437

Porta J B 1593 *De refractione optices parte: Libre novem* (Naples: Carlinum & Pacem)

Rabin J, Gooch J and Ivan D 2011 Rapid quantification of color vision: The Cone Contrast Test *Invest. Ophthalmol. Vis. Sci.* **52** 816–20

Rauscher F G, Chisholm C M, Edgar D F and Barbur J L 2013 Assessment of novel binocular colour, motion and contrast tests in glaucoma *Cell Tissue Res.* **353** 297–310

Rice M L, Leske D A, Smestad C E and Holmes J M 2008 Results of ocular dominance testing depend on assessment method *J. AAPOS Off. Publ. Am. Assoc. Pediatr. Ophthalmol. Strabismus Am. Assoc. Pediatr. Ophthalmol. Strabismus* **12** 365–9

Rodriguez-Carmona M L 2006 *Variability of chromatic sensitivity: fundamental studies and clinical applications* (City University of London) Online: http://openaccess.city.ac.uk/12058/1/433675.pdf

Rodriguez-Carmona M L, Harlow A, Walker G and Barbur J L 2005 The variability of normal trichromatic vision and the establishment of the "normal" range Online: https://pdfs.semanticscholar.org/2f8b/8736eae31794ff6a0100f7103bed7b02876d.pdf

Rose R M, Teller D Y and Rendleman P 1970 Statistical properties of staircase estimates *Percept. Psychophys.* **8** 199–204

Rovamo J, Donner K, Näsänen R and Raninen A 2000 Flicker sensitivity as a function of target area with and without temporal noise *Vision Res.* **40** 3841–51

Różanowski K, Bernat M and Kamińska A 2015 Estimation of operators' fatigue using optical methods for determination of pupil activity *Int. J. Occup. Med. Environ. Health* **28** 263–81

Sadler J R E, Brennen S, Liggins E, Longman P and Bigmore D 2016 *Visual information requirements and image metrics for the rotary wing stability and control task* (QinetiQ)

Safety Regulation Group Civil Aviation Authority 2007 *Helicopter flight in degraded visual conditions.* (Norwich: TSO) Online: https://publicapps.caa.co.uk/docs/33/Paper200703.pdf

Sekiguchi C, Handa Y, Kurihara Y, Nagasawa A and Kuroda I 1978 Evaluation method of mental workload under flight conditions *Aviat. Space Environ. Med.* **49** 920–5

Sharpe L T and Stockman A 1999 Rod pathways: the importance of seeing nothing *Trends Neurosci.* **22** 497–504

Sharpe L T, Stockman A, Jagla W and Jägle H 2005 A luminous efficiency function, V*(λ), for daylight adaptation *J. Vis.* **5** 3–3

Sharpe L T, Stockman A and MacLeod D I 1989 Rod flicker perception: scotopic duality, phase lags and destructive interference *Vision Res.* **29** 1539–59

Shelton B R and Scarrow I 1984 Two-alternative versus three-alternative procedures for threshold estimation *Percept. Psychophys.* **35** 385–92

Shipp S and Zeki S 2002 The functional organization of area V2, I: Specialization across stripes and layers *Vis. Neurosci.* **19** 187–210

Simpson W A, Manahilov V and Shahani U 2009 Two eyes: 2 better than one? *Acta Psychol. (Amst.)* **131** 93–8

Spector R H 1990 The Pupils *Clinical Methods: The History, Physical, and Laboratory Examinations* ed H K Walker, W D Hall and J W Hurst (Boston: Butterworths) Online: http://www.ncbi.nlm.nih.gov/books/NBK381/

Stanley P A and Davies A K 1995 The effect of field of view size on steady-state pupil diameter *Ophthalmic Physiol. Opt.* **15** 601–3

Stiles W S and Crawford B H 1933 The luminous efficiency of rays entering the eye pupil at different points *Proc. R. Soc. Lond. Ser. B Contain. Pap. Biol. Character* **112** 428–50

Stockman A, Sharpe L T, Zrenner E and Nordby K 1991 Slow and fast pathways in the human rod visual system: electrophysiology and psychophysics *J Opt Soc Am* **8** 1657–65

Stot J R R 2013 Orientation and disorientation in aviation *Extreme Physiol. Med.* **2**

Suttle C, Alexander J, Liu M, Ng S, Poon J and Tran T 2009 Sensory ocular dominance based on resolution acuity, contrast sensitivity and alignment sensitivity *Clin. Exp. Optom.* **92** 2–8

Thorn F and Boynton R M 1974 Human binocular summation at absolute threshold *Vision Res.* **14** 445–58

Tinjust D, Kergoat H and Lovasik J V 2002 Neuroretinal function during mild systemic hypoxia *Aviat. Space Environ. Med.* **73** 1189–94

Toet A, IJspeert J K, Waxman A M and Aguilar M 1997 Fusion of visible and thermal imagery improves situational awareness *Displays* **18** 85–95

US Navy 2017 U.S. Navy Aeromedical Reference and Waiver Guide Online: http://www.med.navy.mil/sites/nmotc/nami/arwg/Documents/WaiverGuide/Complete_Waiver_Guide.pdf

Vancleef K, Read J C A, Herbert W, Goodship N, Woodhouse M and Serrano-Pedraza I 2018 Two choices good, four choices better: For measuring stereoacuity in children, a four-alternative forced-choice paradigm is more efficient than two *PLOS ONE* **13** e0201366

Vassie K 1998 Specification and assessment of the visual aspects of cockpit displays *SID Symp. Dig. Tech. Pap.* **29** 1199–203

Vassie K and Christopher W 2000 Just acceptable and desirable luminance levels for fast jet cockpit displays

Vecchi D, Morgagni F, Guadagno A G and Lucertini M 2014 Visual function at altitude under night vision assisted conditions *Aviat. Space Environ. Med.* **85** 60–5

Vos J J 1978 Colorimetric and photometric properties of a 2° fundamental observer *Color Res. Appl.* **3** 125–8

Wald G, Harper P V, Goodman H C and Krieger H P 1942 Respiratory effects on the visual threshold *J. Gen. Physiol.* **25** 891–903

Wangsa-Wirawan N D and Linsenmeier R A 2003 Retinal Oxygen: Fundamental and Clinical Aspects *Arch. Ophthalmol.* **121** 547–57

Watson A B and Pelli D G 1983 Quest: A Bayesian adaptive psychometric method *Percept. Psychophys.* **33** 113–20

Watson A B and Yellott J I 2012 A unified formula for light-adapted pupil size *J. Vis.* **12** 12–12

Wetherill G B, Chen H and Vasudeva R B 1966 Sequential estimation of quantal response curves: A new method of estimation *Biometrika* **53** 439–54

Wilhelm B, Stuiber G, Lüdtke H and Wilhelm H 2014 The effect of caffeine on spontaneous pupillary oscillations *Ophthalmic Physiol. Opt.* **34** 73–81

Williams P and Warwick R 1980 *Gray's Anatomy* (Churchill Livingston)

Willmann G, Ivanov I V, Fischer M D, Lahiri S, Pokharel R K, Werner A and Khurana T S 2010 Effects on colour discrimination during long term exposure to high altitudes on Mt Everest *Br. J. Ophthalmol.* **94** 1393–7

Wilmer W H and Berens C 1918 V. The effect of altitude on ocular functions *J. Am. Med. Assoc.* **71** 1394–8

Winn B, Whitaker D, Elliott D B and Phillips N J 1994 Factors affecting light-adapted pupil size in normal human subjects. *Invest. Ophthalmol. Vis. Sci.* **35** 1132–7

Wong-Riley M T T 2010 Energy metabolism of the visual system *Eye Brain* **2** 99–116

Wood J M, Collins M J and Carkeet A 1992 Regional variations in binocular summation across the visual field *Ophthalmic Physiol. Opt.* **12** 46–51

Wright S, Rousse D, van Atta A, Gaska J, Winterbottom M, Hadley S and Lamothe D 2016 *Automated Vision Test Development and Validation* (School of Aerospace Medicine Wright Patterson AFB United States)

Wright W D 1996 Part II: The origins of the 1931 CIE system *Human Color Vision* (Optical Society of America) pp 534–43

Wuerger S, Ashraf M, Kim M, Martinovic J, Pérez-Ortiz M and Mantiuk R K 2020 Spatio-chromatic contrast sensitivity under mesopic and photopic light levels *J. Vis.* **20** 23

Young R S L and Kennish J 1993 Transient and sustained components of the pupil response evoked by achromatic spatial patterns *Vision Res.* **33** 2239–52

Yu M, Kautz M A, Thomas M L, Johnson D, Hotchkiss E R and Russo M B 2007 Operational implications of varying ambient light levels and time-of-day effects on saccadic velocity and pupillary light reflex *Ophthalmic Physiol. Opt.* **27** 130–41

Zeki S, Watson J, Lueck C, Friston K, Kennard C and Frackowiak R 1991 A direct demonstration of functional specialization in human visual cortex *J. Neurosci.* **11** 641–9

Zekveld A A, Koelewijn T and Kramer S E 2018 The pupil dilation response to auditory stimuli: Current state of knowledge *Trends Hear.* **22** Online: https://www.ncbi.nlm.nih.gov/pmc/articles/PMC6156203/